

https://dspace.org/

Treatment of parameter and model uncertainties through a sensitivity analysis of the seismic hazard for Johannesburg

Manzunzu, Brassnavy

2021
https://hdl.handle.net/10539/33074

Downloaded from a DSpace repository. https://dspace.org/

TREATMENT OF PARAMETER AND MODEL UNCERTAINTIES THROUGH A SENSITIVITY ANALYSIS OF THE SEISMIC HAZARD FOR JOHANNESBURG

Brassnavy Manzunzu

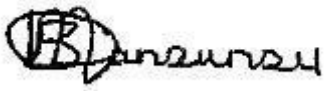
School of Geoscience, University of Witwatersrand

The Dissertation submitted to the Faculty of Science, University of Witwatersrand, Johannesburg, in fulfilment of the requirements for the degree of Doctor of Philosophy

Johannesburg, 2021

DECLARATION

I declare that this Dissertation is my own, unaided work. It is being submitted for the Degree of Doctor of Philosophy in Geophysics at the University of the Witwatersrand, Johannesburg. It has not been submitted before for any degree or examination at any other University.



Brassnavy Manzunzu
(Signature of candidate)

23rd Day of October 2021 in Silverton

ABSTRACT

Seismic hazard analysis is a dynamic process, which requires regular updating with emerging new information. In this regard, quest for new information is always there. However, in order to reduce costs, minimise labour while producing reliable results, efforts must be focused on areas that are influential to the final calculated hazard. In this study, we analyzed the uncertainties associated with various models and input parameters in the computation of the seismic hazard for Johannesburg.
Several uncertainties were assessed and evaluated at different steps in the seismic hazard process. The evaluated uncertainties include uncertainty in the compilation of the seismic catalogue, the selection of ground motion prediction equations (GMPEs), the development of seismic source models as well as the computation of recurrence parameters. A comprehensive homogeneous catalogue was compiled consisting of both historical and instrumental earthquakes. Different declustering techniques were tested on our catalogue on their suitability to remove dependent events in order to come out with a Poissonian distributed catalogue. Both location and magnitude uncertainties were characterized in the catalogue processing. Location uncertainty reduction helps in identification of more refined seismic source zones while magnitude uncertainties influence the computation of recurrence parameters. The catalogue was used in the development of a seismotectonic model. The area under study is characterized by diffuse low magnitude earthquakes, which made it very difficult to identify linear sources of earthquakes. Consequently, areal source zones were developed based on the available and recently determined information on seismicity, focal mechanisms, and active faults. The zones identified in this study were compared to previously identified tectonic source zones in the region. It was noted that although the more information on focal mechanisms and possible active faults were gathered, only a few refinements could be made to the source model. Although there were a few modifications to the previous tectonic studies, sensitivity analysis results showed large variability emphasizing the importance of accurate seismic source zoning in the region. Careful selection of Ground Motion Prediction Equations (GMPEs) was done considering local available data. All the uncertainties were utilized in the sensitivity analysis.

Sensitivity analyses were performed for 2% probability of exceedance in 50 years for the city of Johannesburg. Sensitivity analysis results indicates that the five most important inputs that have a profound impact in controlling the final hazard levels are (1) GMPEs, (2) seismic source model, (3) temporal variation of the seismic catalogue, (4) catalogue homogenisation process, (5) method of computing recurrence parameters. Coefficient of variation values in excess of 0.2 were obtain for these parameters. It shows that the largest contributor to uncertainty in the assessment of Peak Ground Acceleration (PGA) and acceleration at spectral periods 0.15 and 2.0 seconds, which are important for the response of buildings, is the selection of GMPEs. Next are the uncertainties in the processing

of the seismic catalogue and the recurrence parameters. Seismic hazard is not very sensitive to the variability in bedrock velocity. The research findings from this study may serve as a useful guide to facilitate further research studies on influential parameters and models for future seismic hazard assessments. Even so, it should be noted that the degree of sensitivity of the parameters depends on the study site. A meticulous study of these parameters will lead to the reduction of uncertainties in future assessments.

ACKNOWLEDGEMENTS

Firstly, I would like to thank my advisor, Dr. Vunganai Midzi for his invaluable support, guidance, and friendship. His dedication throughout these years was beyond expectation. The countless and interesting discussions we had, helped shape not only this study, but also my future as a scientist and person. I also would like to thank Prof. Raymond Durrheim for his helpful comments and continuous support and for all the encouragement he gave me.

I would like to thank my wife, Sandra, for all she has done to help me reach my goals. Without her support, love, help, and sacrifices, I would never have arrived at this point in my journey. My three beautiful daughters Evernage, Ashley and Tapiwanashe gave me the extra energy and inspiration I needed. I would also like to thank my parents for instilling in me the value of excellence, the desire to learn, and for giving me every opportunity.

My gratitude also goes to my colleagues at the Council for Geoscience, Thifhelimbilu Mulabisana, Tebogo Pule, Sbonelo Zulu, Godfrey Madzivire, Emmanuel Chirenje and Emmanuel Sakala. I also would like to thank the Council for Geoscience for the financial support and providing me time to work on my studies.

Lastly, l would like to give glory to the Almighty Lord for the grace and strength he gave me during this study and all the good things that come of this study.

LIST OF PUBLICATIONS

Peer-reviewed publications

- **Manzunzu B.**, V. Midzi, R.J. Durrheim, T. Pule, N. Flint. (In Press). Quantitative evaluation of source parameters of historical earthquakes in southern Africa, *Journal of Seismology*.
- **Manzunzu B.**, Brandt M. B. C., V. Midzi, R.J. Durrheim, I. Saunders, T.F. Mulabisana. (2020). Towards a homogeneous moment magnitude determination for earthquakes in South Africa: Reduction of associated uncertainties, *Journal of African Earth Science*.
- Midzi, V., Pule, T., Mulabisana, T., Zulu, B., **Manzunzu, B.,** (2020). Reassessment of source parameters of 'major' southern African earthquakes. *South African Journal of Geology*, *123*(1), pp.59-74.
- Midzi, V., **Manzunzu B**., Mulabisana T.F., Zulu B.S., Pule T., Myendeki S., Rathod, G. (2020). The Probabilistic Seismic Hazard Assessment of South Africa. *Journal of African Earth Sciences*.
- **Manzunzu B**., V. Midzi, T.F. Mulabisana, B. Zulu, T. Pule, S. Myendeki and G.W. Rathod (2019). Seismotectonics of South Africa, *Journal of African Earth Sciences*, 149, 271-279
- **Manzunzu B.,** V. Midzi, A. Mangongolo, F. Essrich. (2017). The aftershock sequence of the 5th August 2014 Orkney earthquake, South Africa, *Journal of Seismology*, DOI: 10.1007/s10950-017-9667-z.

Conference presentations

- Determination of shallow shear wave velocity profiles in Johannesburg for Vs30 classification, **SAGA 2019 Conference**, Durban, South Africa, October 2019.
- Relocation of seismic events in South Africa for ground truth identification and classification, **CTBTO Science and Technology 2019 Conference**, Vienna, Austria, June 2019.
- Uncertainties associated with earthquake catalogue: Impacts on Seismic Hazard Assessment for Johannesburg, **CGS 2019 Conference**, Pretoria, February 2019.
- Toward a homogeneous moment-magnitude determination for earthquakes in South Africa: Analysis of uncertainties in magnitude conversion, **African Seismological Commission 2018 General Assembly, Al-Hociema**, Morocco, April 2018.
- Uncertainties associated with earthquake catalogue: Impacts on Seismic Hazard Assessment for Johannesburg, **12th Annual Africa Array Workshop**, Johannesburg, June 2017.

TABLE OF CONTENTS

DECLARATION I

ACKNOWLEDGEMENTS IV

LIST OF PUBLICATIONS V

CHAPTER 1: INTRODUCTION 1

1.1. INTRODUCTION 1

1.2. RESEARCH OBJECTIVES 3

1.3. ORGANISATION OF THE DISSERTATION 4

CHAPTER 2: LITERATURE REVIEW: SEISMIC HAZARD ANALYSIS AND UNCERTAINTIES ASSOCIATED WITH THE PROBABILISTIC SEISMIC HAZARD ANAMYSIS METHOD 5

2.1. INTRODUCTION 5

2.2. DETERMINISTIC SEISMIC HAZARD ANALYSIS (DSHA) 7

2.3. PROBABILISTIC SEISMIC HAZARD ANALYSIS (PSHA) 9

2.3.1. Basic steps in PSHA 10

2.3.2. Step 1: Seismic Sources 12

2.3.3. Step 2: Modelling of Earthquake Occurrences 13

2.3.4. Step 3: Attenuation Relationships (Ground Motion Prediction Equations) 24

2.3.5. Step 4: Seismic Hazard Calculations 27

2.4. REVIEW OF EXISTING PSHA METHODS 29

2.4.1. Cornell (1968) 29

2.4.2. Veneziano et al. (1984) 29

2.4.3. McGuire (1993) 29

2.4.4. Frankel (1995) 30

2.4.5. Kijko and Graham (1999) 30

2.4.6. Stochastic method 31

2.4.7. Monte Carlo method 31

2.5. CONSIDERATION OF UNCERTAINTIES 32

2.6. UNCERTAINTIES IN EARTHQUAKE CATALOGS 34

2.6.1. Earthquake magnitude distribution 34

2.6.2. Uncertainties associated with the recurrence relations 35

2.6.3. Declustering process 35

2.6.4. Uncertainty in M_{max} estimation 37

2.6.5. Uncertainties associated with the magnitude of completeness, M_c 37

2.6.6. Uncertainty in the Spatial Distribution of Earthquakes 38

2.7. UNCERTAINTIES IN SEISMIC SOURCE CHARACTERIZATION 39

2.8. UNCERTAINTY DUE TO ATTENUATION EQUATION 39

2.9. LOGIC TREE APPROACH 42

2.10. SENSITIVITY ANALYSIS 44
2.10.1. Monte Carlo approach 46
2.10.2. Variance Based Global Sensitivity Analysis (VBSA) 47
2.10.3. Practical applications 47

CHAPTER 3: GEOLOGICAL AND TECTONIC SETTING OF JOHANNESBURG AND SURROUNDING AREAS 49

3.1. INTRODUCTION 49

3.2. REGIONAL GEOLOGICAL SETTINGS 49

3.3. LOCAL GEOLOGICAL SETTING 50
3.3.1. Witwatersrand Supergroup 51
3.3.2. Ventersdorp Supergroup 52
3.3.3. Transvaal Supergroup 53

3.4. STRUCTURAL SETTING 53

3.5. GEOPHYSICAL INTERPRETATIONS 56

3.6. NEOTECTONICS 57

3.7. CONCLUSIONS 60

CHAPTER 4: CATALOGUE COMPILATION AND UNCERTAINTY ANALYSIS 61

4.1. INTRODUCTION 61

4.2. SEISMIC MONITORING IN SOUTH AFRICA AND NEIGHBOURING REGIONS 62
4.2.1. South African National Seismograph Network (SANSN) 63
4.2.2. The mining cluster networks 64

4.3. SEISMOLOGICAL STATIONS IN NEIGHBOURING COUNTRIES 65

4.4. GLOBAL SEISMOLOGICAL AGENCIES 66
4.4.1. International Seismological Summary (ISS) 66
4.4.2. International Seismological Centre (ISC) bulletin 66

4.5. PREVIOUS CATALOGUE COMPILATION EFFORTS 67
4.5.1. Early seismological compilations 67
4.5.2. Studies of individual events 69

4.6. CATALOGUE COMPILATION 69
4.6.1. Historical (pre-1899) data 70
4.6.2. Early instrumental (1899-1969) data 71
4.6.3. Modern instrumental (1970-2016) data 77

4.7. HOMOGENISATION OF MAGNITUDES 79
4.7.1. Conversion from local magnitude 79
4.7.2. Conversion from body-wave magnitude M_B 85
4.7.3. Conversion from surface-wave magnitude M_S 86
4.7.4. Conversion from Bulawayo magnitude M_{bLg} 86

4.8. TREATMENT OF UNCERTAINTIES IN THE COMPILED CATALOGUE 86
4.8.1. Location Uncertainties 87
4.8.2. Relocation of instrumental earthquakes 87
4.8.3. Magnitude Uncertainties 94
4.8.4. Magnitude uncertainties for instrumental data 95
4.8.4.1. Direct estimates of 95

4.9. INFLUENCE OF MINING-RELATED SEISMIC EVENTS 97

4.10. DECLUSTERING OF EARTHQUAKE CATALOGUE 99
4.10.1. Window-based approaches 99
4.10.2. Cluster-link models 101
4.10.3. Rate-based methods 103
4.10.4. Declustering results 103

4.11. UNCERTAINTIES ASSOCIATED WITH THE DECLUSTERING PROCESS 104

4.12. CATALOGUE COMPLETENESS 106
4.12.1. Stepp Method 106
4.12.2. Maximum curvature method 107
4.12.3. Temporal variation of M_C 108
4.12.4. Spatial variations in completeness 110
4.12.5. Uncertainty in M_C 111

4.13. CONCLUSIONS 113

CHAPTER 5: SEISMOTECTONIC MODEL AND SEISMIC SOURCE CHARACTERIZATION 114

5.1. INTRODUCTION 114

5.2. PREVIOUS SEISMOTECTONIC STUDIES 114
5.2.1. Partridge (1995) model 115
5.2.2. Hartnady (1996) model 116
5.2.3. Du Plessis (1996) model 116

5.3. REGIONAL TECTONIC STRESS REGIMES 118
5.3.1. In situ measurements 118
5.3.2. Focal mechanism solutions and stress modelling 119
5.3.3. Stress inversion 126

5.4. DEPTH DISTRIBUTION 128

5.5. SEISMOTECTONIC MODEL CONSTRUCTION 129
5.5.1. Classification of available data 130

5.6. DELINEATION OF SEISMIC SOURCE ZONES 132
5.6.1. Criteria for defining seismic sources 133
5.6.2. Seismotectonic sources from tectonic regions 134
5.6.3. Seismic source zones from mining regions 137

5.7. UNCERTAINTIES IN SEISMOTECTONIC MODELLING 139

5.8. CONCLUSIONS 140

CHAPTER 6: MODELLING RECURRENCE PARAMETERS 142

6.1. INTRODUCTION 142

6.2. *B*-VALUE ESTIMATION 143

6.3. EARTHQUAKE *A*-VALUE ESTIMATION 149

6.4. MAXIMUM MAGNITUDE M_{MAX} CALCULATION 155

6.5. CONCLUSION 157

CHAPTER 7: GROUND MOTION MODEL 158

7.1. INTRODUCTION 158
7.2. IDENTIFICATION AND TESTING OF SUITABLE GROUND MOTION PREDICTION EQUATIONS FOR JOHANNESBURG 159
7.3. GMPE PARAMETER ADJUSTMENTS 161
7.3.1. Horizontal component definition 161
7.3.2. Magnitude 161
7.3.3. Distance 161
7.3.4. Style-of-faulting 161
7.4. IDENTIFIED TESTING DATA 162
7.4.1. Results of Comparisons 164
7.5. COMPARISON OF THE ORKNEY EARTHQUAKE STRONG-MOTION DATA WITH PRE-SELECTED GMPES 179
7.6. CONCLUSIONS 182
CHAPTER 8: SENSITIVITY ANALYSIS OF SEISMIC HAZARD OF JOHANNESBURG 183
8.1. INTRODUCTION 183
8.2. SENSITIVITY ANALYSIS RELATED TO GLOBAL VARIABLES 188
8.2.1. Earthquake Catalogue Magnitude homogenisation process 188
8.2.2. Temporal stationarity of the catalogue 192
8.2.3. Declustering process 195
8.2.4. Method of computing recurrence parameters 198
8.2.5. Assessment of seismic source models 200
8.2.6. Effect of individual seismic source zones 204
8.2.7. Local site effects 214
8.2.8. Minimum magnitude, M_{min}, for hazard calculation 216
8.2.9. Ground Motion Prediction Equations 218
8.3. SENSITIVITY ANALYSIS RELATED TO LOCAL VARIABLES 220
8.3.1. *b*-value estimation 220
8.3.2. Activity rate 222
8.3.3. M_{max} determination 224
8.4. DISCUSSIONS 226
8.5. CONCLUSIONS 227
CHAPTER 9: CONCLUSION 229
9.1. LIMITATIONS 232
9.2. RECOMMENDATIONS 233
REFERENCES 235
APPENDIX: 276
APPENDIX A. 276
A.1. List of macroseismic event analysed in this study. 276

List of Figures

Figure 2-1: The four-step process of a deterministic seismic hazard assessment process (Reiter, 1990). 8

Figure 2-2: The four steps in Probabilistic Seismic Hazard Analysis (modified from Reiter, 1990). 11

Figure 2-3: 3D diagram representing some useful data for used in delineating seismic source zones(Le Goff and Fitzenz, 2012). 12

Figure 2-4: Characteristic earthquake model (modified from Youngs and Coppersmith, 1985). 16

Figure 2-5: Linear, Bilinear and Parabolic recurrence relationships. 17

Figure 2-6: Different methods of estimating M_C. a) Stepp (1972) b) Cumulative distribution (Wiemer and Wyss, 200) 21

Figure 2-7: Illustration of possible influence of errors in earthquake locations in seismic source delineations in the West Rand region. Comparison of locations produced by a) cluster network and b) national network location. 38

Figure 2-8: An example of a GMPE developed for Eastern and North America. Log_{10} values of horizontal component 5% pseudo-spectral acceleration (PSA) at frequencies 0.5, 1, and 5.03 Hz, and the peak ground acceleration (PGA) is in units of m/s^2. Dots show PSA from simulations, including aleatory uncertainty, for M 5 (light) and M 8 (dark); Fdist is the distance. Solid lines show predicted amplitudes from regression equations developed from simulated database, for M 5, 6, 7, and 8 (adapted from Atkinson and Boore, 2006). 40

Figure 2-9: An example of a logic tree. The seismic source zone represents an independent node while the activity rate and Mmax are the dependent one. 44

Figure 3-1: Regional geological settings of southern Africa showing mobile belts and Archaean cratons (Manzunzu et al., 2019). 50

Figure 3-2: Detailed stratigraphic unit of the Witwatersrand Supergroup with the lithologies and depositional settings of the Central Rand and the West Rand Groups (modified from Catuneanu and Eriksson, 1999; McCarthy, 2006; Smith et al., 2013). 52

Figure 3-3: Structural settings for southern Africa with major faults (modified from Manzunzu et al., 2019). Blue lines are major faults, red lines are faults green lines demarcate mobile belts. TML is the Thabazimbi Marchinson Lineament. 55

Figure 3-4: The Rietfontein Fault system and the related structural features of the Witwatersrand Basin (modified from Myers et al., 1990). 56

Figure 4-1: Location of early seismograph stations in Southern Africa region from 1899 to 1969. . 62

Figure 4-2: Map of the SANSN network. The three cluster networks also shown in the zoomed picture. 65

Figure 4-3: Seismic events of the early instrumental period (1899-1969) that occurred within the region of interest in southern Africa. 72

Figure 4-4: The location of the earthquakes with source parameters determined in this study. The earthquakes are shown with their ranking. 77

Figure 4-5: Spatial distribution of seismic events that occurred in and around Johannesburg during the modern instrumental period (1970-2016). 78

Figure 4-6: Seismological stations of the SASE project shown as green triangles. The circles represent the locations of the epicentres of the seismic events used in this study (red circles indicate mining-related events, while black circles denote tectonic events). The classification is based on the proximity of the event to the mining boundaries (from Manzunzu et al., 2020). 81

Figure 4-7: Regression analysis of moment magnitude (M_w) calculated in this study and the local magnitudes (M_L) used by the SANSN for the compiled data set as shown in Table 2. (a) Comparison of M_W to M_L as derived using the Hutton and Boore (1987) relation, (b) Comparison of M_W to M_L as derived using the modified Richter relation (Fernández, 1980), (c) Comparison of M_W to M_L as derived using the Saunders et al. (2013) relation. 84

Figure 4-8: Comparison of M_B-M_W data in study region with the three global relations Scordilis (2006) (red line), Das et al. (2011) (orange line) and Johnston (1996) (blue line). 86

Figure 4-9. Comparison of new epicentral locations (black stars) to the published CGS locations (red stars). Black lined boxes represent clusters of seismicity zoomed as in Figure 4-10 for clarity (modified from Midzi et al., 2020). 88

Figure 4-10. Comparison of new epicentral locations (black stars) to the published CGS locations (red stars). Zoomed clusters indicated by boxes in Figure 4-9. (a) Cental Rand, (b) KOSH, (c) Welkom and (d) Koffiefontein clusters. 90

Figure 4-11. Map showing the typical GAP values obtained during the analysis and their distribution with epicentres. 92

Figure 4-12: RMS (in seconds) of relocated epicentres of the events in the dataset. 93

Figure 4-13. Error ellipses of relocated epicentres of the events in the dataset.....94

Figure 4-14: Variation of local magnitude with epicentral distance.....96

Figure 4-15: Mean magnitude residuals with distance local (M_L) magnitude values.....97

Figure 4-16: Frequency magnitude distribution of the current catalogue for seismicity in and around Johannesburg. Effect of mining related seismic events are illustrated by the 2 G-R lines (in red). The first cut-off magnitude M_{C1} shows the G-R distribution for small mining related events and the second M_{C2} shows the G-R distribution for tectonic events.....98

Figure 4-17: Spatial-temporal variation of the dependence windows for the three windows-based declustering techniques. 101

Figure 4-18: Cumulative number of events for the declustered catalogues obtained using several declustering algorithms. G&K is the Gardner and Knoppoff (1974) method; Grue is the Grünthal (1985) method; Reis_min, Reis_std and Reis_max are the minimum, mean and maximum standard deviations for the Reasenberg (1985) method respectively;, Urh is the Uhrhammer method; and Seisan and Zaliapin are the Seisan and Zaliapin methods, respectively.....104

Figure 4-19: Results from the catalogue approach. The red dots represents the start of the completeness for each magnitude unit. 107

Figure 4-20: Estimation of the magnitude of completeness using Maximum-Curvature.....108

Figure 4-21: Variation of the magnitude of completeness (M_c) with time for our catalogue. The green line indicates the average Mc for the time period. The dashed line represents the uncertainty.....110

Figure 4-22: Spatial variation of M_C within the catalogue. 111

Figure 4-23: Comparison of the FMD for the two periods 1970 to 1990 and 2012 to 2016. The two periods have different M_C values. 112

Figure 4-24: Different M_C calculation methods. Green is M_C by the Shi and Bolt method, blue is M_C by EMR and magenta is Maximum curvature method. Both methods were computed using the Gardner and Knoppoff catalogue.....112

Figure 5-1: A seismotectonic model for South Africa proposed by Partridge (1995).....115

Figure 5-2: Hartnady seismic source zones for Southern Africa (modified from Hartnady, 1996).116

Figure 5-3: Modified seismotectonic zones defined by Du Plessis (1996).....117

Figure 5-4: Orientations of the major horizontal stresses from in-situ measurements by Stacey and Wessloo (1998). Red arrow indicate compressive stress, blue lines shows extensional stress orientations. 119

Figure 5-5: Examples of polarities picked. C is the upward first motion and D is the downward first motion. In this figure, station MOPA (BHZ channel) is at an epicentral distance of 210km: Polarity (Down). Station BLWY, (BHZ channel) is in Zimbabwe at 426 KM from the station : (Polarity (UP). BOSA, BHZ, is at epicentral distance of 136 km and station KEVO BHZ located at 221 km from the epicenter. 121

Figure 5-6: Focal mechanism solutions used in this study. Thick black lines represent faults located in the area and yellow circles represent earthquakes (M>4). Black beach balls represent new solutions (Table 5-2) while the red ones are the published solutions in Table 5-1. 122

Figure 5-7: FMS for the Witwatersrand basin. 126

Figure 5-8: Stress inversion from focal mechanism orientation data plotted using the CASMO software (Heidbach et al., 2018) for the inverted focal mechanism solutions. 127

Figure 5-9: Flow chart of the construction of a seismotectonic model as suggested by Terrier et al. (2000). 130

Figure 5-10: Seismotectonic map for Johannesburg and surrounding region used to delineate potential seismic sources. 132

Figure 5-11: Seismic source zones identified for this study. The smaller zones found within the red zone are the mining-related zones. 134

Figure 5-12: The seismotectonic models used in this study for sensitivity analysis used in this study. (a) du Plessis (1995) (b) Partridge (1995) (c) Hartnady (1996) (d) model developed in this study. 140

Figure 7-1: Location of earthquakes used in the testing of GMPEs. The figure shows the spatial distribution of the seismic events and the stations. Triangles represent the stations recording the events with each station having a V_{s30} value indicated with the color; circles are the seismic events. 162

Figure 7-2: Illustration of site classification of the seismic station records representing different site classes based on NEHRP site classification. 164

Figure 7-3: The inter-event residuals of all GMPEs for PGA (T = 0.01s) spectral acceleration versus hypocentral distance. 167

Figure 7-4: The inter-event residuals of all GMPEs for PSA (T = 0.15s) versus hypocentral distance. 169

Figure 7-5: The inter-event residuals of all GMPEs for PGA (T = 2.0s) versus hypocentral distance. 171

Figure 7-6: Intra-event terms, also referred to as the mean residual, for the 10 GMPEs for PGA..174

Figure 7-7: Intra-event terms, also referred to as the mean residual, for the 10 GMPEs T=0.15s spectral period. 176

Figure 7-8: Intra-event terms, also referred to as the mean residual, for the 10 GMPEs for T= 2.0s spectral period. 178

Figure 7-9. Comparison between the spectral accelerations at three spectral periods recorded during the 2014 Orkney earthquake of magnitude *Mw* = 5.5 and the predictions obtained with ten preselected GMPEs. 181

Figure 8-1: Mean 2% probability of exceedance in 50 year seismic hazard maps for Johannesburg computed for the three spectral periods PGA, PSA = 0.15s and PSA = 2.0s. 187

Figure 8-2: G-R curves for the two catalogues used for sensitivity analysis for the homogenisation process. New relation refers to the homogenisation relations developed by Manzunzu et al. (2020) as applied while Global relation refers to the Diechmann (2006) magnitude homogenisation relation. 189

Figure 8-3: COV results for earthquake magnitude homogenisation process. 191

Figure 8-4: G-R curves for the two catalogues used in the assessment of the temporal stationarity of the catalogue. The entire catalogue starts from 1620 to 2016 while the post 1970 catalgogue is from 1970 to 2016. 193

Figure 8-5: COV results for length of catalogue (full catalogue and post 1970 catalogue). 194

Figure 8-6: The G-R distribution for the three declustered catalogues used for sensitivity analysis. Gru is the catalogue declustered with the Grunthal (1985), G&K is from the Gardner and Knoppoff (1975) catalogue and Seisan is from the CLUSTER program in SEISAN. 195

Figure 8-7: COV results for the sensitivity analysis for declustering for the three spectral periods analysed. 197

Figure 8-8: COV results for the sensitivity analysis for methods of computing recurrence parameters. 199

Figure 8-9: Results of different source models used in computing hazard for Johannesburg for the COV. 203

Figure 8-10: Maps showing the % contribution of the delineated zones to the total hazard for PGA for Johannesburg. Note the variation in the percentage value. Each map is scaled according to its own range of values. 207

Figure 8-11: Maps showing the % contribution of the delineated zones to the total hazard for spectral period of 0.15s for Johannesburg. Note the variation in the percentage value. Each map is scaled according to its own range of values. 210

Figure 8-12: Maps showing the % contribution of the delineated zones to the total hazard for spectral period of 2.0s for Johannesburg. Note the variation in the percentage value. Each map is scaled according to its own range of values. 213

Figure 8-13: COV results for the sensitivity analysis for bedrock shearwave velocity Vs. 215

Figure 8-14: COV results for the sensitivity analysis for M_{min} 217

Figure 8-15: COV results for GMPE seismic hazard sensitivity analysis. 219

Figure 8-16: COV results for the sensitivity analysis for *b*-value. 221

Figure 8-17: COV results for the sensitivity analysis for activity rate. 223

Figure 8-18: COV results for the sensitivity analysis for M_{max}. 225

List of tables

Table 2-1: Typical empirical relations between magnitude and some physical parameter of rupture faults. Mw refers to the moment magnitude, L is the rupture length, A is rupture area, S is the slip rate.....18

Table 2-2: Examples of Uncertainties in Seismic Hazard Analysis (McGuire, 2004) 34

Table 4-1: Detailed summary of South African institutions involved in early seismic monitoring and the seismic stations.....63

Table 4-2: Overview of seismological stations in neighbouring countries.....66

Table 4-3: Summary of seismological compilations dealing with pre-SANSN earthquakes. 68

Table 4-4: List of earthquakes analysed in this study with the newly determined source parameters. 75

Table 4-5: Quality ranking of the determined source parameters.....76

Table 4-6: The derived M_L- M_W relations and their period of validity for homogenisation. 84

Table 4-7: Error values and their period of applicability (from Manzunzu et al., 2020).....95

Table 4-8: Input parameters used in the CLUSTER methods in SEISAN. 103

Table 4-9: Results of applying the declustering algorithms of Gardner and Knopoff (1974), Grünthal (1985) and Uhrhammer (1986) to the modern SANSN data subset (1972-2016) of the Johannesburg PSHA project catalogue. 104

Table 4-10: Results of statistical tests for the eight declustered catalogues. 105

Table 4-11: Magnitude completeness using the catalogue based approach.....107

Table 4-12: Time intervals for catalogue completeness analysis 109

Table 4-13: Temporal variation of Magnitude of completeness using the catalogue based approach. 110

Table 5-1: Summary of published FMS in the study region. In the case of multiple solutions for the same event, the preferred solution is indicated in bold. Where NM – Normal faulting, SS – Strike slip, NO – normal oblique.....120

Table 5-2: Summary of FMS determined in this study.....122

Table 5-3: Instrumentally determined depths of South African tectonic earthquakes published in the literature. 128

Table 5-4: Depths of mining events with focal mechanism solution. 129

Table 5-5. Classification of the available information sources for the usefulness of seismic zonation in the region. High (1), Medium (2), Low (3). 130

Table 6-1: *b*–value estimations for the source areas determined in this study. For each source area, different catalogues were created during the catalogue processing step, and for each catalogue, recurrence parameters were calculated to represent the uncertainties associated with each step. Cat 1= Homogenised using M_w-M_L relations developed in this study. Cat 2 = Homogenized using global relations. Cat 3 = post 1970 catalogue. Cat 4 = All events. Cat 5 = Gardner & Knopoff (1974), Cat 6 = Grünthal et al (1985) and Cat 7 = Cluster (Seisan). The three methods used to compute the b-values are ZMAP, SEISAN aand Kijko. 143

Table 6-2: *a*-values for the Sources determined in this study. For each source, different catalogues were created during the catalogue processing and for each catalogue recurrence parameters were calculated to represent the sources of uncertainties. Cat 1= Homogenised using M_W-M_L relations developed in this study. Cat 2 = Homogenised using global relations. Cat 3 = post 1970 catalogue. Cat 4 = All events. Cat 5, Cat 6 and Cat 7 were declustered using the Gardner and Knopoff (1974), Grunthal *et al.* (1985) and Cluster (SEISAN) techniques respectively. 149

Table 6-3: M_{max} values calculated for identified seismic sources determined using different methods. For some source zones where there are identified faults, the Wells and Coppersmith (1994) method was also used to compute M_{max}. M_{max_obs} is the maximum observed magnitude for the source. The five methods used to compute M_{max} are illustrated. ... 156

Table 7-1: GMPEs preselected from different tectonic settings to be used in this study, including the regions for which they were developed. SCR represents stable continental regions, SAC represents shallow active crusts and ISR represents induced seismicity regions. 160

Table 7-2: Number of events and recordings in different magnitude range showing the distance range of the recording stations. 163

Table 7-3: NEHRP site classification scheme (FEMA, 2003). V_{S30} is the shear-wave velocity averaged over the uppermost 30m. 163

Table 8-1: Recurrence parameters for the sources in the du Plessis (1995) model. 200

Table 8-2: Recurrence parameters for the sources determined by Hartnady (1996). 200

Table 8-3: Recurrence parameters for the sources determined by Partridge (1995). 201

Table 8-4: Recurrence parameters for the sources determined in this study. 201

Table 8-5: Coefficient of variation ranges for different spectral periods. 227

CHAPTER 1: INTRODUCTION

1.1. Introduction

Earthquakes are natural events with random characteristics, therefore their potential effects cannot be assessed accurately but can be estimated to some degree. The process of assessing the potential effects of earthquakes is called seismic hazard analysis (SHA). Seismic hazard analysis describes the potential for dangerous earthquake-related natural phenomena such as ground shaking, fault rupture, or soil liquifaction (Reiter, 1990; Beauvual, 2003). It is one of the important inputs to the analysis of seismic risk of an area. Research in seismic hazard began in the 19th century with a simple goal of distinguishing those areas that were more affected by earthquakes from those not affected (e.g. Ballore, 1896). For this purpose, it was sufficient to express seismic hazard in terms of earthquake-felt intensities since there was no desire to express hazard in a quantitative manner. Considering the time scales on which earthquakes occur, (large events may have recurrence intervals of several hundred years) a reliable quantitative evaluation of hazard could not usually be obtained from observational data alone (Musson, 2008; Calais et al., 2016).

The goals of seismic hazard analysis have since changed to quantify the distribution of future shaking that may occur at a site (McGuire, 1993; Abrahamson, 2006; Kılıç et al., 2006; Ansal and Biro, 2004; Bommer et al., 2015a). Therefore, SHA now requires the modelling of observed earthquakes to characterize the generation and propagation of potential future earthquakes. This requires a combination of several disciplines in order to derive and understand procedures and models used to describe location, magnitude, probability of future earthquake occurrences and the spatial distributions of their effects. However, the inclusion of more data might result in propagation of uncertainties especially if the data is not well understood. It is therefore pertinent to utilize more reliable datasets and add more information as it becomes available and more reliable. Therefore, seismic hazard estimation is now a dynamic work and which needs to be updated continuously (Petersen et al., 2014; 2015; Midzi et al., 2020).

According to Bender and Perkins (1993), SHA is associated with many uncertainties due to unknown or inaccurate information about the location and characteristics of seismic sources; the magnitude and recurrence times of earthquakes; the duration and characteristics of ground motion and the geological characteristics. While using probabilistic seismic hazard assessment (PSHA) in many seismic environments and for many purposes, researchers became aware that quantifying uncertainties in PSHA is of major importance in order to provide a good scientific basis to decision makers. For example, recurrence parameters have several uncertainties associated with them, attenuation

equations also have their own uncertainties and the hazard model also adding its own uncertainties (Crammer, 2001; 2002; Barani et al., 2007; Grünthal and Wahlström, 2001). In most cases, these data are known within a range of uncertainty (Kulkarni et al., 1984; McGuire, 1993; Bommer et al., 2005; Abrahamson, 2006).

The uncertainty of input data can be reduced by gathering more data. However, gathering more data can be expensive, time consuming and sometimes may prove not to reduce the uncertainty (Bayraktarli et al., 2011; Kowsari et al., 2017). In recent years, the increase in the availability of instrumental data as well as the advancement of technology has led to significant advances in seismic hazard studies (Hartzell et al., 1997; Balan et al., 2007; Chouinard and Rosset, 2007). However, despite the advanced technology and methodologies now available, it is still impossible to determine the exact seismic effect at a site. To overcome these problems, uncertainty and sensitivity analyses can be performed to estimate the rate of change in the output model with respect to changes in model input parameters. The product of sensitivity analyses highlights the effects of uncertainties on the hazard, allowing the input parameters to be ranked in importance (e.g. Cramer, 2002; Kowsari et al., 2017; Allen, 2020). Uncertainty analysis can be used to evaluate the variability in the outcome variable that is due to the uncertainty in the estimation of the input values (Iman and Helton, 1988). Sensitivity analyses for PSHA studies are useful for evaluating the impact of these uncertainties on the study results as well as give an idea on which uncertainties should be reduced through future studies, and to public or private users for better understanding when using a particular seismic hazard estimate.

The uncertainty in the selection of different models and in the selection of the parameter values of each model is crucial in seismic hazard assessments (Budnitz et al., 1997; Cramer et al., 1996; Rabinowitz et al., 1998; Cramer 2002; Beauval and Scotti, 2004; Barani et al., 2007; Rohmer et al., 2014; Crowley et al., 2015; Kowsari et al., 2017). The logic tree scheme allows one to consider and to quantify the uncertainty in the probability of exceeding a given ground motion. On the other hand, it requires a long computation time due to several branches that might sometimes be unnecessary because they have modest influence on the hazard (Cramer, 2001; 2002; Kowsari et al., 2017). Thus, the identification of input parameters with the highest impact on the hazard and its uncertainty may help in reducing both the calculation time and above all, the time and effort usually required to determine these values as well as how to assign probabilities (Rabinowitz et al., 1998). In other words, sensitivity analysis provides knowledge on how the uncertainty in the output can be allocated to different sources of uncertainty in the model input parameters (Saltelli et al., 2000). This is important, particularly at the early stage of a PSHA where essential modelling decisions have to be made. The

product of sensitivity analyses highlights the most and least important input parameters that influence the hazard.

In this study, sensitivity analysis is used to quantify the relationship between the input parameters and the output distribution. The effects of different sources of uncertainties involved in PSHA methodology on the results are investigated for a number of sites with different source distances. This procedure is useful for evaluating the impact of these uncertainties on the outputs, help identify those uncertainties that can be reduced through the collection of additional data, and provide public or private users with a better understanding of the usefulness of a particular seismic hazard estimate. The probabilistic seismic hazard assessment of Johannesburg was used as the case study to examine the influence of different assumptions on the results based on real data.

For a city like Johannesburg, which has a high population growth and is the hub of the economic activities of the country, a seismic hazard assessment is important. Of late, the city has been hit by a number of moderately sized earthquakes (Midzi et al., 2015a; Midzi et al., 2015b; Durheim et al., 2006). With the recent occurrence of the M_L6.5, 4 April 2017 Botswana and M_L 5.5 5 August 2014 Orkney earthquakes, which rattled the entire city, questions have been raised concerning the preparedness of the city to a large event. The southern part of the city sits on top of mines, most of them already mined out and flooded, which further increase the seismic risk in the area. The closure and flooding of mines in the Central Rand Region has posed a twin threat to the Metropolis of Johannesburg. The first threat is the danger of rising water level in the closed mines and possible contamination of shallow ground water reservoirs beneath the city if the rising water levels are not properly controlled. The second threat is triggered seismicity in the region of Central Rand, which might generate large ground motions.

1.2. Research objectives

The aim of this study is to assess the sensitivity of the parameters that are used in the seismic hazard analysis for the Johannesburg metropolitan municipality and their effect on the output. This is intended to be achieved through the following steps:

- Assessing and modelling the uncertainties in the seismic catalogue and earthquake recurrence parameters.
- Determining the uncertainties in the use of ground motion prediction equations for seismic hazard analysis.
- Establishing uncertainties in seismotectonic sources characterized for the Seismic Hazard Analysis.

- Establishing a methodology for conducting a sensitivity analysis for the parameters and seismic hazard assessment models.
- Identifying the most important parameters that affect the uncertainties in the seismic hazard analysis for the Johannesburg area.

The outputs of this research project should help future researchers and practitioners to gather data that will improve the estimation of seismic hazard, and avoid gathering data that will not significantly alter the hazard predictions. Thus, unnecessary expenditures of effort would be avoided.

1.3. Organisation of the dissertation

After the introduction to the problem and objectives in Chapter 1, the dissertation describes in Chapter 2 the current understanding and treatment of uncertainties in seismic hazard assessment, followed by a description of the seismic hazard assessment methodologies. This description encompasses the analysis of the uncertainties associated with the seismic hazard assessments as well as the sensitivity analysis. Chapter 3 presents the geological framework for the area around Johannesburg. Chapter 4 covers the compilation and processing of the seismic catalogue for the area together with its associated uncertainties. The seismotectonic model for Johannesburg is developed from analysis of previous models and current datasets in Chapter 5. Chapter 6 computes the recurrence parameters for the delineated seismic source zones while chapter 7 looks at the selection process for the ground motion prediction equations to be used in the hazard computations. In all these steps, uncertainties will be analysed and quantified for use in the sensitivity analysis. Chapter 8 presents the sensitivity analysis methodology for seismic hazard assessment for Johannesburg. Finally, in Chapter 9 the concluding summaries and reccommendations will be presented in this chapter.

CHAPTER 2: LITERATURE REVIEW: SEISMIC HAZARD ANALYSIS AND UNCERTAINTIES ASSOCIATED WITH THE PROBABILISTIC SEISMIC HAZARD ANAMYSIS METHOD

2.1. Introduction

Earthquakes are natural events that pose huge threats to humans, therefore their potential effects should be thoroughly assessed. The process of assessing the potential effects of earthquakes is called seismic hazard analysis (SHA; McGuire, 1993; Ansal et al., 2004). SHA maps help to mitigate earthquake losses by expressing the likely severity of ground shaking in a form that can be used to reduce the risk and improve public safety, for example in the development of seismic building codes.

Research in seismic hazard began in the 19th century with a simple goal of distinguishing areas that were most affected by earthquakes from those that were relatively undisturbed (e.g. Montessus de Ballore, 1896). For this purpose, it was sufficient to express seismic hazard in terms of felt intensities of ground shaking since there was no desire to express hazard in a quantitative manner. Considering the time scales on which earthquakes occur (large events may have recurrence intervals of several hundred years), a reliable quantitative evaluation of hazard could not be obtained from observational data alone (Musson and Sargent, 2007). Consequently, the goals of SHA have since changed from qualitative description to quantitative assessment of the likely future ground shaking an earthquake engineers use to ensure that structures can withstand given levels of ground shaking while maintaining desired levels of performance (McGuire, 1993; Ansal et al., 2004; Abrahamson, 2006; Kılıç et al., 2006; Bommer et al., 2015a).

SHA is now a multi-disciplinary process that integrates the understanding of earthquakes produced by several disciplines namely geology, geophysics, geotectonics, seismology, earthquake and structural engineering, geodesy, physics, mathematics and statistics. It involves the modeling of observed earthquakes and the characterization of potential future earthquakes, the processes that govern their generation and the propagation of their effects on the earth surface (Reiter, 1990; Baker, 2008; Ares and Fatehi, 2013). Studies carried out in these disciplines led to the development of procedures followed and models used to describe location, magnitude and probability of future earthquake occurrences, as well as the spatial distributions of their effects. Therefore, SHA has become dynamic process, which should be updated constantly (Frankel et al., 1996; Petersen et al., 2008, 2015a; 2015b; 2018; Ares and Fatehi, 2013; Allen et al., 2018; Midzi et al., 2020).

According to Bender and Perkins (1993), the SHA process is associated with many uncertainties due to unknown or inaccurate information about the location and characteristics of seismic sources, the

magnitude and recurrence times of earthquakes, the duration and characteristics of ground motion and the geological characteristics. In most cases these data are known within a range of uncertainty (Kulkarni et al., 1984; McGuire, 1993; Bommer et al., 2005; Abrahamson, 2006). To reduce some of these uncertainties, more data can be collected. However, these data can be very expensive and time consuming to collect, and sometimes may actually prove not to reduce the uncertainty (Bayraktarli et al., 2011). In recent years, the increased availability of instrumental data as well as the advancement of technology has led to significant advances in seismic hazard studies (Bala et al., 2007; Chouinard and Rosset, 2007; Pagani et al., 2010; Bommer and Strasser, 2011; Kijko, 2012; Hartzell et al., 2013; Budnitz et al., 1997a; 1997b). However, despite the advanced technology and methodologies now available, it is still impossible to determine the exact seismic effect at a site at a particular time. There are widespread misunderstandings regarding the scope of the probabilistic approach, misleading terminology, and lack of representative data to characterize seismic sources and/or seismogenic zones and soil profiles at the site (Bommer, 2003; Krinitzsky, 2002; Klügel, 2008). These may lead to unrepresentative hazard assessments, poor interpretation and improper decision making (Abrahamson and Bommer, 2005; Bommer et al., 2005).

To overcome these problems, uncertainty and sensitivity analyses are performed to estimate the rate of change in the output model with respect to changes in model input parameters (Rabinowitz and Steinberg, 1991; Cramer et al., 1996; Sabetta et al., 2005; Kowsari et al., 2017). It is essential to carry out sensitivity studies to understand the influence of the uncertainties associated with input parameters and how they can be modelled to be included in SHA. For example, in as much as we want to model and characterize the geology surrounding Johannesburg, it has to be known that its complexity is a major source of uncertainty (e.g. Stewart et al., 2004). Thus, uncertainty in such hazard calculations are expected to be especially high and a good control over them is a necessity for the successful use and interpretation of the hazard results. Some researchers have suggested the calculation of seismic hazard without using source zones, especially for low seismicity regions like South Africa, to avoid uncertainties associated with source zoning (Bender and Perkins, 1993; Kijko and Graham, 1998; Woo, 1996). However, such methods are also affected by uncertainties associated with the location, size and occurrence of earthquakes (e.g. Manzunzu et al., 2019; Midzi et al., 2020a).

There are two basic approaches for SHA, namely, deterministic and probabilistic (Reiter, 1990; McGuire, 2004). According to Bulajic and Manic (2006), the basic input data that must be collected are practically the same for both approaches. The data would include all past earthquakes within an area of several hundred kilometers radius around the site of interest, the seismotectonic and geological features of the region, as well as the local soil conditions for different sites and the ground attenuation characteristics. In practice, the two methodologies have strength and weaknesses as well as

proponents and opponents (Bommer 2002; 2003; Krinitzsky, 1995a; 2002; 2003; Musson, 2000; Klugel, 2008; Vermeulen, 2020). The choice of one approach or the other is based on the specific goals and objectives of the particular project, while also taking the quality of the available data into account. Some authors have sought to combine the two methods with schemes that describe the relative contribution of each methodology according to application and utilize the best of each method (McGuire, 2001; Krinitzsky, 2003; Bommer, 2002).

2.2. Deterministic Seismic Hazard Analysis (DSHA)

In the deterministic seismic hazard assessment (DSHA) approach, one or more controlling earthquakes are developed. These earthquakes will produce the largest ground motion at the site. Based on the magnitude, distance and site characteristics, the ground motion at the site is predicted for each controlling earthquake. The basic principle of the DSHA approach is to try to identify the nearest active fault to a particular site and calculate the largest earthquake that could possibly occur on that fault (Kramer, 1996; McGuire, 2001; Bulajic and Manic, 2006). This fault is then used to calculate the largest possible ground shaking at the site. While this method is attractively simple even today (e.g. Krinitzsky, 1995a; Winter et al., 1994; Bulajic and Manic, 2006; Wang and Huang, 2014), its main problem is that dangerous faults can easily go unidentified until an earthquake actually occurs on them, as was the case with the Mozambique earthquake of 2006 (Fenton and Bommer, 2006) and the Botswana earthquake of 2017 (Midzi et al., 2018; Mulabisana, 2021). DSHA implementation is not yet standardized currently and this analysis can therefore vary in different parts of the world (e.g. Peresan et al., 2011; Nekrasova et al., 2014; Panza et al., 2014; Wang and Huang, 2014; Gupta, 2002). However, the general procedure followed is a four-step process described below and illustrated in Figure 2-1.

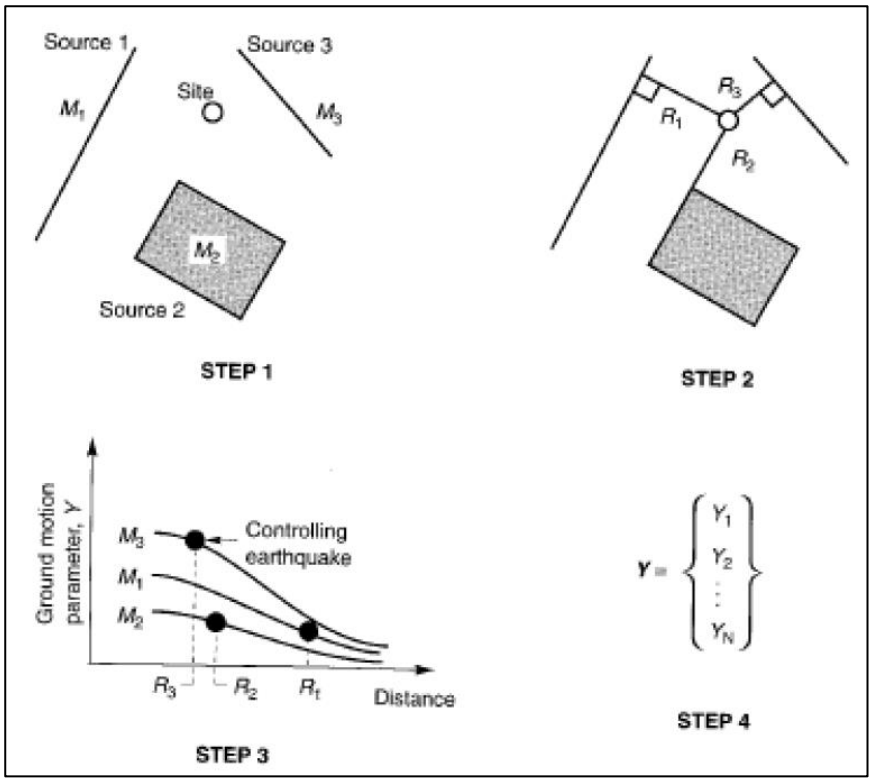


Figure 2-1: The four-step process of a deterministic seismic hazard assessment process (Reiter, 1990).

Firstly, earthquake sources are identified and characterized. Here all earthquake sources that can produce a certain ground motion at a site of interest are identified and characterized by their geometry and potential (Reiter, 1990; Wang and Huang, 2014). Secondly, the appropriate source-site distance is selected. This is the shortest distance from each source to the site. The type of distance might be hypocentral or epicentral distance depending on the distance measure in the GMPEs that are used in the calculation. Thirdly, a decision is made on the appropriate controlling earthquake. The earthquake that is likely to produce the expected strongest shaking at the site is selected. The selection is made by comparing the levels of shaking produced by earthquakes assumed then to occur at the distances identified in step 2. The controlling earthquake is portrayed by its size and its distance from the site. Lastly, ground motions expected to be produced at the site by the controlling earthquake are estimated. Typically, its characteristics are usually described by one or more ground motion parameters obtained from a ground motion prediction equation.

Several modifications to try and improve the performance of the DSHA have been proposed by some researchers (Krinitzsky, 1993; 2003, Amponsah et al., 2009; Huang et al., 2012; Panza et al., 2014; Magrin et al., 2016, 2017). The modifications take account of the inclusion of non-controlling sources (Huang et al., 2012), use of waveform modelling (Panza, 2017) as well as considering the return period for each source contributing to the hazard. The use of waveform modelling have given rise to the neo-deterministic seismic hazard approach which allows for time dependent earthquake scenarios (Amponsah et al., 2009; Nekrasova et al., 2011; Zuccolo et al., 2011; Panza et al., 2014; Panza,

2017). The major advantage of this method is it does not rely on the GMPEs but rather utilizes waveform simulations.

Generally DSHA approach is used in regional studies since it requires less data, computational effort and time (Krinitzsky, 1995b; 2003). However, this approach have a weakness in that it does not take into account for the aleotoric uncertainties involved in the temporal, spatial and magnitude-wise distribution of earthquakes as well as in epistemic uncertainties in each step of the SHA (Kijko, 2011; Wang and Huang, 2014; Panza et al., 2003). Ground motion prediction equations (GMPEs) have also been identified as a major source of uncertainty in DSHA (Amponsah et al., 2009; Atik and Youngs, 2014; Panza et al., 2014). The GMPEs selected for DSHA calculations need to represent the worst case ground motion associated with the selected earthquake however, most empirically derived GMPEs represent the mean with the recorded ground motion showing large scatter around those mean (Atkinson and Boore, 2006; Akkar and Bommer, 2007; Douglas, 2011, 2018). Due to these uncertainties, DSHA may not always guarantee the intended worst-case scenario. Furthermore, selecting the most pessimistic scenario in DSHA is not likely to represent the reality and it is not a good engineering decision (Budnitz et al., 1997b; Abrahamson, 2000; Gupta, 2002; Huang et al., 2012).

2.3. Probabilistic Seismic Hazard Analysis (PSHA)

In contrast to DSHA, in which seismic hazard is based on a single earthquake scenario, PSHA integrates the effects of all future earthquakes of all possible magnitudes, at all significant distances from the site. The PSHA procedure also accounts for the random nature of earthquake occurrences with respect to space and time as well as the uncertainty in attenuation of ground motion and in other input parameters. However, as noted before, there are widespread misunderstandings regarding the scope of the probabilistic approach as well as lack of representative data to characterize seismic sources zones and soil profiles at the site which might lead to unrepresentative hazard assessments, poor interpretation and improper decision making (Castanos and Lomnitz, 2002; Abrahamson and Bommer, 2005; Bommer et al., 2005; Smit, 2019). Several authors around the world developed PSHA methodologies almost simultaneously. Of note is the work of Cornell (1968) together with Esteva (1967; 1968; 1969) who developed the underlying concept which is being widely used now (McGuire, 2008). During the same period, an alternative technique was developed by Milne and Davenport (1969) which is purely based on instrumental seismicity and historical observations of earthquakes of the area. Molchan et al. (1970) developed another extremely powerful technique but it has remained virtually unknown because of its complexity. The Cornell procedure is straightforward, easy to understand, and implement hence, it is more popular than others (McGuire, 1976; 1978). A

non-parametric method based solely on the seismic catalogue was proposed by Veneziano et al. (1984). Kijko and Graham (1998; 1999) later modified this methodology to a parametric-historic method which combines features of both the Cornell (1968) and Veneziano et al. (1984) procedures. Their methodology requires the definition of area specific seismic parameters (i.e. mean seismic activity rate λ, the Gutenberg-Richter parameter b, and the maximum regional magnitude M_{max}), while estimating the normalized empirical distribution of the seismic hazard using the value of magnitude, distance and assumed GMPE for the duration of the seismic catalogue to obtain an annual rate of exceedance of the hazard parameter.

Another approach of PSHA is represented by the procedures based on the Monte Carlo simulations of long-term seismic catalogues (Ebel and Kafka, 1999; Musson, 2000; Shumilina et al., 2000; Assatourians and Atkinson, 2013). This method utilizes the Monte Carlo approach to simulate a number of pseudo synthetic earthquake catalogues by resampling the observed catalogue. The seismic hazard is then calculated from the estimations of the ground motion at a given site or set of sites due to the various earthquakes in the synthetic catalogues.

In the PSHA methodology, the occurrence of earthquakes in time is assumed to be independent and follow the memoryless Poisson distribution (Reiter, 1990). In addition, randomness in the size and location of future earthquakes is also assumed and the frequency-magnitude distribution of future earthquakes is assumed to follow a power law. Such an approach is obviously correct if the catalogue is purely natural and independent events are dominant (McGuire, 2008; Vermeulen, 2020). Nevertheless, there are some regions with low or moderate tectonic seismic activity like South Africa, where contribution of induced earthquakes may be comparable to natural events or even prevail. An estimation of seismic hazard due to induced sources for such regions is as important as that due to natural ones as they can also result in damage and deaths (e.g. Durrheim et al., 2006; Midzi et al., 2015; Bommer et al., 2015b). In principle, calculation of the seismic hazard from induced earthquakes is fundamentally different from that of tectonic earthquakes because the seismic rates of induced earthquakes are not stationary and difficult to model. In addressing issues of induced seismicity, other researchers have calculated hazard maps based on an annual rate of exceedance rather than the 50-year return periods calculated for natural seismicity (Petersen et al., 2015b; 2018; van Elk et al., 2017; Schlittenhardt et al., 2014) while others prefer to identify and remove suspected induced seismicity (Petersen et al., 2015a).

2.3.1. Basic steps in PSHA

The basic steps of PSHA are schematically shown in Figure 2-2. They are similar to DSHA but have a few major differences. First, like DSHA, seismic sources that affect the site of interest are defined.

Then, for each seismic source, the magnitude recurrence relationship, which gives the relative frequency of different earthquake magnitudes, is defined (Reiter, 1990; McGuire, 2001; Baker, 2008; Salazar, 2018). This step of PSHA is fundamentally different from that of DSHA. While in DSHA, only the maximum magnitude earthquake is determined for each seismic source, only this earthquake is considered in the analysis, in PSHA, a probability distribution is determined for earthquakes of a range of magnitudes, and the maximum magnitude is the upper bound of all earthquake magnitudes that will be used in the analysis for each source. Therefore, randomness in earthquake occurrences with respect to magnitude and time is considered in this step. In the third step, similar to DSHA, attenuation relationships are selected to predict the effects of all earthquakes determined in the previous step. At the last step, the effects of all earthquakes, which have different magnitudes and occur at different locations in different seismic sources are combined and displayed in the form of a curve that shows the probability of exceeding different levels of the selected ground motion parameter.

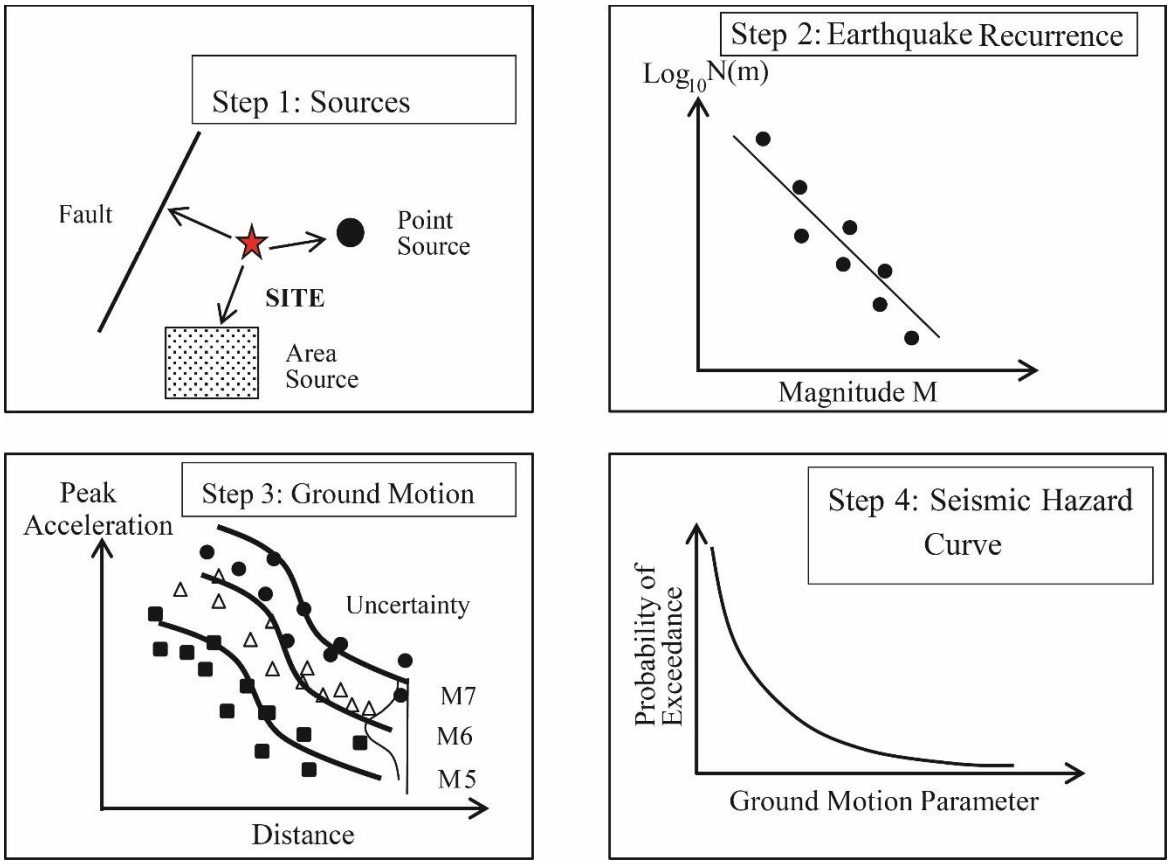


Figure 2-2: The four steps in Probabilistic Seismic Hazard Analysis (modified from Reiter, 1990).

2.3.2. Step 1: Seismic Sources

The first step in PSHA analysis is the determination of the spatial distribution of potential seismic sources of future earthquakes located close enough to the site of interest. In PSHA, a seismic source zone is defined as a geologic feature or group of features with similar style of deformation and tectonic process, where it is possible to infer relationships between the deformation and the seismicity (Estrada, 2012). In this zone, the value of seismicity characteristics; i.e. annual earthquake occurrence rate, b-value and maximum earthquake magnitude value, are considered the same throughout (Reiter, 1990). Geological maps, trenches, seismological data, geophysical data and digital elevation models (DEM), aid in the determination of seismic sources (Figure 2-3).

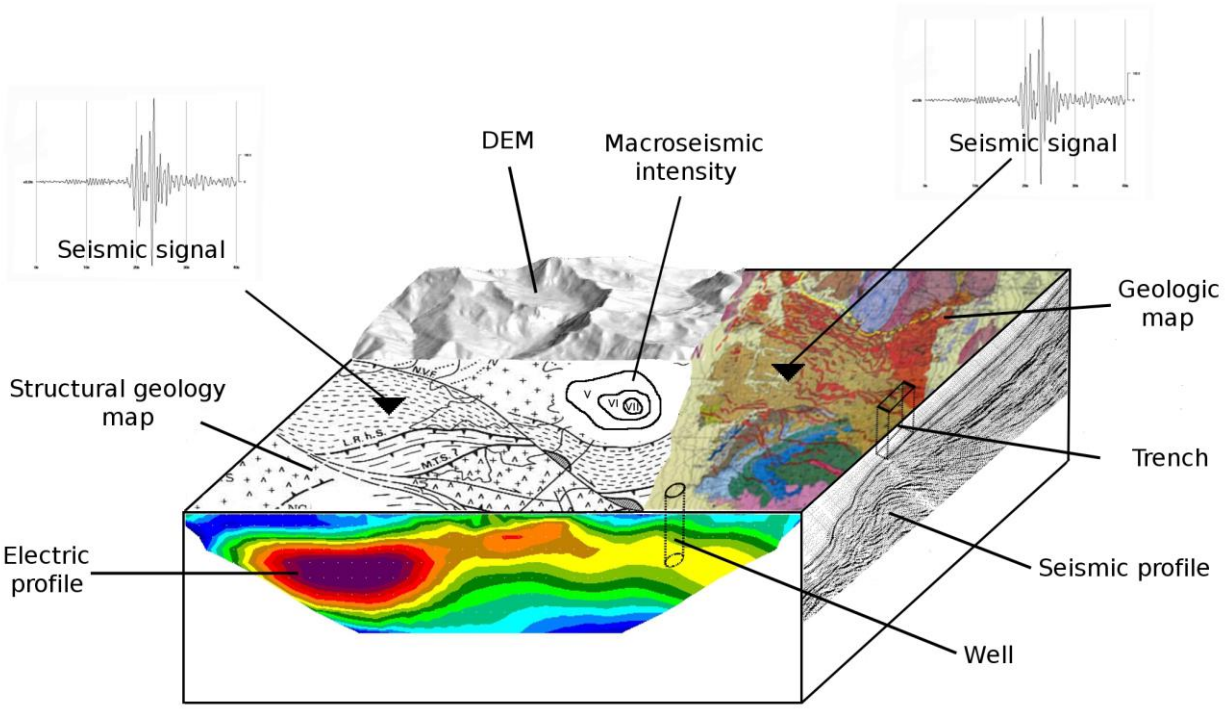


Figure 2-3: 3D diagram representing some useful data for used in delineating seismic source zones(Le Goff and Fitzenz, 2012).

The definition and delimitation of seismogenic zones is based on spatial distribution of epicentres of earthquake catalogues, as well as on available geological, geodetic and paleoseismic evidence related to earthquake activity. Three types of seismic source models are generally described in SHA namely, point, linear (fault model) and areal (area source zone model). Among them, the point source model is the simplest case, which represents epicentres of past earthquakes that are clustered in a relatively small area and are so far away from the site that they can be assumed to emanate from a point in space (Reiter, 1990; Estada, 2012). Therefore, in point source model, there is no randomness with regard to the location of earthquakes. Linear source models are used to model the 2D map view representation of well-defined active faults (Thenhaus and Campbell, 2003; Le Goff and Fitzenz, 2012). It assumes that earthquakes occur with equal probability anywhere along the entire length of the line source.

Therefore, line sources are divided into small segments and each segment is treated as a point source in PSHA calculations. Areal sources are used to model regions that do not have well-mapped faults that are generating earthquakes, but rather an area with uniform diffuse seismic occurrence (Terrier et al., 2000; Le Goff et al., 2010; Le Goff and Fitzenz, 2012). Similar to fault sources, earthquakes are assumed to occur with equal probability anywhere within the areal source and that earthquake locations are uniformly distributed over the area. However, the uniform distribution of epicentres within a source area can be a poor approximation of the actual spatial distribution (Molina et al., 2001; Kijko, 2011; Spada et al., 2011).

In most parts of the world, tectonic provinces as well as active faults are not well mapped and the causes of seismicity are not understood. Therefore the delineation of seismic sources is difficult, subjective and introduces uncertainties in seismic hazard calculations (Reiter, 1990; Budnitz et al., 1997a; Manzunzu et al., 2019; Coopersmith et al., 2009). Even renowned experts rarely agree on the boundaries of source zones for the same region (McGuire, 1993; Frankel et al., 1996; Budnitz et al., 1997b; Giner et al., 2002; Coopersmith et al., 2009) . The specification of different source zones for the same area will most often result in a hazard assessment that is significantly different for that area. In addition, often, seismicity within the seismic sources is not distributed uniformly as assumed (Kijko, 2011).

The difficulties associated with the identification and delineation of seismic source zones as required in the Cornell (1968) procedure have led to the development of alternative PSHA techniques. Methods based on earthquake catalogues (e.g. Milne and Davenport, 1969; Veneziano et al., 1984) are free from subjective decisions on the delineation of seismic sources. However, one significant drawback of these methods is the inability to take into account the stochastic variability of earthquake locations. To overcome this drawback various smoothing techniques have been proposed (Frankel, 1995; Woo, 1996).

2.3.3. Step 2: Modelling of Earthquake Occurrences

Since earthquakes are random events, stochastic models are applied to predict the probability of future earthquake occurrences. In the classical PSHA model, earthquake occurrences are assumed to be independent events both in time and space and modeled as a homogeneous Poisson process (Cornell, 1968; Cornell and Winterstein, 1988; Bommer et al., 2015a). The homogeneous Poisson process is a memoryless stochastic process, which means that the occurrence of an event in any time interval is independent of the occurrence of any previous events (Cornell, 1968). According to the Poisson model, the probability that "n" number of earthquakes having magnitude greater than "m_0" occurring in a time interval, Δt, is;

$$P(N = n, \Delta t) = \frac{\lambda^n}{n!} e^{-\lambda} \quad \text{2-1}$$

where λ is the activity rate. The probability that at least one earthquake occurs in a seismic source within the time interval, Δt, is given as follows;

$$Pr(N \geq 1) = 1 - e^{-\lambda t} \quad \text{2-2}$$

Various alternatives to the homogeneous Poisson model have been considered. For instance, Patwardhan et al. (1980) suggested using a semi-Markov model, where the earthquake occurrence depends only on the previous earthquake. Its disadvantage is that large datasets are required for modelling the recurrence parameters (Anagnos and Kiremidjian, 1988). Shimazaki and Nakata (1980) suggested a time-dependent model that allows the prediction of the time of the next event by assuming the occurrence of an earthquake when a certain level of stress is accumulated. However, stress measurements are very few and difficult to obtain for earthquake prediction. Another model that assumes that each seismic event that occurs in a restricted space-time volume increases the conditional occurrence rate within the volume was proposed by Musmeci and Vere-Jones (1992). Other time-dependent models focus on the statistical modelling of the inter-occurrence times. Other distributions have been used to fit the observed earthquake inter-occurrence times, e.g. the gamma distribution (Udias and Rice, 1975), log-normal distribution (Nishenko and Buland, 1987; Goes, 1996), Weibull distribution (Parvez and Ram, 1997; Yakovlev et al., 2006; Zoller and Hainzl, 2007), the Brownian passage time distribution (Matthews et al., 2002), and the Bayesian combination of the latter three models (Fitzenz and Nyst, 2015).

However, comparative studies aiming to measure the differences between the hazard assessments obtained using the homogeneous Poisson process model and various time-dependent models concluded that, with rare exceptions, these differences were not significant enough to provide a basis for discarding the standard approach (Cornell and Winterstein, 1988; Cramer et al., 2000). Recent studies have shown an increase in hazard of more than 10% caused by the inclusion of dependent events (Boyd, 2012; Iervolino et al., 2014).

2.3.3.1. Magnitude Recurrence Relationship

The recurrence of earthquakes of different magnitudes is an important characteristic of a source zone. The frequency magnitude distribution (FMD), which was discovered simultaneously by Ishimoto and Iida (1939) and Gutenberg and Richter (1944), is the most widely used distribution in seismic hazard studies. It is usually referred to as the Gutenberg and Richter (GR) recurrence law and it specifies the relation between the frequency of occurrence of earthquake and their magnitudes.

$$\log_{10} N(M) = a - bM \qquad 2\text{-}3$$

where N(M) is the number of earthquakes with magnitude equal to or greater than M, a is the level of seismic activity and b describes the ratio between the number of small to large earthquakes. The b value is typically 1.0 for seismically active regions, but varies within the range 0.5 to 1.5 depending on the tectonic environment under consideration (Scholz, 1968). High b-values indicate complex and stressed regions (Enescu et al., 2011; Manzunzu et al., 2017). In its original formulation, the GR law has no upper bound and predicts unlimited earthquake magnitudes. However, the physical requirements of finite energy release (Knopoff and Kagan, 1977), or, equivalently, a finite rate of seismic moment release (Anderson, 1979; Molnar, 1979), imposes restrictions on the FMD. Therefore, the range of magnitudes for which the linear relation (2.3) holds, is bounded from both sides.

The G-R law generally holds for small and moderate magnitudes, but underestimates the frequency of occurrence of certain large earthquakes. Hence particular attention has been devoted to modelling the recurrence of large earthquakes, as these events dominate the seismic hazard at large return periods (Kijko, 2011). These earthquakes are known as characteristic earthquakes, and are described by the characteristic earthquake model, usually derived from paleoseismic observations (Youngs and Coopersmith, 1985; Schwartz and Coppersmith, 1984; Wesnousky, 1994). This model basically suggests that if a fault begins to rupture in a large earthquake, it will tend to rupture the entire fault segment releasing all the seismic energy stored in the fault resulting in a characteristic size of earthquake. This model is appropriate in many cases. Alternative models are based on a combination of the truncated exponential model and the characteristic model. These composite models include a characteristic earthquake distribution for the large magnitude earthquakes and an exponential distribution for the smaller magnitude earthquakes (Figure 2-4). One such composite model is the Youngs and Coppersmith (1985) characteristic model.

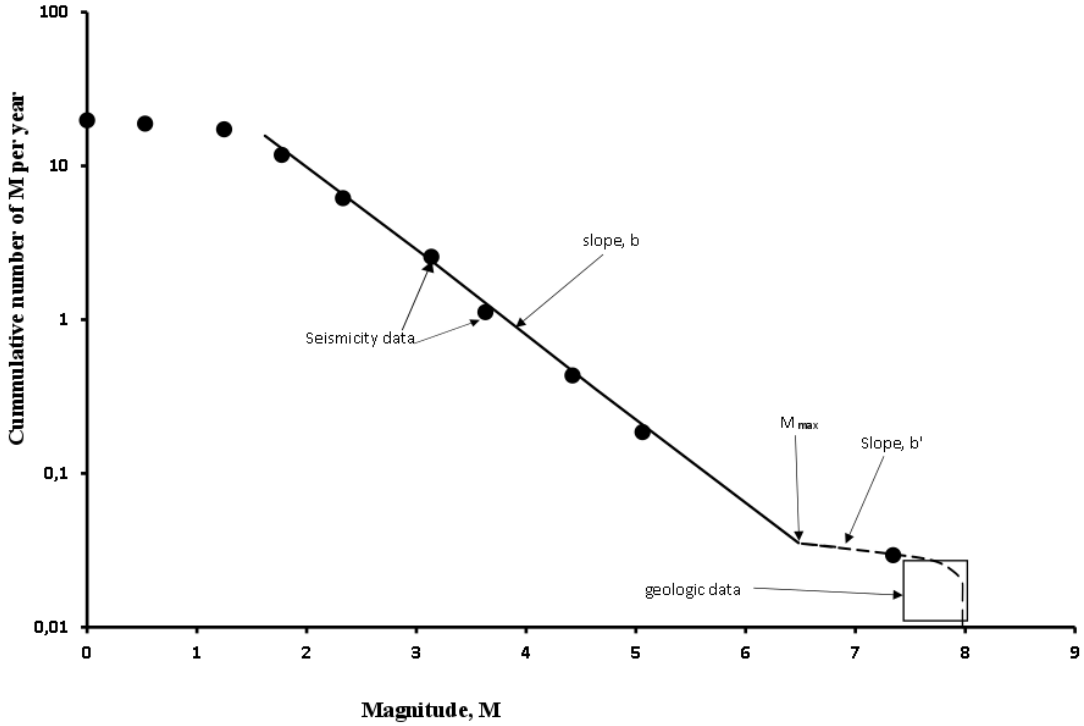


Figure 2-4: Characteristic earthquake model (modified from Youngs and Coppersmith, 1985).

Although the GR law can describe natural seismicity reasonably well and can be applied to various tectonic regimes and large space volumes, it may fail in some instances. Bimodal and other non-linear FMDs have been applied to capture possible deviations from linearity, especially when populations of events with different properties are combined in the same sample (Figure 2-5; Sen, 2012; Main, 2000; Wiemer and Wyss, 2000). Instances that are more complicated can be observed in mining areas, where the FMD can be significantly nonlinear (Ryderand Jager, 2002; Gibowicz and Kijko, 1994; Kijko et al., 2012). Merz and Cornell (1973) used a function with a quadratic magnitude term for seismic risk calculations, whilst Lomnitz-Adler and Lomnitz (1979) modified the GR law to capture the curvature at the higher magnitude end. In seismic hazard analysis, the most common used FMD is the truncated GR recurrence law (Petersen et al., 2014; Pagani et al., 2020; Modzi et al., 2020).

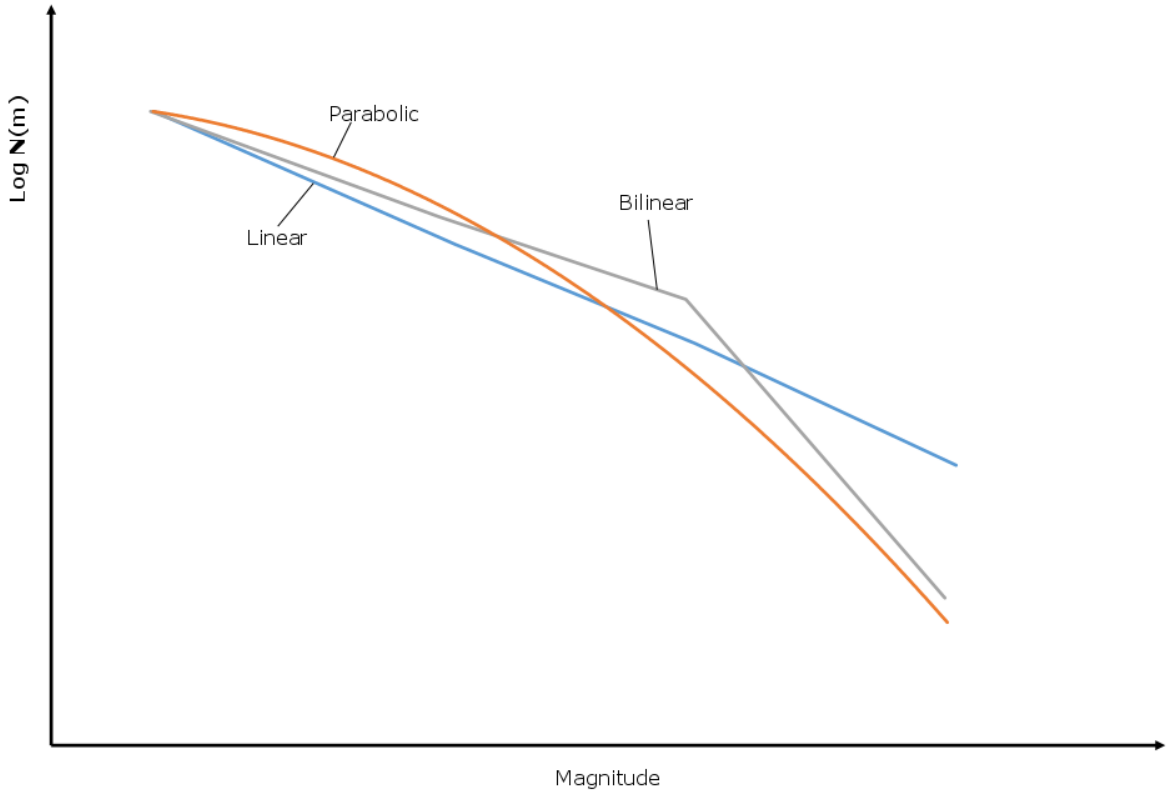


Figure 2-5: Linear, Bilinear and Parabolic recurrence relationships.

2.3.3.2 Estimation of maximum magnitude (M_{max})

The estimation of M_{max} is crucial for seismic hazard analysis because large earthquakes produce the most severe ground motions and dominate the hazard at longer return periods. This is the most difficult parameter to assess for regions of sparse seismicity and short earthquake records such as South Africa but it is a critical parameter in seismic hazard analysis particularly when considering long return periods. At present, there is no generally accepted method for estimating the value of M_{max} (Kijko and Singh, 2011; Singh, 2012). Several methods have been applied in the estimation of M_{max}. More physically based estimates are made using functions that relate magnitude to rupture length (for faults), or to the length of tectonic features (for area sources). In addition, M_{max} can also be constrained by considering geological and tectonic analogues based on ergodicity that is comparing information between the study region and tectonically similar regions (McGuire, 1993; Havskov and Ottemöller, 1999; Holschneider et al., 2011; Bommer et al., 2015a). If the above information is not available, it is obtained by adding an increment value to the maximum observed magnitude with the increment varying from zero (which corresponds to the lower bound estimate of M_{max}) up to one (McGuire, 1993; Wheeler, 2009).

In an area like South Africa, M_{max} is a particularly contentious issue, since there is little to go on. In any low seismicity area, the length of the seismic cycle is such that it is quite likely that the historical time window may not capture the largest possible event (Calais et al., 2016). In addition, considering intraplate seismicity from a global perspective, there are many instances of strong ($M_W > 7$) events occurring in virtually aseismic areas (Johnston, 1994; Calais et al., 2016; Li et al., 2016). Nevertheless, there may still be restrictions on what is likely to occur in South Africa. The available methods for estimating M_{max} are classified as either deterministic or probabilistic.

Deterministic methods: Methods of this category are based on empirical relationships between the magnitude and some physical dimension of the ruptured fault (Kanamori and Anderson, 1975; Leonard, 2010). Seismic moment is proportional to fault rupture area, it appears that magnitude should be more fundamentally related to fault rupture area than fault rupture length (Hanks and Bakun, 2008). The relationships in terms of fault rupture area demonstrate smaller variations compared with the relations of fault rupture length (Wells and Coppersmith, 1994; Hanks and Bakun, 2008; Yen and Ma, 2011). However, due to the complexity in the calculation of rupture area and the determination of the kinematic models for the rupture, models using rupture length are commonly used in the determination of M_{max} (Wald, 2008; Wesnousky, 2008). Several authors have proposed a general correlation between the magnitude and fault length (e.g. Table 2-1; Tocher, 1958; Mark, 1977; Anerson et al., 1996; Wells and Coppersmith, 1994; Wesnousky, 2008). It has to be taken into account that the results of the deterministic estimation of M_{max} are generally associated with significant uncertainties that could be as high as one unit on the magnitude scale (Kijko, 2004).

Table 2-1: Typical empirical relations between magnitude and some physical parameter of rupture faults. Mw refers to the moment magnitude, L is the rupture length, A is rupture area, S is the slip rate.

Tectonic region	**Regression equation**	**Units**	**Type of faulting**	**Reference for regression and comments**
Plate boundary and crustal regions	M_w = log A + 3.98 ± 0.03: For A≤ 537 km^2 M_w = 4/3log A + 3.07 ± 0.04: For A>537 km^2	Area (km^2)	Strike slip	Hanks and Bakun (2008)
	M_w = 3.99 + log A	Area (km^2)	Strike slip	Leonard (2010)
	M_w = 5.56 + 0.87 log L	Surface rupture (km)	Strike slip	Wesnousky (2008)

	M_w = 6.12 +0.47 log L	Surface rupture (km)	Normal	Wesnousky (2008)
	Log A_e = 13.79 + 0.87 log M_0	Effective area	Strike slip; Dip slip	Yen and Ma (2011)
Stable continental regions	Mw = 5.12 + 1.16 log L – 0.20 log S	Surface rupture (km); Slip rate (mm/yr)	Reverse slip; Strike slip	Anderson et al. (1996)
	Log M_0 = 3.65 log L + 21.0	Subsurface fault length (km)	Reverse slip	Nuttli (1983)
	M_w = 1.36 log L + 4.67	Subsurface rupture length (km)	Strike slip	Johnston (1994)
	M_w = 3.98 + 1.02 log A	Rupture area (km^2)	Strike slip	Wells and Coopersmith (1994)
	M_w = log A + 3.82 (±0.02) For A ≤ 251km^2 M_W = 1.33 log A + 3.07 (±0.04) For A > 251km^2	Rupture area (km^2)		Konstantinou (2014)

Probabilistic methods: M_{max} is commonly estimated by extrapolating the FMD derived from the available seismic data to some large recurrence interval, for example, 500 or 1000 years. This method of fitting a distribution to the maxima of earthquake magnitudes have the advantage that no small magnitude data are required, the main drawback of these methods is that the available data are generally incomplete, even for the maxima of magnitudes, in the pre-instrumental period and even in the recent periods of instrumental recordings. Kijko and Singh (2011) gave an overview of different statistical methods of calculating M_{max}, assessing each method's applicability. Various probabilistic methods have been developed for estimating M_{max} (Epstein and Lomnitz, 1966; Karnik and Schenkov, 1974; Yegulalp and Kuo; 1974; Schenkov and Schenk, 1975; Lomnitz-Alder and Lomnitz, 1979; Kijko and Sellevoll, 1987; Kijko, 2012). Among the first, were those based on the extreme value theory. A study by Epstein and Lomnitz (1966) proved that the Type I extreme value distribution for the largest magnitudes could be derived directly from the assumptions usually made in PSHA that the sequence of main seismic events is a Poisson process and that the GR law is satisfied. An estimator of M_{max} can be written in a generic form:

$$M_{max} = M_{max}^{obs} + \Delta \qquad 2\text{-}4$$

where Δ is a positive incremental factor.

Several authors have spent a lot of effort modelling the incremental factor Δ by using the earthquake catalogue within a seismic source to estimate the M_{max} (Kijko and Singh, 2011; Woessner and Giardini, 2012). The methodology makes provision for the earthquake catalogue to containing pre-historic, historic and instrumental seismicity as described in Kijko (2012). The choice of the most appropriate procedure should be based on the assumptions regarding the analysed seismicity and should take into account the quality and quantity of the available information. In areas where seismic data is scarce, the parameter Δ is taken as 0.5 of the magnitude unit (Mavonga, 2011).

2.3.3.3 Estimation of magnitude of completeness (M_C)

The magnitude of completeness of seismic data (M_C) is defined as the lowest magnitude at which 100% of the earthquakes in a space-time volume are detected (Rydelek and Sacks 1989; Wiemer and Wyss, 2000). A fraction of seismic events with magnitudes below M_C is generally removed from the catalogue during catalogue processing. The majority of existing methods for assessing M_C could be subdivided into two categories:

- Methods based on the information from seismic catalogues (Rydelek and Sacks 1989; Woessner and Wiemer 2005; Amorese 2007; Wiemer and Wyss, 2000; Cao and Gao, 2002; Stepp, 1972).
- Methods based on detection capabilities of the seismic network (e.g. Ringdal, 1975; Gomberg, 1991; Kværna et al., 2002; von Seggern, 2004).

The first category prevails in seismic hazard studies; therefore, the present discussion will focus on these methods. Several authors have assessed M_C for different catalogues at different times and a number of procedures have been proposed for the assessment (Stepp, 1972; Albarello et al., 2001; Stucchi et al., 2004). Most of these catalogue-based techniques rely on the validity of the G-R law (Zúñiga and Wyss, 1995; Mignan and Woessner, 2012).

$$\log_{10} N = a - b(M - M_c) \qquad \text{for } M > M_C \qquad 2\text{-}5$$

where M_c is taken as the minimum magnitude at which the frequency magnitude distribution departs from the G-R law. The major uncertainty associated with M_C determination process is that each method yields different result and there is no consensus on which technique is better (Wiemer and Wyss, 2000). A non-exhaustive selection of techniques to assess M_C are described below.

- One of the first methods for estimating M_C was proposed by Stepp (1972), based on the assumption that the sequence of earthquakes follows a stationary Poisson process. In this

instance, the mean rate of earthquake occurrence λ is stable for the complete part of the catalogue, and its standard deviation is inversely proportional to the time interval

$\sigma_\Lambda = \sqrt{\Lambda}/T$ 2-6

A plot of $\sigma_\Lambda(T)$ for each specific magnitude allows points where the graphs start to depart from $1/\sqrt{T}$ behavior to be detected, indicating the end of the period of complete reporting (Figure 2-6).

Wiemer and Wyss (2000) proposed two methods based on the assumption of self-similarity.

- The first method requires the detection of the point of maximum curvature of the frequency magnitude curve. This technique defines the point of the maximum curvature by computing the maximum value of the first derivative of the FMD which matches with the magnitude bin with the highest frequency of events in the non-cumulative FMD. The technique is very easy to apply and requires few events to reach a stable solution than other techniques.
- The second method is based on a comparison between the observed and the synthetic FMDs by using the goodness-of-fit statistic, calculated from the absolute difference between the numbers of events in the same magnitude bins of the two FMDs. M_C is defined as the magnitude cutoff at which the observed data for $M \geq M_{CO}$ is modeled by a straight line (in log –lin plot) for a fixed confidence level (Wiemer and Wyss, 2000; Mignan and Woessner, 2012; Woessner and Wiemer; 2005).

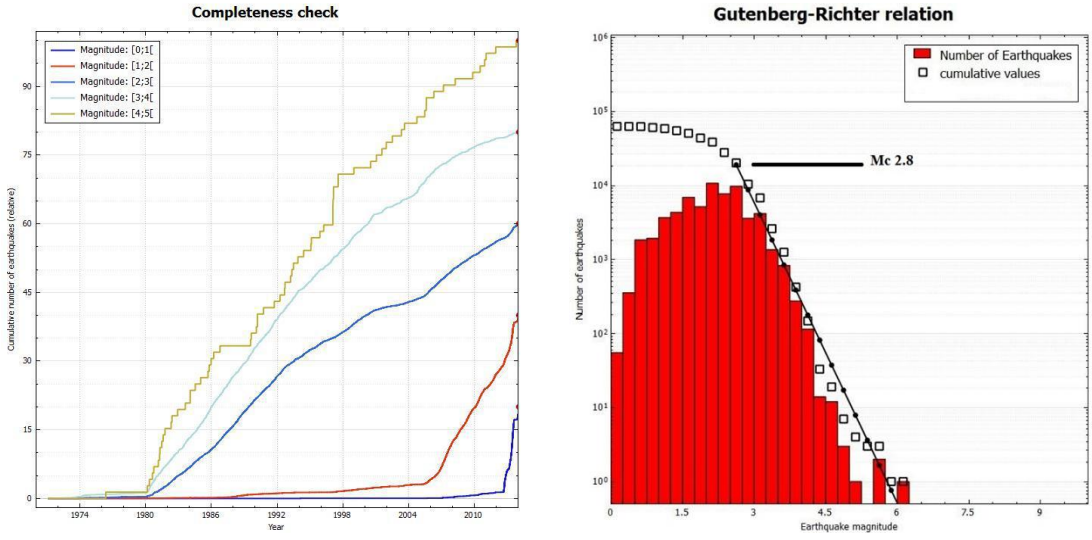


Figure 2-6: Different methods of estimating M_C. a) Stepp (1972) b) Cumulative distribution (Wiemer and Wyss, 200)

- Woessner and Wiemer (2005) developed a method based on modelling of the entire magnitude range. The data below M_c is modelled using the normal distribution, whilst the GR law models

that above M_C. The parameters of the model are estimated by the maximum likelihood method and M_C is defined as the magnitude that maximises the log-likelihood function.

- Cao and Gao (2002) proposed that M_C be estimated using the stabilization of the b-value as a function of the lower cut-off magnitude M_{CO}. Assuming that the b-value increases for $M_{co} < M_c$ and remains almost constant for $M_{CO} \geq M_C$, M_C can be estimated as the magnitude for which the increment between two successive values of b is sufficiently small (e.g. smaller than 0.03) (Cao and Gao, 2002).
- The technique was modified by Woessner and Wiemer (2005) to numerically stabilize it by using the b-value uncertainty as defined by Shi and Bolt (1982).

$$\delta b = 2.3b^2 \sqrt{\frac{\sum_{i=1}^{N} (M_i - <M>)^2}{N(N-1)}} \qquad 2\text{-}7$$

where <M> is the mean magnitude and N the number of events. Mc is then defined as the first magnitude increment at which

$$\Delta b = |b_{ave} - b| \leq \delta b \qquad 2\text{-}8$$

The arithmetic mean b_{ave} is calculated from b−values of successive cutoff magnitudes M_{CO} in half a magnitude range dM = 0.5 such as

$$b_{ave} = \sum_{M_{co}}^{M_{co}+dM} b(M_{co}) \Delta m / dM \qquad 2\text{-}9$$

for a bin size Δm = 0.1.

However, this technique mostly leads to high M_C values compared to the other techniques (Woessner and Wiemer, 2005).

- Marsan (2003) proposed estimating M_C by assessing the likelihood of completeness, which is defined as the probability that the GR law, fitted to the data above the lower cut-off magnitude, would match the number of events in the magnitude bin that precedes the cut-off value. The M_C is selected so that two conditions must be met, namely, drop of the b-value for smaller magnitudes and drop of the likelihood of completeness at M_C.
- Rydelek and Sacks (1989) developed a method to estimate M_C based on the assumptions that earthquakes follow a Poisson distribution and that detection capabilities increase at night relative to daytime (because of lower cultural activity and wind noise). The significant bias in the day-to-night detection of events in the given magnitude interval can be tested by using the Poisson assumption, and the catalogue is classified incomplete at and below this interval if the bias is confirmed. In most of these techniques, what is common is the FMD where M_C is determined as the magnitude where the FMD fails. This phenomenon is important for the

estimation of recurrence parameters for seismic hazard analysis. The variation in the different methods reflects the epistemic uncertainties in M_C determination.

It is known that M_C varies both temporally and spatially (Mignan and Woessner, 2012) and these variations need to be taken into account when calculating seismic parameters. Temporal changes come into play mainly due to the evolution of the seismic network and aftershock sequences. As seismic monitoring improves, the detection of smaller magnitude earthquakes also improves thereby lowering the M_C with time. Transitional phases in a network are usually identified and show clear shifts in M_C estimates (e.g. Hutton et al., 2010; Woessner and Wiemer, 2005; Zulu, 2018).

- Several techniques have been developed for mapping the spatially varying M_C, including the non-parametric method of Schorlemmer and Woesner (2008), the Bayesian method of Mignan et al. (2011), and the multiscale technique of Vorobieva et al. (2013). The commonly used catalogue-based mapping approach estimates $M_C(x, y)$ from the FMD generated from events located in a cylindrical volume of fixed radius R or of fixed number of events N, centred on each node of a spatial grid (Wyss et al. 1999; Wiemer and Wyss 2000). For the constant R approach, the minimum number of events N_{min} is fixed to avoid unstable Mc results. R must be large enough to have sufficient nodes with M_C but small enough to avoid smoothing. This technique has however two basic limitations:
    (1) the choice of a fixed cylinder radius is arbitrary compared to the true M_C resolution (Mignan et al. 2011) while the use of a constant number of events results in an unrealistic and variable relationship to actual seismicity (Rydelek and Sacks 2003) and
    (2) gaps remain in regions of low seismicity (i.e. $N < N_{min}$) where M_C is not computed.

- The Bayesian Magnitude of Completeness (BMC) method to map M_C proposed by Mignan et al. (2011) requires knowledge of the seismic station locations in addition to access to the earthquake catalog. It is a two-step procedure consisting (1) a spatial resolution optimization to minimize spatial heterogeneities and uncertainties in M_C estimates, and (2) a Bayesian approach to merge prior information on the relationship between M_C and the density of seismic stations with locally observed M_C, weighted by their respective uncertainties. The BMC spatial optimization procedure consists in estimating M_C from the FMD that corresponds to events located in a cylindrical volume of radius R,

$$\mathbf{R(d)} = \frac{\mathbf{1}}{\mathbf{2}}\left[\left(\frac{\mathbf{c_1 d^{c_2} + \sigma}}{\mathbf{c_1}}\right)^{\frac{\mathbf{1}}{\mathbf{c_2}}} - \left(\frac{\mathbf{c_1 d^{c_2} - \sigma}}{\mathbf{c_1}}\right)^{\frac{\mathbf{1}}{\mathbf{c_2}}}\right] \qquad 2\text{-}10$$

Where c_1 and c_2 are determined empirically, d is the distance to the k_{th} nearest seismic station and σ is the M_C interval below which variations cannot be resolved. One limitation of the BMC method is that the prior model (equation 2-10) is not well constrained in regions of low seismicity or where seismicity is concentrated in dense areas of the seismic network. If the prior model cannot be defined from regional data, one may try to use the prior model defined for another region (Mignan et al., 2011; Mignan and Woessner, 2012).

2.3.4. Step 3: Attenuation Relationships (Ground Motion Prediction Equations)

When an earthquake occurs, seismic waves will attenuate with respect to distance from the hypocentre, depending on the soil and rock conditions. These waves manifest at the recording site as ground motion, which is characterised by a particular parameter, usually a horizontal peak ground acceleration (PGA), peak ground velocity (PGV), spectral acceleration (SA), or seismic intensity on one of the modern scales. There are two general approaches to estimating the ground motions. The first approach is complex and involves seismogram simulations based on previously determined characteristics of the radiation and propagation of seismic waves (e.g. Taborda and Roten, 2014; Costa et al., 1993; Boore, 2003). The second approach is more typical for PSHA and is based on empirical ground motion prediction equations (GMPEs), derived using regression analysis of recorded strong ground motions (Boore and Joyner, 1982; Abrahamson and Youngs, 1992; Joyner and Boore, 1981; Douglas, 2003).

In seismic hazard analysis, GMPEs are the crucial tools used to estimate the ground motion parameters at a site located at a distance from the source of an earthquake (Cramer, 2001; Gupta, 2002; Bommer et al., 2005; Pavlenko, 2018). They give an estimate of the ground motion parameter as a function of the source (faulting mechanism, magnitude, radiation pattern, and spectral characteristic), the propagation path (source distance, geometrical spreading, and frequency-dependent inelastic absorption of seismic waves in the medium), and local site effects (the influence of surface topography and soil conditions). GMPEs allow estimation of median or mean ground motion at the site, and the associated uncertainty as functions of magnitude, source-to-site distance, and other parameters:

$$\mathbf{ln(y)} = \mathbf{f(m, r, \theta)} + \boldsymbol{\varepsilon\sigma} \qquad 2\text{-}11.$$

where y is the ground motion parameter of interest, f is the regression function linking earthquake magnitude m, distance r, and θ, a vector of additional explanatory parameters (e.g. site effects, style of faulting etc.).. The term $\varepsilon\sigma$ represents the observed variability of ground motions for the specific earthquake scenario.

The GMPEs can then be used to find the cumulative distribution function (CDF) for the ground motion parameter that is being evaluated such as PGA, PGD, PGV. The GMPEs account for factors that contribute to surface ground motion and at the same time, preserve a reasonable degree of simplicity to remain a useful tool in practical applications. GMPEs can be divided into three groups according to the methodology used to derive them:

(1) Empirical models,
(2) Stochastic models,
(3) Hybrid empirical models.

Empirical models are derived by regression of observed data in regions with large amounts of strong ground-motion data, like the western North America and Japan (Chiou and Youngs, 2008; Fukushima, 1996). Stochastic simulation processes involve repeatedly exercising the model for a range of magnitudes and distances, as well as other parameters, adopting a proper functional form for a regression equation. The final step is to performing regression analyses to determine coefficients for mean, median and percentile predictions as well as variability about the mean, median and percentile for the target region (Silva et al., 2002; Atkinson and Boore, 2006; Allen, 2012). The hybrid empirical method is usually used to develop GMPEs in areas with sparse records of ground-motions like northern Europe, eastern North America and Australia. This method employs the stochastic simulation to adjust empirical GMPEs developed for a region with infinite strong-motion recordings, like the western North America and Japan, in order to estimate strong-motion parameters in a region with small amounts of native dataset (Campbell, 2014). The adjustments account for regional differences between the host and the target region in the earthquake source, wave propagation, and site-response characteristics between the two regions (Pezeshk et al., 2011).

Recent GMPEs have more complex forms taking into account the local site effects, style of faulting and non-linear relations (e.g. Abrahamson and Silva, 2008; Atkinson and Boore, 2006; Chiou and Youngs, 2008; Douglas et al., 2006; Douglas, 2001). Most of the GMPEs are derived from the statistical analyses of strong ground motion records and they are updated as new records become available (Ambrasseys et al., 2005; Atkinson, 2004; Akkar et al., 2014). Ideally, it is preferable to use a GMPE derived from local data. However, this is not always possible in many parts of the world due to a lack of sufficient records of strong ground-motion data. In such cases, GMPEs are usually selected from other regions of similar tectonic settings, adjusted and used in target regions (Bommer et al., 2005; Douglas et al., 2006; Scherbaum et al., 2004; 2011). This process of selecting and

adjusting GMPEs has been observed to be very complex due to the existence of a lot of different GMPEs which will result in propagation of uncertainties (Abrahamson and Bommer; 2005; Douglas, 2011; 2018).

There are more than 280 GMPEs for PGA and more than 180 for other spectral ordinates derived all over the world, going as far back as 1964 (Douglas, 2018). Selecting appropriate models for a target region is, therefore, both important and challenging. Fortunately, several researchers have provided guidance to make the process easier (e.g. Cotton et al., 2006; Delavaud et al., 2009; Bommer et al., 2010). The selection process should result in the minimum number of independent GMPEs that capture the expected range of all possible ground-motions in the target region (Cotton et al., 2006). This minimum number of independent GMPEs must be weighted in a logic tree to address the associated uncertainty if more than one GMPE is used. The uncertainty parameters are described in the branches of the logic tree and weighted according to the relative confidence (Bommer et al., 2005) or degree of belief by the analyst using available information. It is critical to compare observed seismic data with ground motion predicted by GMPEs as proposed by Scherbaum et al. (2009), to test if the models capture the observed ground-motions. This does not mean that the expected median ground-motions will be exactly equal to the model median ground-motions. Cotton et al. (2006) proposed a six-step rejection criterion, which was later updated to a ten-step criterion by Bommer et al. (2010). GMPEs need to pass this rejection procedure to be considered for use in seismic hazard assessment in the target region. The procedure by Bommer et al. (2010) is outlined below where a GMPE is rejected if:

1. The model is derived for an inappropriate tectonic environment (e.g. a model from the subduction-zone cannot be used in South Africa).
2. The model is not published in a peer-reviewed journal (although an exception can be made for an update to a model that did meet this criterion).
3. The dataset used to derive the model is not presented in an accessible format; the minimum requirement would be a table listing the earthquakes and their characteristics, together with the number of records from each event.
4. The model has been superseded by a more recent publication.
5. The model does not provide spectral predictions for an adequate range of response periods, chosen here to be from 0 to 2s.
6. The functional form lacks either non-linear magnitude dependence or magnitude-dependent decay with distance.

7. The coefficients of the model were not determined with a method that accounts for inter-event and intra-event components of variability; in other words, models must be derived using one- or two-stage maximum likelihood approaches or the random effects approach.
8. Model uses inappropriate definitions for explanatory variables, such as M_L or R_{epi}, or models site effects without consideration of V_{S30}.
9. The range of applicability of the model is too small to be useful for the extrapolations generally required in PSHA: $M_{min} > 5$, $M_{max} < 7$, $R_{max} < 80$ km.
10. Model constrained with insufficiently large dataset, fewer than 10 earthquakes per unit of magnitude or fewer than 100 records per 100 km of distance.

Bommer et al. (2010) noted that if one accepts this general approach, then it would not be necessary to develop and publish GMPEs that would subsequently be excluded from use because of not satisfying one or more of the 10 criteria requirements. Stewart et al. (2015) give an example discussion of the selection process of GMPEs for hazard assessments for the three principal tectonic regimes, which led to a much-reduced set of models. Predictions of median ground motions from GMPEs show great dispersion (Douglas 2010; Douglas et al., 2012; 2013) demonstrating the large epistemic uncertainties involved in the estimation of earthquake shaking. This uncertainty should be accounted for within seismic hazard assessments by, for example, logic trees (e.g. Bommer and Scherbaum, 2008; Atik and Youngs, 2014).

2.3.5. Step 4: Seismic Hazard Calculations

The seismic hazard is quantified by the probability $P(y \geq a_0, T)$ that the ground motion parameter y will exceed the value a_0 at a given site at least once during a specified time T. The random variable y may generally represent an arbitrary hazard-relevant quantity describing the ground shaking such as PGA, PGV or spectral acceleration at different periods. This probability is found from the mean rate $\lambda(a_0)$ of events that induce ground motions at the site, such that y exceeds a_0:

$$\mathbf{P(y \geq a_0, T) = 1 - e^{-\lambda(a_0)T}} \qquad \text{2-12}$$

This equation is based on the assumptions that the rate $\lambda(a_0)$ is constant in time and that the earthquake occurrences are modeled by the Poisson distribution. The probability of exceedance of a specified ground motion level is obtained by calculating the contribution of each seismic source independently and aggregating them based on the theorem of total probability. In the modern PSHA calculations, $\lambda(a_0)$ is obtained by using the following equation based on the total probability theorem (Baker, 2008; Pavlenko, 2018; Salazar, 2018):

$$\boldsymbol{\lambda(a_0) = \sum_i \nu_i \int_M \int_R P(y \geq a_0 | m_k, r_k) f_{m_i}(m) f_{r_i}(r)\, dr\, dm} \qquad \text{2-13}$$

where ν_i is the activity rate of the i-th seismic source, $f_{mi}(m)$ and $f_{ri}(r)$ are the PDFs of magnitude and distance at the i-th source respectively, and summation is performed over all the seismic sources near the site. By repeating these calculations and using 2-13, the seismic hazard curve can be constructed for any specific time interval. In order to construct a seismic hazard curve for a specific site, a set of ground motion values are selected and the annual frequency of the ground motion parameter, y, exceeding each ground motion value, a_0, is calculated from the following expression:

$$\mathbf{H(y \geq a_0) = \sum_{i \epsilon I} H_i(y \geq a_0) = \sum_{i \epsilon I} \upsilon_i \int_{m_{min}}^{m_{max}} \int_{r_{min}}^{r_{max}} P(y \geq a_0 | m, r) f_{R_i|M_i}(r|m) f_{M_i} \, dr \, dm} \qquad 2\text{-}14$$

where υ_i is the annual rate of occurrence of earthquakes with a magnitude higher than threshold value m_{min}. f_M and $f_{Ri|Mi}(r|m)$ are the probability density functions on magnitude and distance and $P(y > a_0|m, r)$ is the probability that the expectation A that the ground acceleration is exceeded under the condition that an earthquake of magnitude m occurred at distance r.

The seismic hazard map can be constructed by applying this procedure to a grid of points. Throughout the analysis, we assume that the number of earthquakes happening during a time interval Δt can be adequately approximated by a Poisson distribution (Cornell, 1968; McGuire, 2004; Bommer et al., 2015a; Midzi et al., 2020). Assuming a Poisson distribution implies that the events are statistically independent, which is only true if the fore- and aftershocks are removed from the seismicity catalogue. Therefore, the catalogue has to be de-clustered, thus reducing it to a set of uncorrelated earthquakes that can be considered as main shocks.

Input parameters for seismic hazard analysis can be divided into two variable classes (Kowsari et al., 2019). The first class of variables, called "global" variables, are those that affect multiple seismic sources. The choice of these variables and how they affect the hazard parameters is quite flexible. Global variables may be sub-divided into two main categories, as follows:

- Variables related to alternative global zonation approaches and the existence of sources. These variables typically control the existence and geometry of the various seismic sources.
- Variables related to the calculation of source parameters. Examples of these include the catalogue to use, catalogue-completeness model and approaches to use for calculating recurrence parameters.

The second class of variables, called "local" variables, are those that affect only one source. These are the quantities that actually enter the hazard calculations. Multiple, alternative values of these variables represent the conditional epistemic uncertainty in the source parameters, given the values of the global variables. Recurrence parameters falls within the local variables.

2.4. Review of existing PSHA methods

Several methods have been developed for the calculation of PSHA, although the basic principles of PSHA are conserved. Each model has its advantages and disadvantages as outlined below.

2.4.1. Cornell (1968)

Cornell (1968) originally developed the most commonly employed methodology for PSHA. This approach incorporates the influence of all potential sources of earthquakes and their corresponding activity rates. A potential source of earthquakes can be in the form of a point, a fault, or a region where future earthquakes are likely to occur (McGuire, 2004). To describe a potential source of earthquakes, one must decide its form, size, boundary, and the activity rates of earthquakes of different magnitudes. Hence, this method is fundamentally a source-based approach. The basic assumption of this approach is that earthquake activity will recur where it was observed in the past or where it can be expected in future i.e. areas that are tectonically prone to earthquakes that were not recorded in the historical past (Reiter, 1990). Cornell (1968) suggested randomising the observed seismicity in both time and space. This is achieved by modelling the seismicity in zones with uniform spatial and temporal probability of earthquake occurrence. These so-called 'source zones' are chosen based on structural geology, neotectonic data and the seismicity recorded in the study area. The Cornell approach is considered difficult to apply in regions lacking adequate information on the source characteristics, or with a scarcity of recorded strong motion data (Kijko and Graham, 1998). However, this method has been applied worldwide and is well established (Cramer, 2001; Bommer et al., 2015a; Ahulu et al., 2019; Midzi et al., 2020).

2.4.2. Veneziano et al. (1984)

Veneziano et al. (1984) introduced a non-parametric method that was based solely on the information obtained from a seismic catalogue. The method estimates the seismic hazard from each event in the catalogue using the event location and site location through an assumed GMPE and then normalizes the calculated hazard for the duration of the catalogue, to obtain an annual rate of the exceedance.

2.4.3. McGuire (1993)

McGuire (1993) proposed a so-called historic method, which is based on historical earthquake events and does not involve characterization of sources. The major assumption of this method is that the probability distribution of the ground motion is statistically modelled from the historical seismicity of the site. By summing up the distribution functions of all historical earthquakes and dividing the whole function by the number of years of the historical catalogue, the annual rates at which different levels of ground motion are exceeded can be obtained. Although the method is fairly simple to apply,

its major disadvantage is its unreliability at low probability, especially for low-seismicity regions where major events might not exist in the earthquake catalogue (Kijko and Graham, 1998). The approach is heavily dependent on the catalogue, therefore it is not suitable for regions of low seismicity where large earthquakes have long recurrence periods.

2.4.4. Frankel (1995)

Frankel (1995) developed a method that eliminated the need to characterize seismic sources that is suitable for hazard calculation for regions far from active faults. This method is based on smoothing the historical seismicity during the calculation of the probabilistic amplitude. It describes a regular grid that is superimposed over the area of study, and the number of events with magnitudes above a threshold m_0 is counted from the seismic catalogue for each cell of the grid. This number of events in a cell is converted from a cumulative value to an incremental value. The total incremental number of all cells within a certain distance increment r_k from the site is denoted by N_k, and the annual rate $\lambda(a_0)$ is calculated as follows:

$$\boldsymbol{\lambda(a_0) = \sum_k \sum_l 10^{-b(m_i - m_0)} P(y \geq a_0 | m_k, r_k)} \qquad 2\text{-}15$$

where i is the index for magnitude bin, the b-value is taken to be uniform throughout most of the area, and summation over magnitude is carried out to some maximum value. The uncertainties associated with the historical catalogue, such as the location error, can be reduced by smoothing the historical seismicity spatially to different length scales.

2.4.5. Kijko and Graham (1999)

Kijko and Graham (1998; 1999) later developed a parametric-historic method which combines features of both the Cornell (1968) and Veneziano et al. (1984) procedures. Their methodology requires the definition of area specific seismic parameters (i.e. mean seismic activity rate λ, the Gutenberg-Richter parameter b, and the maximum regional magnitude Mmax), while estimating the normalized empirical distribution of the seismic hazard using the value of magnitude, distance and assumed GMPE for the duration of the seismic catalogue to obtain an annual rate of exceedance of the hazard parameter. This method also does not require the characterization of seismic source, but retains some features of the conventional source-based method (Vermeulen, 2014). The advantage of this method is that earthquake catalogues of different completeness conditions could be combined in the hazard assessment, rendering it suitable for regions where the seismicity is not well-understood (Kijko and Graham, 1999). A limitation has, however, been posed on the choice of GMPEs that does not allow non-linear magnitude scaling.

2.4.6. Stochastic method

This technique combines parametric or functional descriptions of the ground motion amplitude spectrum with a random phase spectrum modified such that the motion is distributed over a duration related to the earthquake magnitude and to the distance from the source (Woo, 1996; Abd El-Aal et al., 2015). One of the essential characteristics of this method is that the total spectrum of the motion at a site is formed of contributions from earthquake source, path and site (Abd El-Aal, 2008, 2010). By separating the spectrum into these components, the stochastic models can be easily modified to account for specific situations or to account for improved information about particular aspects of the model (Boore, 2003). This method is based on the point source assumption and it is well known that this assumption fails in the near source region of large earthquakes.

2.4.7. Monte Carlo method

The Monte Carlo method is based on the generation of synthetic earthquake catalogues using a Monte Carlo approach (Ebel and Kafka, 1999; Musson, 2000; Hong and Goda, 2006; Assatourians and Atkinson, 2013). The hazard is then calculated from the estimations of ground motion at a given site or set of sites due to various earthquakes in the synthetic catalogue. Because the method allows identification of those events that contribute at any given hazard probability, the ground motion corresponding to that probability can be directly related to earthquakes of specific magnitudes and at specific locations (Musson, 2000; Hong and Goda, 2006). Furthermore, some or all of the inputs needed in the computation can be found non-parametrically using observed datasets.

Seismic source zones and seismicity rate parameters are not required for the analysis, since these are implicitly in the observed earthquake catalogue. Monte Carlo method can use for the GMPEs, either a set of observed ground motion from which estimates are randomly selected, a table of ground motion values as a function of epicentral distance and magnitude or a parametric ground motion attenuation relation (Ebel and Kafka, 1999). On the other hand, if desired the method can also use postulated seismicity that obeys the standard Gutenberg-Richter or other recurrence relations, characteristic earthquakes, spatial variations in the occurrences of earthquakes of different sizes, distance, frequency, or other variables.

However, the hazard values depend to some extent on the duration of the synthetic catalogue and the specific ground motion attenuation used, and the uncertainty in the ground motions increases with decreasing hazard probability. The Monte Carlo method assumes that the catalogue represents the whole sample of earthquakes expected to affect the site, however all available catalogues of historic earthquakes are much too short to truly represent the long-term seismic activity (Ebel and Kafka, 1999).

2.5. Consideration of Uncertainties

It is well understood that there is uncertainty in SHA because of the uncertainties inherent in input parameters that are used, especially for low seismicity regions like South Africa (Kijko and Graham, 1998; McGuire, 1993; Cramer et al., 1996; Hassaballa et al., 2011; Main et al., 2011). While using PSHA in many seismic environments and for many purposes, scientists became aware that quantifying uncertainties in PSHA is of major importance in order to provide a good scientific basis for decision makers. Uncertainties in PSHA arise from different inputs such as the recurrence parameters and attenuation equations, as well as the hazard model itself (Reiter, 1990; Cramer, 2002; Rebez and Slejko, 2000; Kowsari et al., 2017).

These uncertainties are usually subdivided into two categories that need to be handled differently, namely, aleatory and epistemic uncertainties (Budnitz et al., 1997b). The former describes the inherent uncertainty due to the unpredictable nature of events, while the latter results from incomplete knowledge in the predictive models and variability in the interpretations of the data used to develop the models (Abrahamson, 2006; Thenhaus and Campbell, 2003). The reason that it is convenient to have this distinction within an engineering analysis model is that the lack-of-knowledge part of the uncertainty can be represented in the model by introducing auxiliary non-physical variables (Bommer, 2003). These variables capture information obtained through the gathering of more data or use of more advanced scientific principles.

Several authors have noted the importance of recognizing the difference between epistemic and aleatory uncertainty, and considering them correctly in order not to overestimate the hazard (Kulkarni et al., 1984; Toro et al., 1997; Newman et al., 2001; Thenhaus and Campbell, 2003; McGuire, 2004; Abrahamson, 2006). The nature of uncertainties and the manner of dealing with them has been a topic of discussion by statisticians, engineers and other specialists for a long time (see, e.g., Paté-Cornell, 1996; Vrouwenvelder, 2003; Faber, 2005). In principle, epistemic uncertainties can be reduced with improved knowledge (both empirical and theoretical), whilst aleatory uncertainty cannot. However, in reality, such a distinction is idealistic because some of the observed aleatory uncertainty are in fact due to the epistemic uncertainty (Krinitzsky, 2002). Despite this idealization, the separation of aleatory and epistemic uncertainties has been argued as beneficial from a conceptual view over the past decades and has led to a better treatment of each uncertainty (Bommer et al., 2005; Kulkarni et al., 1984). Therefore, the nature of uncertainties and how one deals with them depends on the context and the application.

In PSHA, the aleatory uncertainties in the parameters are described by suitable probability distributions and are included directly into calculations by quantifying the appropriate statistical

parameters (i.e., standard deviation, coefficient of variation). Epistemic uncertainties, on the other hand, are considered by including alternative models and combining them through a logic tree methodology. For example, the selection of M_{max} for source zone is an example of epistemic uncertainty. Due to the short length of a seismic catalogue, M_{max} may be poorly determined, but as we get more information from paleoseismic investigations and geological mapping its uncertainty will be reduced. However, ground motion variability falls into the aleatory uncertainty category because GMPEs are derived from very uncertainty datasets and their scatter is highly uncertain (Cramer, 2002).

Epistemic uncertainties can be classified into two major categories: parameter and model uncertainties. Parameter uncertainties stems from the difficulties in estimating the input parameters of models due to the limited number, poor representativeness and imprecision of observations. Models are simplified representations of the phenomena, i.e. they are based on assumptions, and compliance between the model assumptions and the properties of the system being analysed do not exist in an absolute sense (Nilsen and Aven, 2003).

Taking into account that our understanding and knowledge of available models for the median values may be quite different from those of aleatory uncertainty in seismic hazard analysis, the separate treatment of epistemic and aleatory uncertainty has its difficulties (Scherbaum et al., 2005). Therefore, it may be desirable to use the probabilistic approach, defining separate logic trees for median values (epistemic) and sigma values (aleatory), through a composite seismic hazard model, which contains the same information as the complete set of end-branch models, but just arranged differently (along median and aleatory variability scales). The composite seismic hazard model treats uncertainties in a clear way, considering the dependence of models represented by branches of a logic tree.

The categorisation of uncertainties is very useful because, in practice, actions affected by the aleatory uncertainty are different from those due to epistemic uncertainty (Der Kiureghian and Ditlevsen, 2009). Aleatory uncertainties usually do not have direct actions that can be taken to reduce them and thus rely on indirect actions to minimise them. On the other hand, epistemic uncertainties require direct actions to reduce them that can be achieved by setting priorities for data collection and analysis based on the identified most influential source of uncertainties (Ellingwood and Kinali, 2009). They do reflect the incomplete knowledge and can be reduced as more data are collected, more information acquired and more research completed therefore are more important to model especially in regions where few large earthquakes with large recurrence periods dominate the overall hazard (Newman et al., 2001). Some examples of uncertainties in PSHA are presented in Table 2-2.

Table 2-2: Examples of Uncertainties in Seismic Hazard Analysis (McGuire, 2004)

Aleatory Uncertainties	Epistemic Uncertainties
Future earthquake locations	Ground motion at a site given the median value of motion
Future earthquake source properties (e.g., magnitudes)	Geometry of seismotectonic and seismogenic zones
Details of the fault rupture process (e.g., direction of rupture)	Median value of ground motion given the source properties
Distributions describing source parameters (e.g., activity rate, b value, maximum magnitude)	
Limits on ground shaking	

2.6. Uncertainties in Earthquake Catalogs

Earthquake catalogs are the most important sources of information used in seismic hazard analysis since they describe the spatial and temporal distribution of past earthquakes in the region of interest. This is usually of use in several aspects of the SHA (e.g. source delineation, recurrence parameter calculations and M_{max} determination). Unfortunately, a certain degree of uncertainty results from the earthquake catalogs. Typically, the following uncertainties have been observed:

- Those associated with type of magnitude reported (i.e. catalogues produced for the same area by different authors have different magnitude types) and magnitude distribution
- Those associated with incompleteness of catalogues
- Spatial distribution of earthquakes (earthquake locations)
- Temporal distribution of earthquakes (conforming with the Poisson distribution)

Typical information associated with these uncertainties is given below.

2.6.1. Earthquake magnitude distribution

Generally, over time, different catalogues have been compiled by different authors and institutions for the same region. These catalogues have earthquake magnitudes reported in different magnitude scales and it is desirable to convert them into a common one. Castellaro et al. (2006) discussed in detail the influence of magnitude conversions on the estimates of seismic parameters. Converting magnitudes from one scale to another is a conventional step of pre-processing the data in seismic hazard studies, since a homogenised earthquake catalogue is required. In their study, Castellaro et al.

(2006) highlighted the superiority of the generalised orthogonal regression in deriving the relations for converting magnitudes. Application of the standard linear regression for this purpose leads to significantly biased assessment of λ and b, while unbiased estimates can be obtained by employing the generalized orthogonal regression.

2.6.2. Uncertainties associated with the recurrence relations

Uncertainty in the magnitude of a future earthquake that will occur in a seismic source is incorporated into PSHA by defining an appropriate magnitude recurrence relationship. The most widely used models in seismic hazard studies are the truncated exponential distribution, characteristic earthquake model developed by Youngs and Coppersmith (1985) and the maximum magnitude model. The uncertainty in the recorded magnitudes is a factor that has significant influence on the estimation of seismic parameters. Tinti and Mulargia (1985) introduced the terms apparent magnitude $\dot{M}$ and true magnitude M. According to this terminology, the reported apparent $\dot{M}$ is the true magnitude, perturbed by a random error ε:

$$\dot{M} = \mathbf{M} + \boldsymbol{\varepsilon} \qquad 2\text{-}16$$

Considering the normally distributed ε, Tinti and Mulargia (1985) concluded that the presence of magnitude uncertainty generally led to an overestimation of activity rate (λ), whereas the b-value remained unaffected. Therefore, to reduce the uncertainty in the recurrence parameters, there is need for an accurate and reliable catalogue. The magnitude of completeness M_C identifies the lower end of the linear segment in the FMD, and therefore, accurate knowledge of M_C is essential for reliable estimation of the b-value and the activity rate (λ). Overestimating M_C reduces the amount of data, whereas underestimating it could potentially lead to incorrect results in further PSHA analyses (Wiemer and Wyss, 2000). The problem of estimating M_C has attracted much attention, as knowledge of this value is essential for many studies that involve statistical analysis of seismic catalogues.

2.6.3. Declustering process

In natural seismicity models, the usual assumption of a Poissonian distribution is made to characterize earthquake occurrences in time and space (Gardner and Knopoff, 1974). Under this assumption, the rate parameter of the Poissonian distribution characterizes the long-term rate of seismicity. This assumption requires events to occur independently from one another; therefore, events whose occurrence is causally linked to that of other events, such as foreshocks and aftershocks, which effectively represent short-term perturbations of seismicity rate, need to be removed from the

catalogue prior to undertaking the rate calculations (Luen and Stark, 2012; van Stiphout et al., 2012). This is done using algorithms identifying dependent events, often called declustering algorithms. Options for identifying dependent events fall into three main categories:

- Window-based approaches, which as their name indicates, identify dependent events based on spatio-temporal windows;
- Cluster-link approaches, such as the frequently-used Reasenberg (1985) algorithm, which link sequences of events into clusters considering multiple levels of dependencies;
- Rate-based and stochastic approaches, which essentially consider deviations from the long-term background rate and/or the Poissonian distribution assumption.

The windows-based approach essentially consists in defining magnitude-dependent windows in space and time around each event of the catalogue (Gardner and Knopoff, 1974; Grünthal, 1985). If an event falls into the spatio-temporal window of another, the two events are classified as members of the same cluster. Once all events have been assigned to clusters or found to be independent, the largest event in each cluster is labelled as the mainshock of the cluster, and all other events within its spatio-temporal window as dependent events. The latter are then deleted to obtain the declustered catalogue.

Cluster-link models, such as the widely used Reasenberg (1985) algorithm, group events into the same cluster as long as they fall within the window of any event that is already in the cluster. This allows the inclusion of higher-level dependencies (e.g., aftershocks of aftershocks), which could be missed in a simple windowing approach. Another feature of cluster-link approaches is that the clusters grow with the number of events analysed.

Stochastic methods utilise the clustering nature of earthquakes by comparing with the background seismicity and modelling the earthquake occurrence models. Well-studied types of clustering include aftershocks, foreshocks, pairs of large earthquakes, swarms and bursts of aftershocks. Zaliapin et al. (2008) demonstrated the existence of two statistically distinct subpopulations in the observed seismicity of southern California: one corresponds to the background seismicity, which is stationary in time but may be inhomogeneous in space, while the other corresponds to clustered events, which are much closer to each other in time and space.

The various approaches for identification of dependent events reviewed above gives different results in terms of the identity and proportion of dependent events identified (Hainzl et al., 2006; Van Stiphout et al., 2012; Luen and Stark, 2012). This, in turn has implications for seismic hazard analysis if the estimation of the long-term rate of seismicity is biased. An important fact to acknowledge is that not all of these approaches have been developed with the aim of removing dependent events prior to rate calculations for seismic hazard analysis, therefore their performance in terms of returning a

declustered catalogue from which unbiased estimates of recurrence parameters can be obtained also varies. Some of the methods listed above (e.g., Reasenberg, 1985) are more targeted at the identification of aftershocks for the purpose of keeping them to study the connections between events, rather than getting rid of them as noise affecting the estimation of the background rate. One consequence of this is that these methods may keep more data in the "declustered" catalogue, which may also deviate from the Poissonian model (Van Stiphout et al., 2012).

Most of the methods described above require the specification of parameters that have typically been derived empirically for a specific catalogue and a given geographic region. This raises the issue of whether this calibration can be considered universal and applied to other regions, or whether locally derived parameters may be required. In the context of seismic hazard analysis, this may need to be considered, since the improvement in methodology may be counter-acted by increased epistemic uncertainty regarding the parameters. This is particularly an issue in cases where empirical data available for calibration are very sparse, as is the case in South Africa.

2.6.4. Uncertainty in M_{max} estimation

According to Reiter (1990), Kijko (2011) and Wheeler (2016), M_{max} refers to the maximum possible earthquake magnitude that can occur within a seismic source. There are a number of methods for estimating M_{max} but none is universally acceptable. These methods include Wells and Coppersmith (1994), Slejko et al. (1998), Kijko (2004) and Wheeler (2016) amongst others. Wheeler (2009) and Kijko and Singh (2011) provide reviews of different procedures for the evaluation of M_{max}. It has been observed that if the period of observation is short and there are few large events, then M_{max} cannot be assessed reliably (Kijko, 2004; Zöller and Holschneider, 2016; Wheeler, 2016).

2.6.5. Uncertainties associated with the magnitude of completeness, M_c

Earthquake catalogues are generally incomplete for small magnitude earthquake, especially in historical times, due to inadequate instrumental coverage (Deniz, 2006; Beauval et al., 2013). As time progresses and the number of seismic stations as well as the processing methods increases, the detection capabilities of local networks improves, which results in changes in M_c for many catalogues (Saunders et al., 2016). It has also been observed that M_c varies spatially depending on the station configurations. The incompleteness of earthquake catalogues creates biases in the database in both time and space (Rydelek and Sacks, 2003). Accordingly, the resulting recurrence relationships may not represent the true long-term rates. In other words, the annual rate of occurrence of smaller magnitude earthquakes and the value of the slope of the recurrence relation are underestimated from the incomplete databases (Vermeulen, 2020). For this reason, it is necessary to determine the time period over which the data in a given magnitude interval is completely reported. Therefore, the annual

rate of earthquake occurrence for earthquakes of that magnitude and above is computed by considering only that time interval. Due to the short period covered by instrumental earthquake catalogues, pre-instrumental datasets are usually employed to expand the volume of available information (Kijko and Sellevoll, 1989).

2.6.6. Uncertainty in the Spatial Distribution of Earthquakes

In PSHA, the uncertainty in the occurrence of future earthquake locations is compensated by delineating line or area sources. In the earlier PSHA models (e.g. Bender and Perkins, 1993), line sources were divided into infinitely small parts and each part was treated as a point source. Since then, many GMPEs that use the shortest distance between the site of interest and a fault rupture as the distance measure have been developed (e.g. Akkar and Bommer, 2007; Akkar et al., 2014). In most PSHA calculations, the uncertainties due to the delineation of seismic zones have been observed to have a substantial impact on the hazard (Cramer, 2001a; 2001b; Santulin et al., 2017). Location errors have an influence on the spatial distribution of earthquakes, which in turn influence the characterization of seismic sources. Accurate determination of earthquake source parameters is very important is SHA. In seismic source characterization, the location of earthquakes has to be accurately known in order to delineate sources reliably. This can be achieved by improving the seismic network distribution and configuration within a region in order to locate active faults. A localized dense network is more useful than a sparse network with poor station configuration (e.g. Figure 2-7).

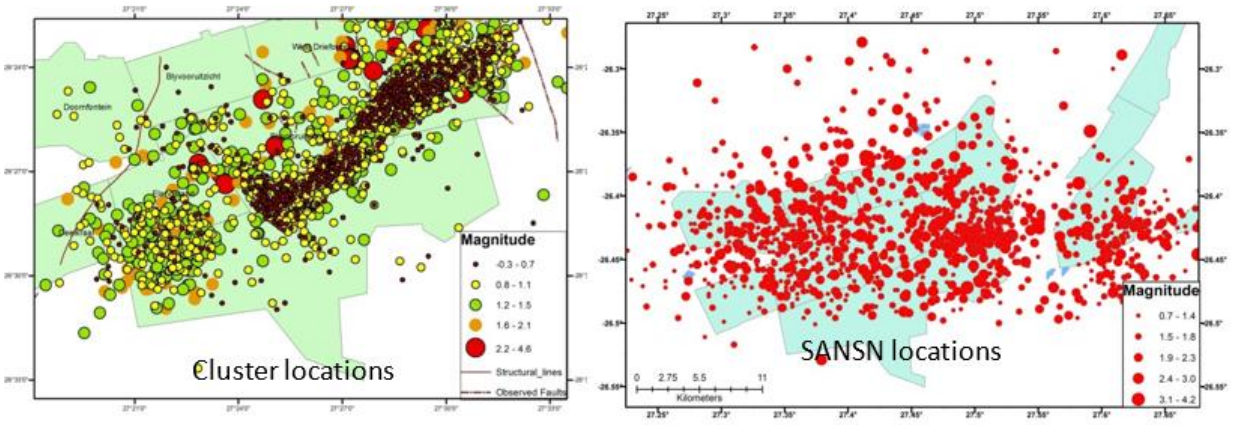


Figure 2-7: Illustration of possible influence of errors in earthquake locations in seismic source delineations in the West Rand region. Comparison of locations produced by a) cluster network and b) national network location.

2.7. Uncertainties in seismic source characterization

Source characterization describes the rate at which earthquakes of a given magnitude, and rupture dimensions (length and width) occur at a given location. The first step in the source characterization is to develop a model of the geometry of the sources (Estrada, 2012). There are two basic approaches used to model geometries of seismic sources in hazard analyses: areal source zones and fault sources. Once the source geometry has been modelled, models are developed to describe the occurrence of earthquakes in the source. This includes models that describe the distribution of earthquake magnitudes, the distribution of rupture dimensions for each earthquake magnitude, the distribution of locations of the earthquakes for each rupture dimension, and the rate at which earthquakes occur on the source (above some minimum magnitude of interest).

Because most earthquakes in stable continental regions do not rupture to the surface, sources of seismicity are not known precisely and thus are delineated using catalogue information. Due to poor distribution of seismic stations within the regions, large errors occur in the location of the earthquakes. The poor locations obtained from these networks are then used to delineate seismic source zones. Association of earthquakes with faults becomes difficult. For regional hazard studies, areal zones may be sufficient to delineate source zones but for localized studies, more information that is accurate needs to be defined (e.g. Bommer et al., 2015a).

2.8. Uncertainty due to attenuation equation

One of the most important steps in seismic hazard analysis is the selection of models to predict the ground-motion in the target region (Scherbaum et al., 2009). In both DSHA and PSHA, the effect of a likely future earthquake in terms of the desired ground motion parameter at a certain distance is estimated by using available GMPEs. Since GMPEs are generally derived from statistical analysis of recorded ground motion, they deviate from the values observed and using them results in the propagation of uncertainties (Bommer et al., 2005). Uncertainty in the ground motion parameter at specified magnitude and distance levels is represented by a lognormal distribution. Developed ground motion relations have errors inherent in them associated with the modeling of the data used (Figure 2-8). The errors are usually indicated as standard deviations (σ) defined for each set of the GMPE coefficients.

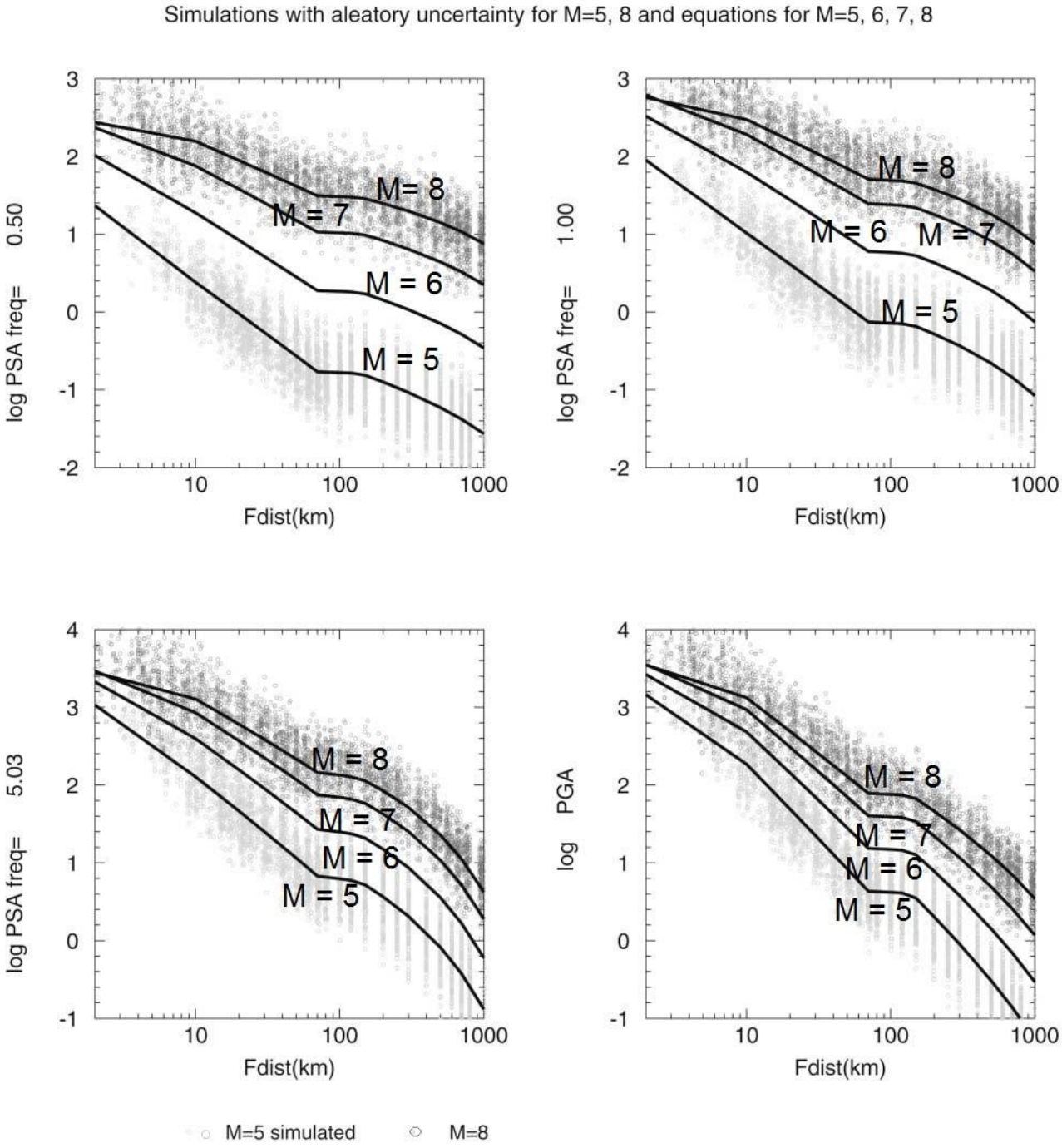


Figure 2-8: An example of a GMPE developed for Eastern and North America. Log_{10} values of horizontal component 5% pseudo-spectral acceleration (PSA) at frequencies 0.5, 1, and 5.03 Hz, and the peak ground acceleration (PGA) is in units of m/s^2. Dots show PSA from simulations, including aleatory uncertainty, for M 5 (light) and M 8 (dark); Fdist is the distance. Solid lines show predicted amplitudes from regression equations developed from simulated database, for M 5, 6, 7, and 8 (adapted from Atkinson and Boore, 2006).

The application of GMPEs to quantify attenuation effects is generally recognized to be the major source of uncertainty in seismic hazard estimates, particularly for low annual frequencies of exceedance (Cramer, 2001a; b; Lombardi et al., 2005). Due to lack of strong motion data, GMPEs developed for stable continental regions (SCRs) tend to be biased towards small earthquakes at short distances and large earthquakes at long distances (Musson, 2008; Frisenda et al., 2005, Massa et al.,

2008, Sabetta and Pugliese, 1987, Douglas, 2011). Procedures for selecting and adjusting GMPEs from other regions of similar tectonic settings have been developed. However, the propagation of uncertainties has been observed in some studies.

GMPEs use a wide variety of definitions for the basic predictor variables, such as the horizontal component of motion, the magnitude scale, and the measure of source-to-site distance (Douglas, 2011). Some GMPEs account for the style of faulting and local site effects, while others do not. These have to be properly adjusted in order to combine the corresponding equations in a logic tree. Otherwise, these parameter incompatibilities will result in systematic differences between the ground motion predictions from the individual models and distort the estimate of the total uncertainty (Scherbaum et al., 2005). When several GMPEs are combined in a logic tree for PSHA to capture the epistemic uncertainty in predicted median ground motions, adjustments need to be made for compatibility if these equations are based on different parametric measures. Such empirical adjustments can lead to severely inflated standard deviations of the adjusted GMPEs, which will exert a strong influence on the results of the PSHA (Bommer and Akkar, 2012).

Most modern GMPEs use definitions more realistic of the source-to-site distance, while traditional models use point-source measures relative to the epicentre. The appropriate distance measure should be used with each GMPE considered. However, definition and delimitation of seismic source and/or seismogenic zones for PSHA almost invariably include areas of distributed point-source seismicity and linear fault sources. Bommer and Akkar (2012) demonstrated the errors that can result from combining point-source simulations and extended-source distance metrics. They suggested that in order to minimise uncertainties, GMPEs have to be derived in pairs, one using an extended-source distance measure, and another using a point source measure (Bommer and Akkar, 2012).

Incompatibilities in terms of magnitude scale and definition of the horizontal component of motion (larger, random or geometric mean) may be corrected using empirical correlations. Another potential source of incompatibility is when the logic tree contains equations that include a predictor variable that is not used in others (e.g. style-of-faulting), which also may be corrected through a procedure to achieve compatibility among the median values. All procedures applied to treat the various incompatibilities imply an increase in the corresponding aleatory uncertainties in the individual predictions (Bommer et al., 2003).

GMPEs are probabilistic descriptions of the ground motion, the median ground motion, characterized by the standard deviation, and the form of the distribution. Ground motions greater than one standard deviation above the median can and do occur. However, statistical evaluations of recorded ground motion data indicate that the data begin to deviate from a lognormal distribution two standard

deviations above the median, indicating that the probability model for ground motion is less reliable from two standard deviations above the median (Abrahamson, 2000).

2.9. Logic tree approach

In seismic hazard analysis, a logic tree is a tool used to capture and quantify the epistemic uncertainties associated with the input variable used in the analysis (Kulkarni et al., 1984; Coppersmith and Youngs, 1986; Reiter, 1990; Bommer et al., 2005). The uncertainties are separated into branches with each branch being assigned a normalized weight to reflect the analyst's confidence in the choice of that branch. The hazard calculation are then performed following all the possible branches and the total hazard is the sum of all the branches. Despite the widespread use of the methodology, guidelines on setting up logic trees and assigning weights to the branches are lacking in the current literature (Bommer et al., 2005; Bommer and Scherbaum, 2008). The process of constructing the logic tree and assigning weights to the branches is not a trivial matter, and if not done correctly might lead to underestimation of the seismic hazard (Abrahamson, 2000). Bommer et al. (2005) provided a detailed analysis of the issues related to this process by using a logic tree for capturing epistemic uncertainties related to the selection of appropriate GMPEs.

A logic tree consists of nodes and branches (Figure 2-9). Each node represents a model, an input parameter, or an assumption that is uncertain. Branches extending from each node are the discrete alternatives for that model, input parameter, or assumption and are assigned a normalized weight that reflects expert opinion regarding the degree of feasibility of that particular hypothesis (Abrahamson and Bommer, 2005). The nodes would be ordered in such a way that independent nodes be placed to the left while dependent ones are located to the right (Figure 2-9). The end branches of the logic tree represent mutually exclusive and collectively exhaustive states of all uncertain parameters, models and assumptions. According to the applicability and credibility of each model, an expert or group of experts assigns a degree-of-belief value or weight to each branch of the logic tree. For the calculation of seismic hazard, these branch weights are subsequently used as subjective (conditional) probabilities. Then, it is necessary to be bound by the rules of probability to assign logic tree weights, in order to avoid logical inconsistencies, because deviant tree branch weights will lead to some unexpected and most likely unintended results. These results might actually look formally correct (because of the normalization), but if normalization is seen only as a matter of convenience, and not as a part of a theoretical framework in which this normalization must reflect the fact that the model set is mutually exclusive and collectively exhaustive, the normalization process can lead to an apparent insensitivity to the weights. Treating the weights as probabilities from the start would mean

that a weight must reflect a logically consistent degree-of-belief (Scherbaum and Kuehn, 2011; Abrahamson, 2000).

The hazard calculations are performed for all the possible branches of the logic tree, resulting in a distribution of hazard curves, from which the mean, the median or other fractiles can be obtained. The development of the logic tree allows for the consideration of alternative models and the values of their parameters to be used in PSHA, with each alternative possibility given a degree of belief such that the sum of the possibilities adds to unit.

Various options can be taken into account in the hazard computation with each branch representing the confidence analysts have in each terminal of the input parameter. The hazard calculations follow all the possible branches through the logic tree, each analysis producing a single hazard curve showing ground motion against annual frequency of exceedance. The weighting of each hazard curve is determined by multiplying the weights along all the component branches. The estimation of the hazard mean and variance is made possible by the similarity in its probability to that of the normal distribution, hence efficient computation of the confidence levels for the exceedance values can be done.

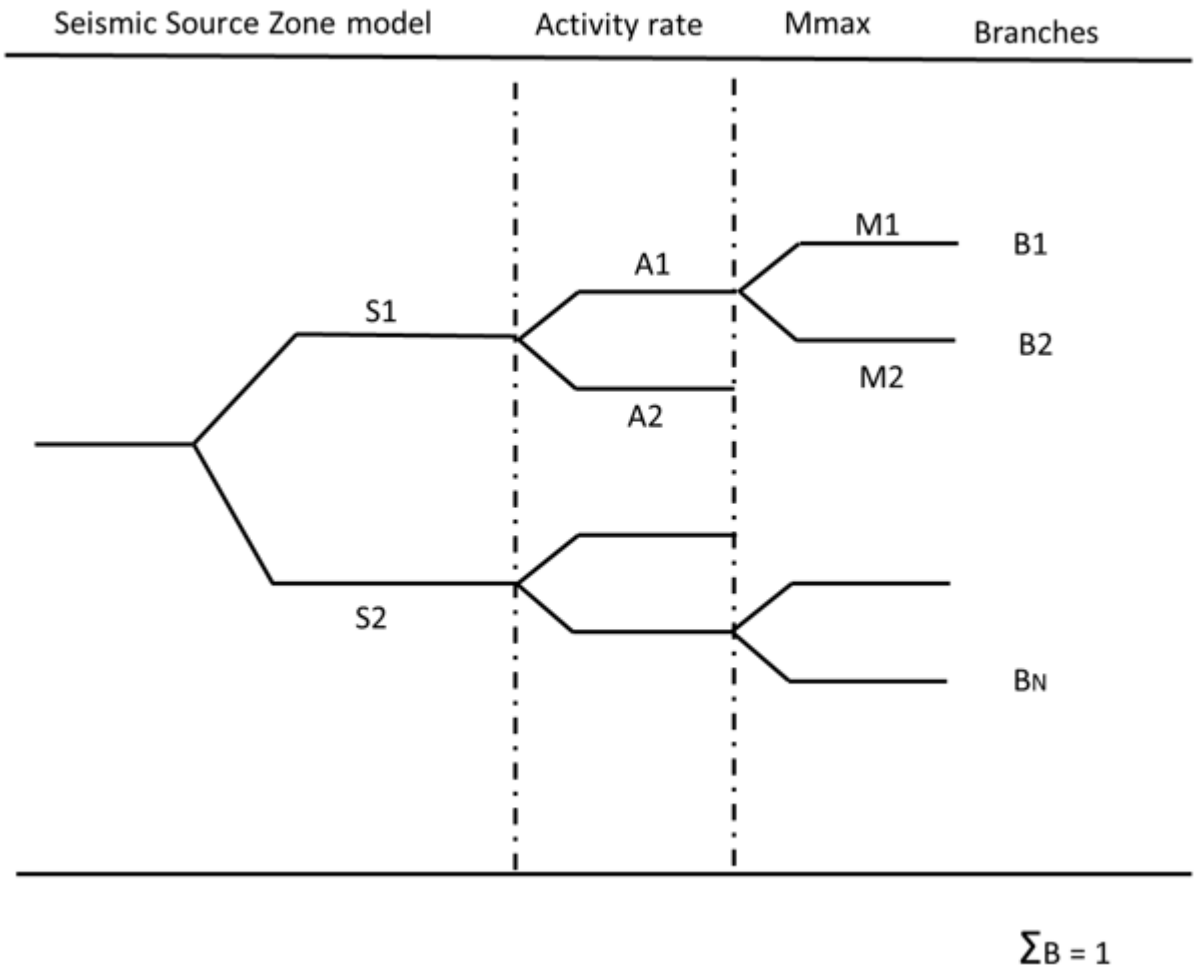


Figure 2-9: An example of a logic tree. The seismic source zone represents an independent node while the activity rate and Mmax are the dependent one.

The use of logic trees in probabilistic seismic hazard analysis often involves a large number of branches that reflect the uncertainty in the selection of different models and input parameters assigned to each model. The calculation would then require a long computation time, though some of the branches actually have little to no impact on the hazard results. Therefore, sensitivity analysis is useful to discriminate which parameters contribute the most to the seismic hazard and its uncertainty, and can be used as a preliminary step for the construction of logic trees focusing efforts on the parameters found to be most sensitive (Barani et al., 2007).

2.10. Sensitivity analysis

In order to evaluate the impact that inputs to PSHA have on the computed hazard, one needs to carry out a sensitivity analysis. This type of analysis can identify critical inputs, provide insight to the model behavior, and help understand underlying mechanisms (Cramer, 2001; 2002; Barani et al., 2007;

Kowsari et al., 2017). This is important, particularly at the early stage of a PSHA where essential modeling decisions have to be made. The aim of a sensitivity analysis is to identify the input parameters that have the greatest impact on hazard assessment and its uncertainty. Many authors have conducted sensitivity analyses for seismic hazard focusing on different aspects of the PSHA process (Cramer et al., 1996; McGuire and Shedlock, 1981; Rebez and Slejko, 2000; Rabinowitz et al., 1993). Some studies focused on assessing the influence of individual input parameters (e.g. McGuire and Shedlock, 1981; Rebez and Slejko, 2000; Crowley et al., 2005; Molina and Lindholm, 2007), while other sophisticated approaches explored the combined effect of uncertainty in a number of input parameters (Rabinowitz and Steinberg, 1991; Rabinowitz et al., 1998). Barani et al. (2007) applied this approach in an Italian case study.

The Senior Seismic Hazard Advisory Committee (SSHAC) report emphasizes that sensitivity analysis for PSHA is crucial, both during the modeling process (for preliminary hazard calculations) and for understanding the final hazard results that are obtained (Budnitz et al., 1997b). To reduce epistemic uncertainties, sensitivity analysis can provide valuable information by addressing the following questions:

- What sources of uncertainty contribute the most to the uncertainties in the predicted hazard?
- At what stages of the hazard assessment procedure (e.g., source characterisation, recurrence rate calculation or GMPE selection) do we have large uncertainties?
- How to rank these sources of uncertainties?
- How to set priorities for future investigations?

The great value of addressing such questions has long been recognized in PSHA relying on logic trees (Rabinowitz et al., 1998; Kulkarni *et al*., 1984; Peruzza and Pace, 2002).

Uncertainty appears in the structure/form of the model, which depends on the choice of variables, dependencies, processes and so forth regarded as relevant and prominent for their purpose in the model. Yet, in some cases, a set of different models (e.g. differing in their structure and input variables) are either considered equally adequate (e.g., they equally fit the observations), or they are associated with different confidence levels. The extensively debated issue of selecting an appropriate GMPE (e.g., Bommer et al., 2010) exemplifies this. Lombardi et al. (2005) investigated the parametric and overall uncertainties in the GMPE, b-value and maximum magnitude for Northern and Central Italy. Their analysis showed that the results are more sensitive to GMPE variations than any other parameters. Giner et al. (2002) discovered that the nodes related to the relation used to convert intensity to peak ground acceleration, the area source model, and the ground-motion relation have the highest sensitivity. Most researchers have pointed out that the degree of sensitivity of the

logic-tree nodes depends on the study site. However, the advantage of using sensitivity analysis in seismic hazard is that it provides a useful tool for identifying the most important parameters for seismic hazard analysis.

In recent years, different approaches have been suggested to assess sensitivity issues in PSHA and for components of PSHA. The approaches that have been considered include using analytical expressions of the hazard integral for simple cases of PSHA (Vanmarcke and Cornell, 1969; Ordaz, 2004) and using factorial design (Rabinowitz and Steinberg, 1991). Cramer et al. (1996) carried out a sensitivity study for a regional seismic-hazard assessment by using classical Monte Carlo methods, while Rabinowitz et al. (1998) pointed out the duality between an efficient construction of logic trees and sensitivity analysis in PSHA. The study by Scherbaum et al. (2005) examined sensitivity issues based on Monte Carlo methods and a two-level factorial design regarding epistemic uncertainties in a key component of a PSHA, namely, ground motion prediction. The SSHAC report gave examples of sensitivity analyses based on partial derivatives of the hazard results with respect to input parameters using finite-differences methods (Budnitz et al., 1997a).

The model that represents the uncertainties of the seismic hazard results is usually determined by studying the behaviour of the weighted distribution of the solutions provided by the logic-tree procedure (Kulkarni et al., 1984; McGuire, 1993; Boomer et al., 2005; Coppersmith and Youngs, 1986) or by a Monte-Carlo approach (Cramer et al., 1996).

In order to carry out sensitivity analysis, Kowsari et al. (2017) divided the input parameters for seismic hazard analysis into two variable classes. The first class of variables, called global variables, are those that affect multiple seismic sources (e.g. ground motion prediction equations, earthquake catalogue, site effects etc.). The choice of these variables and how they affect the hazard parameters is quite flexible. The second class of variables, called local variables, are those that affect only one source (e.g. b-value, activity rate and M_{max}). These are the quantities that actually enter the hazard calculations. Multiple, alternative values of these variables represent the conditional epistemic uncertainty in the source parameters, given the values of the global variables.

2.10.1. Monte Carlo approach

In the Monte Carlo approach, a series of hazard results are generated by randomly varying the input parameters in the source model. All the parameters are assumed to have a normal distribution and are represented by a standard deviation of a mean value (Kowsari et al., 2017). For each site, the series of hazard values generated by Monte Carlo runs are sorted into ascending order, and the 2nd, 50th, and 98th percentiles determined (Cramer et al., 1996).

Some studies have combined the logic tree and Monte Carlo approach for the evaluation of hazard uncertainties (Cramer et al., 1996; Cramer, 2001a; 2001b). Here, parameters at the single nodes of the logic tree are described using continuous probability distributions and the tree is sampled using a Monte Carlo approach. All parameters are taken simultaneously into account by using best estimate values for all but one parameter. Results are given as peak ground acceleration maps together with coefficient of variation maps to highlight areas where uncertainties or lack of knowledge in the input parameters most influences the hazard assessment and its uncertainty.

2.10.2. Variance Based Global Sensitivity Analysis (VBSA)

Sensitivity analysis has also been conducted in earthquake loss estimates using the variance based global sensitivity analysis (VBSA) relying on quasi-Monte Carlo simulations (Rohmer et al., 2014). VBSA is a stochastic method providing a quantitative measure of sensitivity (Sobol, 1993; Sobol and Kucherenko, 2005) assigned to each source of uncertainty (represented by any kind of probabilistic distribution, e.g. uniform, normal or discrete). VBSA presents the advantages of exploring the sensitivity over the whole range of variation (i.e. in a global manner) of the input random variables and of fully accounting for possible interactions between them. This is contrary to the 'one factor at a time' technique, as discussed by Saltelli and Annoni (2010). VBSA allows identification of:

- which input parameters contribute the most to the output variability;
- which input parameters interact with one another;
- which input parameters are insignificant and can be eliminated to "simplify" the model.

By comparing the main and total effects, this technique improves insight into the nature of the considered model. For instance, the case where main and total effects are of equal importance and the sum of the main effects nearly reach unity, indicates that the uncertainty of the output (i.e. the variance) is only due to the sum of the effects of each uncertain parameter taken alone, and not from interactions among them. Thus, the model can be simplified and be represented as a sum of elementary one-dimensional functions of the input parameters.

2.10.3. Practical applications

Uncertainty analysis in seismic hazard assessment should include all input parameters. One cannot investigate the effect by varying the seismicity parameters only without also specifying source zone locations and providing site locations and attenuation functions for the study. Varying the values of the seismicity parameters affects the calculated ground motion levels differently at different sites, for

different times and when different attenuation functions and source configurations are used. This means that sensitivity studies must be viewed in a specific context without generalizing results performed at individual sites under a particular set of conditions. A sensitivity study may be performed to show the effects of varying values of each seismicity parameter without specifying a distribution or a probable range for the parameter. However, without an estimate of the most likely value and of the uncertainty in each parameter, the study may not be helpful (Bender and Perkins, 1993).

CHAPTER 3: GEOLOGICAL AND TECTONIC SETTING OF JOHANNESBURG AND SURROUNDING AREAS

3.1. Introduction

An understanding of the geological and neotectonic setting of the region helps in the preparation of a seismotectonic model of the region, which usually includes the identification of active or potentially active faults. To understand the behavior of these faults, there is a need for detailed geological and geophysical analysis of relevant data and information. In this chapter, we review available geological, neotectonic and geophysical information related to the structural setting of the study region.

3.2. Regional geological settings

The foundation of southern African geology is a core of cratonic rocks that have been subjected to periods of deposition, erosion, extension and consolidation with other continents. Of these cratons, the Archaean Kaapvaal and Zimbabwe cratons are the oldest (3.7 - 2.6 Ga) and they form the core of the Kalahari craton. It is rimmed by the Palaeoproterozoic Damara-Irumide Belt and Kheis province to the west, the Mesoproterozoic Namaqua-Natal Belt to the south, and the Palaeozoic Cape Fold Belt even further to the south (de Wit and Ransome, 1992; Adams and Nyblade, 2011; Cornell et al., 2011; Johnston et al., 1994). The Namaqua sector of the Namaqua-Natal Belt is separated on its north-eastern boundaries from the Kaapvaal craton by the Palaeoproterozoic Kheis province (Adams and Nyblade, 2011) which could either be an orogenic belt (~1.8 Ga) or a northern branch of the Namaqua-Natal Belt (~1.2 Ga) (Eglington, 2006; Cornell et al., 2011).

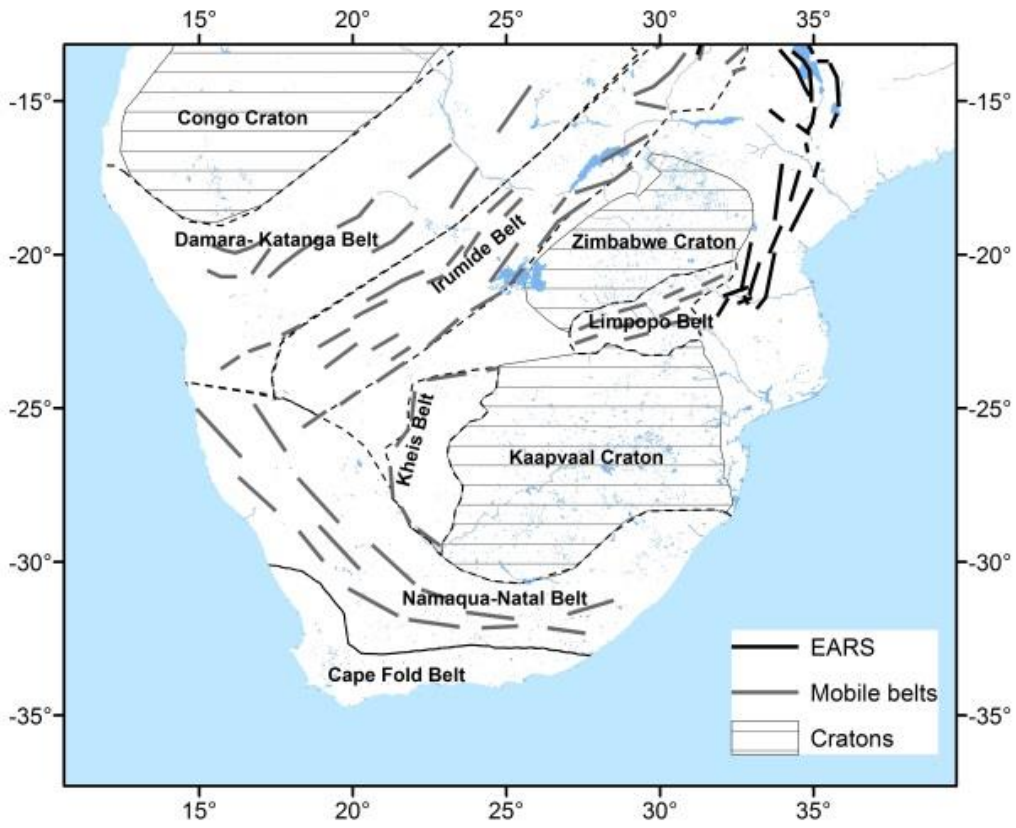


Figure 3-1: Regional geological settings of southern Africa showing mobile belts and Archaean cratons (Manzunzu et al., 2019).

3.3. Local geological setting

There are four major geological domains associated with the study area. The oldest, the Archaean Granite, underlies the northern portion of the area and is unconformably overlain by the sediments of the Witwatersrand, Ventersdorp, and Transvaal Supergroups, which crop out in the central and southern parts of Johannesburg (Kositcin and Krapež, 2004; Crow and Condie, 1988; Manzi et al., 2013). The Witwatersrand basin is a folded basin, created by the crustal thickening initiated flexural subsidence of the craton and is overlain both conformably and uncomformably by the Ventersdorp Supergroup, a complex sequence of volcanic and sedimentary rocks (Beach and Smith, 2007; Dankert and Hein, 2010; Van der Westhuizen et al., 1991). The Witwatersrand and Ventersdorp successions were then covered by the Transvaal Supergroup. Much of the Witwatersrand basin was exhumed by the pre-Karoo (Permian) erosion and is currently buried directly beneath the Karoo sediments (Myers et al., 1990).

3.3.1. Witwatersrand Supergroup

The Witwatersrand Supergroup, well known for the wealth of its gold deposits, is composed of an epi-continental sequence that grades into a more restricted basinal sequence and is underlain largely by the Kaapvaal craton (Barton et al., 1986). The formation of the Witwatersrand basin is complex and several interpretations have been proposed (Myers et al., 1990; Tankard et al., 1982; Cornell et al., 2011). Some authors argue that it was formed due to the collision between the Zimbabwe and the Kaapvaal cratons, while others believe it formed after the subsidence of the Dominion Group below sea level (Myers et al., 1990; Tankard et al., 1982). It is divided into the lower West Rand Group and the upper Central Rand Group (Cornell et al., 2011).

About 2.7 Ga the sea depth fluctuated as sediments accumulated, forming the lower most formations in the Witwatersrand Supergroup, called the Hospital Hill Subgroup. During this period, the glacial process also started which deposited diamictites, forming the Government and Jeppestown Subgroups (Tankard et al., 1982). These three sub groups are collectively called the West Rand Group and attain a maximum thickness of 5 000m. The Kaapvaal craton later collided with the subducting oceanic crust, forming large faults that moved relative to each other resulting in mountainous terrains that later were eroded to low lying areas forming sediments of the Central Rand Group i.e. the Johannesburg and Turfontein Subgroups (McCarthy, 2006; Ryder and Jager, 2002). A detailed stratigraphy of the Witwatersrand Supergroup is shown in Figure 3-2, showing the depositional sequences.

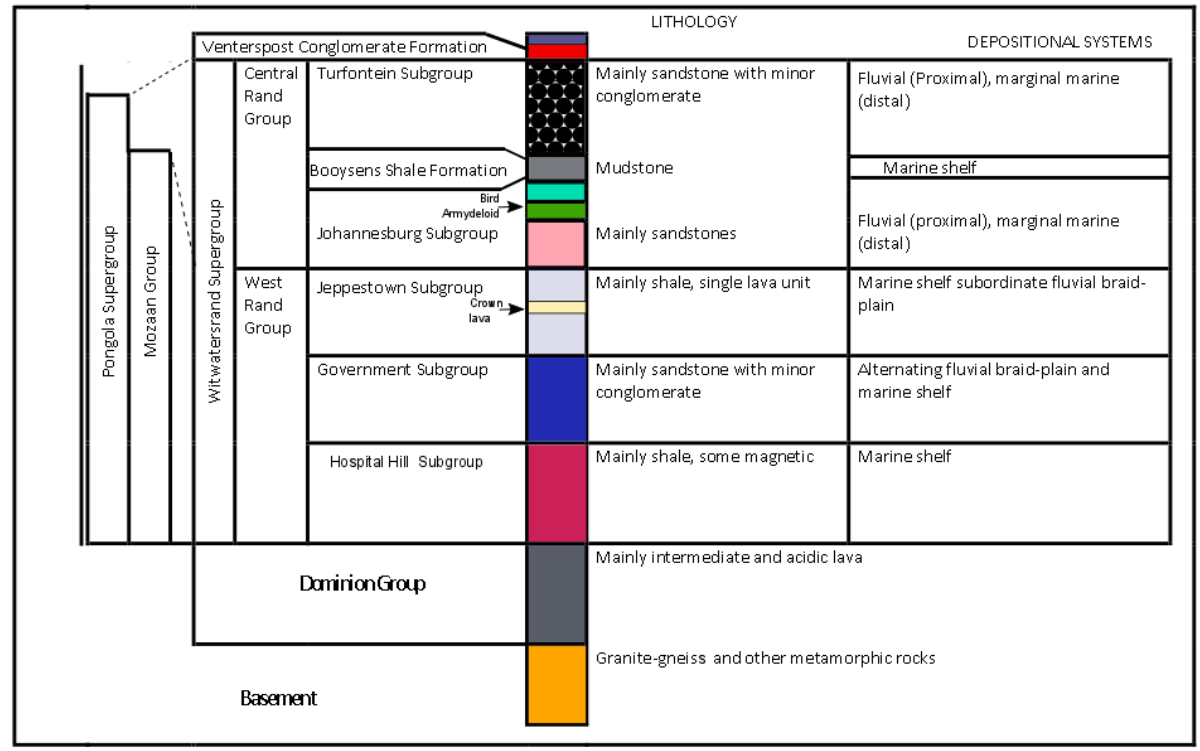


Figure 3-2: Detailed stratigraphic unit of the Witwatersrand Supergroup with the lithologies and depositional settings of the Central Rand and the West Rand Groups (modified from Catuneanu and Eriksson, 1999; McCarthy, 2006; Smith et al., 2013).

3.3.2. Ventersdorp Supergroup

The Ventersdorp Supergroup (2.71 Ga) overlies the Witwatersrand Supergroup and contains the thickest volcanic rocks on the Kaapvaal (Johnson ,et al., 2006). It comprises the Klipriviersberg and Platberg Groups. The sedimentation and deposition of the Witwatersrand basin was terminated when the Kaapvaal craton ruptured. erupting basalt which flowed across the whole basin, covering the entire land and river systems. Even though the event was short-lived, the lava attained a thickness of about 2 000m and covered more than 1 000 000 km^2 and is known as the Klipriviersberg Group (McCarthy and Rubidge, 2005).

The structures created in the closing events of the formation of the Central Rand Group were also active in the Klipriviersberg Group, suggesting that a compressive tectonic style continued during Klipriviersberg times (McCarthy et al., 1990; Van der Westhuizen et al., 1991). However, the eruption of the Klipriviersberg Group was marked by a change in the tectonic style from compression (which characterizes the Central Rand Group) to extensional. Although there was a change in the tectonic style, the extensional structures formed along the same lines of weakness, which previously accommodated the compression phase (Myers et al., 1990). The movement of the normal faults resulted in the disturbance of the post- Klipriviersberg lavas, thus developing the Bezuidenhout

Valley graben and other minor localized basins in which the sediments of the Platberg Group were deposited (McCarthy, 2006).

3.3.3. Transvaal Supergroup

The Palaeoproterozoic Transvaal Supergroup comprises relatively undeformed, unmetamorphosed volcanic and sedimentary rocks (Eriksson and Clendenin, 1990). The Supergroup includes dolostones and iron formations of the Chuniespoort Group, which is overlain by the Pretoria Group. Both groups have been subjected to low grade metamorphism (Eriksson et al., 2006). It consists .of three parts the Transvaal Basin in the east, Griqualand Basin in the west and Kanye Basin in southern Botswana (Cheney, 1996; Eriksson and Altermann, 1998; Moore et al., 2001).

Transvaal sedimentation began with predominantly clastic sedimentary rocks (Black Reef-Vryburg Formations), followed by carbonate rocks and banded iron formations (Chuniespoort-Ghaap-Taupone Groups) (Eriksson et al., 1995). After the erosional process was paused, the clastic sedimentary rocks and volcanics of the Pretoria-Postmasburg-Segwagwa Groups were deposited within the three basins, largely under closed-basin conditions. A final stage of predominantly volcanic succession (Rooiberg Group-Loskop Formation) is limited to the Transvaal Basin (Eriksson and Altermann, 1998).

3.4. Structural Setting

The structural geology of the study area reflects a very long and complex geological history that included significant tectonic events that have all left their scars on the ancient crust. The structures and features created by these events have been reactivated and have the potential to be reactivated again in later stress regimes. Therefore, a short summary of the tectonic history of southern Africa is necessary for understanding the neotectonic setting in the region.

After the deposition of the Witwatersrand Supergroup, the continent cooled and subsided below sea level. The interior of the continent began to experience severe compressional stresses, which ruptured the crust leading to the development of large-scale fractures across the craton (e.g. Thabazimbi-Murchison Lineament, Zoetfontein fault, Zebediela fault, Rietfontein fault, Sugarbush fault and the Border fault) extending in an E-W orientation, following the axis of the compressional stresses (Chunnet and Rompel, 2004; McCarthy and Rubidge, 2005; Basson, 2019). The most prominent one is the Thabazimbi-Murchison-Lineament, which extents for approximately 500 km in an ENE–WSW direction across the Kaapvaal craton (Figure 3-3; Good and De Wit, 1997). Significant faults within this system of lineaments (e.g. the Thabazimbi and Zebediela faults) are associated with a number of

thermal springs and also had some control over the structure of the Bushveld Complex's chamber and the injection of magma at 2.06 Ga (Singh *et al.,* 2011; Kinnaird and McDonald, 2005; Basson, 2019).

The Zebediela fault reactivated as an extensional fault that resulted in the formation of a half-graben structure as the Karroo sediments and basalts accumulated near the Springbok flats (Armitage *et al.*, 2007). The Zoetfontein fault, located in eastern Botswana, is one of the major faults that were reactivated during the Karoo sedimentation and developed as a growth fault trending NW – SE (Modie, 2007; Segwabe, 2008). Mulabisana et al. (2021) suggested that there is evidence of a seismic cycle along the Khurutse fault scarp as reflected by cumulative surface defomation. Further west, the Ellisras Basin is bound by the Eenzaamheid fault to the south and the Mhalapshwe Fault in the north (Figure 3-3 Fourie *et al.*, 2014). The latter structure is close to the Zoetfontein Fault, which appears to influence the distribution of exposures and may be continuous with the Melinda fault further east (Brandl, 1995).

The collision between the Kaapvaal and Zimbabwe cratons (~2.5 Ga) also resulted in the formation of E-W or NE-SW structures within the Limpopo Mobile Belt (Coward, 1976; Gore *et al.*, 2009). Of note are the Tshipise and Bosbokpoort, faults that have scarps ranging from 2 to 10 metres in height (Singh *et al.*, 2009). They appear to form and/or influence the boundary between the Archaean Kaapvaal craton and the southern margin of the Limpopo Mobile Belt, the northern margin of the Archaean–Proterozoic Transvaal Basin, southern margin of the Mesoproterozoic Waterberg Basin, and the emplacement of the Mesoproterozoic Bushveld Complex (Good and De Wit, 1997).

To the south east of the Kaapvaal craton is the Ciskei-Swaziland Axis, along which the Cedarville and Tugela faults are located (Singh *et al*., 2011). Along the Lesotho Highlands, E-W synclinal structures impose linear faults and fractures which have been associated with deep earthquakes at the base of the Highlands (Letlatsa, 2004). To the northeast of the Kaapvaal craton, the East African Rift System (EARS) runs in an N-S direction with several faulting systems. As it propagates southwards, the EARS becomes diffuse and difficult to delineate. However, the occurrence of the 22 February 2006 Mozambique earthquake of magnitude M7.0, confirms the extension of the EARS into southern Africa (Fenton and Bommer, 2006).

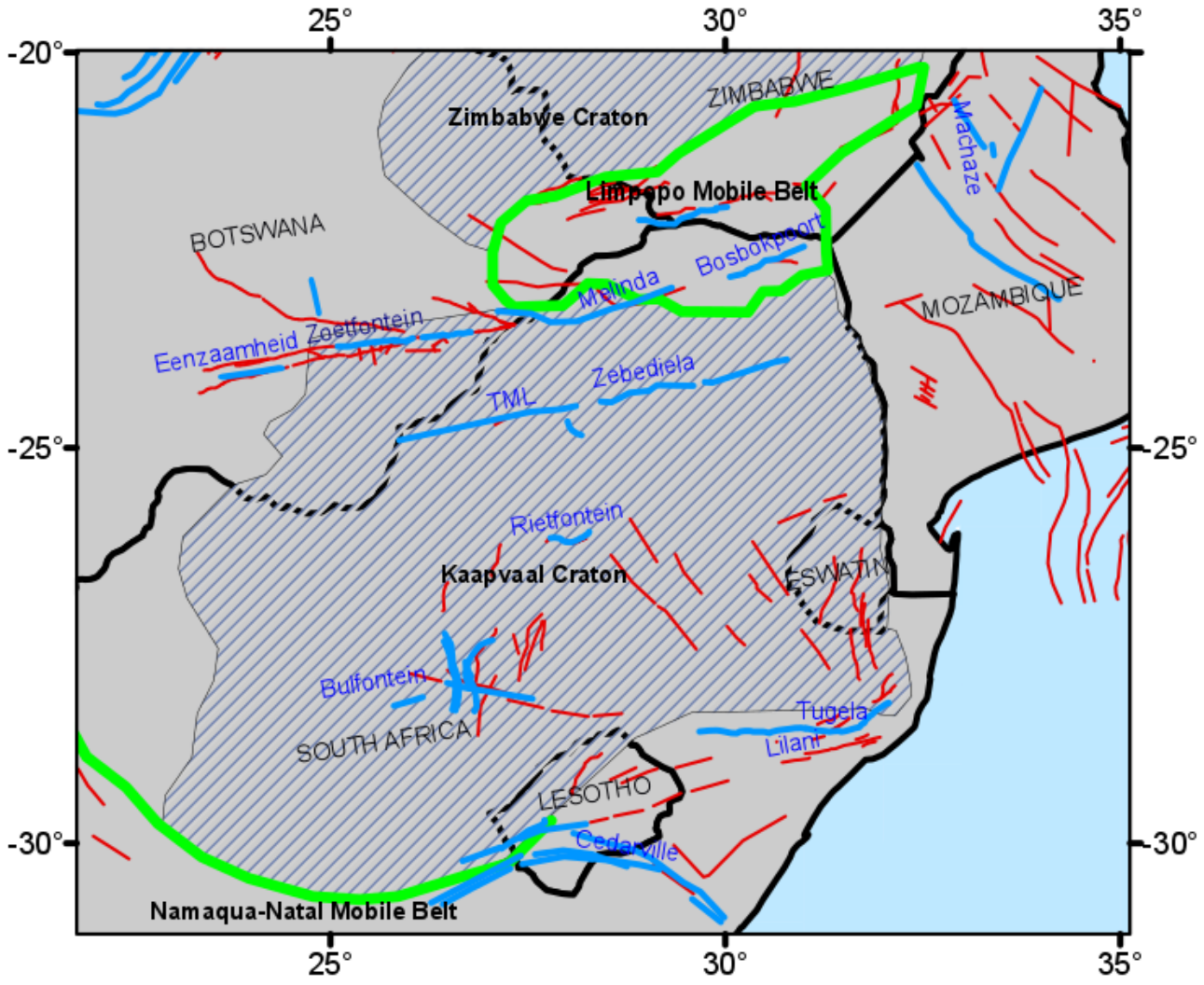


Figure 3-3: Structural settings for southern Africa with major faults (modified from Manzunzu et al., 2019). Blue lines are major faults, red lines are faults green lines demarcate mobile belts. TML is the Thabazimbi Marchinson Lineament.

The Rietfontein fault system is found near the northern margin of the Witwatersrand Basin and it occurs in curvilinear form, which extends for over 60km in an E-W direction (Charlesworth and McCarthy, 1990). Due to the complex geological evolution of the Witwatersrand basin, complex faulting is also observed in the Rietfontein fault system. The fault system can be traced westwards towards the West Rand area, where it intersects the northern margin of the main West Rand Syncline and spreads into numerous south-trending faults. To the east of the Central Rand area, the fault system occurs in the southern margin of the Bezuidenhout Valley graben and it consists of a linked set of faults which form a border around the Witwatersrand rocks (McCarthy, 1994). At the far east, the fault system widens to form curved faults which are northerly orientated (Stanistreet et al., 1986. According to Charlesworth and McCarthy (1990), the Rietfontein Fault also underwent oblique reverse movement, associated with left-lateral strike-slip faulting, resulting in NW-SE oriented fold axes. In recent years, the Rietfontein Fault has been observed to be reactivated as evidenced by localized low-level seismicity in the adjacent area. Although Marlservisi et al. (2013) did some

comutation on geodetic strain rate in South Africa, their results did not discern any movement above their error margins.

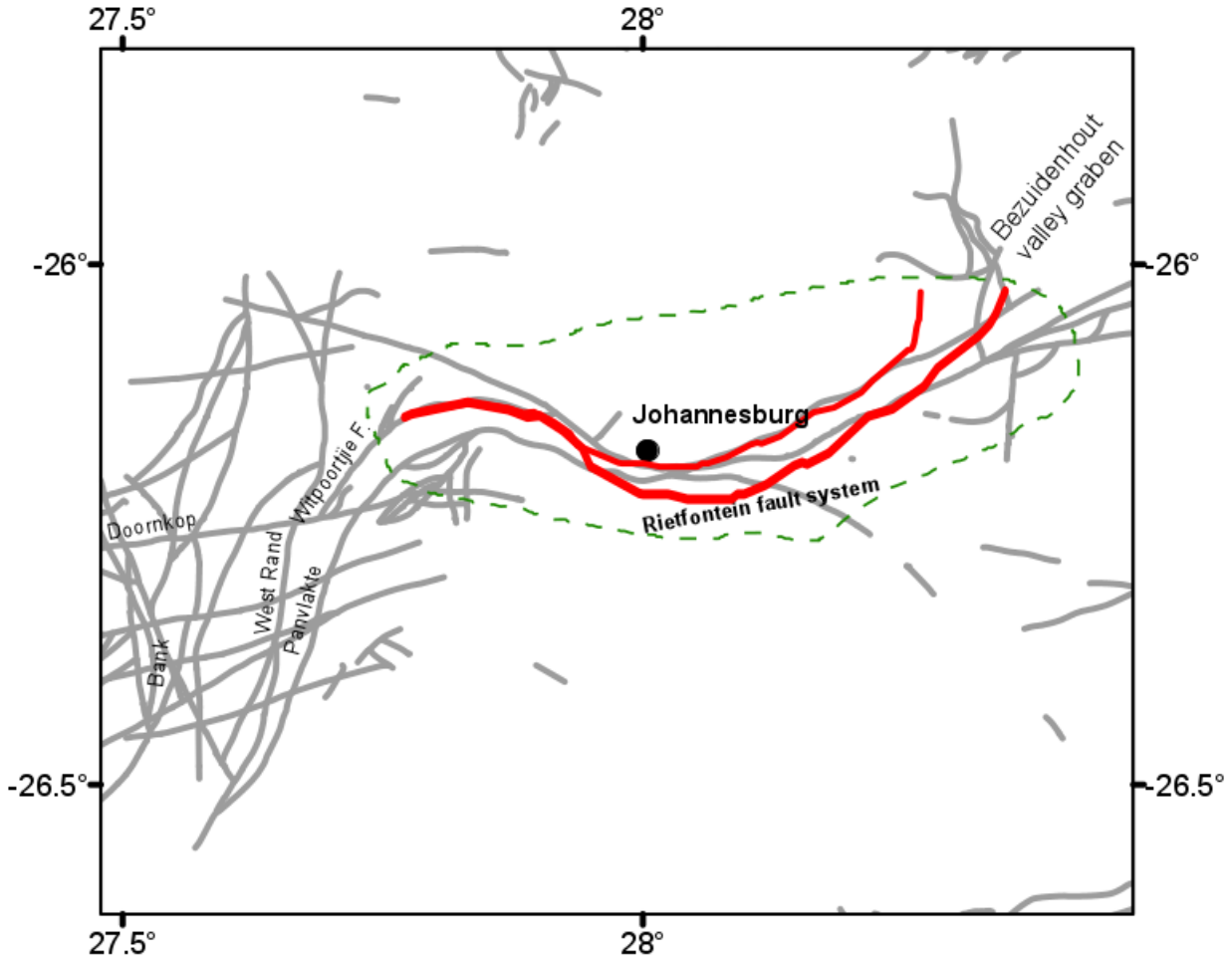


Figure 3-4: The Rietfontein Fault system and the related structural features of the Witwatersrand Basin (modified from Myers et al., 1990).

3.5. Geophysical interpretations

The role of deep-seated geodynamics in the present-day seismic domains is an important element for the understanding of localized deformation zones. A number of projects have been conducted in the last decade to study the crustal thickness and lithosphere-mantle structure of the African continent (e.g. Wright et al., 2002; Pasyanos and Nyblade, 2007; Simon et al., 2002; 2003; Fishwick and Bastow, 2011). Information from such studies are useful to investigate the thickness of the seismogenic layer for each province.

Simmons et al. (2006) indicated that the African Superplume might be an active, buoyant upwelling structure directly beneath South Africa with significant lower chemical density signatures that that has entrained intrinsically-dense material from a pile at the base of the mantle. The long term interaction between upwelling in the mantle and the lithosphere have been associated with the relative stationarity of the continent and associated hot spots (Morgan, 1983; Burke, 1996; Nyblade and Robinson, 1994; Lithgow-Bertelloni and Silver, 1998; Simmons et al., 2006). Thin-sheet crustal modelling indicates that although buoyancy forces may advance rifting, they are not great enough to initiate rifting (Stamps et al., 2008) as mantle upwelling may also have a role in rifting. Using seismic tomography, Brandt et al., (2011) mapped in high detail the African Superplume under southern and eastern Africa. The EARS and related plume extending from Malawi to the Red Sea illustrate the geodynamics of the mantle below Africa and the underlying mantle convection. One-dimensional shear-wave velocity models of the upper mantle beneath the Kalahari craton are similar to those of other cratons indicating a possible lower mantle source for high topography in southern Africa (Brandt, 2012). Hartnady and Partridge (1995) noted that the most uplifted areas correspond with large negative Bouguer gravity anomalies, which possibly reflects the continuing southerly development of the African Superswell, which may, in turn, be related to the southward propagation of the EARS. The crust structural thickness within South Africa ranges from 27 – 45 km within the cratons while the mobile belts have thicker crustal structures of more than 50 km (Nguuri et al., 2001; Durrheim and Mooney, 1994).

A number of localized geophysical studies have been conducted especially in the mining regions in order to understand the structural settings of the area (Manzi et al., 2012; 2013; 2015; Stevenson et al., 2003). Manzi et al. (2013) used 3D seismic modelling to confirm that the West Rand Group is unconformably overlain by the Central Rand Group. Their seismic sections also confirm that an unconformable relationship exists between the Central Rand Group and the Ventersdorp Contact Reef, with an easterly-verging fold-thrust belt being initiated simultaneously to deposition of the Ventersdorp Contact Reef at approximately 2.72 Ga.

3.6. Neotectonics

Earthquakes are usually of tectonic origin and occur along the boundaries of the tectonic plates that make up the surface of the Earth. In southern Africa, low earthquake recurrence rates and a short seismic catalogue inhibit the study of the modern stress regime. Recent studies have begun the process to analyze the regional modern stress regime using seismic events, GPS and geological strain indicators, such as jointing, in conjunction with stress field modelling (Stamps et al., 2014; Manzunzu

et al., 2019). Stamps et al. (2018) developed a geodetic strain rate model for Sub-Saharan Africa that incorporates geodetic velocity fields, regions of deforming zones and constraints on block rotations. This model provides fundamental constraints on long-term tectonic deformation in the region and an improved seismic hazards assessment in Sub-Saharan Africa. However, Stamps et al. (2018) noted that the EARS remains one of the least monitored tectonic plate boundaries, which makes it challenging to constrain present-day seismic hazards.

Simulation results from the CRUST 2.0 model (Calais et al., 2006; Stamps et al., 2010) indicated that deviatoric stress alone cannot overcome the strength of the lithosphere. Rather, lateral crustal density variations are necessary to achieve the dynamic topography of southern Africa. Deep mantle convection may also be a primary driver of plate motions (Bird et al., 2006). The presence of the Wegner Stress Anomaly in southern Namibia - western South Africa is believed to have an influence on the intraplate seismicity of South Africa including the moderately large events in the mining regions (Andreoli et al., 1996; Bird et al., 2006).

Using GPS data from 14 sites and slip vectors from 53 earthquakes, Calais et al. (2006) proposed southward-dipping asthenospheric flow associated with the EARS as the cause of normal faulting in the Kaapvaal and other southern African cratons. The splitting of the African plate into Nubia and Somalian plates results in extensional structures along the rift with some rotation between them (Jestin et al., 1994; Saria et al., 2014; Stamps et al., 2018). Modelling of plate motion data indicates that the Nubian and Somalian Plates may be separated by smaller plates (Hartnady, 2002; Horner-Johnson et al., 2007; De Mets et al., 2010; Saria et al., 2014). Hartnady (2002) identified four aseismic blocks and predicted a clockwise rotation of 0.089°/Myr in the Nubian reference frame. Saria et al. (2014) included in their model the Lwandle plate and a fourth plate (the Rovuma plate), and it significantly improved the fit of their model to observations. Bird et al. (2006) and Calais et al. (2006) also modelled the relative rotation between the two plates with an Euler pole between South Africa and the southwest Indian Ridge.

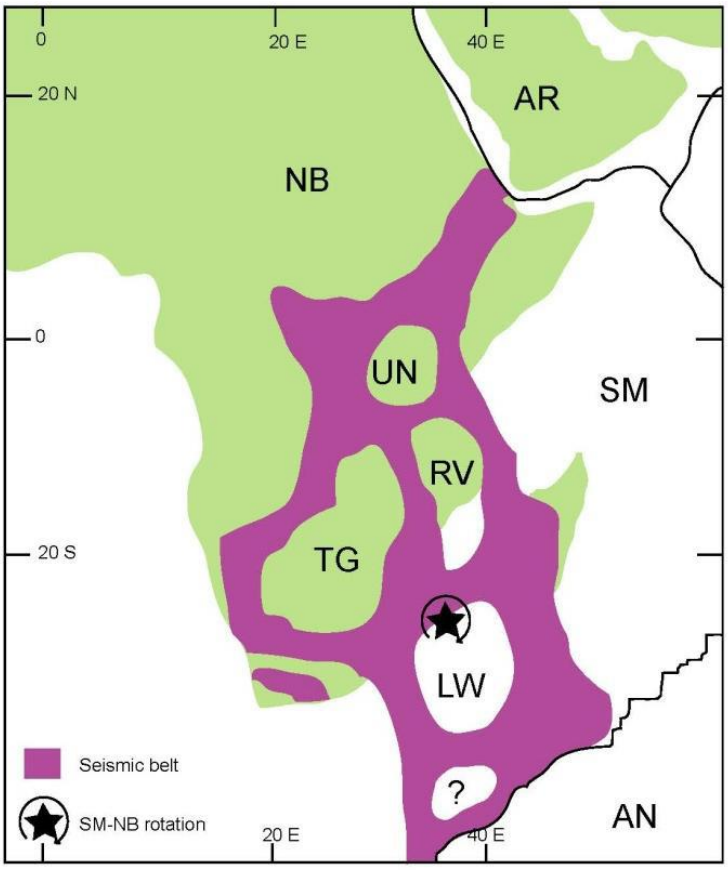


Figure 4.6: African composite plate, subdivided into smaller, relatively stable blocks separated by seismically active belts (shaded zones). Star symbol at 27.3°S, 36.2°E off the Mozambique coast marks the pole of SM finite rotation (clockwise at 0.089°/Myr) over the last 3 Myr, in the NB reference frame. (from Hartnady, 2002.)

Analysis of GPS data shows that the South African plate is slowly deforming and the vector directions confirm the effects of the southward propagation of the EARS into northern South Africa (Malservisi et al., 2013; Calais et al., 2006), although there is no evidence of higher strain rates wrapping around the Kaapvaal craton as suggested by Bird et al. (2006). Jestin et al. (1994) predicted a velocity of 3-4 mm/yr for the southern Africa portion of the Somalia plate in an eastward direction. Malservisi et al. (2013) determined the present day velocity fields for South Africa using GNSS recording of more than 1000 days per station. The results show that the South African region behaves rigidly, with deformation in the order of one nanostrain/year or less. The Trignet data were compared with data for the Nubian plate, and it was found that the South African block is rotating in a clockwise direction with respect to the African continent, which is consistent with the propagation of the EARS along the Okavango region. Therefore, although there is very little measurable deformation within southern Africa, it is difficult to quantify the deformation rates for seismic hazard analysis purposes. However, stress analysis results confirm the extensional stress regime within South Africa (Bird et al., 2006).

Intraplate earthquakes appear to cluster both temporally and spatially on a complex system of ancient faults or crustal weaknesses with long dormancy periods (Calais et al. 2016, 2011; Liu et al. 2011; 2014). South Africa is not an exception to this point of view, with historical and instrumental significant seismicity (M> 5) concentrated in few well-localized clusters, for example the Ceres cluster and the Koffiefontein cluster (Midzi et al. 1999; Davies and Kijko 2003; Brandt, 2008; Hartnady, 1990; Singh et al. 2009; 2011).

3.7. Conclusions

Although there is evidence of tectonic deformation in southern Africa, it is small in comparison to observations along the EARS or at plate boundaries. It is evident that South Africa behaves like a stable continental region (SCR) with intraplate earthquakes that vary spatially and temporally along complex ancient faults. Geological and structural data indicate that the region has undergone both extensional and compressional stresses in the past. Observed seismicity indicates the propagation of the EARS into southern Africa in Mozambique as well as to the southwest along the Zambezi valley into Okavango delta. Several authors support this proposed model for the southward propagation of the EARS. The information gathered in this chapter will assist in the development of a seismotectonic model for Johannesburg.

CHAPTER 4: CATALOGUE COMPILATION AND UNCERTAINTY ANALYSIS

4.1. Introduction

A critical input in all seismic hazard assessments is a reliable and accurate catalogue of earthquakes. The catalogue is usually of use in several aspects of the assessments, such as in the identification and delineation of earthquake sources, in recurrence parameter calculations and in the determination of maximum expected magnitude (M_{max}). In selecting earthquakes to use in a seismic hazard assessment, the boundaries of the region for which the seismicity catalogue is compiled are usually selected to cover the geographic extent of the seismic source zones that have been identified as potential contributors to the seismic hazard for site under investigation (such as the city of Johannesburg in this case). The catalogue developed here covers all known events in the region of study up to and including December 2016. The city of Johannesburg is surrounded and underlain by mines hence seismicity in and around the city is contaminated by anthropogenic sources. In this regard, all the seismicity is considered and care taken in defining the seismic sources.

Several versions of catalogues have been compiled for South Africa and in each catalogue, more information is added as both monitoring and the techniques for catalogue analysis improve. The first catalogue for South Africa was compiled by Gane (1939). Gane and Oliver (1953), Fernández and Guzman (1979), and Brandt et al. (2005) updated the catalogue as the years went by and new events were recorded. A number of regional catalogues that also include the study area have been also compiled. Turyomurugyendo (1996) compiled a catalogue that covered the whole of east and southern Africa, which was used in the GSHAP seismic hazard assessment for the same region (Midzi et al., 1999). Malephane (2007) also compiled the Lesotho catalogue as part of her seismic hazard calculations for Lesotho. Recently, Mulabisana (2016) compiled a regional catalogue for seismic hazard analysis but deleted seismicity in the mining regions below magnitude 4. In this current study, a synthesized catalogue from different sources was compiled by carrying out the following steps:

- Collection of available data mainly from the databases at the Council for Geoscience (CGS). Other data was obtained from organisations such as the Advanced National Seismic System (ANSS), the Goetz Observatory Zimbabwe, the Botswana Geoscience Institute (BGI, previously Geological Survey of Botswana), the International Seismological Centre (ISC) and the National Earthquake Information Centre (NEIC). Valuable data were also obtained from other published and unpublished sources (e.g. Turyomurugyendo, 1996; Wood, 1913; Finsen, 1950; Gane and Oliver, 1953; Flint, 2016; Mulabisana, 2016),

- The merging of all collected data into one catalogue,
- The removal of duplicate events,
- The homogenisation of the earthquake magnitudes to moment magnitude,
- The declustering of the homogenised catalogue, and
- The analysing the completeness levels for the new catalogue.

In each step, uncertainties were thoroughly assessed and documented for the compiled catalogue. The nature of the information available is closely linked to the history of seismic monitoring in South Africa and neighbouring countries, which is detailed in the following sections.

4.2. Seismic monitoring in South Africa and neighbouring regions

Seismic monitoring in Southern Africa started in the late 19th Century, although very few stations were installed in the early days (

Figure 4-1; Table 4-1). The information was taken from the references and materials cited in Table 4-1, as well as from the summaries by Wright and Fernández (2003) and Saunders et al. (2008).

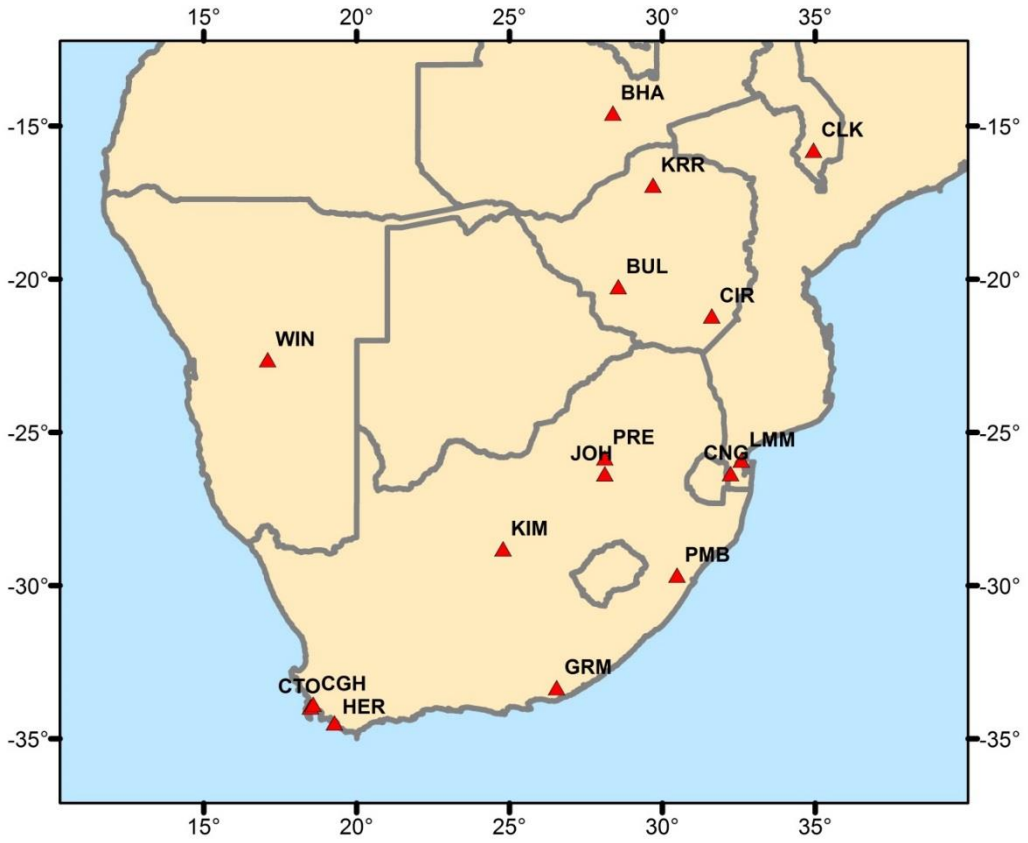


Figure 4-1: Location of early seismograph stations in Southern Africa region from 1899 to 1969.

Table 4-1: Detailed summary of South African institutions involved in early seismic monitoring and the seismic stations.

Institution	Responsibilities and Contributions	Instruments
Royal Observatory at the Cape of Good Hope [CGH, Cape Town, 1820-1931]	Reports and letters describing felt effects of 19th century earthquakes. Instrumental readings from 1899 onwards. Communication with international seismological institutions	Milne seismograph (CGH) installed August 1899. Upgraded to Milne-Shaw instrument in 1920. Ceased operation in 1931 (moved to CTO)
Union Observatory, later Republic Observatory [Johannesburg, 1910-1972]	Primary focus on monitoring of seismic activity in the Gauteng gold-mining regions. Macroseismic monitoring through correspondence with the general public. Communication with international seismological institutions	200kg Wiechert seismograph operational from July 1910 to April 1972
University of Cape Town, Department of Applied Mathematics [CTO, Cape Town, 1931-1950]	Operation of CTO seismograph 1935-1947 and publication of bulletins for part of this period	Milne-Shaw instrument previously at CGH, plus another horizontal Milne-Shaw seismograph
Hermanus Magnetic Observatory [Hermanus, 1950-1986]	Operation of seismological instrument and publication of seismological bulletin. Focus mostly on teleseismic events.	Milne-Shaw instruments previously at CTO
University of the Witwatersrand, Bernard Price Institute (BPI) [Johannesburg, 1949-1968]	Macroseismic monitoring Analysis of seismograms from Geological Survey (1949-1968) and Bulawayo networks (1959-1964) Publication of regional catalogue 1949-1956	Network of short-period Benioff seismographs installed 1949-1951 at Kimberley (KIM), Grahamstown (GRM), Pietermaritzburg (PMB), Pretoria (PRE) and Windhoek (WIN).PRE, GRM and WIN upgraded to WWSSN in 1964-1965
Geological Survey of South Africa, later Council for Geoscience [PRE, Pretoria, 1932-present]	Macroseismic monitoring from 1932 onwards Owner of network analysed by BPI 1949-1968 Operation of SANSN from 1970 onwards	See BPI for pre-SANSN See text for SANSN

4.2.1. South African National Seismograph Network (SANSN)

Following the destructive 1969 earthquake in the Tulbagh/Ceres region and the reorganisation of the South African Astronomical Observatories, the responsibility of monitoring seismicity at a national level fell to the Geological Survey, now the CGS. The South African National Seismic Network (SANSN), described in detail in Saunders et al. (2008), was established as a network of seven analogue stations in 1970. The network has since evolved and from 1991 onwards, analogue instruments were supplemented and eventually replaced by digital instruments. Currently the network consists of 28 permanent broadband stations (Figure 4-2).

The data collected through the SANSN is processed at the CGS head office in Pretoria by the Engineering and Geohazards unit staff. Regularly published quarterly and yearly bulletins are available that summarise the source parameters of all earthquakes recorded by the SANSN.

4.2.2. The mining cluster networks

Mining-induced seismicity and its hazardous manifestation, rockbursts, were first encountered in the early 1900s, when mining operations went deeper into the ground (Wood, 1913; 1914). This prompted the monitoring of rockburst-induced seismicity. The Ophirton Earth Tremors Committee conducted the first investigation into the causes of mine tremors in 1908. Based on the recommendations of the committee, two seismographs were installed in 1910, one at the Union Observatory in Johannesburg and the other in the village of Ophirton. The Ophirton seismograph was moved to Boksburg in 1913, where tremors were beginning to be felt. Later in 1939, a network of five stations was deployed on the northern rim of the Witwatersrand Basin to augment the few stations that were in operation. Over the years, a couple of networks were installed at the surface in the mining regions to monitor mining induced seismicity and data analysis was done by several research groups (Durrheim and Reimer, 2016). Underground networks were later introduced to better locate and improve monitoring but these mainly focus on individual mines. In this study, data from underground networks was not used.

In response to concerns raised on the increase in seismicity felt within the mining regions, CGS installed some cluster networks to monitor the seismicity in the mining regions (Brandt and Saunders, 2010; Cichowicz et al., 2010; Grobelaar et al., 2017). The three clusters are referred to as the Strategic Water Management Program (SWMP) in the Central and East Rand, Japan International Cooperation Agency (JICA) network in the West and Far West Rand and the Klerksdorp-Stilfontein-Orkney-Hartesbeespoort (KOSH) network as shown in

Figure 4-2. The Engineering and Geohazards unit staff also process the data collected through these networks. The SWMP network was installed in 2010 while the JICA and KOSH were later installed in 2012. More than 50 broadband and accelerometers were installed in these cluster networks.

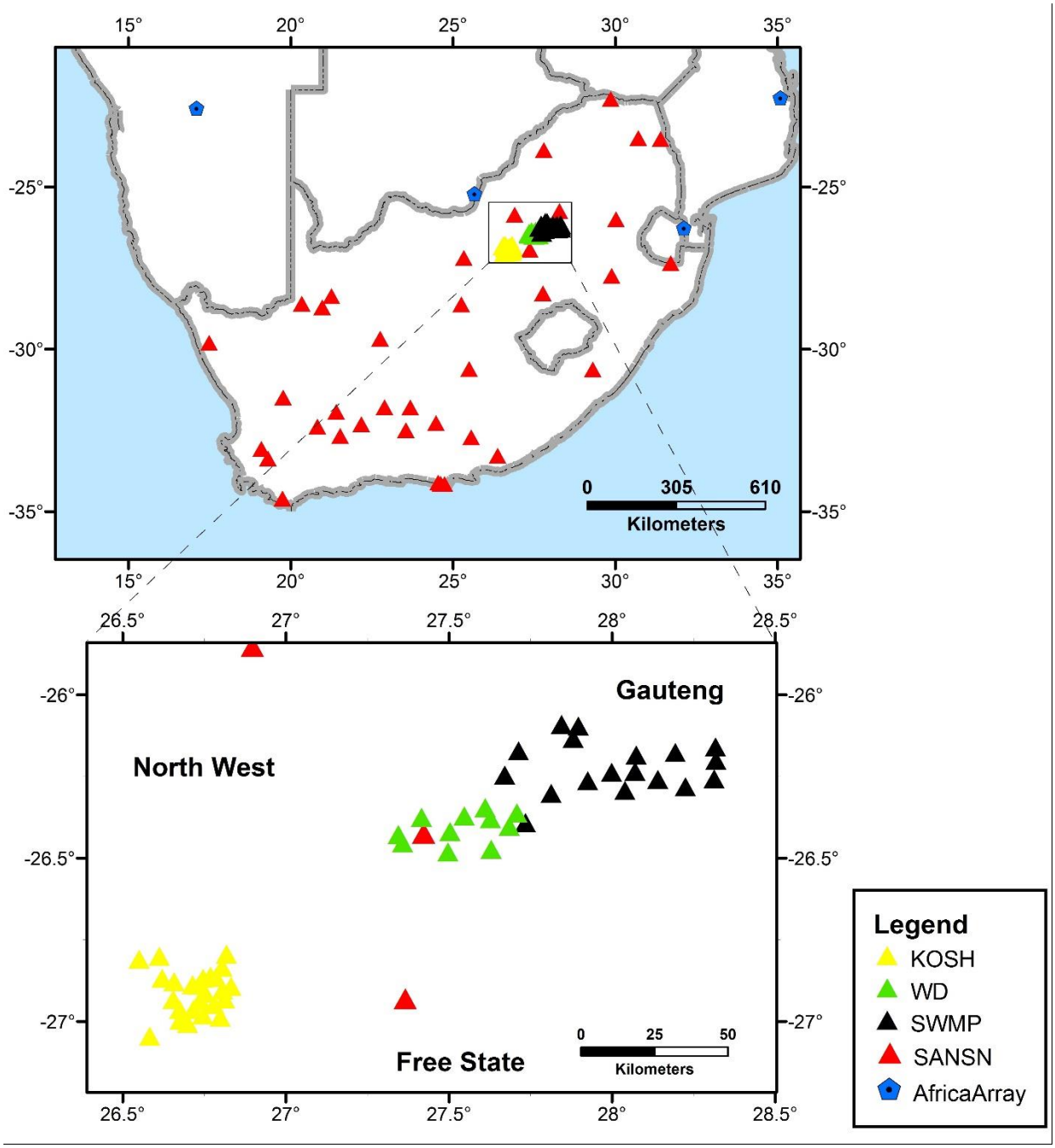


Figure 4-2: Map of the SANSN network. The three cluster networks also shown in the zoomed picture.

4.3. Seismological stations in neighbouring countries

Apart from the SANSN data, a number of networks in neighbouring countries also contributed data to this catalogue, an overview of which is given in Table 4-2. However, after the establishment of the SANSN, the importance of these stations became increasingly marginal due to the densification of the local network, and their contributions are essentially through inclusion in the listings of global agencies.

Table 4-2: Overview of seismological stations in neighbouring countries.

Country	Network/Stations	Contributions to the Johannesburg catalogue
Zimbabwe (+ Zambia, Malawi)	Goetz Observatory, Bulawayo, network from 1959 onwards. Included stations in present-day Zimbabwe (BUL, CIR, MTD, KRR), Zambia (BHA) and Malawi (CLK). From 1959 to 1964, the data was analysed at BPI, after which the responsibility was passed on to the Goetz Observatory.	Main contributor outside South Africa of regional seismological data. Epicentral solutions and magnitudes were determined for both local and regional events. Early studies of regional attenuation (Henderson, 1974; Chow *et al.*, 1980)
Mozambique	Station LMM at Maputo from 1951 onwards. Station CNG at Changalane operational from the mid-1950s onwards, regularly providing readings to the ISC.	Data from these stations helped to constrain the locations of some of the early events in the catalogue. Provided some phase readings to the ISC.
Namibia	Station WIN at Windhoek station since 1951. Modern network provides readings to ISC.	Recordings from this station were routinely incorporated into the South African bulletins. Routine data exchanges with South Africa continue to the present day.
Botswana	Permanent station in Lobatse (LBTB) near the South African border.	Data incorporated in SANSN analyses.

4.4. Global seismological agencies

In addition to local and regional sources, information about source parameters of South African earthquakes can be retrieved from compilations of earthquakes determined at the global scale by international agencies. These sources are reviewed below.

4.4.1. International Seismological Summary (ISS)

The South African stations regularly contributed to the International Seismological Summary (ISS), which constitutes one of the main sources of information for instrumentally recorded earthquakes in the time period between its inception in 1918 and the establishment of the World Wide Standardised Seismographic Network (WWSSN) in the 1960s. Phase data from the ISS summaries were used for the determination of source parameters for large events between 1918 and 1964. Manzunzu and Midzi (2015) used these summaries to discard the so-called 1919 Swaziland earthquake, which was in the South Africa earthquake database as an M_S6.5 earthquake, where M_S indicates a surface wave magnitude.

4.4.2. International Seismological Centre (ISC) bulletin

The International Seismological Centre (ISC) was formed in 1964 concurrently with the establishment of the WWSSN. Its mission was to continue the gathering of instrumental recordings worldwide, previously undertaken by the ISS, in order to calculate source parameters that are well constrained. The ISC Bulletin typically presents the source parameters calculated by the individual

agencies contributing the data, followed by a reappraised solution considering all available data as calculated by ISC staff.

For southern Africa, the ISC bulletin lists source parameters from 1964 onwards, contributed mainly by the CGS and the Goetz Observatory at Bulawayo (BUL). The National Earthquake Information Center (NEIC) of the US Geological Survey also contributes solutions for larger events, but these have been found not to be as well constrained and hence less reliable than the ISC solutions as far as southern Africa is concerned (Johnston et al., 1994). The ISC maintains seismic databases containing data from worldwide seismic networks. The data is available freely online on the following website http://www.isc.ac.uk/iscbulletin/search/catalogue/.

4.5. Previous catalogue compilation efforts

Besides systematic compilations of instrumentally recorded data released by the operating networks described above, a number of regional earthquake catalogues based on instrumental recordings and on reports of felt effects were compiled. These cover in particular the historical (pre-1900) and early instrumental (1900-1969) periods. South African researchers have collected a number of local contemporary reports of historical earthquakes over time.

4.5.1. Early seismological compilations

Early seismological compilations, whether contemporary with the events compiled, or collated later, are the principal contributors of data up to 1970. An important aspect to acknowledge is the overlap and interdependencies that exist between these different compilations, as noted in Albini (2012), in order to avoid treating related assessments as if they were independent. Table 4-3 provides a summary overview of these compilations, highlighting the type of information provided as well as the links between the different studies.

Table 4-3: Summary of seismological compilations dealing with pre-SANSN earthquakes.

Reference(s)	Description	Information provided
Wood (1913), Finsen (1950)	Summary of the information gathered at the Union Observatory in Johannesburg, predominantly based on macroseismic information gathered from newspaper clippings or reports sent by members of the public to the observatory. Some instrumental information included. Finsen (1950) also includes a compilation of earthquake reports in historical sources.	Dates and summary of felt reports with associated locations, occasionally instrumental radii. Finsen (1950) whenever possible provides coordinates for epicentral locations and locations of intensity observations, but not magnitudes. Wood (1913) includes isoseismal maps for 3 events.
Sieberg (1932)	The global compilation by Sieberg (1932) listed some events for the 20th century that match the local records of Wood (1913) and Finsen (1950). Earlier listings of unknown origin mostly redundant or erroneous.	Dates and summary of felt observations, some with intensity assignments. Summary map of felt areas. Isoseismal map for 1912 Koffiefontein event.
Krige and Maree (1951)	compilation of individual studies of eleven events having occurred in South Africa between 1938 and 1944	
Gane and Oliver (1953) and Oliver (1956)	They listed earthquakes in the southern Africa region reported at the Union Observatory and the Bernard Price Institute of Geophysics from 1949-1952 as well as 1953-1955. Exact locations (i.e., epicentral coordinates) are only provided for a subset of events, for which recordings at three or more stations are available. For the other events, the earthquake location is given only as a geographical region, sometimes supplemented by the distance from a single station.	These catalogues also list local magnitude (M_L) values for some of the larger events but is not clear on how they calculated the magnitude. However, Johnston et al. (1994) noted that the values of M_L listed by Gane and Oliver (1953) and Oliver (1956) were likely to have been inferred from maximum intensity values.
Fernández and Gúzman (1979)	First catalogue systematically listing times, epicentral coordinates and magnitudes for events in southern Africa, covering South Africa and neighbouring countries (Namibia, Botswana, Zimbabwe, Mozambique). Reappraises previous South African studies as well as including additional information gathered from archival records and seismological sources.	Epicentral coordinates and magnitude estimates in terms of local magnitude M_L, along with epicentral intensity values.
Ambraseys and Adams (1991, 1992)	Ambraseys and Adams (1991, 1992) reappraised the macroseismic and instrumental data for a number of larger events located south of 20°N that occurred in the time period 1900-1930.	Review of intensity data. Reappraised locations and magnitudes based on re-examination of intensity and the limited instrumental recordings available.
Turyomurugyendo (1996)	Catalogue developed for the Eastern and Southern Africa Global Seismic Hazard Assessment Program (GSHAP) study (Midzi et al., 1999)	Source times, epicentral coordinates and magnitudes. Magnitudes expressed uniformly in terms of surface-wave magnitude M_S, but the consistency of the conversions applied and their applicability to the South African region was not tested within that study.
Brandt et al. (2005)	Update of the Fernández and Gúzman (1979) catalogue, revising the source parameters of historical earthquakes from the Finsen (1950) studies.	Epicentral coordinates, epicentral intensities and magnitudes expressed in terms of the M_L scale, in some cases converted from magnitude values determined using other magnitude scales.
Singh and Hattingh (2009)	Collected intensity information and created isoseismal map for earthquakes that occurred from 1932 to 2005.	14 events with maximum intensities up to VII were compiled
Albini (2012) and Albini et al. (2014)	Detailed study of the seismicity of the	Individual studies of 30 events in the

	Southern and Eastern Cape regions was undertaken specifically for the Thyspunt Nuclear Site Project. This study focused in particular on the seismic history of the region, collecting negative as well as positive evidence in order to establish historical catalogue completeness.	time span 1850-1936, including macroseismic intensity points where relevant (435 IDPs at 277 locations).
Midzi et al. (2013)	Compilation of macroseismic information for earthquakes with instrumental locations in South Africa	57 earthquakes that occurred from 1964 to 1981 were re-assessed
Strasser et al. (2015)	Detailed study on source parameters for earthquakes that occurred in the Koffiefontein region using macroseismic information	5 earthquakes relocated using third generation macroseismic analysis method
Mulabisana (2015)	Compiled a homogeneous declustered catalogue which includes all available events, i.e. historical, and instrumental events from 1690 to December 2011 for southern Africa (i.e. South Africa, Namibia, Lesotho, Botswana and Swaziland)	This is the first regional catalogue for Southern Africa. It contains 932 events with $M_W \geq 4$ whereas GSHAP had only 100 events with $M_S \geq 4$ in Southern Africa. It completely removed earthquakes within mining regions that were below magnitude 4 as a way of dealing with induced seismicity.

4.5.2. Studies of individual events

Prior to the establishment of the SANSN, the staff of the South African Geological Survey (now CGS) described more notable events in a number of monographs. These monographs focus predominantly on macroseismic information, but also present instrumental phase readings when available. They include the monograph about the 31 December 1932 Cape St Lucia earthquake by Krige and Venter (1933), the 12 and 16 January 1936 Swaziland and Fauresmith events by Krige (1936). Von Veh (1988) analysed 33 new events along the KZN coastal region. The MSc thesis of Jensen (1991) contains monographs of three African events that occurred in the stable part of the continent, including the 1 July 1976 Koffiefontein event. A number of more recent studies investigate the source parameters of a few moderate South African events (Fan and Wallace, 1995; Bowers, 1997; Brandt and Saunders, 2011, Midzi et al., 2015a; b; Manzunzu et al., 2017), but with a strong focus on mining-related events.

4.6. Catalogue Compilation

Using the data sources listed in the previous section, a catalogue was compiled using the following rules and criteria. In the case of multiple determinations of the source parameters (date, location and magnitude), all possible options were reviewed and the solution considered the best constrained and/or the best documented was retained as the preferred solution, with the remaining data informing parameter uncertainty. Where duplets exist, the CGS solution was preferred for reasons of completeness and consistency. Two events were considered identical if they describe earthquakes that lie within a period of 20 s and a space-frame of 50 km of each other. The estimated magnitude

for these identified identical events usually corresponded well, though some exceptions were found to differ by close to ±1 magnitude unit especially for events before 1970.

The specific assumptions made in the determination of source parameters for each subset are detailed in the following sections. The catalogue was divided into the following three subsets to reflect the varying nature of the information on which the estimation of source parameters is based:

- **Historical period:** This subset includes all events reported that occurred prior to the installation of the first seismograph in South Africa at the Royal Observatory of the Cape of Good Hope in Cape Town in August 1899.
- **Early instrumental period:** This subset includes all events in the study region starting with the first instrumentally recorded South African earthquake, from 1899 up to 1969.
- **Modern instrumental data:** This subset includes all events recorded since the establishment of the SANSN in 1970.

The assessment of historical and early instrumental periods is mainly influenced by the availability of macroseismic information. Several studies have investigated source parameters for historical and early instrument earthquakes in South Africa (e.g. Krige and Venter, 1933, 1936; Krige and Maree, 1948; Gane and Oliver, 1953; Oliver, 1956; Theron, 1974; Fernández and Guzman, 1979; Brandt et al., 2005; Albini et al., 2014; Strasser et al., 2015; Manzunzu et al., In press).

4.6.1. Historical (pre-1899) data

The assessment of source parameters for this subset is based exclusively on macroseismic data (Wood, 1913; Finsen, 1950; Brandt et al., 2005; Albini, 2012). For events falling into this period, the primary source of data is the compilation by Brandt et al. (2005), which builds on work by previous authors, and in particular the compilation by Fernández and Gúzman (1979) by incorporating information that had not been available to these earlier authors. Most of the events in this period were analysed using the 1st generation method. The magnitudes were inferred from the observed maximum intensity value (Fernández and Gúzman, 1979). The conversion to local magnitude was carried out using an empirical relation by Gutenberg and Richter (1954):

$$\mathbf{M_L = \frac{2}{3} I_0 + 1.0} \qquad 4\text{-}1$$

where M_L is the local magnitude, and I_0 is the macroseismic intensity at the epicentre. The maximum observed intensity I_{max} is often used as a proxy for I_0, although in cases of sparse data coverage this value might be smaller than the true value of I_0, resulting in the underestimation of the magnitudes.

Therefore, the obtained and reported magnitude values have to be considered lower bound estimates. For our study region, only eleven events were recorded during this period.

4.6.2. Early instrumental (1899-1969) data

The primary source of information for the early instrumental dataset is the compilation by Brandt *et al.* (2005) complemented by information from the ISC. The data for this period (1899 to 1969) can be split into two subsets, with the split being defined by the establishment of the first national seismograph network operated by BPI in 1949.

From 1899 to 1949, the approach adopted is very similar to that of the historical period. For larger events, macroseismic information is in some cases supplemented by instrumental information from the two South African seismographs and early global networks. Due to the sparse distribution of the seismograph stations as well as recording limitations stemming from instrument characteristics, this early instrumental information is mostly useful for confirming the occurrence of seismic events, and to provide constraints on the magnitude, with epicentral locations still largely controlled by macroseismic data.

For the later part of the time span (1949 to 1969), the locations determined by the BPI using the five-station Geological Survey network represent the preferred solutions for South African events when they are available. For some events, these solutions also considered the recordings on the Wiechert seismograph at the Union Observatory in Johannesburg. The quality of the solutions depends mainly on the number of stations available, and thus improves with the magnitude of the event. It is noteworthy that the epicentral locations published in Gane and Oliver (1953), Oliver (1956) and the BPI Seismological Bulletins include confirmatory macroseismic evidence where available, and that the authors include information regarding the quality of the solution. Where additional macroseismic data was available from the compilation of De Klerk and Read (1988) or other sources investigated as part of the compilation of the intensity database described in Midzi et al. (2012), these data were used as an additional check on the BPI instrumental location and uncertainty estimate. Three hundred and eighty-six early instrumental events were identified and their spatial distribution is shown in Figure 4-3.

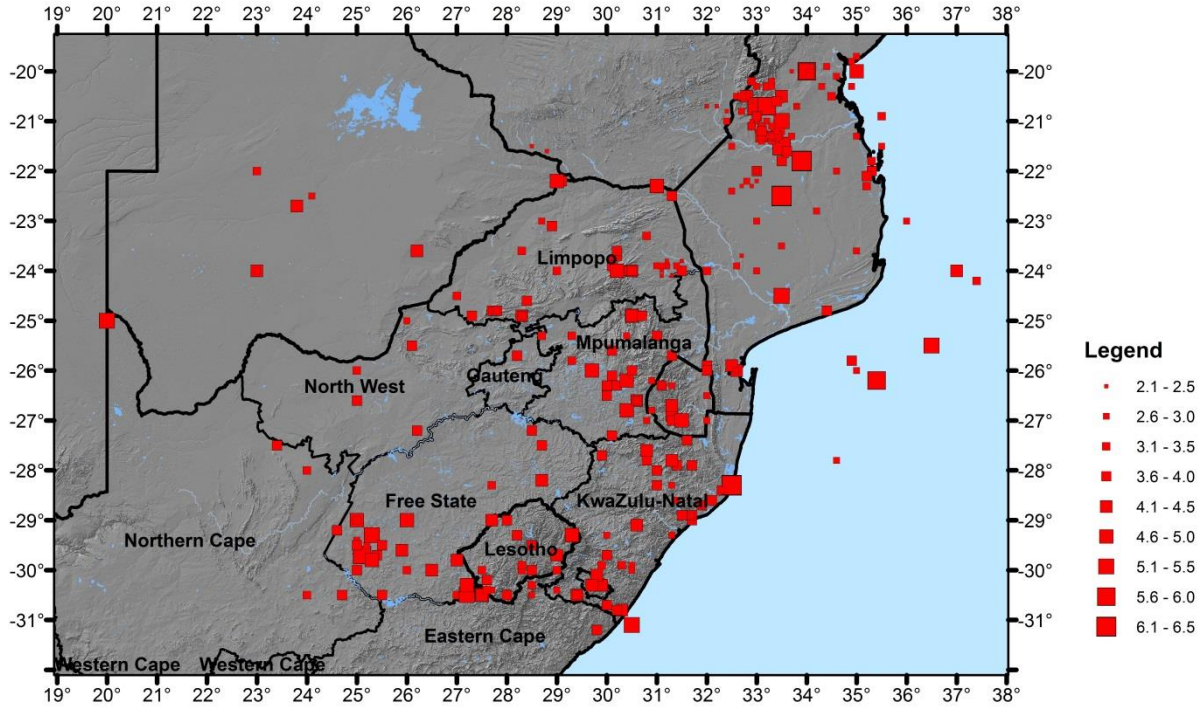


Figure 4-3: Seismic events of the early instrumental period (1899-1969) that occurred within the region of interest in southern Africa (Brandt et al., 2005 and references therein; Midzi et al., 2012).

In an effort to improve historical and early instrumental catalogue, some additional earthquakes were reanalyzed in this study (Manzunzu et al., In Press). A summary of the analysis is given in the next section.

4.6.2.1. Reappraisal of earthquakes with available macroseismic data

Macroseismic intensity information is the key to evaluating historical seismicity. However, this information is not always reliable since it relies on human perception. A number of methods for evaluating source parameters of historical earthquakes have been developed and these methods depend largely on the distribution of the intensities, number of intensities as well as their locations (Musson, 2009; Gasperini et al., 1991). Musson (2009) defined three levels of methods (1st generation, 2nd generation and 3rd generation) used for source parameter estimation of macroseismic information. These methods differs according to the complexity in their analysis (Strasser et al., 2015).

1st Generation: Based on a single intensity assignment. The earthquake location is assigned to the location of the epicentral intensity, I_o, whilst the magnitude is also inferred from, I_o. I_o is defined as the epicentral intensity value. However, in many cases a slightly different parameter is used, I_{max}, the maximum observed intensity value. Many of the historical parameters in the CGS database were

determined using this parameter (Krige and Venter, 1933, 1936; Krige and Maree, 1948; Gane and Oliver, 1953; Oliver, 1956; Theron, 1974; Fernández and Guzman, 1979; Brandt et al., 2005). It should be noted though that this value, I_{max}, is very much dependent on location of population as well as type of building structures in the settlements. Thus in some cases I_{max} actually results in an underestimate of an earthquake magnitude, such that the values published can be considered the minimum possible values.

2nd Generation: Based on isoseismals created using all available intensity values. Source location is assigned at the centroid of isoseismals, whilst the magnitude is estimated from the area enclosed by the isoseismals (Gasperini et al., 2010). The determination of isoseismals is not a straightforward method hence determination of source parameters is not very reliable. Singh and Hattingh (2009) assessed thirty two earthquakes in South Africa using the 2G methodology.

3rd Generation: Based on techniques that interpret the distribution and magnitude of intensity values. These techniques utilizes IDPs evenly distributed for location and magnitude determination (Musson 2009). Ideally, 3G methodologies assume radial distribution of seismic energy from the source thus the more concentric intensity levels the better constraint the solution. Four of these techniques are implemented in the MEEP2 software (Musson, 2009) and are outlined below.

- *The Macroseismic Estimation of Earthquake Parameters (MEEP) approach (Musson, 2009).* It combines the Köveslingethy's (1906) equation with the Frankel (1994) model. Köveslingethy's (1906) equation links the average spacing of isoseismal contours to regional attenuation properties, whilst Frankel's (1994) model allows the estimation of magnitude based on felt area.
- *The Bakun and Wentworth (1997) approach.* It is based on an intensity prediction equation (IPE), which gives macroseismic intensity as a function of magnitude and distance.
- *A Centroid method, which is based on the BOXER algorithm of Gasperini et al. (1999).* It determines the optimal epicentral location based on the spatial distribution of the IDPs with the highest intensity levels.
- *Pairwise comparisons of IDPs*, It favours epicentral locations closer to the IDP with the highest intensity. Musson (2009) implemented this method in his MEEP2 software.

A review was conducted for pre-selected historical and early instrument earthquakes that had enough macroseismic information to be reanalyzed using state of the art 3rd Generation techniques to determine their source parameters (Manzunzu et al., In press). The source parameters obtained in this study were determined using currently available IDPs (Flint, 2017). It should be noted that intensity

values discussed in this study were assigned according to the Modified Mercalli (MMI-56) intensity scale (Richter, 1958). A summary of the analysed events is shown below (Table 4-5).

Forty-six earthquakes with at least eight IDPs were analyzed using the 3rd Generation techniques in Manzunzu et al. (In press). For each event, the spatial distribution and intensity values were used in the determination of the source parameters. Of the events already in the catalogue, our analysis was compared with the original solutions as we had new IDP that help in obtaining improved solutions. It was observed in this study that significant variations of solutions were obtained using different methods. For each event, the locations and magnitudes obtained from the different methods were combined to obtain the best estimate values using event specific weights as suggested by Strasser et al. (2015).

An improvement to the current CGS database is evident as more events that occurred in the early instrumental period but were not recorded by the sparse network are located. These results ascertain the fact that macroseismic information still plays an important role in earthquake location. Some improvements in the new locations with events being clustered in present day known sources of seismicity. Magnitudes are generally higher than previously determined. However, not all analyzed events produced reliable solutions. This was observed for earthquakes that had a single intensity value and were located very close to each other. The newly computed locations are shown in Figure 4-4. The obtained solutions are shown in Table 4-4. A number of the events had poor intensity distribution making it difficult to analyze; however, the MEEP2 software tried to optimize the solutions by performing bootstrap analysis (Musson, 2009). A number of events near Johannesburg had high intensity values at close distances but were barely perceptible 30 km away. These indicate small earthquakes at shallow depths (Musson, 2008), very likely related to mining activity. These events attenuate fast, as evidenced by a few localised IDP on a number of events.

Table 4-4: List of earthquakes analysed in this study with the newly determined source parameters.

ID	Time of the event					Previously published locations by CGS			Solutions obtained in this study				Province
	Year	Mon	Day	Hr	Min	Lat	Long	Mag	Lat	Long	Mag	Rank	
1	1870	8	3	13	20	-28.3	29.1	5.0	28.25	29.42	5.5	2	KZN
2	1903	7	31	20	43				-28.84	24.88	4.8	2	NC
3	1906	12	10	8	12	-26.9	31.3	4.3	-26.67	31.13	5.3	2	ESWAT
4	1908	2	2	22	25				-26.19	28.07	3.0	3	GP
5	1908	2	7	18	20				-26.25	28.05	3.4	3	GP
6	1908	9	10	17	53				-26.18	28.04	2.8	2	GP
7	1908	9	24	18	50	-24	30.5	4.0	-23.81	30.13	3.4	2	LIM
8	1908	9	26	21	7	-29	26	5.0	-29.07	26.00	5.8	1	FS
9	1908	12	25	14	8	-26.0	28.0	3.7	-26.00	27.95	4.1	2	GP
10	1909	6	23	22	25				-26.21	28.02	3.1	2	GP
11	1909	8	5	8	37	-22.2	29	5.0	-22.62	29.09	5.1	2	BOTS
12	1910	3	9	1	29				-26.21	28.03	3.1	3	GP
13	1910	8	16	11	15				-26.21	28.05	3.2	3	GP
14	1910	9	9	13	30				-26.26	27.99	3.0	2	GP
15	1910	10	21	18	40	-30.5	24.7	5.0	-29.50	25.00	6.2	1	NC
16	1912	2	20	13	0	-29.5	25	6.2	-29.50	25.00	6.2	1	FS
17	1912	5	25	18	34				-26.21	28.05	3.1	2	GP
18	1912	5	27	18	43				-26.20	28.06	3.3	3	GP
19	1912	11	16	23	43	-29.7	25.1	4.0	-29.21	25.09	5.7	2	FS
20	1913	3	15	18	28				-26.18	28.06	3.1	2	GP
21	1913	4	5	23	11				-26.20	28.04	2.8	2	GP
22	1913	9	5	14	37				-26.20	28.05	3.1	3	GP
23	1913	12	21	0	28				-26.22	28.06	3.3	3	GP
24	1914	11	11	2	14				-26.21	28.05	3.3	2	GP
25	1914	12	2	21	40				-26.19	28.05	3.0	2	GP
26	1915	1	19	18	32				-26.21	28.07	3.5	2	GP
27	1915	4	19	20	44				-26.21	28.04	3.8	2	GP
28	1915	6	19	21	53				-26.18	28.05	3.7	2	GP
29	1915	6	24	7	49				-26.18	28.06	3.3	2	GP
30	1915	6	28	4	15				-26.20	28.04	3.6	3	GP
31	1916	7	27	17	45	-25.7	31.3	4.0	-25.27	30.93	4.4	2	MP
32	1916	8	27						-26.22	28.07	3.3	2	GP
33	1918	7	17	20	10				-26.21	28.07	3.3	2	GP
35	1924	10	16	1	10				-26.23	28.02	3.6	2	GP

ID	Time of the event					Previously published locations by CGS			Solutions obtained in this study				Province
	Year	Mon	Day	Hr	Min	Lat	Long	Mag	Lat	Long	Mag	Rank	
36	1924	11	25	2	31	-24.9	28.2	3.7	-24.91	28.30	3.9	3	LIM
37	1927	5	2	6	52				-26.20	27.99	3.3	2	GP
38	1928	11	19	18	34				-26.21	28.03	3.6	2	GP
39	1932	8	9			-33.3	26.5	5.0	-33.40	26.50	5.7	1	EC
40	1932	12	31	6	30	-28.3	32.5	6.3	-28.43	32.22	6.1	1	KZN
41	1936	1	12	5	17	-27.00	31.00	5.0	-27.34	31.61	5.1	1	SWAZ
42	1936	1	16	9	32	-29.8	25.3	5.0	-29.40	25.42	5.4	1	FS
43	1938	2	10	20	4	-27.8	31.3	4.3	-28.14	31.75	4.3	2	KZN
44	1940	2	29	23	40	-28.6	28.2	4.3	-28.10	28.85	4.4	2	KZN
45	1940	5	19	18	16	-22.5	33.5	6.2	-22.55	30.78	6.5	2	LIM
46	1940	11	10	21	0	-24	30.2	5.0	-24.12	30.15	5.2	2	LIM
47	1944	11	12	10	55	-29	27.7	4.3	-29.09	27.62	4.5	3	SA-LES

Due to the non-uniform distribution of the IDPs per event, the performance of the 3rd Generation techniques was variable. In this regard, a ranking technique was derived to rank the solutions according to the reliability of input IDPs. The ranking classes are presented in Table 4-5. Earthquakes with a ranking of 1 and 2 have more reliable source parameters and these were added into our current catalogue. For events with a rank of 3, either the original solution was kept or 1st Generation technique was applied since the data could not fit the criteria for 3rd Generation techniques. Solutions with a ranking of 3 need to be improved and continual search of more information is being done.

Thirty-seven earthquakes were assigned a ranking of either 1 or 2, implying high confidence in the obtained solutions. These events were added into our catalogue for further analysis of hazard parameters, while those with a ranking of 3 were recomputed using 1st Generation technique. Although some of the events were assigned a ranking of 3 it was important to note that they did not exist in the current catalogue hence their inclusion is crucial. There were some events that had epicentral locations determined previously from 1st Generation technique and were updated in this study (Table 4-4).

Table 4-5: Quality ranking of the determined source parameters.

Rank level	Description
1	The IDPs are well distributed and have at least 8 IDPs with different intensity levels and the solutions close to each other.
2	The IDPs not well distributed. The intensity levels are evenly distributed or almost similar but few. At least 2 solutions agree.
3	The distribution of IDP is poor and the IDPs have only one intensity value.

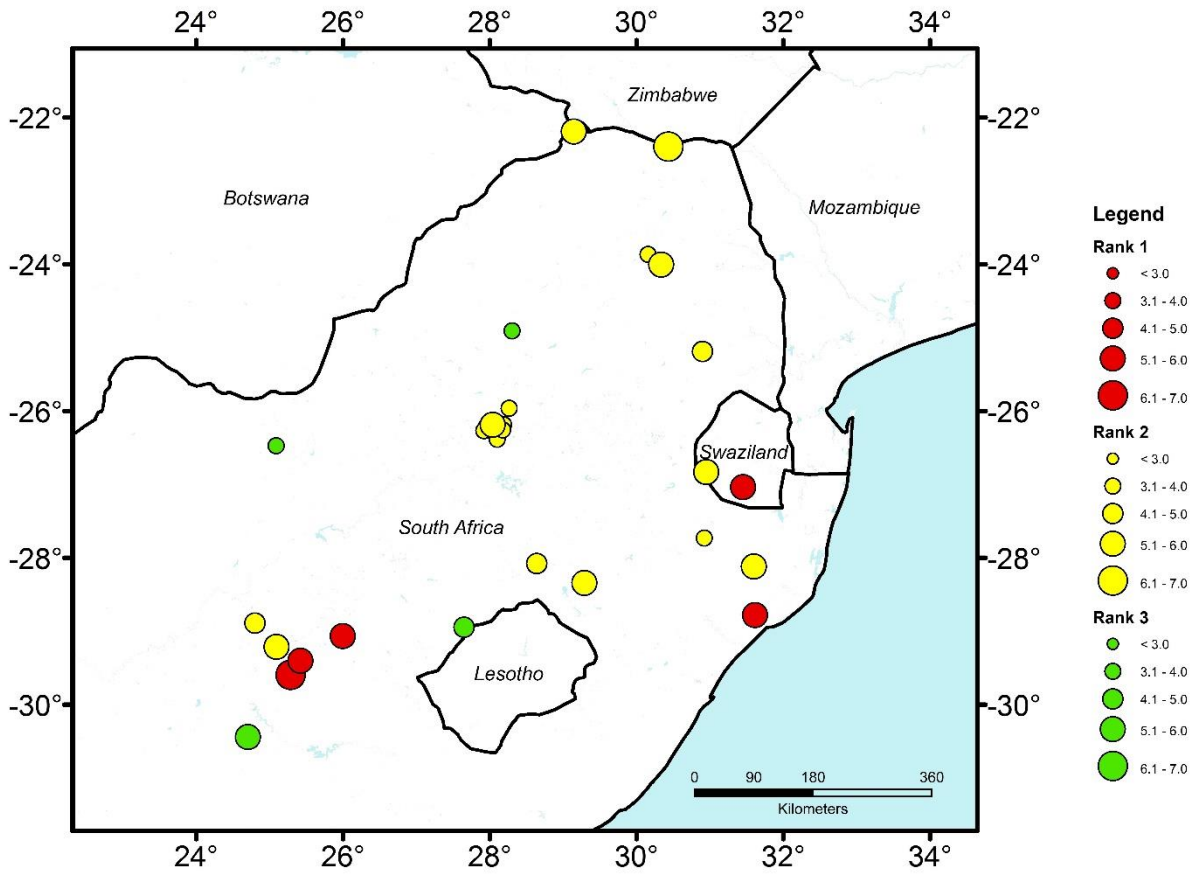


Figure 4-4: The location of the earthquakes with source parameters determined in this study. The earthquakes are shown with their ranking.

These events were added to the current catalogue with historical and early instrumental catalogue. In total 433 events were obtained for the historical and early instrumental catalogue.

4.6.3. Modern instrumental (1970-2016) data

Locations and magnitudes for this period are determined from instrumental data. The primary source of information is the CGS database. Alternative solutions determined by the Goetz Observatory in Bulawayo (BUL) and by the ISC are available for larger events (until 1993 for BUL, until 2014 for ISC). BUL also provides a number of additional events for the period from 1970 to 1983, for which no determinations are available from other agencies.

In the case of multiple solutions, the preferred solution would normally be the ISC solution, since it is calculated using additional data compared to the solutions provided by the individual networks, and thus better constrained. ISC solutions also have the advantage of systematically providing an estimate of the uncertainty associated with the location. Therefore, the following approach for addressing duplicates is adopted:

- If the ISC and CGS epicentral locations are significantly different, macroseismic information is used to support the more credible solution;
- If no macroseismic information is available, or if the difference in location is small, the ISC solution is retained as it is of better quality (smaller location uncertainty and azimuthal gap as a result of using regional and international stations).
- If the solutions do not include the ISC, then the CGS solution is taken.

For the instrumental data between 1997 and 2016, locations determined from fewer than three stations were not included in the catalogue because it was assumed that these locations are azimuthally unconstrained and thus extremely uncertain. Despite the sparse nature of the network, the improved detection thresholds of modern seismographs limit such cases to events with very low magnitudes. The exclusion of these events therefore has no significant impact on downstream applications such as the estimation of recurrence parameters. A total of 61310 events were compiled for the modern instrumental period 1970 to 2016 (Figure 4-5). The seismic catalogue compiled for the region within 500 km radius from Johannesburg contains 61743 earthquakes, which span from 1620 to 2016.

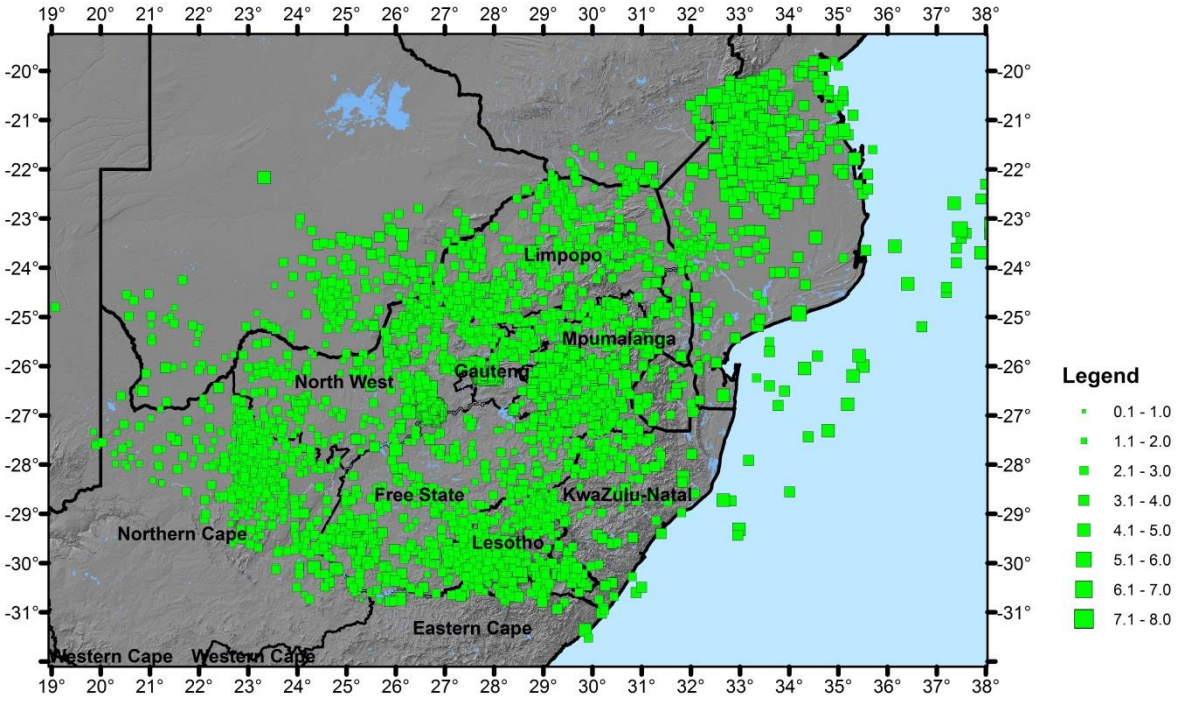


Figure 4-5: Spatial distribution of seismic events that occurred in and around Johannesburg during the modern instrumental period (1970-2016).

4.7. Homogenisation of magnitudes

The catalogue presented in this study was developed in terms of moment magnitude (M_w, Hanks and Kanamori, 1979) for compatibility with future manipulations as part of the seismic hazard analysis, in particular to avoid conversion issues when using modern GMPEs formulated in terms of M_w. The use of magnitude scale that does not saturate is also important in the selection and testing of source scaling relations although this does not affect our catalogue since there are no large earthquakes in our region.

There are, only a handful of large magnitude earthquakes in the catalogue for which a value of M_w has been directly determined from the long-period part of the spectrum of available recordings through moment tensor inversion or waveform modelling. The limited number of such determinations is due to the rare occurrence of events large enough to allow a teleseismic determination, combined with the sparse nature of the local recording network, which usually yields insufficient data for a moment tensor inversion of local events. For those events for which no direct estimate of M_W is available, a conversion was made from the primary magnitude scale to M_W. The most common primary magnitude scales in this catalogue are:

- Local magnitude, M_L (determined by SANSN)
- Body-wave magnitude, m_B (determined internationally by ISC and other agencies)
- Surface-wave magnitude, M_S (determined internationally by ISC and other agencies)
- Magnitude determined by the Goetz Observatory in Bulawayo, m_{BUL}

Additionally, for historical events as well as a number of events from the early instrumental period, M_W was estimated from macroseismic intensity observations. The homogenisation process have been identified as one of the sourcses of uncertainty in the compilation of the seismic catalogue for Johannesburg. This is mainly because the currently available data is insufficient to define magnitude relations for homogenisation. Therefore, global relations are generally used for conversion to M_W.

4.7.1. Conversion from local magnitude

By far the greatest fractions of magnitudes requiring conversion are expressed in terms of local magnitude, M_L, which is the magnitude routinely reported by CGS and its predecessor organisations. According to Saunders et al. (2013), several M_L scales have been used in the calculation of local magnitude as the SANSN evolved. In South Africa, Saunders et al. (2013) derived the first M_L scale calibrated using a selection of high-quality local recordings from tectonic events recorded at a minimum of five stations. In their study Saunders et al. (2013) prepared a new local magnitude relation specifically for South African conditions. Their relation was substituted into the analysis

procedure as from 2012 soon after it was published. Recalculation of the old M_L to the new M_L was not done after the switch since some of the earthquakes in the catalogue did not have period and amplitude values. The derived relation is

$$\mathbf{M_L = \log_{10}(A) + 1.149 \log_{10}(R) + 0.00063R + 2.04 - S} \quad 4\text{-}2$$

where A (mm) is the maximum amplitude, R (km) is the hypocentral distance and S is the station correction term.

Prior to this, South African magnitude determinations were based on the calibration derived for Southern California and strictly speaking applicable only to horizontal components measured on Wood-Anderson seismometers, while until recently the South African instruments consisted predominantly of short-period vertical instruments (Brandt, 1997; Saunders et al., 2013). Prior to 1997, a modified version of the Richter (1935) local magnitude relation was used to estimate magnitude values of South African earthquakes (Saunders et al., 2013; Fernández, 1980). The relation used in South Africa as modified from the Richter equation is given by (Fernández, 1980):

$$\mathbf{M_L = \log_{10}\left(\frac{A_V}{T}\right) + 0.84 \log_{10} \Delta + 1.26} \quad 4\text{-}3$$

where Δ (km) is the epicentral distance. From 1997, the SANSN was upgraded from analogue to digital seismometry, this change introduced the use of the SEISAN software for analysis as well as a new magnitude relation by Hutton and Boore (1987) given by:

$$\mathbf{M_L = 1.10 \log_{10}\left(\frac{r}{100}\right) + 0.00189(r - 100) + \log_{10} A + 3} \quad 4\text{-}4$$

Where r (km) is the epicentral distance and A is the maximum amplitude. Both these magnitude relations were developed for North America although they were applied in South Africa. Given the variation in the local magnitude scales, it was necessary to convert each scale to M_W in order to avoid propagation of uncertainties. Both equations are not similar and hence usually gives different M_L values for the same earthquake. In this regard, each equation was converted to M_W independently.

4.7.1.1. Derivation of the M_L - M_W relations

In order to derive M_L-M_W conversion relations, spectral analysis was performed to a total of 90 well located earthquake events recorded by the temporary network of stations in the South African Seismic Experiment (SASE) project conducted during the period 1996 to 1999 (Figure 4-6; Manzunzu et al., 2020). The moment magnitude values ranged from 2.8 to 4.6 and represent shallow depth events from both mining and tectonic sources. Of these, 38 earthquakes were located in the mining areas and the

rest were of tectonic origin. The data set consists of continuous seismic waveforms at 20 samples per second with triggered waveforms at 100 samples per second in miniseed format from more than 85 stations (Kgaswane et al., 1999). All the events selected fulfilled the requirement of having at least 4 stations recording the S/Lg waves with an adequate signal to noise ratio to identify, from the displacement spectrum, the plateau at low frequencies, the corner frequency and decay for frequencies higher than f_c. The spectral analysis for the derivation of the Mw was done in SEISAN software package (Ottemöller et al., 2018). The same data set was used to compute three different M_L that were used in the SANSN for the comparison with M_W as described in Manzunzu et al. (2020).

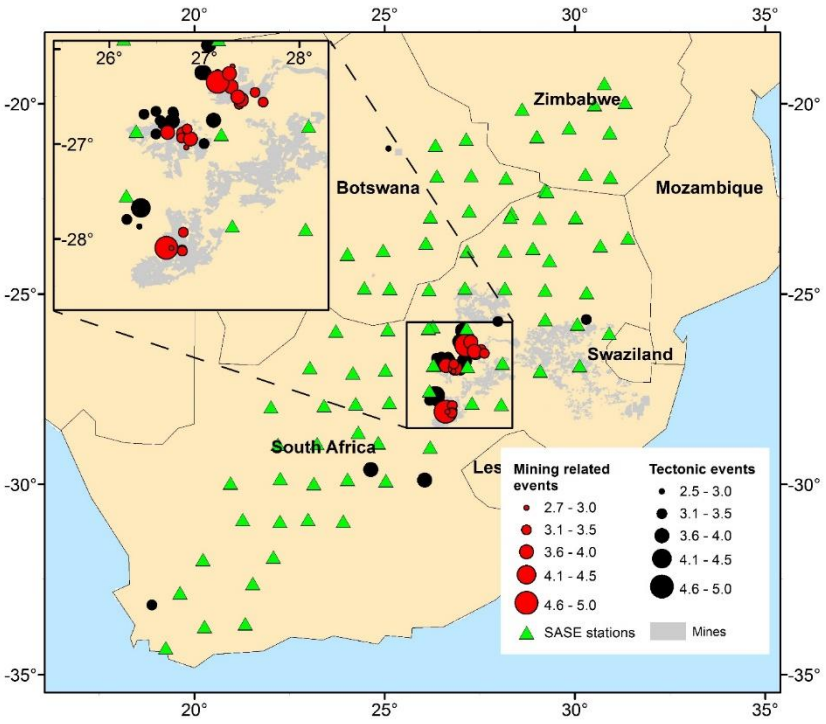


Figure 4-6: Seismological stations of the SASE project shown as green triangles. The circles represent the locations of the epicentres of the seismic events used in this study (red circles indicate mining-related events, while black circles denote tectonic events). The classification is based on the proximity of the event to the mining boundaries (from Manzunzu et al., 2020).

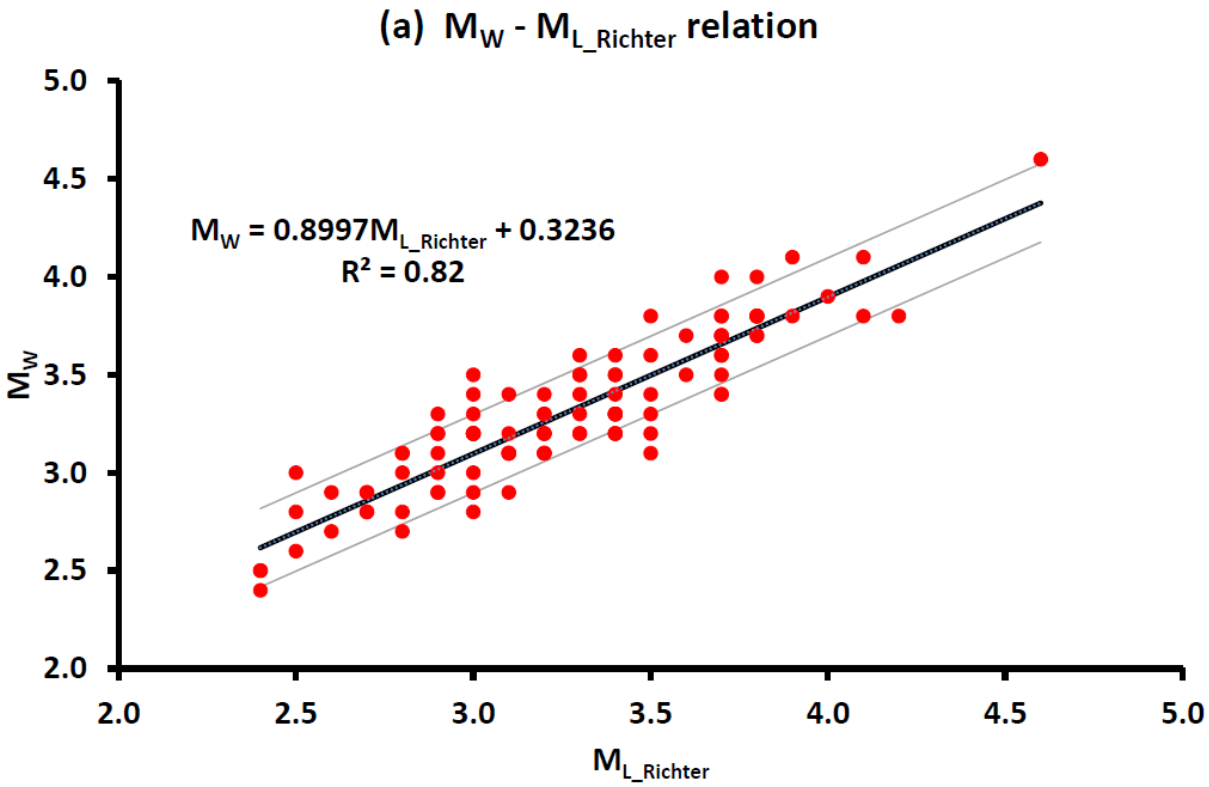
Relations between moment magnitude M_w and the three common local magnitude scales that have so far been used in South African catalogue were developed by Manzunzu et al. (2020) using a generalized orthogonal regression technique since both estimates of M_L and M_w are subject to measurement and modelling errors. The general orthogonal regression relation takes both M_L and M_w errors into account by minimizing the squares of the distances to the best fit line, whereas standard linear regression only considers the squares of the vertical offset (e.g., Das et al., 2012). Three regression relations obtained are:

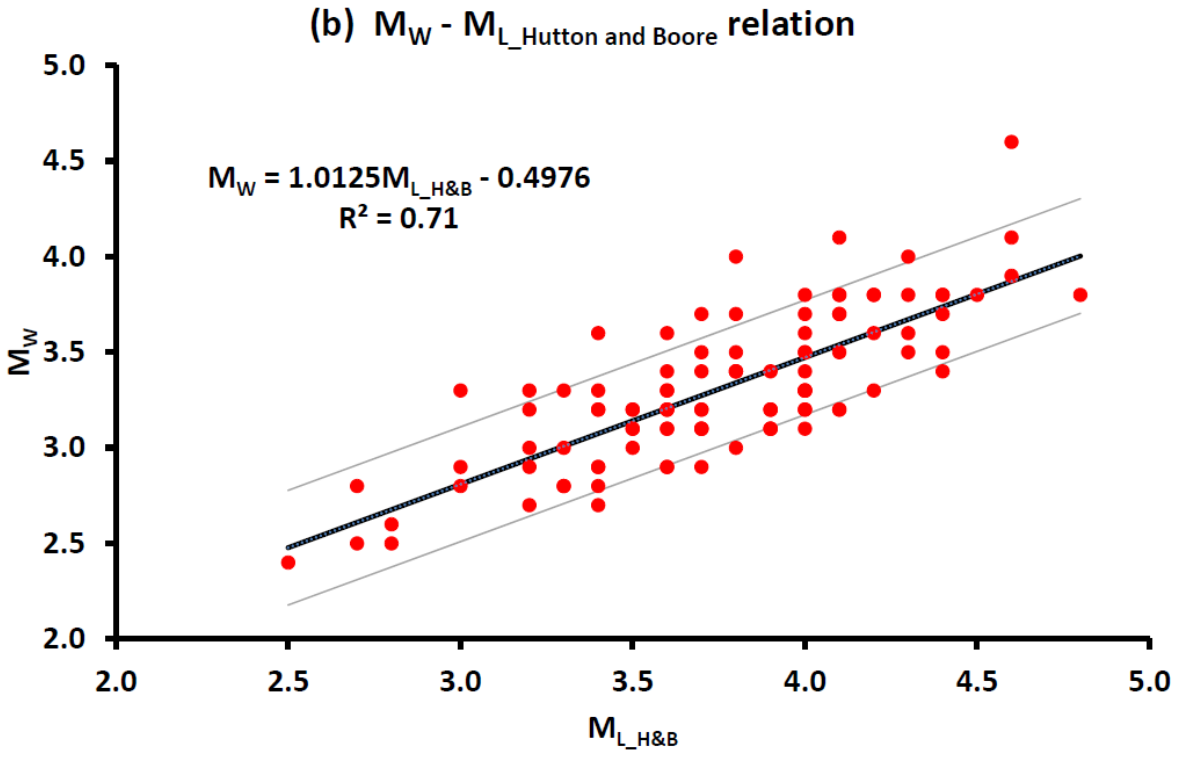
$$\mathbf{M_W = 0.8997 M_{L_Richter} + 0.3236} \qquad 4\text{-}5$$

$$\mathbf{M_W = 1.0125M_{L_{HuttonandBoore}} - 0.4976} \quad \text{4-6}$$

$$\mathbf{M_W = 1.0957M_{L_Setal} - 0.4409} \quad \text{4-7}$$

The three relations indicate that M_W is lower than M_L for all M_L relations used in South Africa. M_{L_Setal} by Saunders et al. (2013) seems to be closer to M_W than the other two scales. This observation might be in agreement with the conclusions made by Deichmann (2006) in which he postulated that M_W is proportional to M_L over the range $4 < M_L < 6$. Table 4-6 shows the periods where each equation can be applied in the homogenisation process. These are the time periods that the equations were used in the routine magnitude determination.


(a) M_W - $M_{L_Richter}$ relation
$M_W = 0.8997M_{L_Richter} + 0.3236$
$R^2 = 0.82$
M_W
$M_{L_Richter}$
5.0
4.5
4.0
3.5
3.0
2.5
2.0


(b) M_W - $M_{L_Hutton\ and\ Boore}$ relation
$M_W = 1.0125M_{L_H\&B} - 0.4976$
$R^2 = 0.71$
M_W
$M_{L_H\&B}$
5.0
4.5
4.0
3.5
3.0
2.5
2.0

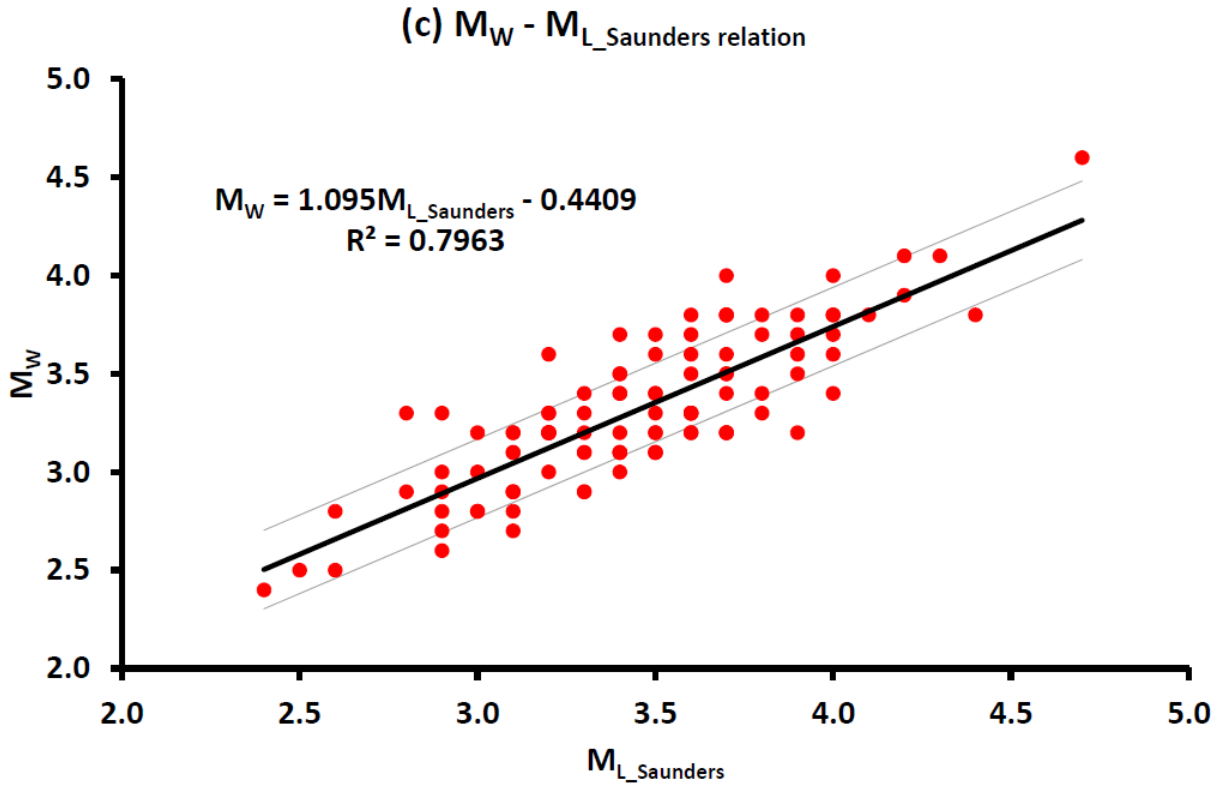


Figure 4-7: Regression analysis of moment magnitude (M_w) calculated in this study and the local magnitudes (M_L) used by the SANSN for the compiled data set as shown in Table 2. (a) Comparison of M_W to M_L as derived using the Hutton and Boore (1987) relation, (b) Comparison of M_W to M_L as derived using the modified Richter relation (Fernández, 1980), (c) Comparison of M_W to M_L as derived using the Saunders et al. (2013) relation.

The scatter in the observed data indicates the uncertainties associated with the derivation of the relations. These uncertainties, as indicated in equations 4-5 to 4-7, are captured and should be incorporated when homogenising the rest of the catalogue. For the homogenisation to be done, the catalogue was split into three sets, the first one 1970 to 1997 was converted using equation 4-5, the second one from 1997 to 2012 was converted using equation 4-6 while the other set 2012 to 2016 was converted using equation 4-7.

Table 4-6: The derived M_L- M_W relations and their period of validity for homogenisation.

Equation	Homogenisation period	Comments
$M_W = 0.8997M_{L_Richter} + 0.3236$	1970 – 1997	Original Richter relation derived for Southern California.
$M_W = 1.0125M_{L_{HuttonandBoore}} - 0.4976$	1997 – 2012	Derived for Southern California.
$M_W = 1.0957M_{L_Setal} - 0.4409$	2012 – present	M_L derived with South African data

To test the efficiency of the derived magnitude relation equations, two catalogues were computed and used for sensitivity analysis. One catalogue was developed using the newly determined conversion relations while the other one was developed using a global relation.

4.7.2. Conversion from body-wave magnitude M_B

For a small number of events in the catalogue, teleseismic body-wave magnitudes have been calculated by ISC and/or NEIC (or its predecessors). The ISC determinations are generally preferred as being based on a larger number of stations. For a fraction of the events for which M_B was determined, a moment magnitude value is usually available. The available M_B-M_W data are compared with the published conversion relations of Das et al. (2011) and Johnston (1996) for SCR, as well as the global relation of Scordilis (2006), all of which are shown beyond their range of applicability in Figure 4-8. Note that this comparison plot of available data versus existing M_B-M_W relations is used not so much to select the most appropriate M_B-M_W relation (which is precluded by the paucity of the data), but simply as a check that imported relations are not in contradiction with the very limited number of local data available. Out of the three relations available, the Johnston (1996) relation appears to be the best-behave and was therefore chosen for the conversion.

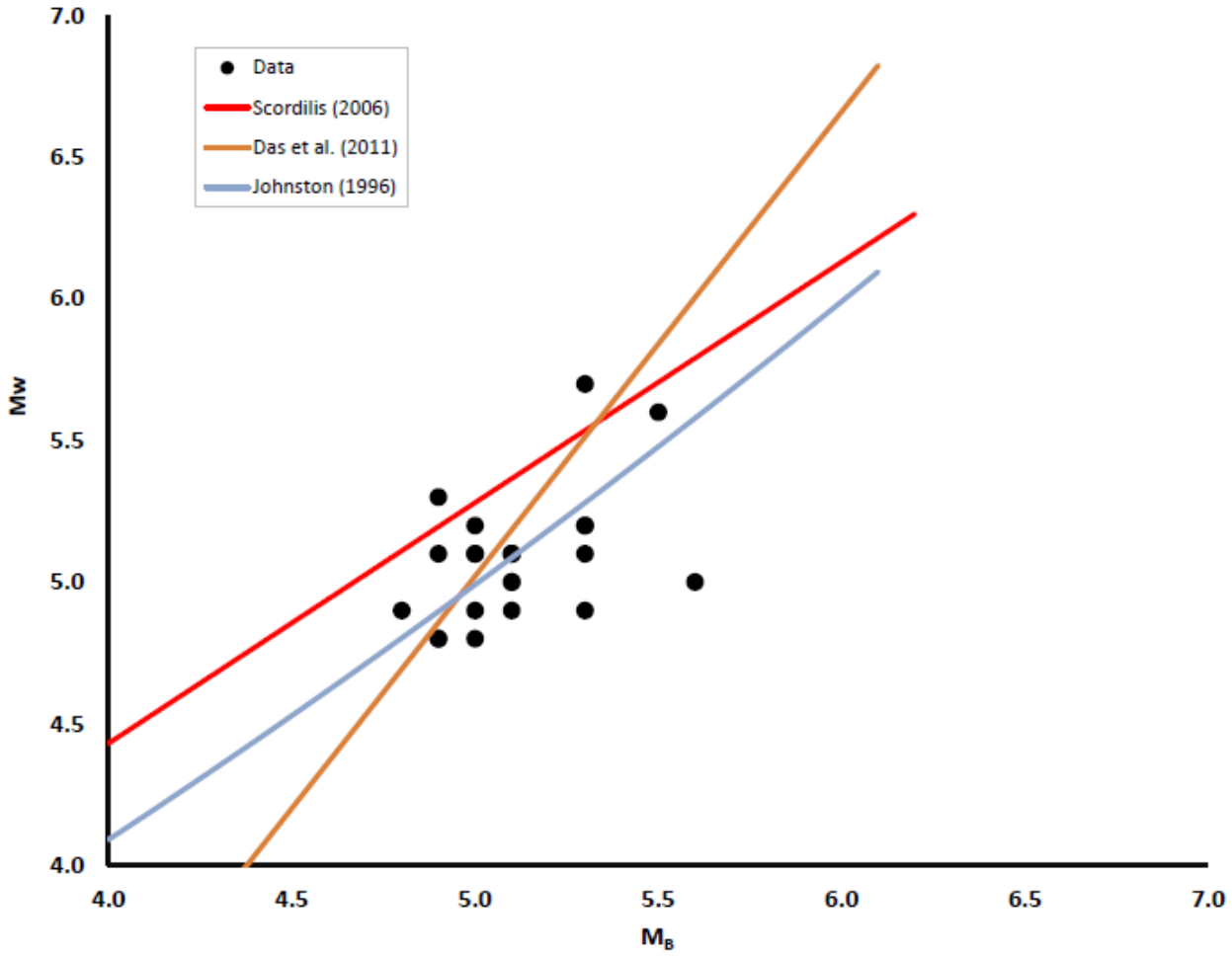


Figure 4-8: Comparison of M_B-M_W data in study region with the three global relations Scordilis (2006) (red line), Das et al. (2011) (orange line) and Johnston (1996) (blue line).

4.7.3. Conversion from surface-wave magnitude M_S

The conversion from surface-wave magnitude M_S is included here mainly for the sake of completeness, since for the modern instrumental data, estimates of M_S are only available for events large enough to have an M_W estimate, thus not requiring conversion; these generally support the M_W=M_S scaling assumed for larger events in published conversion relations (e.g., Scordilis, 2006).

The ISC catalogue contains multiple events for which mutual estimates of M_W, M_S, and M_B are given. In that case the original M_W value is of course kept. If values for both M_B and M_S are available, M_W is preferably derived from M_B using the Johnston (1996) relation.

4.7.4. Conversion from Bulawayo magnitude M_{bLg}

Another instrumental magnitude scale for which a conversion is required is the magnitude calculated by the Goetz Observatory in Bulawayo based on the data registered by the network of stations located in present-day Zimbabwe, Zambia and Malawi. This conversion concerns events that occurred in the late 1960s and early 1970s, for which no other reliable estimate of magnitude is available. This magnitude is close to an m_{bLg} magnitude (Nuttli, 1973).

Given the excellent agreement found between these magnitude values and the body-wave magnitude (m_B) values determined by the US Geological Survey (Goetz Observatory, 1972), these values were treated as equivalent to m_B values and converted to moment magnitude using the relation developed by Johnston (1996).

4.8. Treatment of uncertainties in the compiled catalogue

The process of compiling an earthquake catalogue for seismic hazard analysis brings in many uncertainties that needs to be taken into account when calculating the hazard. Each step in the catalogue compilation needs to be assessed on the sources and influence of the uncertainties. Presented in this section is the scheme implemented to assess and classify the uncertainties associated with the magnitude and locations of the seismic events included in the catalogue presented in this study. A subset of the catalogue was selected for the assessment of the uncertainties.

4.8.1. Location Uncertainties

Uncertainty in the location influences the delineation of seismic zones. Identification of seismic source zones requires accurately located earthquakes, especially for our region where active faults are not mapped and active zones are delineated in terms of seismicity. Therefore, if events are not well located it becomes difficult to delineate the zones. Earthquake location uncertainties are routinely determined as part of the location process. CGS provides estimates in terms of latitude and longitude error, whereas ISC provides the dimensions of the major and minor axes of an error ellipse, S_{maj} and S_{min}. The error ellipses for the events in the current dataset are mostly oriented NS or EW, hence the CGS and ISC location error parameters can be considered equivalent. For ease of comparison with the uncertainties determined from macroseismic data, which are expressed as radii, equivalent error radii are defined by taking the geometric mean of the two location error parameters and used as estimates of the location uncertainty.

For determinations based on instrumental data, the quality of the location depends critically on the number of stations, their distance to the source, as well as their azimuthal distribution (Midzi et al., 2020). The best-constrained solutions are obtained from dense, close-in networks surrounding the source. The CGS has recently installed three cluster networks within the mining regions that have good stations distribution. This have since improved location uncertainty in events within the mining regions.

4.8.2. Relocation of instrumental earthquakes

To constrain our location uncertainty, especially for older events, 500 (2000 to 2013) events with phase data at more than five stations were selected for relocation. The data for all these events were reanalysed using the SEISAN software and earthquake epicentres determined through the iterative, least squares method using the HYPOCENTER routine (Lienert and Havskov, 1995). A comparison was made of the new source parameters (epicentre, magnitude, errors) to the existing CGS parameters. The comparison of the epicentres is shown in Figure 4-9 and Figure 4-10.

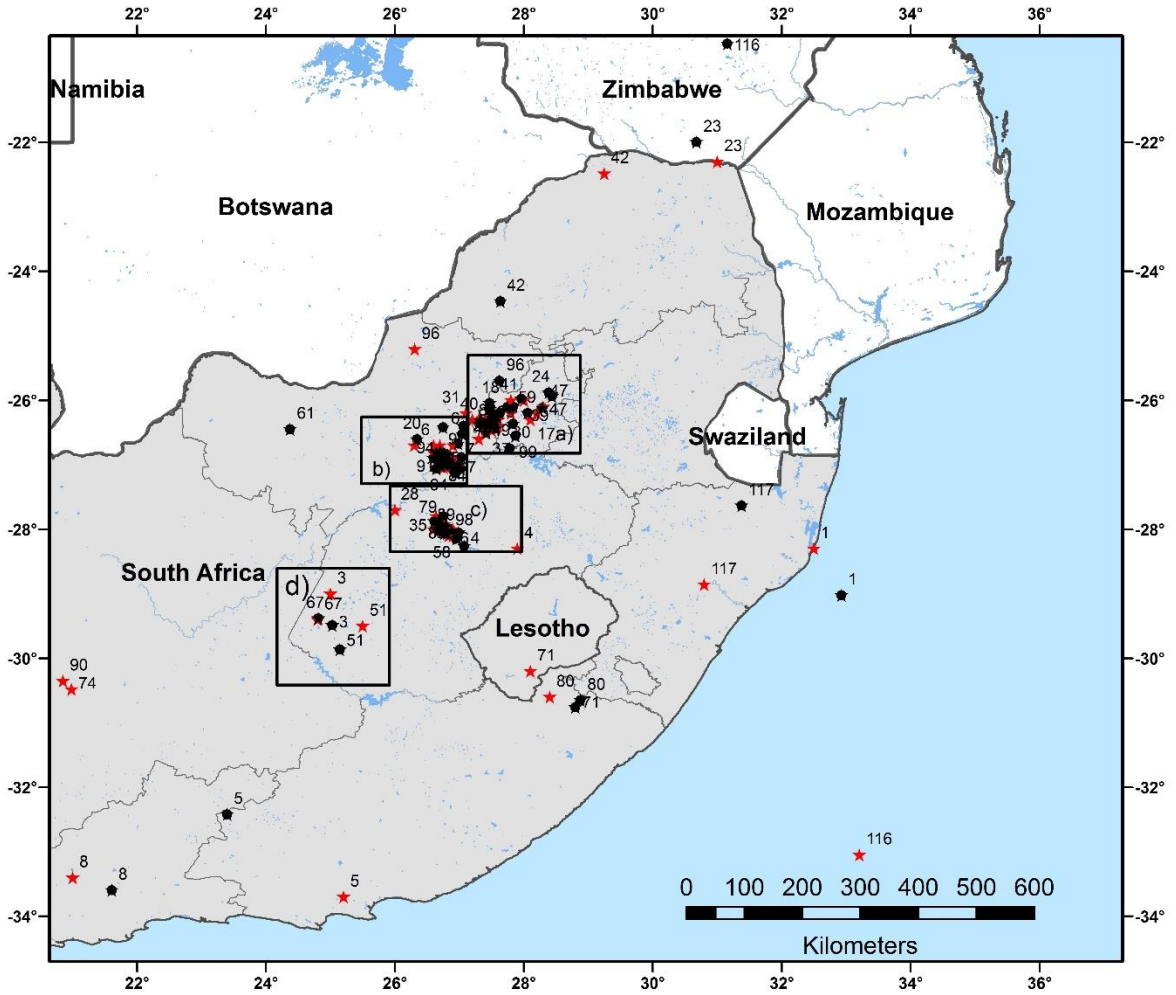
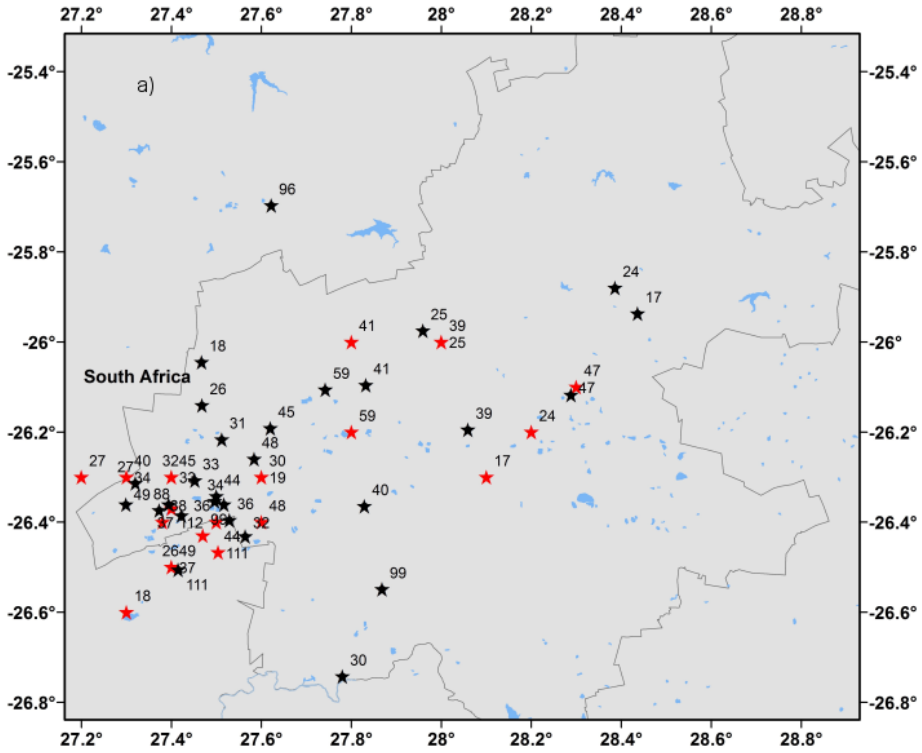
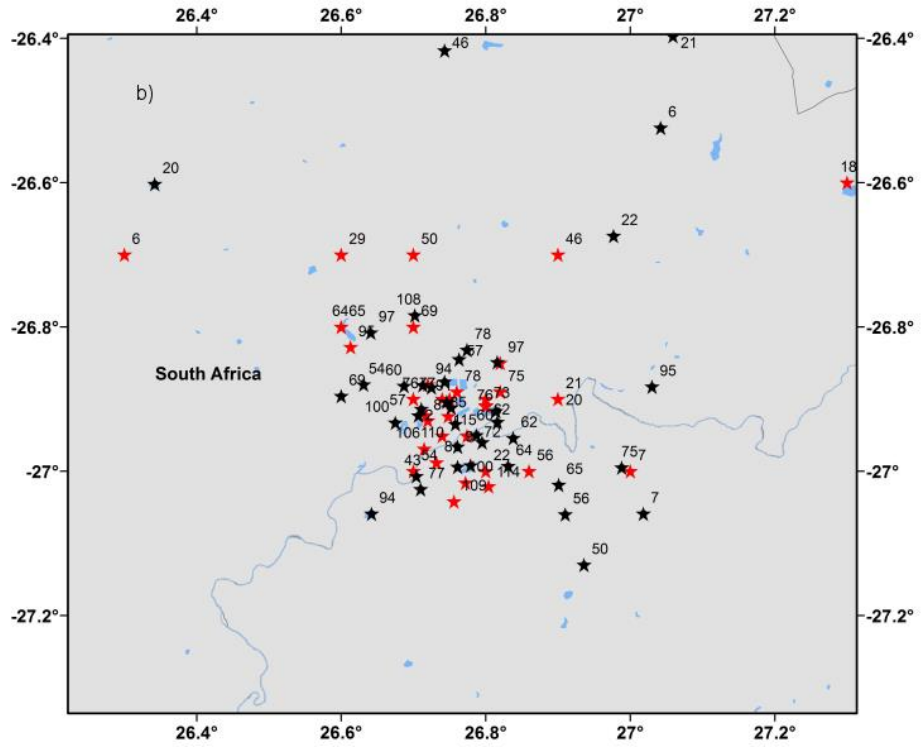


Figure 4-9. Comparison of new epicentral locations (black stars) to the published CGS locations (red stars). Black lined boxes represent clusters of seismicity zoomed as in Figure 4-10 for clarity (modified from Midzi et al., 2020).

Mostly small changes were observed in the actual location of the events on comparing the new epicentres to those in the CGS database. The largest change observed was that for event 116 whose location moved from the South West Indian Ocean just off the South African southeast coast all the way to eastern Zimbabwe. This movement is logical because arrival phases arrived at Zimbabwean and Zambian stations before being recorded in South Africa. This means the epicentre must be located closer to the Zimbabwe and Zambia stations. A closer look at the changes in the clusters indicated in Figure 4-9, are shown by zooming on the clusters as in Figure 4-10.


a)
South Africa
27.2°
27.4°
27.6°
27.8°
28°
28.2°
28.4°
28.6°
28.8°
-25.4°
-25.6°
-25.8°
-26°
-26.2°
-26.4°
-26.6°
-26.8°


b)
South Africa
26.4°
26.6°
26.8°
27°
27.2°
-26.4°
-26.6°
-26.8°
-27°
-27.2°

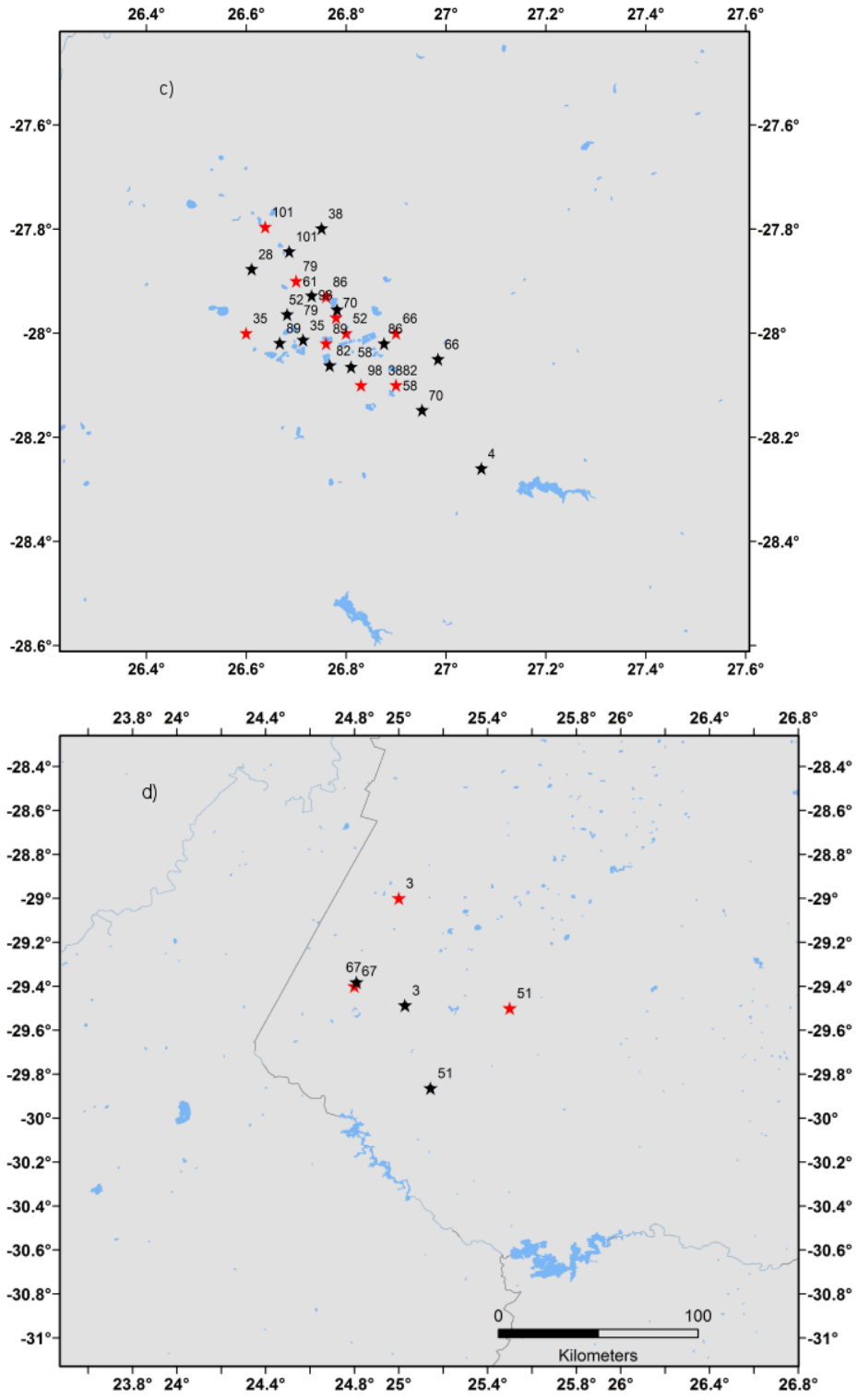


Figure 4-10. Comparison of new epicentral locations (black stars) to the published CGS locations (red stars). Zoomed clusters indicated by boxes in Figure 4-9. (a) Cental Rand, (b) KOSH, (c) Welkom and (d) Koffiefontein clusters.

The Central Rand (a) and KOSH (b) clusters do not really show significant change in epicentres. Most of these events were recorded by sparse network of stations. This also might influence the location uncertainties. The new epicentres in the Welkom cluster (in window (c)) appear to be more clustered than the published CGS epicentres, with epicentres moving in towards the cluster. The clustering will assist in source delineation.

4.8.2.1. Assessment of the quality of new locations

The question that arises after observing these various changes in the epicentres, is which, then, of the new locations and CGS published locations are more reliable. Without more information on the actual sources or faults along which the earthquakes occurred, it is difficult to decide which of these two datasets is correct. However, their accuracy and / or reliability can be given by assessing the three parameters, GAP, RMS and errors in location. GAP refers to the largest azimuthal gap between azimuthally adjacent stations (in degrees) and it defines the spatial distribution of stations whose records are used in determining the epicentres. This value is obtained for each event. The smaller the angle the better the station distribution and more confident one is of the obtained solution.

GAP values from the analysed data are found to range from a low of 26° to almost 335° (Figure 4-11). Most events with low values are located in the centre of the country in the mining regions. This is expected because there is good station coverage in the central parts of the country. Thus, these moderately sized events are expected to be recorded widely by most stations. Interestingly, some events close to the coast also have low GAP values (26-71). This is possible because some teleseismic stations were now used in the location (e.g. the 31 December 1932 event of magnitude ML6.3 has a low GAP of 74^0). Its large size enabled it to be recorded by distant stations located all around the globe, which then contributed data towards the analysis. Events with smaller GAP values are located using stations that are well distributed and this gives confidence in the location.

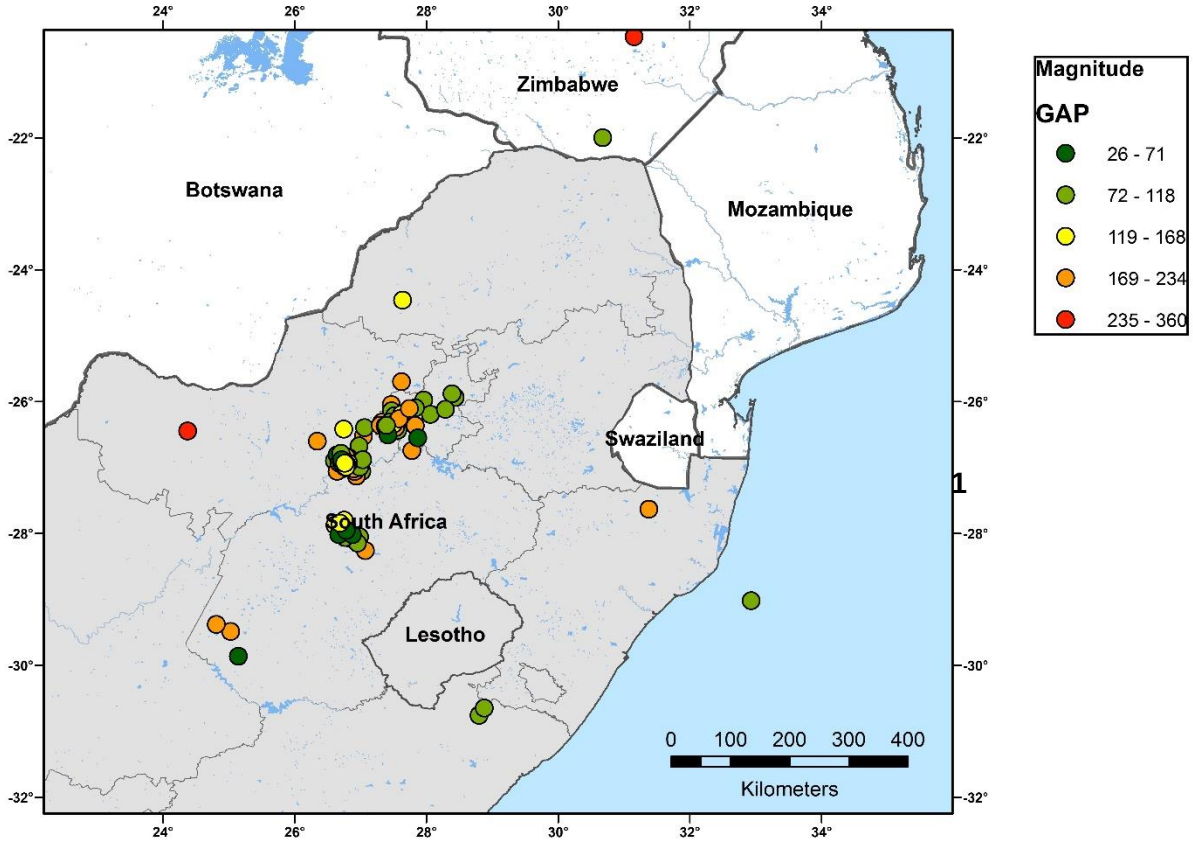


Figure 4-11. Map showing the typical GAP values obtained during the analysis and their distribution with epicentres.

Errors in the location are illustrated by RMS (Figure 4-12) and error ellipse (Figure 4-13) values. RMS values are square root of the mean squares of average station travel time residuals for each event. Ideally the best solutions are those associated with low RMS values. The closer RMS is to zero the better the solution. Most solutions obtained in the relocation have values less than 2 seconds (Figure 4-12). Though the low values observed give the impression of well constrained solutions, it should be noted that these values depend a great deal on the velocity model used. Thus, low values do not necessarily mean accurate location, but a relative statistical result that can be used to assess quality of location given the available data.

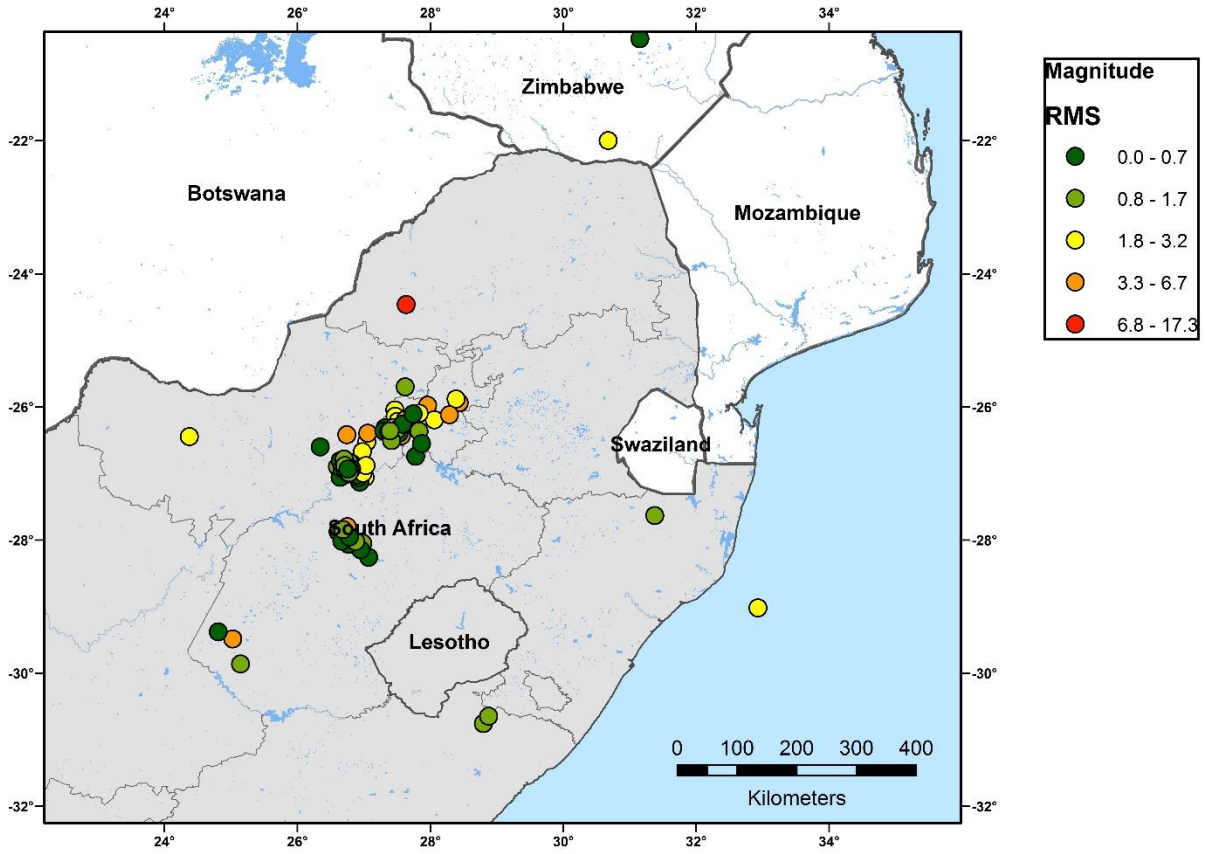


Figure 4-12: RMS (in seconds) of relocated epicentres of the events in the dataset.

An error ellipse is defined as a contour within which there is a 67% probability of finding the epicentre (Bormann, 2002). Such results were estimated during the relocation of the dataset in this study and are presented in Figure 4-12. Most of the events show small ellipses indicating small errors in the locations, however few events in Koffiefontein and NorthWest resulted in high error ellipses. However, as discussed above, this value alone cannot be used as a conclusive indicator of the accuracy of the location.

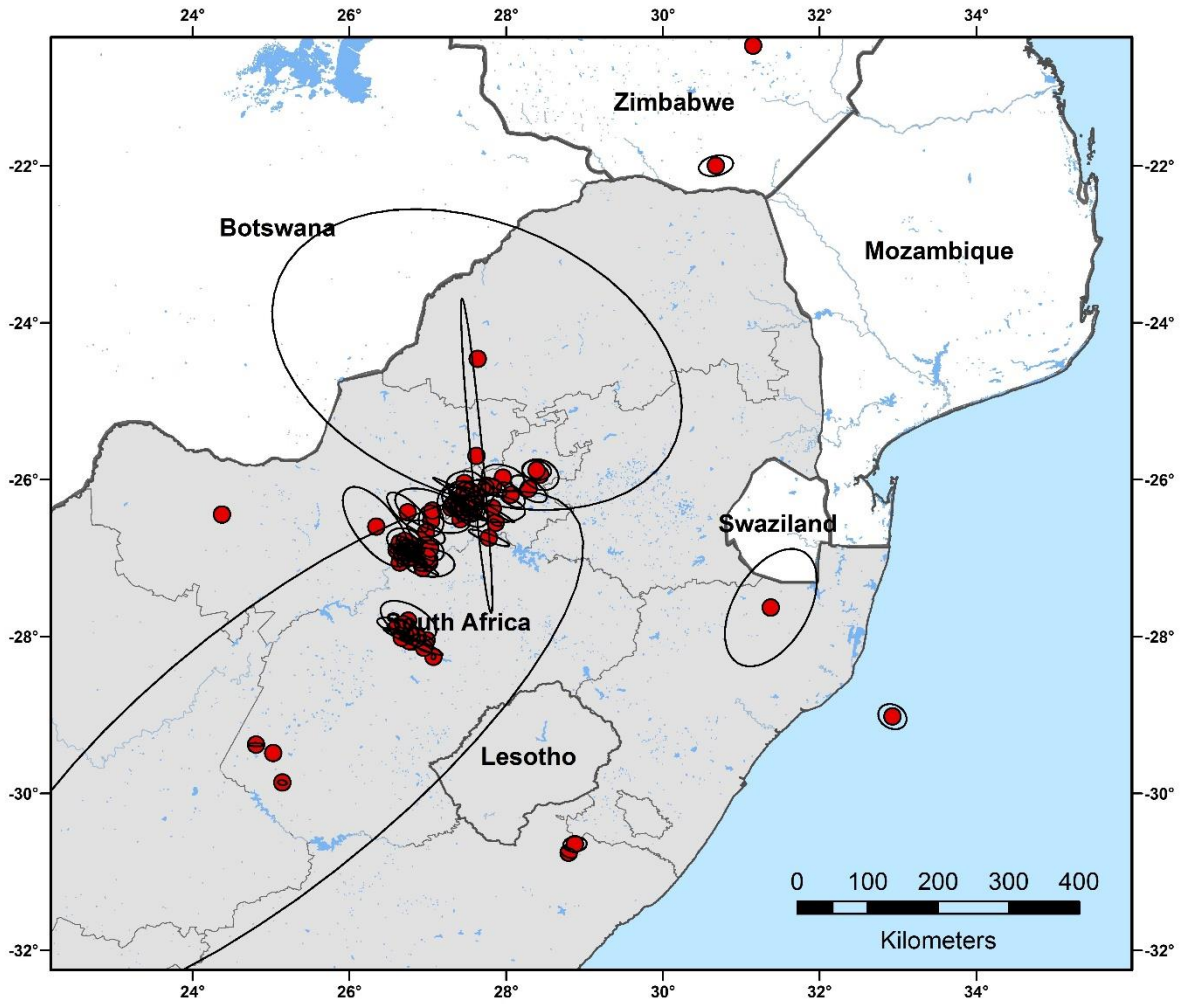


Figure 4-13. Error ellipses of relocated epicentres of the events in the dataset.

Analysis of a combination of GAP, RMS, and error ellipse values is likely to help in getting a better constraint on the accuracy of the locations. Events located in Gauteng, North West and Free State have low GAP, RMS and small error ellipses. This is because they are located in the middle of the South African National Seismic Network. A few events have high error ellipses, because they were they were located by few stations which influenced their accuracy. Instrumental data located with a few stations have high GAP and large error ellipses meaning they are not well constrained. Most of the events in the central parts of South Africa are well constrained. Except for a few events near Koffiefontein and in the North West Province that had high error ellipses.

4.8.3. Magnitude Uncertainties

Earthquake magnitude is an important parameter in seismic hazard analysis. It influences the activity rate as well as the b-value calculations hence it needs to be calculated with high accuracy. Magnitude uncertainties are propagated from the determination of the average magnitude from different recording stations. It has been observed that the same earthquake, recorded by different stations at different epicentral distances give different magnitudes. This difference will generate uncertainties in

the magnitude determination process. An assessment of this effect was done for different magnitude scales in this study. Given the limited amount of data available for the vast majority of the magnitude determinations, as well as the significant uncertainties associated with the conversions to moment magnitude, the specification of the uncertainties associated with the magnitude values is an essential component of the catalogue.

4.8.4. Magnitude uncertainties for instrumental data

4.8.4.1. Direct estimates of M_W

For the small number of events for which a direct estimate of M_W is available, a magnitude uncertainty of 0.16 magnitude units is assigned following USNRC (2012).

4.8.4.2. Conversions from M_B

For M_W estimates obtained from M_B using the Johnston (1996) equation, the magnitude uncertainty is set to the standard deviation associated with this equation, namely 0.26 magnitude units. Using a number of selected events with amplitude and period used to calculate M_B, a re-computation of the M_B yielded was performed.

4.8.4.3. Conversion from M_L

The developed M_L - M_W regression relations derived in Manzunzu et al. (2020) and discussed in section 4.7.1.1 had their standard deviation calculated. These were used as the uncertainty in the converted data (Table 4-7).

Table 4-7: Error values and their period of applicability (from Manzunzu et al., 2020).

Period	Error	Relation
1970 – 1997	0.25	Equation 6
1997 – 2012	0.33	Equation 7
2012 - 2016	0.19	Equation 8

Illustrated in Figure 4-14 are plots for a number of earthquakes showing the variation of M_L values determined at each station plotted according to the distance of the stations from the epicentre. These variations are expected because the radiation pattern at the source is different in each direction and each ray path from the source to station passed through different geological units, thus introducing uncertainties in the determination of earthquake magnitudes. This variation in the magnitude reflects the uncertainties associated with the magnitude calculation process. However, M_L values appear to be relatively stable with distance (Figure 4-14). This probably indicates that the attenuation curve derived during the study by Saunders et al. (2013) consistently estimates magnitude correctly over different hypocentral distances.

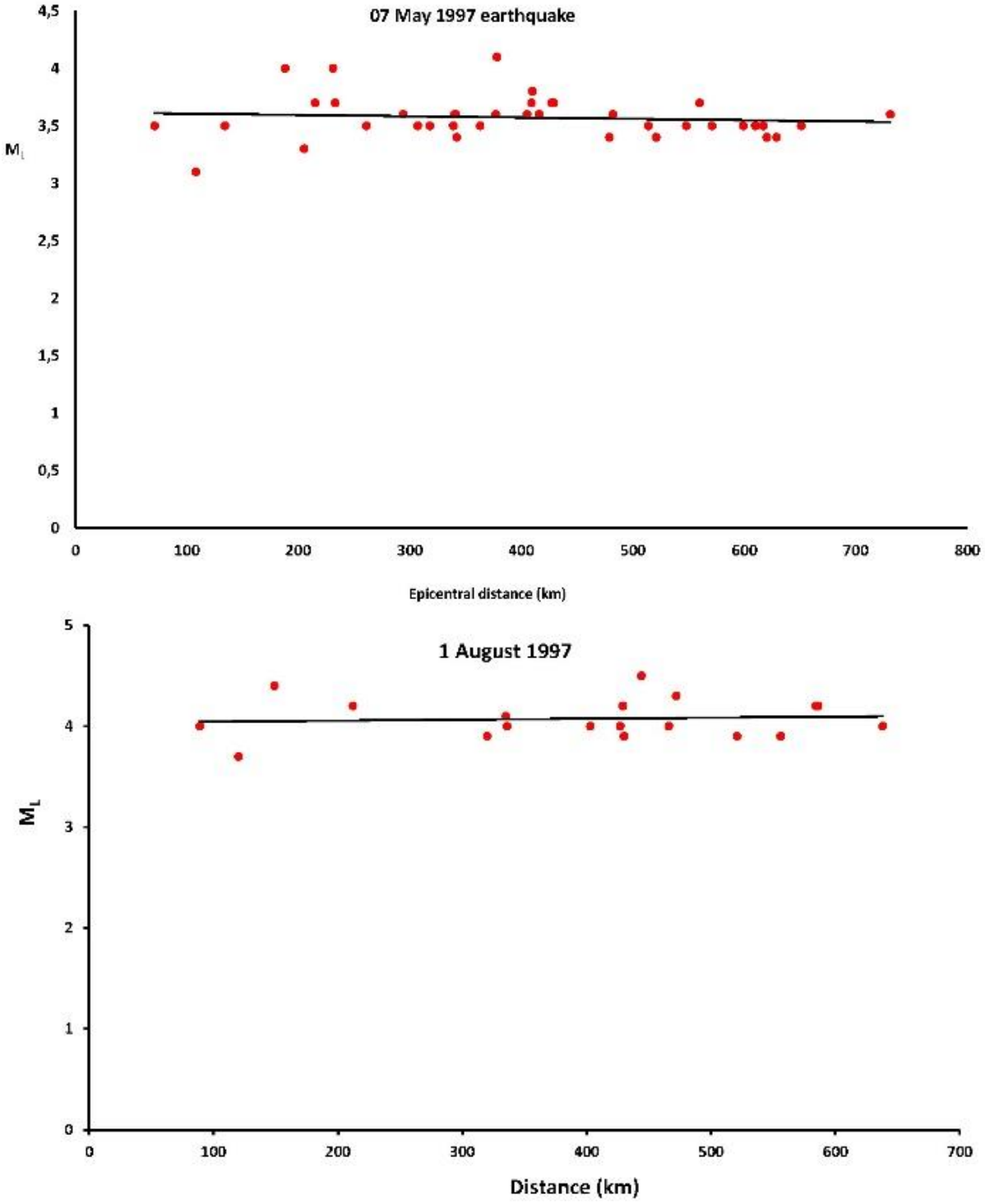


Figure 4-14: Variation of local magnitude with epicentral distance.

The values of the mean magnitude residuals obtained by subtracting M_L, independently calculated for each recording station, from the arithmetic mean of M_L determined from all stations are illustrated in Figure 4-15.

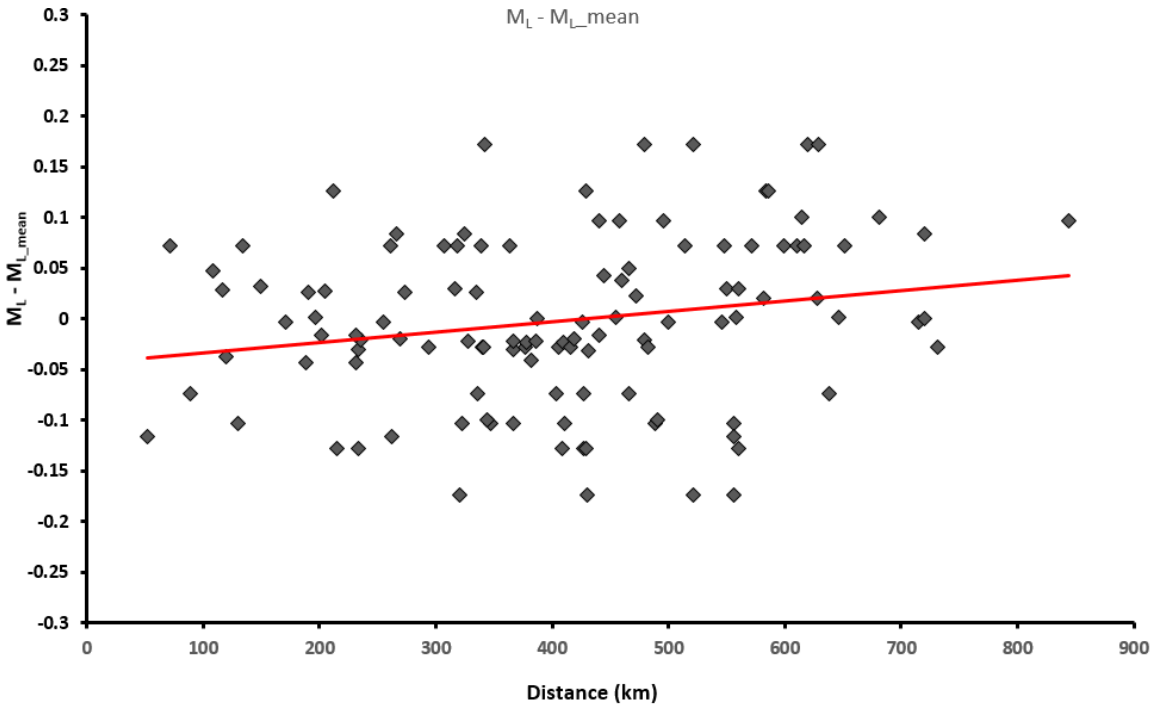


Figure 4-15: Mean magnitude residuals with distance local (M_L) magnitude values.

The mean values, plotted against the epicentral distance for local magnitude derived by Saunders et al. (2013) values, follow the zero baseline closely. Again, this trend appears to confirm the earlier mentioned conclusion that the relationship between attenuation and hypocentral distance in the region is accurately modelled by their attenuation curve. The maximum error in M_L is less than 0.2.

4.8.4.4. Conversion from M_{B_Lg}

The values converted from M_{B_Lg} have been assigned an uncertainty of 0.5. The rationale behind this assignment is that based on the definition of this magnitude, associated uncertainties are expected to be slightly higher than those for a regional M_S scale.

4.9. Influence of mining-related seismic events

A catalogue of 61743 earthquakes was compiled for the period 1620 to 2016 for an area of 500 km radius around Johannesburg. In order to carry out a seismic hazard analysis, the catalogue has to be independent and should follow a Poisson distribution. In view of the proximity of the study area to anthropogenic seismic sources, the seismicity will not follow the natural Poissonian model. Due to their possible impact on people and infrastructure, all such events are included in the assessment of seismic hazard in the region. However, no models of seismic occurrence have been so far developed that caters for long term mining-related seismic occurrence in hazard calculations (Petersen, 2014; 2015; Lasocki and Orlecka-Sikora, 2006). Both natural and mining-related seismicity of moderate

magnitude occur in the mining regions of South Africa. The Poissonian assumption becomes the major source of uncertainty when dealing with seismicity in the mining regions.

In a Poisson process, occurrences are very irregular and the probability of an event remains constant regardless of how much time elapsed since a previous event. Orderliness precludes the possibility of multiple events at a single point in time or space or the possibility of an infinite number of events in a finite interval of time or space. Over the short term, small seismic events in mines tend to occur in clusters in space and in time in response to rock extraction. Seismic activity within a mine is driven mainly by transient convergence of excavations in response to rock extraction. Smaller events are highly correlated in space and in time with mining. Such processes are neither stationary nor independent. However, if a number of such processes are superimposed over a longer time and over a larger area the outcome may be random. The inter-event time distribution of larger seismic events in most of the mines tested turns out to be random. Hence, the Poisson process may provide an asymptotic fit to the distribution of larger events in the time or volume mined domains. Note that stationary models apply to the long and the intermediate terms of hazard assessment. It is evident that there are two slopes in the G-R distribution curves for our catalogue (Figure 4-16). The first one at lower magnitudeswhich is relatively steeper than the second one at high magnitudes.

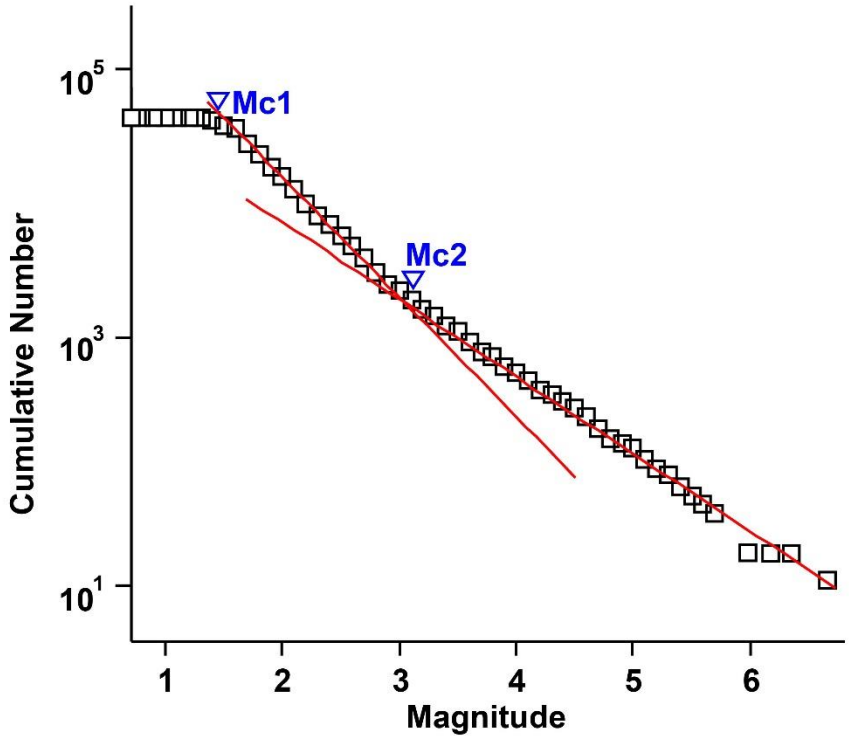


Figure 4-16: Frequency magnitude distribution of the current catalogue for seismicity in and around Johannesburg. Effect of mining related seismic events are illustrated by the 2 G-R lines (in red). The first cut-off magnitude M_{C1} shows the G-R distribution for small mining related events and the second M_{C2} shows the G-R distribution for tectonic events.

The purpose of this study is to assess the influence of ground motion due to moderate and large earthquakes hence the presence of the smaller magnitude earthquakes is invaluable. However, these events will have an influence on the computation of recurrence parameters and therefore needs to be taken into account. For the purpose of simplicity, events of magnitude less than 2.5 were assumed to be due to mining related events. The influence of mining seismicity can be illustrated through the splitting of the catalogue into two nodes. Each node was treated differently. The first node include all the seismic events in the catalogue and the second node only events of magnitude 2.5 and above.

4.10. Declustering of earthquake catalogue

Catalogue of tectonic events are often found to be non-Poissonian due to the existences of foreshocks and aftershocks. In order to test the independency, a Chi-squared test was performed on the data with a null hypothesis that "the catalogue follows a Poisson distribution". The null hypothesis was rejected at 95% confidence interval meaning the catalogue is not Poissonian. Therefore, the catalogue needs to be declustered to remove dependent events. The three techniques *viz.* Window-based, Cluster-link and rate-based approaches were applied in this study to test which one best applies to our catalogue. For further evaluation of the catalogue, the subset of the catalogue corresponding to modern instrumental data (1970-2016) was studied in more detail. This subset of 51689 events with Mw ranging from 1.3 to 7.2 was selected in order to avoid potential issues related to the uncertainties in the magnitude conversion, which are expected to be considerable for the pre-1971 data in view of the heavy reliance on macroseismic information and data from other networks.

4.10.1. Window-based approaches

There are three common window-based declustering methods named after their developers (Figure 4-17). The simplest and longest-established method is that of Gardner and Knopoff (1974), which is based on earlier efforts by Knopoff and Gardner (1972). Its spatial-temporal windows were originally derived empirically from southern Californian data but have been applied to other geographical regions, as well as global catalogues (e.g., Shearer and Stark, 2012; Luen and Stack, 2012). The distance and time of occurrence of the aftershocks is related to the magnitude according to the following equations:

$$\mathbf{Distance} = \mathbf{10}^{\mathbf{0.1238M+\ 0.983}} \qquad 4\text{-}8$$

$$\mathbf{Time} = \mathbf{10}^{\mathbf{0.032M+\ 2.7389}}\ , \text{if } M \geq 6.5 \qquad 4\text{-}9$$

$$\mathbf{Time} = \mathbf{10}^{\mathbf{0.05409M-\ 0.547}},\ \text{if } M < 6.5 \qquad 4\text{-}10$$

where M is the magnitude, time is in days and distance is in kilometres.

Grünthal (1985) independently derived alternative windows using Central European data. Interestingly, these remain close to the Gardner and Knopoff (1974) windows, with the consequence that applying these two algorithms often produces very similar results. Grünthal (1985) as cited by Burkhuard and Grünthal (2009) applied the following equations:

$$\mathbf{Distance} = \mathbf{e}^{1.77+\sqrt{0.037+1.02M}} \qquad 4\text{-}11$$

$$\mathbf{Time} = \mathbf{e}^{3.95+\sqrt{0.62+17.32M}} \quad \text{if } M \geq 6.5 \qquad 4\text{-}12$$

$$\mathbf{Time} = \mathbf{e}^{6.44+0.055M} \quad \text{if } M < 6.5 \qquad 4\text{-}13$$

Updated windows developed for California by Uhrhammer (1986), however, are significantly different and thus lead to different results.

$$\mathbf{Distance} = \mathbf{e}^{-1.024+0.804M} \qquad 4\text{-}14$$

$$\mathbf{Time} = \mathbf{e}^{-2.87+1.235M} \qquad 4\text{-}15$$

In all the equations, the time is in days while distance is in kilometres. The diversity of the window parameters illustrates the non-uniqueness of the declustering process. For comparison, the three window were applied with suggested spatial-temporal windows (Gardner and Knopoff, 1974; Gruenthal, 1985; Uhrhammer, 1986).

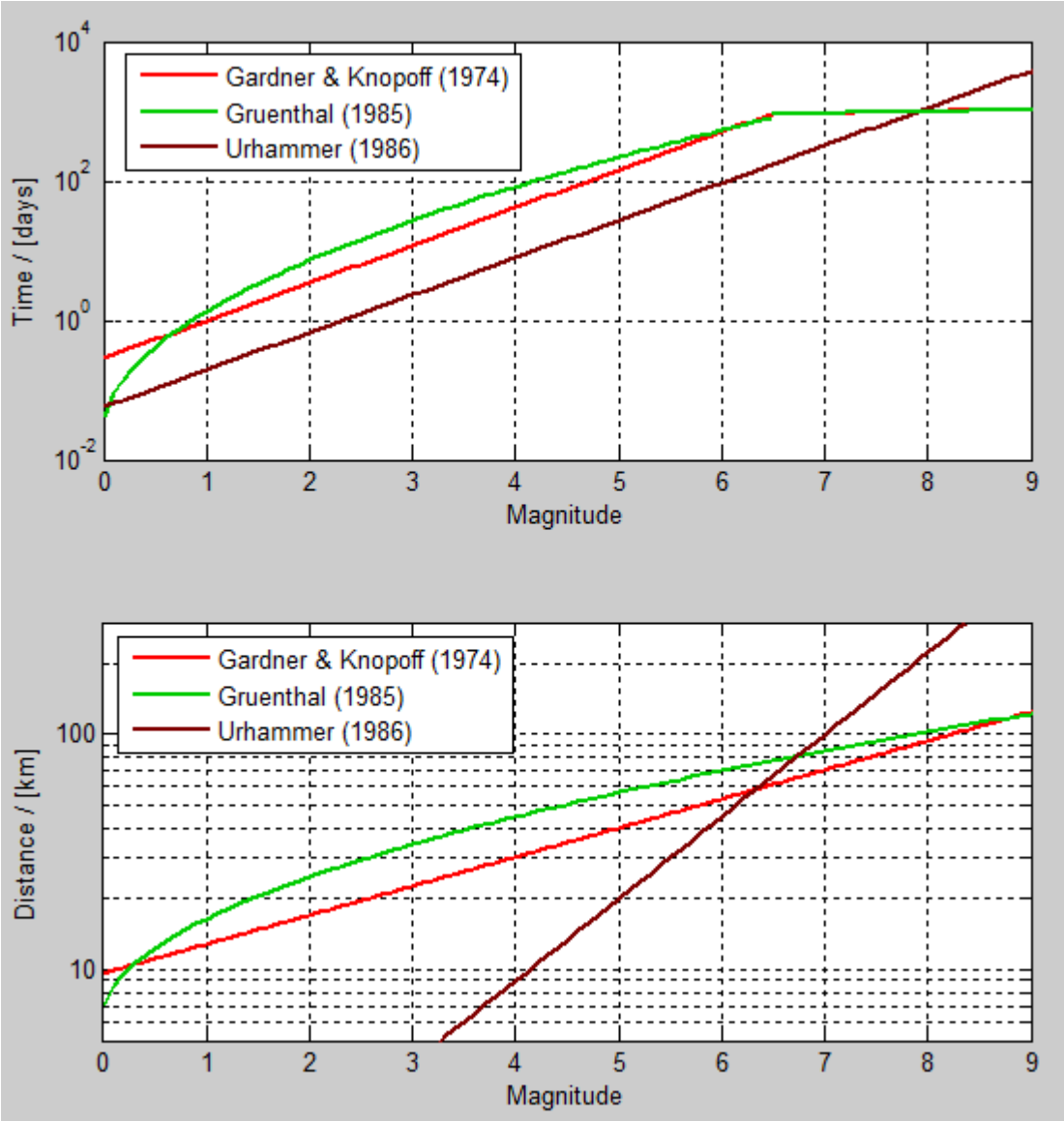


Figure 4-17: Spatial-temporal variation of the dependence windows for the three windows-based declustering techniques.

4.10.2. Cluster-link models

Cluster-link models, such as the widely used Reasenberg (1985) algorithm, group events into the same cluster as long as they fall within the window of any event that is already in the cluster. This allows the inclusion of higher-level dependencies (e.g., aftershocks of aftershocks), which could be missed in a simple windowing approach. Another feature of cluster-link approaches is that the clusters grow with the number of events analysed.

The Reasenberg (1985) algorithm requires the specification of several calibration parameters. These parameters characterises the bounds on the interaction time window (r_{fact}), the empirical decay factor of the modified Omori law (p_1), the effective lower magnitude cut-off of the catalogue (x_{meff}) alongside as a multiplicative factor by which this parameter is raised during a cluster, as well as

parameters characterising errors in epicentral location and depth (r). The default values provided in the ZMAP implementation of this algorithm correspond to empirical values determined for Central California. The Reasenberg (1985) algorithm is often implemented with these default parameters, even for regions outside Central California. This choice may not always be appropriate for other regions, since these parameters may depend on catalogue quality and completeness. A recent study by Ebel (2009) found that Omori-law parameters determined for aftershock sequences for a number of SCR areas were in good agreement with each other, as well as being similar to those of California aftershock sequences. The parameters applied in this study for the Reasenberg method are as follows

- r_{fact} = 8 (dimensionless)
- x_{meff} = 1 (units of magnitude)
- x_k = 0.5 (dimensionless)
- p_1 = 0.95 (dimensionless probability)
- min = 1 day
- max = 5 days.
- r = $0.01 \times 10^{0.5M}$ km, (Interaction distance scaling as suggested by Wells and Coppersmith, 1994)

To account for uncertainties, the Reasenberg method is usually applied using the mean and standard deviation in the input parameters. This will create three datasets for the minimum (mean – standard deviation), maximum (mean + standard deviation) and mean of the above parameters.

The cluster method implemented within the SEISAN software as a program called CLUSTER was also applied in this study. Depending on pre-set search parameters, the program identifies and removes dependent events (foreshocks, aftershocks and swarm events) from a catalogue using time difference, epicentral distance and magnitude limit parameters. These parameters are magnitude dependent and can be different before and after the main event. The method looks at each earthquake as a possible main shock then searches for the largest aftershock for that event within a certain hypocentral distance at a localized time. The program requires an input parameter file, which defines the parameters. In this study, the parameters used are shown in Table 4-8.

Table 4-8: Input parameters used in the CLUSTER methods in SEISAN.

Magnitude	Magnitude limit	Aftershocks		Foreshocks	
		Distance (km)	Time (days)	Distance (km)	Time (days)
2.5	1.5	19.5	6.0	19.5	6.0
3.0	2.0	22.5	11.5	22.5	11.5
3.5	2.5	26.0	22.0	26.0	22.0
4.0	3.0	30.0	42.0	30.0	42.0
4.5	3.5	35.0	83.0	35.0	83.0
5.0	4.0	40.0	155.0	40.0	155.0
5.5	4.5	47.0	290.0	47.0	290.0
6.0	5.0	54.0	510.0	54.0	510.0
6.5	5.5	61.0	790.0	61.0	790.0
7.0	6.0	70.0	915.0	70.0	915.0
7.5	6.5	81.0	960.0	81.0	960.0

4.10.3. Rate-based methods

Rate-based declustering methods assume that each event is correlated within each cluster. The probability of each event being classified as a dependent event decrease as we move away from the main event. Declustering an earthquake catalogue using rate-based methods is accomplished by reducing every cluster to its largest event (van Stiphout et al., 2012). Zaliapin et al. (2008) achieved this with the aid of a correlation metric proposed by Baiesi and Paczuski (2004), through the identification of independent events by exploring the graphical representation of space-time windows (T_N and R_N). The metric used decreases as two events get closer in space and time, and also as the first event increases in size. The MATLAB code written and provided by Zaliapin was used to also decluster the catalogue with the following parameters:

- d_f is the fractal dimension of epicenters ($0 < d_f \leq 2$)
- b is the b-value from the Gutenberg Richter slope
- p is the weight parameter for defining T_N, R_N ($0< p < 1$)
- m_{min} is the lower magnitude cutoff.

4.10.4. Declustering results

Declustering results from the eight methodologies implemented in this study are shown in Table 4-9. Examination of the declustering results shows that the Gardner and Knopoff (1974) and Grünthal (1985) algorithms give similar results, removing less than 20% of the events. In contrast, the Uhrhammer (1986) algorithm labels more than 85% of events as dependent events. The cluster method by Reasenberg (with its standard deviations), were conservative removing between 13 and 45 % of the events while the rate-based method removed 45% of the events. The SEISAN

implementation removed the least events with only 9%. From this analysis it can be concluded that the Uhrhammer (1986) algorithm does not appear appropriate for the catalogue under investigation, and that there is no significant difference between applying the Gardner and Knopoff (1974) and Grünthal (1985) algorithms.

Table 4-9: Results of applying the declustering algorithms of Gardner and Knopoff (1974), Grünthal (1985) and Uhrhammer (1986) to the modern SANSN data subset (1972-2016) of the Johannesburg PSHA project catalogue.

Method	Initial	Declustered	Dependent	Clusters	% reduction
Gardner and Knopoff (1974)	51689	41874	9815	3542	18.99
Grünthal (1985)	51689	41875	9814	3730	18.99
Uhrhammer (1986)	51689	5732	45957	5959	88.91
Reasenberg (minimum)	51689	44783	6906	1802	13.36
Reasenberg (standard)	51689	38764	12925	1745	25.01
Reasenberg (maximum)	51689	29937	21752	1895	42.08
Cluster (Seisan)	51689	47028	4661	1034	9.02
Zaliapin et al. (2008)	51689	28801	22888	4452	44.28

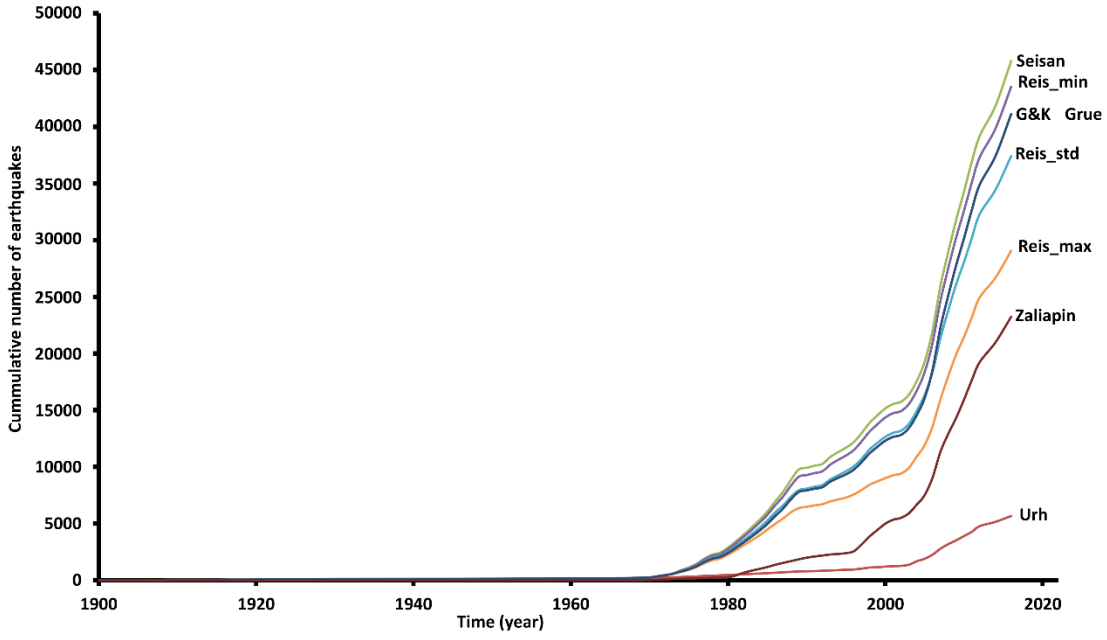


Figure 4-18: Cumulative number of events for the declustered catalogues obtained using several declustering algorithms. G&K is the Gardner and Knoppoff (1974) method; Grue is the Grünthal (1985) method; Reis_min, Reis_std and Reis_max are the minimum, mean and maximum standard deviations for the Reasenberg (1985) method respectively;, Urh is the Uhrhammer method; and Seisan and Zaliapin are the Seisan and Zaliapin methods, respectively.

4.11. Uncertainties associated with the declustering process

In view of the downstream use of the declustered catalogue, namely the estimation of recurrence parameters assuming a Poissonian process, the ability of the selected algorithm to provide a declustered catalogue that follows the Poissonian model is critical. While some of the algorithms

reviewed above are specifically designed to meet this condition (e.g., Hainzl et al., 2006), others, in particular Reasenberg (1985), have been found to be in violation of this assumption even in cases where calibration should not be an issue (Hainzl et al., 2006; Van Stiphout et al., 2012; Luen and Stark, 2012). Comparing the results of the Reasenberg (1985) method using standard parameters and varying parameters, the variation due to the parameter settings becomes obvious (Figure 4-18 and Table 4-9). Depending on the choice of the declustering algorithm and its parameter settings, clustered seismicity is either completely removed or remains in the catalogue. The outcome depends on the choice of the declustering method and on its parameter settings, which are often chosen after a trial-and-error process to make the outcome match with the empirical definition. Thus, this non-unique process of declustering acts as the largest source of uncertainty for the estimation of background rate changes. This huge variety of seismicity-rate changes raises the question of which declustering method is correct. Unfortunately, this question cannot be answered, because no physical basis exists to distinguish independent events from clustered seismicity- like aftershocks. Moreover, the applied declustering algorithm inherently defines independent events. Therefore, when declustering for background seismicity analysis, one should be aware of the arbitrariness of the solution. The results will not implicitly reflect real seismicity, and therefore, the process of declustering should not be regarded as part of unique data processing, but as part of the model uncertainty to achieve and analyze background seismicity.

To assess the influence and dependence of the declustering methods, statistical tests were performed to verify that the declustered catalogues indeed are temporally independent and follow Poissonian distribution. The statistical tests performed are the Kolmogorov-Smirnov (K-S), the student's T-test and the Chi-squared ($\chi 2$) tests (Table 4-10). We tested the null hypothesis at 95% significant level that the declustered catalogues are temporally Poisson distributed after our declustering algorithms were applied. For all tests, we set the minimum magnitude of investigated events to $Mw = 2.6$.

Table 4-10: Results of statistical tests for the eight declustered catalogues.

Method	Sample size	KS test @ 95% significance level		χ^2 test @ 95% significance level		T-test @ 95% significance level	
Gardner and Knoppoff (1974)	41875	0,1	accept	0,001	reject	0,001	reject
Uhrhummer (1986)	5732	0,0002	reject	0,001	reject	0,001	reject
Reasenberg minimum	44783	0,001	reject	0,001	reject	0,001	reject
Reasenberg standard	38764	0,001	reject	0,001	reject	0,001	reject
Reasenberg maximum	29937	0,001	reject	0,001	reject	0,001	reject
Grunthal (1985)	41875	0,100	accept	0,001	reject	0,001	reject
CLUSTER (Seisan)	47028	0,023	accept	0,001	reject	0,001	reject
Zaliapin et al. (2008)	28208	0,001	reject	0,001	reject	0,013	reject

Of the three statistical tests used, only the K-S test accepted the null hypothesis for the Gardner and Knoppoff (1974), CLUSTER and Grunthal (1974) catalogues at 95% significant level. The Gardner and Knopoff (1974) approach has been widely used outside of California, and found to provide reasonable results even when the windows have not been calibrated to local data. The similarity between the independently derived Grünthal (1985) and the original Gardner and Knopoff (1974) windows, as well as the good performance of the Gardner and Knopoff (1974) algorithm when applied at a global scale (Shearer and Stark, 2012) further point to the fact that the spatial-temporal windows required in this approach are not region-dependent. The accepted catalogues will be tested through sensitivity analysis to assess their influence on the hazard.

4.12. Catalogue completeness

The minimum magnitude of completeness (M_C) of a compiled catalogue is considered to be an important factor in accurate seismic hazard parameter estimation, and it can vary on both temporal and spatial basis (Sagar and Leonard, 2007; Wiemer and Wyss, 2000). M_C needs to be taken into account in the recurrence calculations, since failure to do so may result in biased estimation of seismicity rates and b-values, and thus may affect the final hazard results. A variety of approaches are available to address the issue of catalogue completeness namely the maximum-curvature method or the catalogue-based method (Mignan and Woessner, 2012; Stucchi et al., 2009; Wiemer and Wyss, 2000) and the Stepp method (Stepp, 1972). In this task, we used the Gardner and Knoppoff, (1974) catalogue to evaluate M_C.

4.12.1. Stepp Method

The most common method for estimating completeness period (T_C) has been proposed by Stepp (1972) and consists of making plots of the cumulative number of events against time, from which, the period since present during which reporting has been complete, can be judgmentally estimated (Figure 4-19).

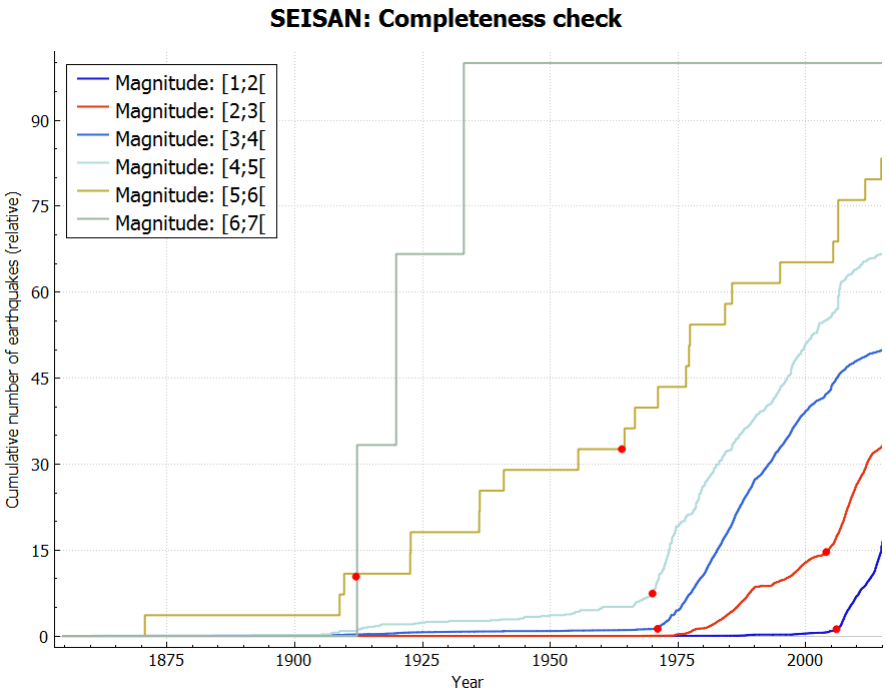


Figure 4-19: Results from the catalogue approach. The red dots represents the start of the completeness for each magnitude unit.

Estimation of T_C is often difficult and involves a high degree of subjective judgment. This plot allows for defining catalogue completeness for different magnitude classes (Table 4-12).

Table 4-11: Magnitude completeness using the catalogue based approach.

M_C	**T_C using Stepp method**
1-2	2013 – 2017
2-3	2003 – 2017
3-4	1972 – 2017
4-5	1970 – 2017
5 -6	1964 - 2017
6-7	1912 - 2017

4.12.2. Maximum curvature method

The maximum curvature method plots the frequency-magnitude distribution of events, as proposed by Gutenberg and Richter (1956) and Richter (1958). The frequency-magnitude distribution describe the relationship between the frequency of occurrence and magnitude of earthquakes as in equation 4-16.

$$\mathbf{log_{10}\, N(M) = a - b(M)} \qquad 4\text{-}16$$

where N(M) is the number of earthquake of magnitude ≥ M, a is the activity rate of earthquakes of magnitude larger than M and b describes the relative distribution of small and large earthquake.

This is commonly known as the Gutenberg-Richter (G-R) power law distribution of magnitudes (Wiemer and Wyss, 2000). By assuming that the declustered catalogue has a stationary characteristic, then the deviation of the seismicity from the theoretical stationary model is assumed to be due to the incompleteness of the catalogue. The magnitude of completeness is the value at which the slope of the G-R frequency-magnitude distribution starts to flatten out. This method of determining M_C is regarded as the simplest method (Wiemer and Wyss, 2000).

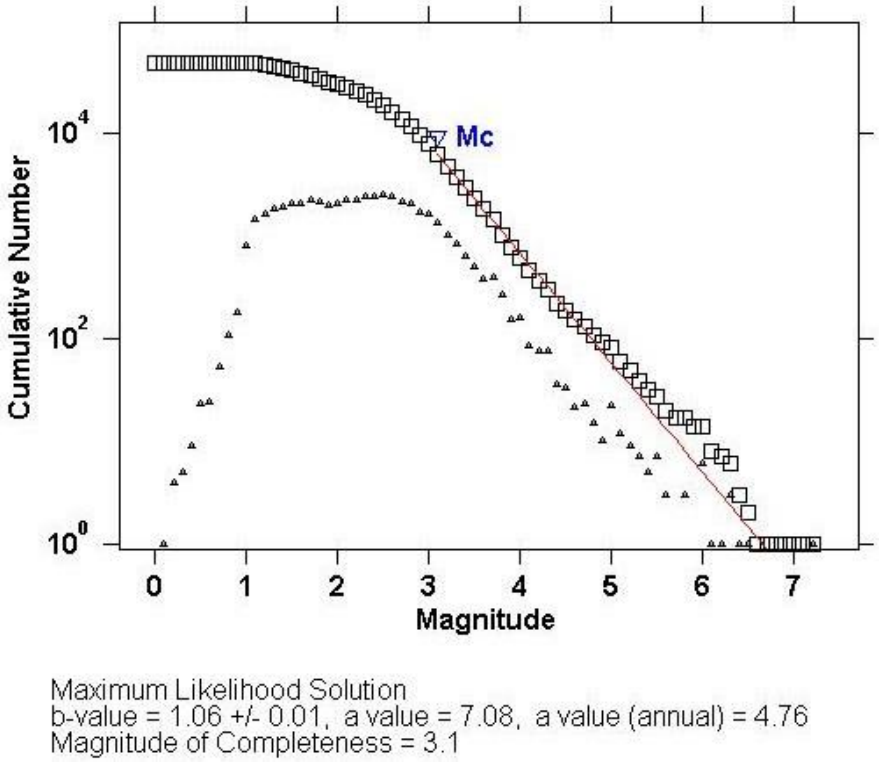


Figure 4-20: Estimation of the magnitude of completeness using Maximum-Curvature.

4.12.3. Temporal variation of M_C

Based on the knowledge of earthquake reporting and monitoring in the region, the time intervals listed in Table 4-13 were determined. These intervals correspond to dates delimiting periods for which the probability of detection is expected to remain uniform. The completeness levels of the whole catalogue are determined by inspecting visually the seismic history of the region. The observed completeness levels are summarised in Table 4-13. Though M_C is observed to vary with time, a major change is seen around 2005, where the values drop drastically to $M_C = 1.5$. The fluctuations observed show a general decrease in the M_C values, which are a reflection of improved monitoring capabilities.

Table 4-12: Time intervals for catalogue completeness analysis

Interval	**Dates**	**Justification**
1	1650-1909	Milne seismograph installed in Cape Town. Macroseismic reports collected across the country are the major source of information.
2	1910-1936	Undamped Wiechert seismograph and continuous monitoring in Johannesburg. Re analysis of macroseismic information for Eastern Cape was covered by Albini (2012) study while Strasser et al., (2015), did the Koffiefontein.
3	1937-1949	No longer covered by Albini (2012) study. Data mainly from Johannesburg-based sources (Finsen, 1950; Krige and Maree, 1951) or global compilations.
4	1950-1963	Short-period Benioff network installed (Gane and Oliver, 1953). Continuous monitoring, bulletins available
5	1964-1968	Early WWSSN period. Local network continues as before.
6	1969-1971	Bulletin production stopped due to reorganisation of South African scientific institutions, but recording continues. Ceres sequence. Heavy reliance on Bulawayo data collection and analysis
7	1972-1979	Early SANSN, still very sparse.
8	1980-1996	SANSN mostly analogue, but network densifies.
9	1997-2002	Transition to SEISAN and digital recording
10	2003-2006	Digital upgrade of the network
11	2007-2011	Modern, fully digital network
12	2012 to present	Installation of cluster networks in the mining regions and upgrading of the national network.

The minimum magnitude of completeness M_C of the available catalogue was estimated using a technique similar to the Goodness-of-Fit technique proposed by Wiemer and Wyss (2000). The technique employs a comparison between the observed and the theoretical frequency magnitude distribution with the aim of minimizing the root mean square for a set of trial values for M_C, while the uncertainty is obtained using a Monte Carlo approach (Figure 4-21). The temporal variation of M_C is calculated by a standard moving-window technique (Wiemer and Katsumata, 1999; Wiemer et al., 1998; Wiemer and Wyss, 1997). It was calculated for a time-window containing 100 seismic events, advancing in steps of 100 events, by calculating the derivative of the frequency-magnitude distribution as implemented in ZMAP (Wiemer, 2001).

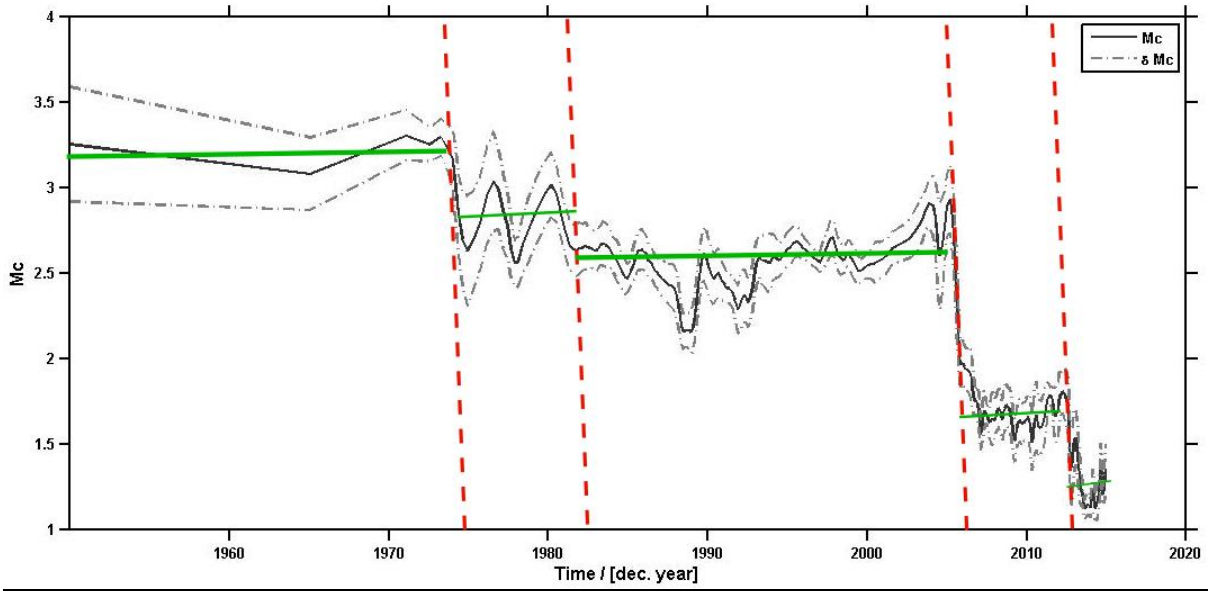


Figure 4-21: Variation of the magnitude of completeness (M_c) with time for our catalogue. The green line indicates the average Mc for the time period. The dashed line represents the uncertainty.

M_C varies significantly with time. Five different Mc values can be identified in Figure 4-23, before 1975, M_C was around 3.3 and from 1975 to 1983, it fluctuates around 3.0. From 1983 to 2006, it fluctuates again around 2.5 then it drastically drops to 1.7 from 2006 to 2012 then to 1.2 since then until now (Table 4-16). The temporal variation in M_C is also influenced by the network detection capabilities within the area.

Table 4-13: Temporal variation of Magnitude of completeness using the catalogue based approach.

Interval	**Magnitude of completeness**
Before 1900	5.0
1900 - 1970	3.5
1970 – 1983	3.0
1983 -2006	2.5
2006 2012	1.7
2012 to present	1.2

4.12.4. Spatial variations in completeness

The station configuration and distribution within a region influences the spatial variation in M_C. Large interstation distances will result in limited detection of small events. Therefore, the evolution of the SANSN is closely related to the M_C variation in South Africa. Although the number of stations in the SANSN has significantly improved, Brandt (2019) have shown the need for improvement in the distribution of the station to be able to detect small magnitude earthquakes. The spatial mapping of M_C was done using ZMAP software by (Weimer (2001). Event sampling was completed using a regularly spaced grid, set at 0.1-degree intervals, to extract 200 events closest to each node. This

method resolve the problem of sparse events over a large area by increasing the search distance there by keeping the required number of events to calculate M_C. The general spatial variation in M_C is shown in Figure 4-22. High M_C values between 3.5 and 4.0 can be observed in some regions. M_C values within Gauteng and some parts of North West province range from 1.0 to 1.9. These regions have cluster network of stations that are capable of detecting small magnitude earthquakes. The source radius to sample 200 events might be extending to areas with low magnitude earthquakes there by influencing the M_C calculation for this region. This phenomenon is also observed in the Limpopo-Mozambique region where low M_C values are observed. The improvement in the SANSN influenced the temporal and spatial variation in M_C values. Therefore, it is recommended that for seismic hazard studies, M_C must be evaluated for each source. High M_C values observed to the eastern and southern parts of Gauteng maybe attributed to the sparcity of the seismic stations in these areas.

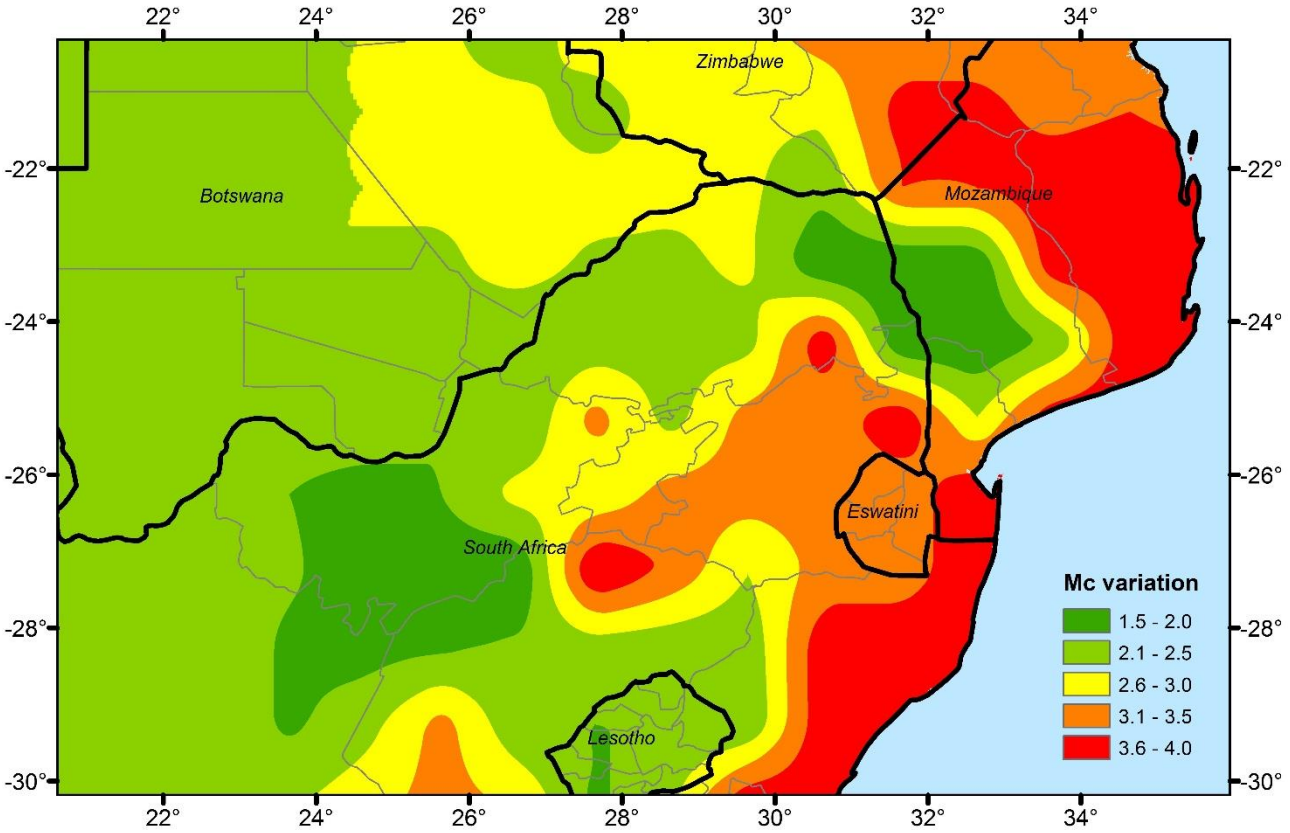


Figure 4-22: Spatial variation of M_C within the catalogue.

4.12.5. Uncertainty in M_C

It was noted that the observed variations in M_C is not entirely natural but is also influenced by the sensitivity of the seismic station networks in the region. It has to be emphasised that the inclusion of cluster networks in the current catalogue also influence the determination of M_C both spatially and temporally. The networks are localised in mining regions hence improved detection capabilities are

seen in these localised regions while the rest of the area is located using the national network. These networks started operating from 2012 with the SWMP network having only eight stations (section 4.2.2) and have been increasing the number of stations until 2014, this has direct influence on the M_C values as shown in Figure 4-23. The change in M_C also influence the productivity of earthquakes, which in turn influence the seismicity rate parameters.

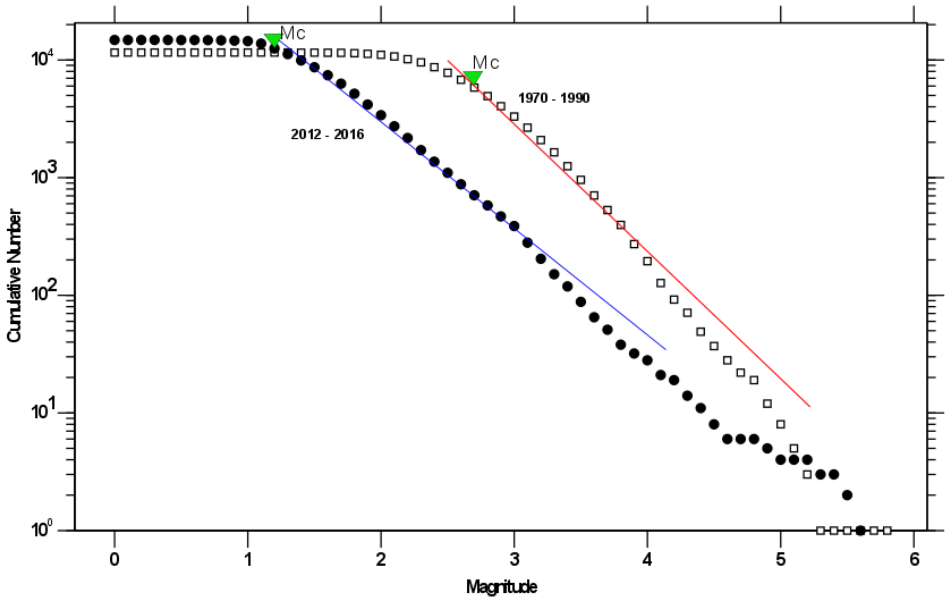


Figure 4-23: Comparison of the FMD for the two periods 1970 to 1990 and 2012 to 2016. The two periods have different M_C values.

Different M_C estimation methods yields different results which makes the process ambiguous (Figure 4-24). The FMD is based on the linearity assumption, which works well in high seismicity regions but not so well in South Africa. The EMR method is very conservative and gives low M_C values, which also affects the hazard calculations.

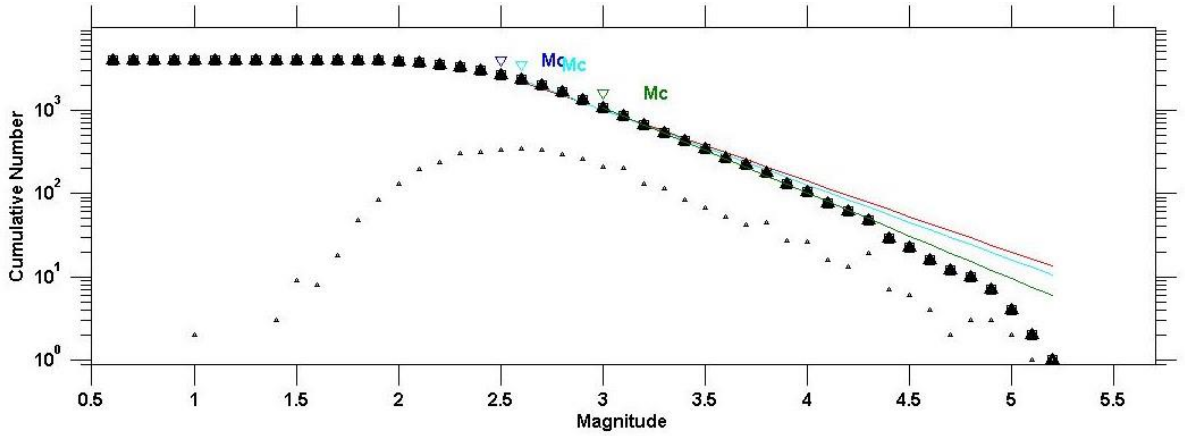


Figure 4-24: Different M_C calculation methods. Green is M_C by the Shi and Bolt method, blue is M_C by EMR and magenta is Maximum curvature method. Both methods were computed using the Gardner and Knoppoff catalogue.

4.13. Conclusions

The main aim of this part of the project was to asses uncertainties associated with the compilation of the seismic catalogue for Johannesburg. Different catalogues were identified emanating from different catalogue processing methods. The different catalgoues will be used for sensitivity anlysis to assess the influence of each processessing method. Because the area extends into other countries, the catalogue has to include events located by those countries. This results in uncertainties of uniformity in the earthquake reporting. Different magnitude scales have been used over the years for magnitude determination at CGS, these results in propagation of uncertainties within our catalogue and careful analysis of the homogenisation process was performed. Identification of duplicated in the catalogue is a subjective process that can be influenced by human perception especially for small magnitude earthquakes. Uncertainties in determination of sources parameters for historical earthquakes was also done. This arise from the spatial distribution of IDPs used for source parameter calculations. Anthropogenic events were carefully removed by applying an indirect approach. The catalogue was then declustered to remove dependent events. Eight declustering methods were implemented to cater for the uncertainties in the process. Statistical analysis was done to test each declustered catalogue for Poissonian distribution and only three methods were accepted. Of the eight declustering methods used, only the Gardner and Knoppoff (1974), Seisan and the Grunthal (1985) were statistically significant for Poissonian distribution. These three methods were applied to all the previously determined catalogues to produce 12 catalogues, which were kept for further processing. The analysed catalogues will be used in the next chapters for the delineation of seismic zones and the calculation of hazard parameters. The different catalogues developed during the uncertainty analysis at different levels will be used for the computation of different recurrence parameters. Spatial and temporal analysis of Mc reveal the uneven distribution of the current catalogue. The distribution of seismicity is influence by the station network configuration, magnitude scale variation as well as the method applied to calculate M_C.

CHAPTER 5: SEISMOTECTONIC MODEL AND SEISMIC SOURCE CHARACTERIZATION

5.1. Introduction

A conceptual seismotectonic model for Johannesburg was developed and it characterizes the modern tectonic settings and processes, the contemporary stress regime, and the rate of active deformation in the region. An ideal delineation of seismotectonic units requires a complete comprehension of the general geological setting and regional tectonics, neotectonic features as well as seismological information (Terrier et al., 2000). However, information of this kind is often found to be incomplete, particularly in regions of low-to-moderate seismicity such as South Africa (Manzunzu et al., 2019; Midzi et al., 2020). Although a large number of faults are known to exist in the study area, there is limited evidence to suggest that any of these are tectonically active. In general, tectonic activity over the last 0.2 Ga years has been muted and the Kaapvaal Craton is an area of comparative tectonic stability (Schulte and Mooney, 2005). However, the existence of clusters of seismicity in the region is an indication that there are active faults, though it is not easy to associate the seismicity to individual faults as is common for stable continental regions (Calais et al., 2005; 2011; 2016; Liu et al. 1992; 2011; 2014). Based on previous seismotectonic studies, a simplified seismotectonic model was created supported by latest information described in chapters 3 and 4 for an area of 500 km radius around Johannesburg. Focal mechanism solutions were calculated to complement the few that were already available.

5.2. Previous seismotectonic studies

The seismotectonics of South Africa is not well understood though a number of studies have been done to try to model it (e.g. Partridge, 1995; Hartnady, 1996; Du Plessis, 1996; Brandt, 2008; Singh et al., 2009; Manzunzu et al., 2019). Of note are the three studies by Partridge (1995), Hartnady (1996) and Du Plessis (1996). Although these studies interpreted different datasets, they identified important seismotectonic units especially in the study area. Brandt (2008) discussed the three hypotheses and outlined the limitations in each hypotheses in comparison to available data. Singh et al. (2009) developed a regional seismotectonic model using both seismological and geophysical information, and Singh (2016) discussed the seismotectonic setting around the KwaZulu Natal area. However, they did not incorporate stress information. Manzunzu et al. (2019) recently updated the seismotectonics of South Africa where more information was considered (e.g. seismicity, focal

mechanisms, stress indicators, fault data etc.). The following sub-sections are reviews of the studies previously presented by Partridge (1995), Hartnady (1996) and du Plessis (1996).

5.2.1. Partridge (1995) model

Partridge (1995) proposed that the seismotectonics of southern Africa are characterised by incipient rifting in a southward propagation of rift fractures from the present EARS into South Africa. He used global plate tectonics data, the seismogenic mechanism inferred from an interpretation of the erosional surfaces, geomorphic evolution as well as seismicity to divide the region into two broad zones with differing horizontal stress regimes. He argued that the south western part of South Africa consists of an E-W horizontal stress regime that prevails due to compressional forces originating at the Mid-Atlantic Ridge, while the northern and eastern South Africa is of extensional stress regime influenced by the presence of the EARS. The eastern zone extends from Mpumalanga to the Urema Graben in the lower Zambezi River catchment, and from the Mozambique Channel via northern Kwazulu-Natal through Cedarville and Koffiefontein to Okiep near the West Coast (Figure 5-1). In addition, Partridge identified potentially capable major faults in both seismically-active zones and seismically-quiet zones. He did not consider the influence of mine seismicity on seismic hazard analysis. The zones identified in this hypothesis are part of our study area, except for the Port Elizabeth and the Cape Town zones.

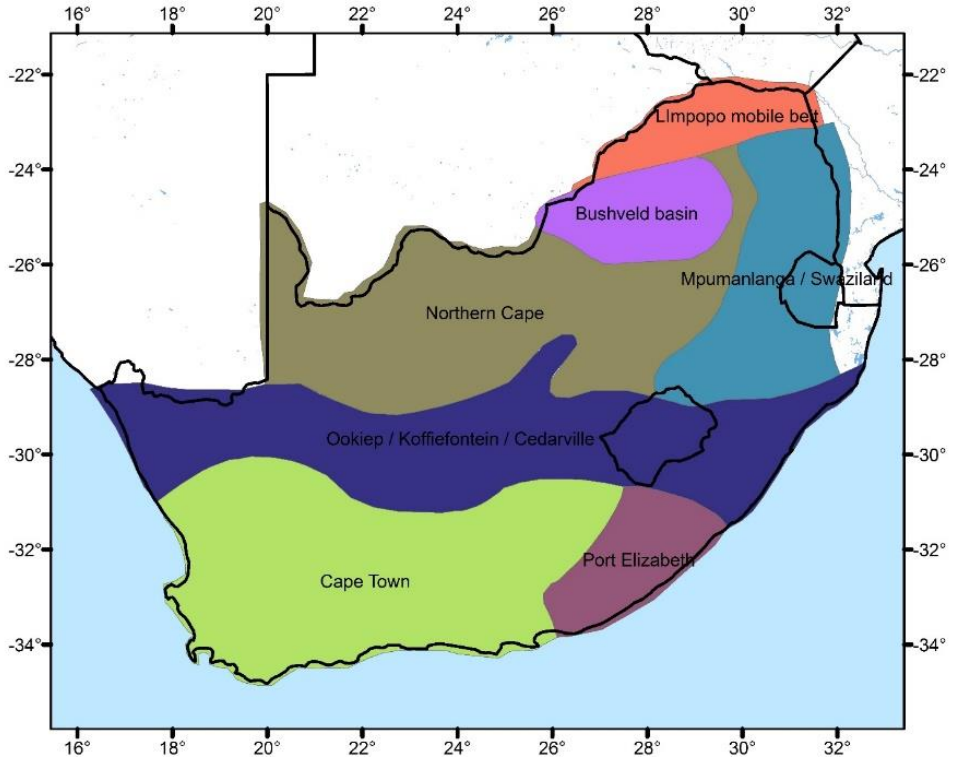


Figure 5-1: A seismotectonic model for South Africa proposed by Partridge (1995).

5.2.2. Hartnady (1996) model

Hartnady (1996) proposed that southern Africa is a developing plate boundary zone which extends from the EARS through its western branch into southern Africa. The model was derived from seismological database, the NUVEL-1 global plate tectonics data set, crustal stress regime data, spatial seismic-moment release and tectonic deformation rates. He proposed that in southern Africa relatively aseismic "blocks" are bounded by seismically active "belts". Eight seismic zones were identified in Southern Africa (Figure 5-2). For our study region, four source zones can be identified from this model, *viz.* the Transgariep, Mpumalanga, Mozambique, Kwahlamba and the broad E-W-trending zone of Ulwandle, Koffiefontein and Cedarville. This model is very basic and no detailed information was available to refine it.

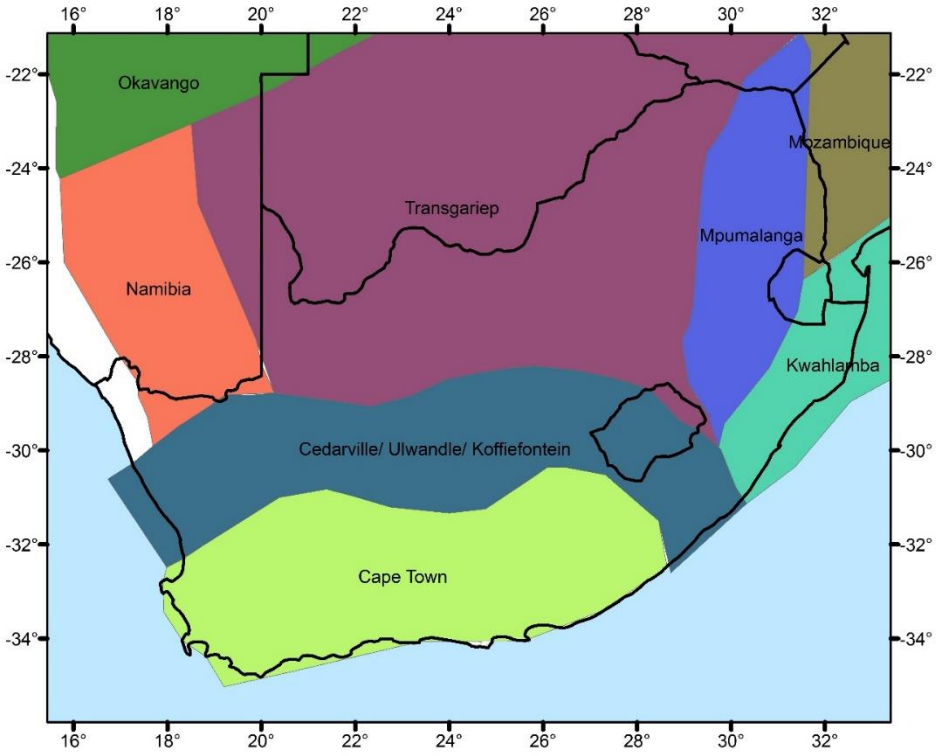


Figure 5-2: Hartnady seismic source zones for Southern Africa (modified from Hartnady, 1996).

5.2.3. Du Plessis (1996) model

The model was derived from seismological, geological, geophysical and geomorphological data to construct a regional seismotectonic model consisting of what was termed 'seismogenic structures'. The model proposes that a regional seismotectonic model always consists of two types of seismogenic structures, namely, those that can be identified using the available databases, and the remaining areas characterised by diffuse seismicity, which cannot be attributed to specific structures. Five major seismic zones were identified and these were further split into smaller zones related to seismicity

clustering (Figure 5-3). The zones identified in our study area include the Central South Africa, Koffiefontein, FreeState, Koffiefontein, Matatiele, Lesotho, Lephepe and the Mupumalanga, Northern Natal, Swaziland zone.

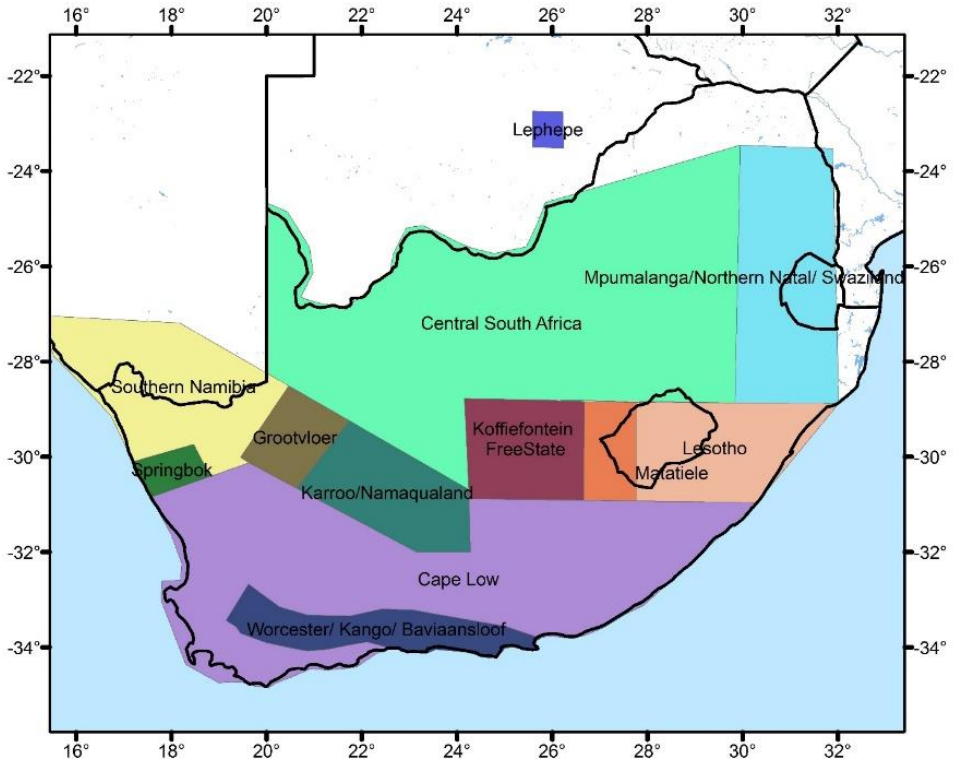


Figure 5-3: Modified seismotectonic zones defined by Du Plessis (1996).

Although the three models were developed using different datasets, they identified a number of similar zones. They agreed that the Koffiefontein, Cedarville, Lesotho zone consist of several clusters trending in an E-W direction. They also identified the N-S zone in the east, stretching from Limpopo into the Eastern Cape, although there were some differences in interpreting this zone. These models were specifically interested in natural tectonic structures and they avoided looking at how structures in the mining regions influence the seismicity. Since their development, a lot of information has been gathered and new theories brought forward that are important in characterizing seismic source zones (e.g. Stamps et al., 2018; Calais et al., 2016; Meghraoui et al., 2016; Malservisi et al., 2003). Recent studies have begun to analyze the modern stress regime using seismicity, Global Positioning System (GPS), and geological strain indicators, such as jointing, in conjunction with stress field modelling (Stamps et al., 2014). A review of models proposed using recent information is provided in the following sections.

5.3. Regional tectonic stress regimes

Earthquakes are usually of tectonic origin and occur along the boundaries of the tectonic plates that make up the surface of the Earth. In southern Africa, low earthquake recurrence rates and a short seismic catalogue inhibit the study of the modern stress regime. As in most stable continental regions of the world, the tectonic seismicity in southern Africa is driven by regional stresses originating from large-scale features that include intra-continental rifts, large-scale topographic elevations, and the network of mid-oceanic ridges (Hartnady, 1990; Andreoli et al., 1996; Calais et al., 2016). More specifically, the stress pattern in southern Africa appears to be dominated by two main fields:

1. Predominant NE-oriented trend corresponding to the East African Rift System (e.g. Mozambique, KwaZulu Natal, Limpopo, Botswana)(Midzi et al., 1999; Kinabo et al., 2008; Meghraoui et al., 2016; Manzunzu et al., 2019);
2. A NW/NNW trend that affects a very broad region, which includes the central and north-western portion of South Africa (Hartnady, 1990; Andreoli et al., 1996; Viola et al., 2005; Calais et al., 2016: Mulabisana et al.,. 2021).

Whereas the NE –orientated trend is roughly parallel to the direction of the plate's motion, the NW-trending stress field is less easily explained and was referred to as the Wegener Stress Anomaly (Andreoli et al., 1996; Viola et al., 2005). The EARS is one of the major source of seismicity in Africa with almost all the largest earthquakes occurring along this zone (Midzi and Manzunzu 2014, Meghraoui et al., 2016). However, Stamps et al. (2018) noted that the EARS remains one of the least monitored tectonic plate boundaries, which makes it challenging to constrain present-day seismic hazards.

A geodetic strain rate model was developed by Stamps et al. (2018) for Sub-Saharan Africa that incorporated geodetic velocity fields, regions of deforming zones and constraints on block rotations. This model provides fundamental constraints on long-term tectonic deformation in the region and an improved seismic hazard assessment in Sub-Saharan Africa. However, this data currently have little information that can be used to characterize the seismotectonics of our region (Meghraoui et al., 2016).

5.3.1. In situ measurements

Many in situ stress measurements have been carried out in mining and civil engineering projects in southern Africa in the last century (Stacey and Wessloo, 1998). The information contained in the database indicates that horizontal to vertical stress ratios in the mining regions (i.e. Carletonville, Klerksdorp and Rustenburg) are high indicating predominance of normal faulting. As indicated in

Figure 5-4 below, a variety of stress orientations are found and this was also identified by Manzunzu et al. (2017). However, no local stress information is available for detailed zonation taking into account stress field variations. The lack of local information is limiting the relevance to broad scale zonation and for assessing the potential for reactivation under given stress regime.

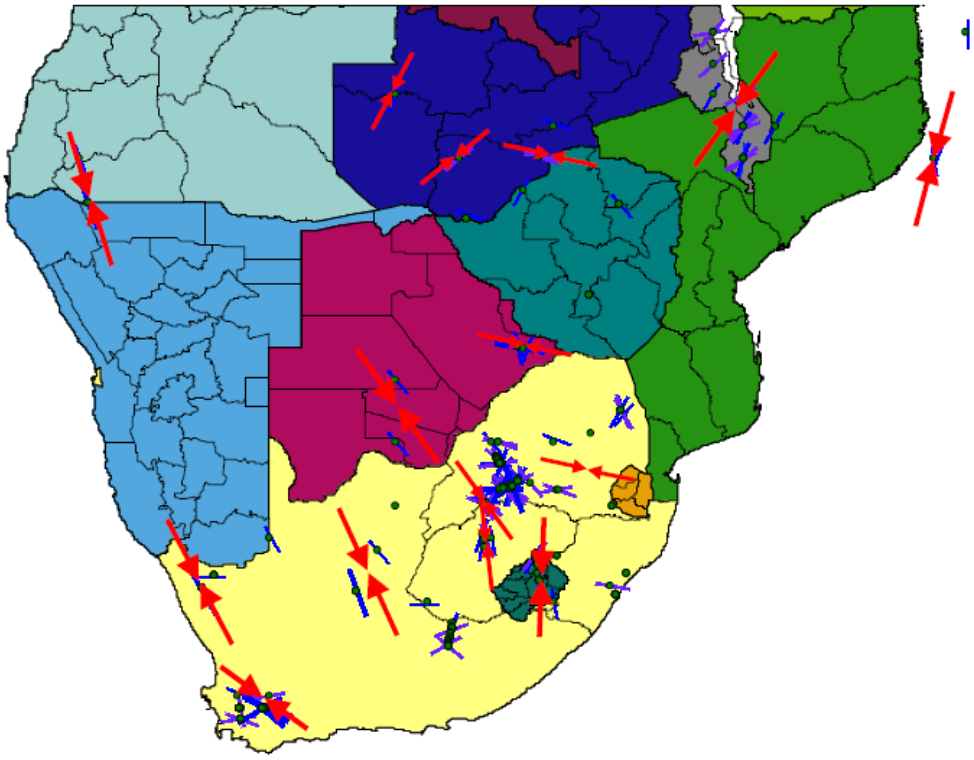


Figure 5-4: Orientations of the major horizontal stresses from in-situ measurements by Stacey and Wessloo (1998). Red arrow indicate compressive stress, blue lines shows extensional stress orientations.

5.3.2. Focal mechanism solutions and stress modelling

A major problem with SCR regions is to associate seismicity with active faults as the fault movement and deformation are very slow (Calais et al., 2005, 2011; Li et al., 2016; Allen 2018). Paleoseismic studies are needed to understand the recurrence rates for some of the faults assumed to be active. However, in the absence of paleoseismic information, focal mechanism solutions (FMS) derived from earthquakes can be used to explain the present day stress regimes. FMS are important in the characterization of style-of-faulting and fault geometries of future earthquakes. About 26 seismic events have published FMS in the study region. This compilation includes 19 tectonic earthquakes and 8 mining related events with magnitudes Mw ranging from 3.0 to 7.0 (Table 5-1).

Table 5-1: Summary of published FMS in the study region. In the case of multiple solutions for the same event, the preferred solution is indicated in bold. Where NM – Normal faulting, SS – Strike slip, NO – normal oblique.

Event	Mining-related (M) or Tectonic (T).	**ID**	**Reference**	**Strike**	**Dip**	**Rake**	**Style of Faulting**
1986-10-05 Matatiele	T	**1**	Dziewonski et al. (1987)	168 348	47 53	-90 -90	NM
1990-09-26 Free State Gold Mines	M	**2**	Dziewonski et al. (1991)	11 153	45 52	-61 -115	NM
1994-10-30 Free State Gold Mines	M	3a	Fan and Wallace (1995)	345	14	-105	NM
		3b	Bowers (1997)	190	45	-70	NM
1997-09-25 Far West Rand	M	**4**	Brandt and Saunders (2011)	354 167	49 41	-86 -95	NM
1998-04-24 Augrabies	T	**5**	Mangongolo et al. (2017)	132	80	18	SS
1998-06-22 Three Sisters	T	**6**	Mangongolo et al. (2017)	19	41	-121	NO
1998-09-06 Lesotho	T	**7**	Mangongolo et al. (2017)	148	48	-67	NM
1998-10-05 Fraserburg	T	**8**	Mangongolo et al. (2017)	9	67	-19	SS
1998-12-05 Far West Rand	M	**9**	Brandt and Saunders (2011)	296 28	88 54	144 3	NM
1999-01-07 Koffiefontein	T	**10**	Mangongolo et al. (2017)	148	18	-68	NO
1999-02-04 Fauresmith	T	**11a**	Brandt and Saunders (2011)	170 269	70 66	-25 -159	NO
		11b	Mangongolo et al. (2017)	98	78	-121	NO
1999-06-21 Koffiefontein	T	**12**	Mangongolo et al. (2017)	95	58	-152	NO
1999-07-03 Koffiefontein	T	**13**	Mangongolo et al. (2017)	68	58	-174	NO
2006-02-22 Machaze earthquake	T	**14**	Fenton and Bommer (2007)	325	27	-114	NO
2007-03-11 Leeu-Gamka	T	**15**	Saunders (2018)*	212	61	28	SS
2010-11-21 Augrabies	T	**16**	Saunders (2018)*	21	52	18	SS
2010-12-25 Augrabies (18:29)	T	**17**	Saunders (2018)*	16	53	17	SS
2010-12-25 Augrabies (23:28)	T	**18**	Saunders (2018)*	10	53	14	SS
2010-12-28 Augrabies	T	**19**	Saunders (2018)*	10	52	16	SS
2011-01-04 Augrabies	T	**20**	Saunders (2018)*	22	58	20	SS
2011-12-18 Augrabies	T	21a	Saunders (2018)*	2	46	10	SS
		21b	USGS NEIC	254 349	78 70	-21 167	SS
2013-11-02 Johannesburg	M	**22**	Midzi et al. (2015a)	135	45	-82	NO
2013-12-18 Bela Bela	T	**23**	Midzi et al. (2015a)	72	51	-77	N
05-08-2014 Orkney	M	**24**	Midzi et al (2015b); Manzunzu et al. (2017)	182.6	72.77	-10	SS
27-08-2014	M	**25**	Manzunzu et al. (2019)	44.15	71.25	-68	NO
03-04-2017 Orkney	M	**26**	Pule et al., (2018)	75	33	-61	NO
31-10-2019 Bongwana earthquake	T	**27**	Manzunzu et al. (2020)	185	68	-52	NO

*Unpublished solutions provided by Saunders

These, however, are insufficient to fully characterize the stress regime of the study area. To complement them, a further 149 events with high quality seismic waveforms were carefully selected for focal mechanism analysis. The waveforms collected from both the national network and the cluster network as well as the temporary network of the AfricaArray stations were used. The waveforms were processed using the SEISAN Software (Ottemöller et al., 2018), where the location of the events was performed using the program HYPOCENTER (Lienert and Havskov, 1995). The selected earthquakes were analysed using the FOCMEC program (Snoke et al., 1985) as implemented in SEISAN software. FOCMEC has good control because it performs an efficient systematic search of the focal sphere and reports acceptable solutions based on a selection criteria for the number of polarity uncertainties. The program utilises the grid search method to find all possible double couple solutions based on first motion polarities and/or amplitude information. The first motion polarity methodology was applied for most of the events while others especially mining related ones were

computed using the amplitude ratio (Snoke et al., 1984). P-wave polarities were picked on the vertical component waveform for each station with high signal to noise ratio (>2.5). For most of the events, the waveforms were very clear so that no filtering was needed during data processing (Figure 5-5), while data for all the other events that were not clear were discarded.

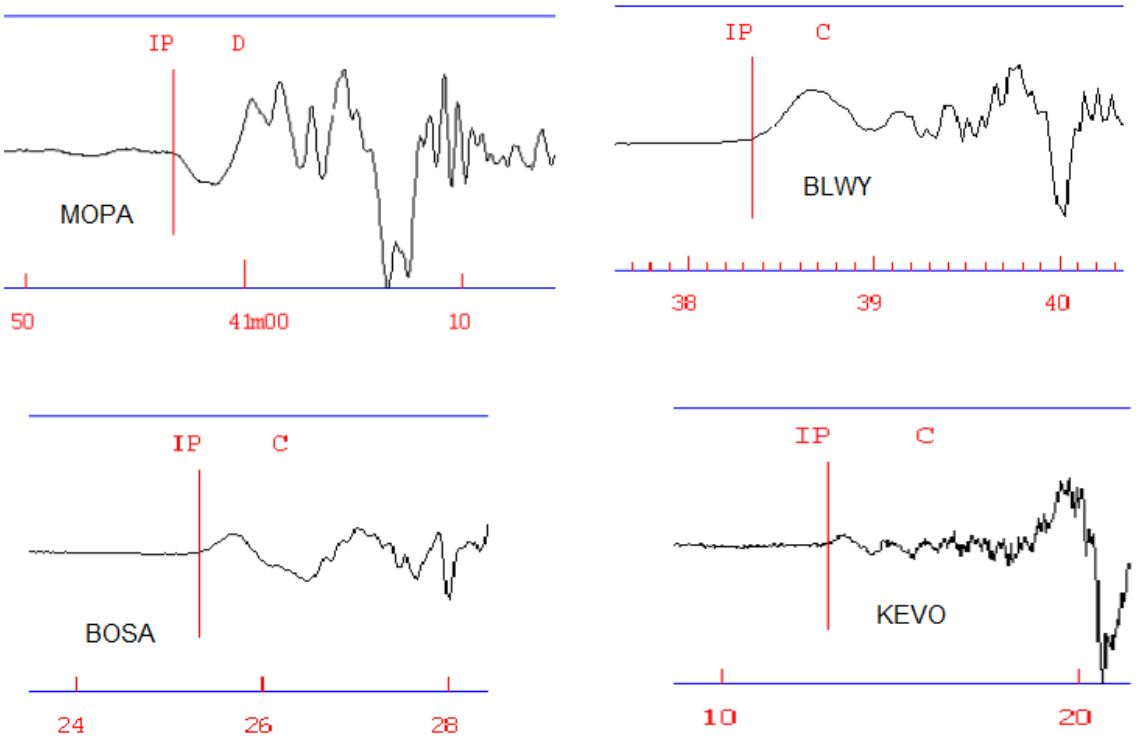


Figure 5-5: Examples of polarities picked. C is the upward first motion and D is the downward first motion. In this figure, station MOPA (BHZ channel) is at an epicentral distance of 210km: Polarity (Down). Station BLWY, (BHZ channel) is in Zimbabwe at 426 KM from the station : (Polarity (UP). BOSA, BHZ, is at epicentral distance of 136 km and station KEVO BHZ located at 221 km from the epicenter.

At least 10 polarities were used for each event with the best polarity errors. Only two polarity misfits were allowed during inversion. In order to obtain reasonable solutions, good azimuth coverage and distance are of paramount importance. A full description of the process followed is given in the manual for the SEISAN software (Ottemöller et al., 2013), where the primary program used is FOCMEC (Snoke et al., 1984). The selection criteria for both polarities and angles allow for correction or weightings for near-nodal solutions. The majority of the solutions indicate normal faulting, with a few showing transtensional faulting. In a few cases, reverse faulting mechanisms were observed, suggesting that those areas are likely to be highly faulted with faults oriented in all directions (Manzunzu et al., 2017). Solution of events from this study and previously published solutions are shown in Figure 5-6 and listed in Tables 5-1 and 5-2.

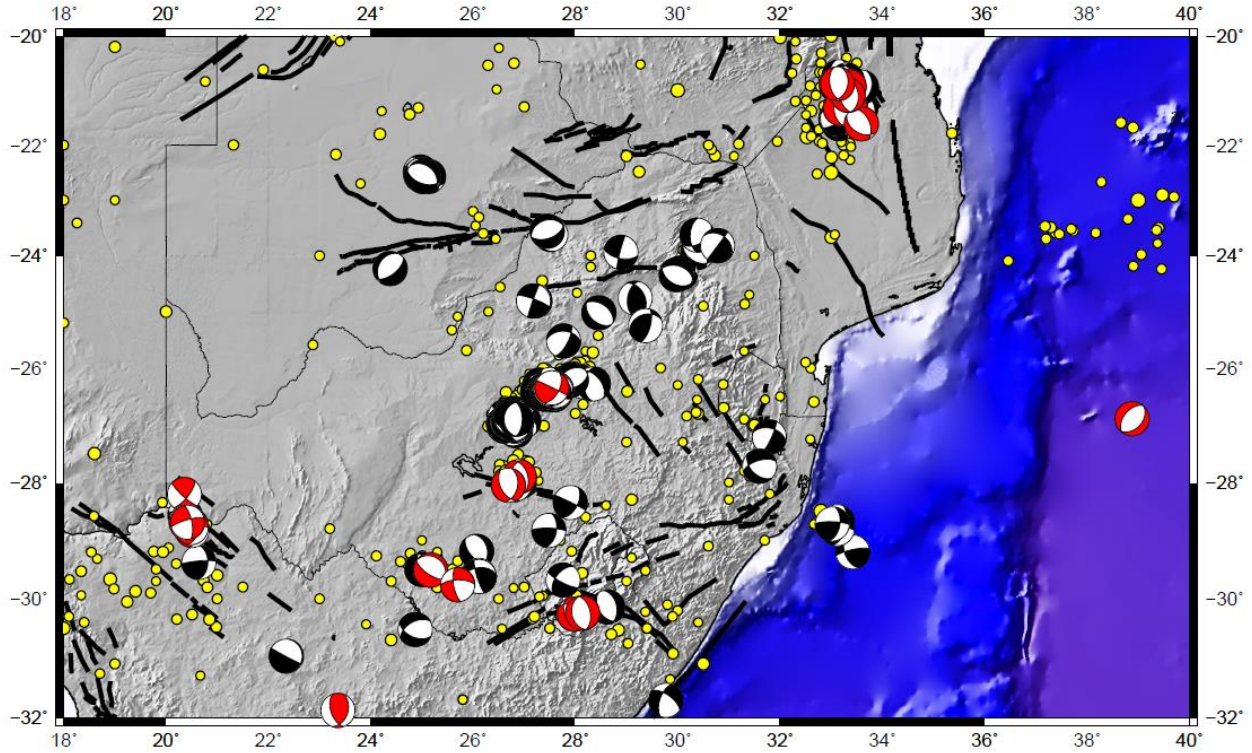


Figure 5-6: Focal mechanism solutions used in this study. Thick black lines represent faults located in the area and yellow circles represent earthquakes (M>4). Black beach balls represent new solutions (Table 5-2) while the red ones are the published solutions in Table 5-1 (Faults were extracted from Manzunzu et al., 2019; background topography was extracted from Amante et al., 2009).

Table 5-2: Summary of FMS determined in this study.

Year	Month	Day	Hour	Minute	Second	Long	Lat	Depth	Strike	Dip	Rake	Magnitude
2012	3	24	4	43	51.7	26.07	-29.19	17.2	138	58	-109	4.9
2013	1	8	14	33	19.8	26.822	-26.893	2.4	334.41	25.46	78.3	2.9
2013	1	10	13	24	48.6	26.78	-26.886	2.8	59.19	40	-74.02	3.8
2013	1	31	7	54	39.9	26.855	-26.942	2	302.43	46.92	-69.25	3.6
2013	2	10	12	16	10.5	26.789	-26.895	4.5	288.51	30	-90	3.2
2013	2	25	11	16	42.3	26.819	-26.963	2	230.4	54.07	37.45	2.8
2013	3	4	2	12	3.4	26.803	-26.884	0.7	355.76	67.48	20.36	2.4
2013	3	9	6	0	9.8	26.736	-26.886	2.1	199.74	20	-63.9	2.6
2013	3	10	16	57	9.2	26.844	-26.941	2	180	45.21	-88.72	2.8
2013	3	18	18	14	39.4	26.778	-26.894	2	199.74	30	-55.05	2.9
2013	3	20	12	53	8.5	26.811	-26.965	3.1	78.06	46.92	69.25	2.7
2013	3	20	22	35	40.1	26.788	-26.939	2.9	68.38	72.77	-58.43	3.8
2013	3	21	12	10	39.8	26.743	-26.885	3	283.6	45	-46.32	2.7
2013	3	22	3	1	17.5	26.743	-26.882	3.9	189.8	77.2	152.3	3
2013	3	22	3	1	33.1	26.739	-26.887	2.5	95.02	45.22	82.95	3.3
2013	4	4	12	17	0.7	26.806	-26.963	2	219.46	73.02	-90	3.3
2013	4	5	2	43	15.2	26.741	-26.886	3	288.51	40	-65.61	2.6
2013	4	5	21	1	32	26.716	-26.938	2	214.49	34.55	-56.98	3.6
2013	4	6	3	21	0.4	26.717	-26.934	2.9	328	60	-90	2.9

2013	4	21	9	13	39.8	26.777	-26.942	2	314.1	67.48	20.36	3.4
2013	4	22	13	39	32.7	26.82	-26.92	2.8	254	26.4	-89	2.9
2013	4	23	2	38	44.2	26.805	-26.985	2.7	288.51	37.64	-74.98	2.9
2013	4	23	21	27	45.8	26.778	-26.945	2	239.21	30	-63.11	2.9
2013	4	25	17	20	3.6	26.745	-26.867	2	152.17	54.37	58.67	3.1
2013	4	28	23	36	4.3	26.799	-26.993	2.8	275.9	65.41	-78.99	3
2013	4	30	15	49	46.1	26.775	-26.943	2	9.86	50	90	3.3
2013	5	1	8	0	17	26.741	-26.883	3	199.73	80	-70.71	3.3
2013	5	2	17	6	13.9	26.805	-26.985	2.6	9.86	50.9	-68.9	3.1
2013	5	12	0	58	59.6	26.831	-26.87	2	209.62	30	-97.48	3.5
2013	5	14	22	4	45.5	26.739	-26.884	3.4	69.05	90	90	3.9
2013	5	15	1	4	52.8	26.806	-26.965	2.1	337.8	58.2	-70.5	2.8
2013	5	15	6	38	32.1	26.742	-26.871	2	224.4	60	-90	3.5
2013	5	15	10	51	32.5	26.783	-26.878	1.8	50	81	-83.2	2.8
2013	5	16	19	27	1	26.788	-26.993	2.5	82.36	48.44	-30.79	2.6
2013	5	20	3	46	47.1	26.762	-26.925	4.4	28.2	75.7	155	2.8
2013	5	20	19	57	12.8	26.721	-26.895	2	290	55	-29.86	3.3
2013	5	21	16	33	24.6	26.779	-26.893	2	217.2	69.3	40.89	3.3
2013	5	21	16	33	24.6	26.779	-26.893	2	237.4	50.14	56.6	3.3
2013	5	26	22	35	15.1	26.767	-26.92	2	180	30	-59.31	2.9
2013	5	30	16	50	2	26.829	-26.979	2	291	89.1	-130.1	3.5
2013	6	5	13	7	11.4	26.778	-26.894	2	232.81	52.84	64.59	3.1
2013	6	9	21	33	11.2	26.752	-26.922	3.1	30.11	7.07	44.89	3.2
2013	6	12	8	41	22.5	26.783	-26.898	2.5	25	75	90	4.1
2013	6	13	0	19	52.7	26.831	-26.977	2	311.16	43.96	60.48	3.3
2013	6	22	18	33	15.1	26.787	-26.941	2	176.41	41.03	-74.66	2.4
2013	6	25	11	30	31.4	26.787	-26.989	1.8	1.4	82.3	-2.9	3.4
2013	6	26	4	37	14.4	26.706	-26.923	2	300	65	-123.81	3.3
2013	7	1	3	46	27.5	26.771	-26.944	2	199.74	55.61	-90	3.7
2013	7	2	10	6	28.7	26.764	-26.92	2	327.73	46.03	54.04	3.1
2013	7	6	9	30	0.9	26.812	-26.899	2	180	30	-90	3.3
2013	7	6	14	43	57.7	26.782	-26.941	3.1	99.37	64.34	-16.1	3.9
2013	7	7	1	8	44.1	26.765	-26.92	2	260.67	34	-87.9	3.8
2013	7	12	9	39	28.2	26.832	-26.933	3	357.63	17.82	-61.23	3.2
2013	7	12	11	2	55.6	26.764	-26.923	3	88.78	12.38	-104.29	3.7
2013	7	13	4	21	56.2	26.814	-26.9	2	340	50	-45.22	4
2013	7	14	5	22	37.5	26.773	-26.909	2	209.6	28.47	-33.49	3.4
2013	7	27	13	1	37.4	26.823	-26.923	2.3	0	75	74	3.4
2013	7	29	6	55	30.2	26.821	-26.926	3.1	194.8	73.97	-77.65	3.2
2013	8	1	20	48	38.4	26.705	-26.928	2	278.68	50	-86.92	3
2013	8	4	21	24	11.4	26.719	-26.939	2	219.47	47.86	-61.09	2.4
2013	8	13	18	50	2.3	26.801	-26.847	2	58.98	35.53	-53.95	2.7
2013	8	26	21	7	22.5	26.818	-26.929	2.8	258.51	52.84	-64.59	3
2013	8	31	11	48	1.5	26.781	-26.941	2	243.4	52.84	64.59	2.6
2013	9	1	4	47	7.1	26.803	-26.91	2	219.47	30	-90	3
2013	9	1	7	56	11.1	26.765	-26.92	2	309.96	50.73	-77.04	3.3
2013	9	2	9	54	9.7	26.827	-26.991	2	298.42	30	-74.95	3.7

2013	9	12	7	51	40.5	26.79	-26.993	2	180	40	-90	3.2
2013	10	7	3	38	8.6	26.832	-26.933	2.9	348.85	67.48	62.77	3.4
2013	10	8	3	30	42.8	26.866	-26.883	2	69.85	72.77	-58.43	3.1
2013	10	8	7	45	59.4	26.748	-26.872	2	219.47	70	-90	3.5
2013	10	18	22	26	59.3	26.718	-26.947	2	242.96	48.44	48.07	3.4
2013	10	18	22	27	54.7	26.721	-26.948	3	207.51	64.34	-56.31	3.7
2013	10	21	21	19	11.6	26.828	-26.903	2	209.62	30	-81.12	3
2013	10	27	0	28	20.2	26.823	-26.934	2	199.74	50	-99.34	4
2013	10	27	1	18	12.9	26.83	-26.93	3.3	180	70	-33.48	3.4
2013	10	28	0	42	56.9	26.761	-26.922	2.8	1.52	64.34	56.31	2.9
2013	10	31	1	41	51.1	26.781	-26.899	2	290	54.32	-70.63	3.5
2013	11	1	9	7	30.4	26.608	-26.99	2	318.16	50	-90	3.4
2013	11	4	8	56	0.6	26.717	-26.962	2	41.7	47.8	-86.9	2.8
2013	11	7	9	49	25.6	26.822	-26.958	3.9	195	80	-90	3.2
2013	11	16	17	52	8.3	26.819	-26.929	2	0	60	-66.73	2.8
2013	11	18	7	53	49.3	27.92	-26.21	5	72	51	-77	3.6
2013	12	2	19	18	7.7	28.46	-25.02	5	135	45	-82	3.9
2014	8	5	10	22	31	26.81	-27	4.7	182.6	72.77	-10.31	5.5
2014	8	6	12	43	53	26.84	-26.94	2.2	142.6	50.73	-77.04	2.1
2014	8	6	15	42	19	26.82	-26.91	3.4	133.06	71.78	29.21	1.7
2014	8	6	21	33	30	26.81	-26.92	1.6	182.45	62.97	-37.45	1.3
2014	8	6	21	33	30	26.78	-26.9	6.6	163.48	75.97	32.4	1.3
2014	8	7	13	10	38	26.83	-27.1	0.2	219.47	70	-90	2.1
2014	8	7	15	10	5	26.81	-26.9	5.7	349.57	84.03	29.45	3.1
2014	8	7	16	58	45	26.84	-26.97	1.3	57.84	49.37	80.76	1.9
2014	8	9	5	58	0	26.81	-26.96	0.1	194.8	45	-90	2.6
2014	8	9	11	7	42	26.79	-26.93	0.1	122.5	42.06	-50.89	2
2014	8	9	12	40	57	26.81	-26.98	4.3	52.72	56.17	53	2.6
2014	8	15	10	2	2	26.82	-27.02	6.8	57.99	52.24	-50.77	1.8
2014	8	16	7	40	8	26.79	-26.95	2.2	71.67	43.37	-72.38	1.3
2014	8	16	17	6	1	26.83	-27.02	2	1.25	30	0	0.9
2014	8	16	20	16	1	26.8	-26.95	3.8	264.02	65.91	-73.53	0.8
2014	8	25	12	6	20	26.8	-26.98	3.3	126.64	46.92	14.51	2
2014	8	27	23	18	54	26.8	-26.97	2	44.15	71.25	-68.83	3.7
2014	8	31	11	57	15	26.75	-26.96	2	121.26	34.63	-77.62	1.6
2016	7	6	15	22	42	27.58	-26.47	2	347.7	70	-90	3.1
2016	7	19	9	20	41.5	26.81	-28.04	2	160.46	54.37	19.53	3.2
2016	8	10	0	35	35.2	26.72	-26.84	2	90.04	46.03	-26.73	2.5
2016	8	18	18	40	57.9	28.63	-30.14	5	347.03	45.86	-76	4.1
2016	8	31	23	26	50.6	26.6	-27	2	357.17	45.86	-76	3.1
2016	9	2	0	21	58.4	26.6	-26.99	2	8.49	55.15	-83.9	2.4
2016	9	5	6	22	49.3	27.76	-29.68	10	117.32	77.3	-38.26	3.4
2016	9	5	16	37	8.9	27.36	-26.41	2	235.92	26.81	-67.35	2.5
2016	9	11	13	34	35.6	26.6	-26.98	2	347.03	45.86	-76	2.2
2016	9	11	20	49	42.4	26.6	-27	2	10.72	52.84	-64.59	2.2
2016	9	14	18	55	39.3	26.77	-26.94	2	265.44	65.82	-51.04	2.6
2016	9	17	14	11	26.2	27.43	-26.44	2	197.14	42.27	-67.37	2.8

2016	9	19	16	18	39.6	27.59	-26.44	2	177.14	11.3	44.72	2.5
2016	9	26	3	15	3.9	27.38	-26.44	2	328.8	80.15	-79.85	2.5
2016	9	30	19	21	41.1	27.56	-26.39	2	135.88	80.04	-84.92	2.5
2016	10	28	16	45	24.7	24.87	-30.52	5	113.66	52.24	-50.77	2.7
2016	12	21	23	23	43.6	31.79	-27.21	20	284.54	46.92	-14.51	2.8
2017	2	7	14	2	46.2	27.58	-26.43	2	15	35	90	3.1
2017	4	3	3	8	50	26.75	-26.89	2	16	40	-122	4.6
2017	4	3	17	40	13.4	25.13	-22.57	10	330.42	45.71	-61.46	6.3
2017	4	3	18	11	23.5	24.97	-22.49	10	331	43.96	-60.48	4.1
2017	4	5	0	55	48.4	24.98	-22.54	10	336	42.27	-67.37	4.6
2017	4	8	19	55	30	24.99	-22.54	10	343.68	39.67	-57.6	4.3
2017	4	9	18	39	57.4	31.6	-27.72	10	133.9	47.85	-39.32	3.3
2017	4	22	20	50	36.8	26.61	-27.02	2	160	90	30	3.4
2017	6	13	4	4	38.1	27.55	-26.42	2	313.3	41.41	40.89	2.8
2017	6	13	4	14	5.3	27.59	-26.41	2	260.7	60.5	-42.39	2.8
2017	7	2	2	53	50.3	26.74	-26.84	2	276.8	46.92	-69.25	3.4
2017	7	4	11	37	3.7	25.03	-22.57	10	310.55	36.22	-72.91	4.4
2017	7	9	22	54	4.8	26.77	-26.92	2	17.1	35.31	-81.33	3.6
2017	7	25	4	18	54.4	27.56	-26.43	2	214.17	28.9	-57.62	3.4
2017	8	8	21	47	23.6	28.15	-26.24	2	148.47	70.32	79.37	2.4
2017	9	15	13	31	5	26.11	-29.62	5	250.15	51.62	12.25	3.7
2017	9	15	13	52	12.2	26.11	-29.6	5	254.88	48.36	18.88	3.4
2017	9	16	11	17	16.8	26.12	-29.62	5	262.52	46.92	14.51	3.5
2017	10	25	22	16	56.3	27.4	-26.43	2	14.98	45.22	-82.95	2.8
2018	1	9	13	19	2	27.77	-25.52	5	273.6	42.06	-31.11	2.1
2018	1	15	1	53	30.6	27.21	-24.81	2	46.32	50.73	-77.04	2
2018	1	15	9	16	40.4	30.38	-23.63	5	56.1	48.44	-48.07	3
2018	1	15	14	29	32.2	30.06	-24.31	5	279.35	52.84	-64.59	1.8
2018	1	16	12	1	28.7	29.17	-24.76	5	331.99	43.96	60.48	1.8
2018	1	24	12	0	38.4	28.89	-23.94	0	101.27	60.5	-5.73	0.9
2018	1	25	11	44	36.1	27.52	-23.62	0	168.36	14.11	44.56	2
2018	1	26	14	21	59.4	29.97	-24.34	5	123.94	45.86	-76	1.6
2018	2	4	12	7	10.9	27.45	-23.56	0	250.91	35	-90	2
2018	2	7	12	38	25.5	29.37	-25.25	0	15.99	67.48	62.77	2.9
2018	2	16	12	4	15.5	30.78	-23.82	5	306.61	35	0	3.4

The focal mechanism data and fault orientations generally indicate a remarkably consistent regional stress pattern with maximum extension in the NE-SW and NW–SE directions. A mixture of reverse and strike slip faulting is also observed in central South Africa (e.g. in Klerksdorp and some parts of Limpopo) indicating the complex tectonic setting in the area. To the north and north east of the study area (i.e. Botswana, Mozambique and Zimbabwe), normal faulting is predominant due to the presence of the western branch of the EARS. As shown in Figure 5-6, the FMS reveals that the majority of the events in Witwatersrand Goldfields have normal fault mechanisms (Figure 5-7). The FMS in these

mining zones are in agreement with the stress measurements made by Stacey and Wesloo (1998). It shows that mining activities are reactivating normal faults. However, the occurrence of the 5 August 2014, Orkney earthquake (M5.5) is still difficult to explain with the observed stress orientations, but can be attributed to flexural adjustment (Manzunzu et al., 2017).

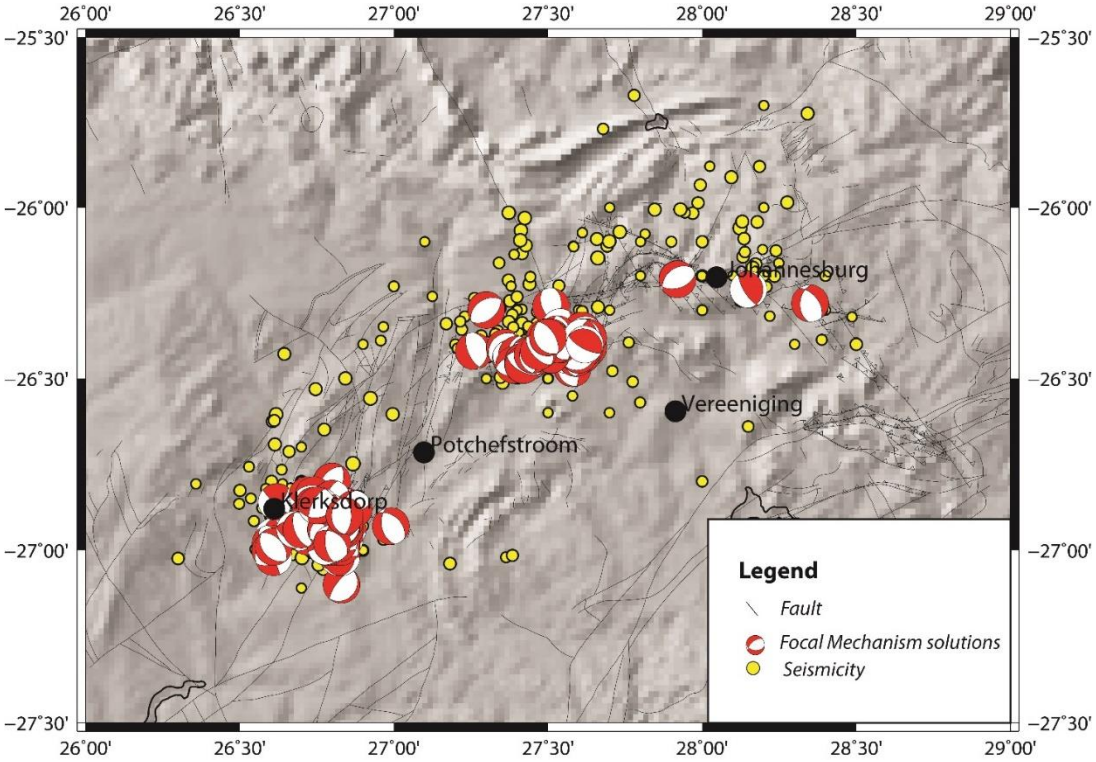


Figure 5-7: Zoomed in focal mechanism solution for the Witwatersrand basin. The seismicity is for magnitude 3.5 and above for the period 1602 to 2017 (Faults were extracted from Manzunzu et al., 2019; background topography was extracted from Amante et al., 2009).

5.3.3. Stress inversion

FMS shown in Figure 5-6 were used in conducting stress inversions. Several methods have been proposed for determining tectonic stress from focal mechanisms of earthquakes (e.g. Gephart and Forsyth, 1984; Michael, 1987; Delvaux and Barth, 2010; Maury et al. 2013). However, stress inversions from focal mechanisms are faced with a problem of identifying the auxiliary plane from the primary fault plane. If the primary fault plane and the auxiliary plane are interchanged in the stress inversions, the results can be biased. To overcome this problem, some additional information (e.g. geological evidence or indications from aftershock analysis) is required. For this reason, Lund and Slunga (1999) proposed applying the so-called fault instability constraint and identified the fault with that nodal plane which is more unstable in the given stress field. Using this criterion, they modified the Gephart and Forsyth (1984) method by calculating the stress in iterations thereby improving its efficiency. This method was applied through the software Stressinverse as provided by Vavrycuk

(2014). 175 focal mechanism solutions were inverted. The FMS were grouped into sub zones and each sub zone is inverted for stress computation. Results of the stress inversion are shown in Figure 5-8. The CASMO software (Heidbach et al., 2018) was used for plotting these results.

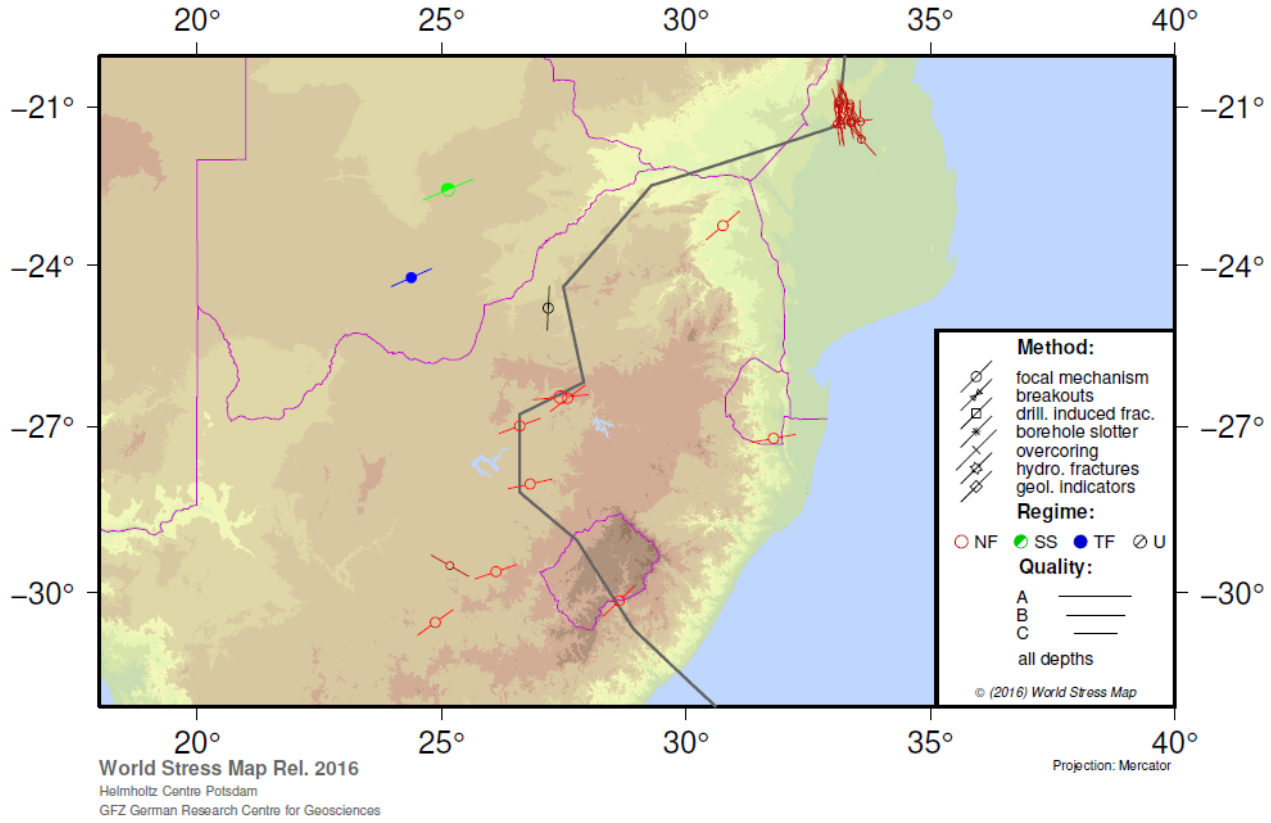


Figure 5-8: Stress inversion from focal mechanism orientation data plotted using the CASMO software (Heidbach et al., 2018) for the inverted focal mechanism solutions.

NE- to ENE-oriented trend dominates the stress pattern that is consistent with the EARS. Stress orientation in the Witwatersrand basin might also be influenced by anthropogenic stress changes due to mining operations, but no evidence can support this from the current analysis. Reactivation of dormant faults is possible and careful analysis is required in assessing the stress regimes. In a few regions (e.g. Koffiefontein and the Klerksdorp mining district), the NW- to NNW-trend is also dominant. Although regional stress field are dominant, the deformation process is quite slow and recurrence periods for large earthquakes are very long. Therefore, it can be concluded that South Africa is located in a stable continental regions. Movement of faults is very slow which results in difficulties in associating seismicity to individual faults.

5.4. Depth distribution

The earthquake location process incorporates the determination of the hypocentral parameters (longitude, latitude and depth) and the origin time of the earthquake. Of these parameters, the most difficult to determine is the depth, especially with a sparse seismic network like the SANSN. As a result, it is common practice to fix the hypocentral depth and attempt to solve for epicentral coordinates only when a well-constrained location in three dimensions cannot be achieved due to data limitations. As discussed in Chapter 4, the CGS tends to fix depth values depending on location of events, 2 km for events located in mining regions, 5 km for natural / tectonic events and 0 km for explosions (Saunders et al., 2010). For a very small number of South African events where instrumental information was sufficient to obtain a reasonably well-constrained estimate of depth, mostly when more advanced analyses such as moment tensor inversion and/or waveform fitting could be performed, the depth was determined (Brandt, 2014; Brandt and Saunders, 2011; Mangongolo et al., 2017). However, even when such techniques are used, resulting depths are not always reliable (Mangongolo et al., 2017). Table 5-2 summarizes published depth values for tectonic events in South Africa gathered from the literature. Overall, these results point to shallow crustal depths (<20 km).

Table 5-3: Instrumentally determined depths of South African tectonic earthquakes published in the literature. Note: No estimate of depth uncertainty was given in some cases.

Event	Mw	Reference	Type of study	Depth (km)	Remarks
1976-07-01 Koffiefontein	5.8	Shudofsky (1985)	Rayleigh-wave inversion and body-wave modelling	6.0	Focal depth from minimising residuals between observed and predicted waveforms.
		Jensen (1991)	Body-wave inversion of long-period WWSSN data	5.5	Use both P- and SH-waves to obtain focal solution
		Storchak (2009)	Reanalysis of ISC data	7.0 to 11.0	Original ISC depth 28 km
1986-10-05 Matatiele	5.3	Dziewonski et al. (1987)	Harvard centroid moment tensor solution	15.0	Default depth value for shallow earthquakes, probably fixed.
		EHB Bulletin	Reanalysis of ISC data	11.7± .7	Slight increase of the error ellipse compared to the ISC fixed depth solution
1989-09-29 SA-Lesotho border	5.0	ISC Bulletin	Routine location	6.8 ± 22.7	Large error indicative of poor constraints.
		EHB Bulletin	Reanalysis of ISC data	7.7	Error unspecified, slight increase of error ellipse with respect to ISC.
1998-04-24 Augrabies	4.3	Mangongolo et al. (2017)	Regional depth phase modelling using SASE temporary array data	7.3 ± 2.3	
1998-06-22 Three Sisters area	3.5	Mangongolo et al. (2017)	Regional depth phase modelling using SASE temporary array data	6.3 ± 0.3	
1998-07-05 Lesotho	3.0	Mangongolo et al. (2017)	Regional depth phase modelling using SASE temporary array data	14.8 ± 1.5	
1998-09-06 Lesotho	3.4	Mangongolo et al. (2017)	Regional depth phase modelling using SASE temporary array data	18.6 ±3.0	
1998-10-05 Fraserburg	3.9	Mangongolo et al. (2017)	Regional depth phase modelling using SASE temporary array data	5.6 ± 0.3	
1999-01-07 Koffiefontein	2.7	Mangongolo et al. (2017)	Regional depth phase modelling using SASE temporary array data	6.3 ± 0.9	
1999-02-04 Koffiefontien	4.5	Mangongolo et al. (2017)	Regional depth phase modelling using SASE temporary array data	8.1 ± 1.5	
1999-02-04 Fauresmith	3.8	Brandt and Saunders (2011)	Regional moment tensor solution using SASE temporary array data	11.0	Event in Koffiefontein region

1999-06-21 Koffiefontien	3.3	Mangongolo et al. (2017)	Regional depth phase modelling using SASE temporary array data	7.5 ± 1.4	
1999-07-03 Koffiefontein	4.5	Mangongolo et al. (2017)	Regional depth phase modelling using SASE temporary array data	7.5 ± 2.2	

Again, larger mining events provide some insights into the limitations of the various approaches when data are scarce. Table 5-4 summarizes the depths determined for such events using techniques similar to those used to determine the depths of tectonic events listed in Table 5-3. Some of these large mining events have shown to be occurring at depths deeper than the 2 km expected for normal operations.

Table 5-4: Depths of mining events with focal mechanism solution.

Event	**Mw**	**Type of study**	**Depth**	**Reference**
1990-09-26 Free State Gold Mines	5.0	Harvard centroid moment tensor solution	28.3 ± 8.8 km (later revised to 5 km)	Dziewonski et al. (1991)
1994-10-30 Free State Gold Mines	4.9	Regional moment tensor solution	9-12 km	Fan and Wallace (1995)
		Global moment tensor inversion using broadband data	2.3 km	Bowers (1997)
1997-09-25 Far West Rand	4.1	Regional moment tensor solution using SASE temporary array data	2 km	Brandt and Saunders (2011)
1998-12-05 Far West Rand	4.1	Regional moment tensor solution using SASE temporary array data	1 km	Brandt and Saunders (2011)
2014-08-05 Orkney event	5.5	Routine location using SANSN as well the 3 cluster networks to constrain depth.	4.7 km	Midzi et al. (2015)

5.5. Seismotectonic model construction

From the gathered information, a seismotectonic model can be constructed. Terrier et al. (2000) suggested a methodological flow chart for the construction of a seismotectonic model (Figure 5-9). This flow chart was utilized in compiling the seismotectonic model of the study region. A number of databases were selected as described in Chapter 2, Chapter 3, and Chapter 4 as well as section 5.2 and 5.3. In this chapter, each database is classified according to its importance and the model will be developed based on the classified datasets.

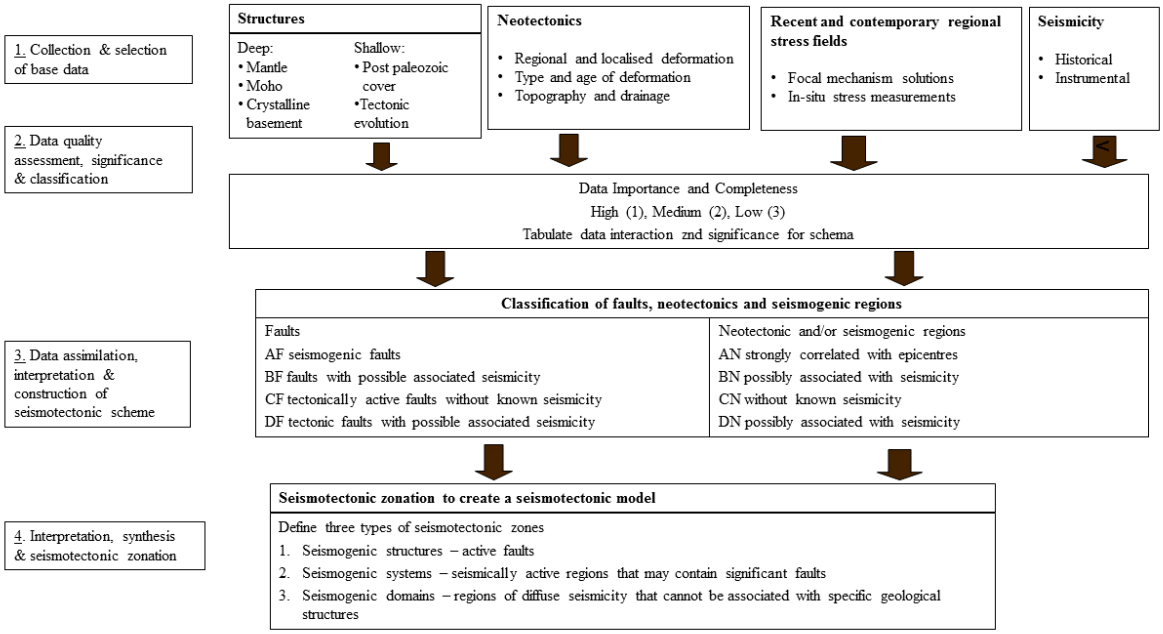


Figure 5-9: Flow chart of the construction of a seismotectonic model as suggested by Terrier et al. (2000).

5.5.1. Classification of available data

The available information was evaluated and prioritized with respect to their usefulness for source zonation. The data classification scheme as implemented in Terrier *et al.* (2000) was followed in this study (Table 5-5). From this classification, the most important data source for zonation are the seismicity (both instrumental and historical), focal mechanism solutions, faults and the overall geological and rheological units.

Table 5-5. Classification of the available information sources for the usefulness of seismic zonation in the region. High (1), Medium (2), Low (3).

Type of information	Class	Remarks
Large-scale geological/ rheological units	1	Differences between crustal-scale units are meaningful as they coincide with differences in earthquake depth distribution, differences in the density of earthquakes and differences in isostatic behaviour. However, major boundaries between these regions show no signs of recent activation in historical or geological data.
Historical catalogue	1	While highly relevant, recurrence times of large events are impossible to establish based on the historical data alone. In areas of moderate seismicity, the uncertainty in magnitude and location is important and most likely large and poorly quantified.
Instrumental seismicity:	1	Important to constrain source zones and in order to construct a recurrence model, if combined with the historical catalogue. However, it is unclear to what extent the extrapolation from small events to larger ones, and from the most recent times to longer periods, is valid. Depth of most South African earthquakes is fixed. The few events that had depth determined are used to estimate seismogenic depth distribution.
Focal mechanism	1	Useful for defining the potential for reactivation of existing faults, for general style of faulting, and to check consistency of zoning. However, it is unclear to what extent the observed small events can be extrapolated to hazard relevant larger ones. The available dataset has more than 200 solutions which is well distributed within our study region (Figure 1-7).
Paleoseismicity	3	'Paleoseismic' events older than 3 Myrs are considered to provide no pertinent information for current earthquake hazard. Younger, Holocene evidence is more critical. However, the available paleoseismic evidence (e.g., Andreoli et al., 1996) is sparse, fragmented, incomplete, and uncertain in both space and magnitude. This is because very few such investigations have been carried out in the country

		mainly due restrictive costs. Lack of information from such studies means there is no data that can be used to characterise active faults for them to be used in seismic hazard assessments. Only area source zones will be used. Therefore, it provides, no conclusive evidence of size and time of occurrence of large magnitude historical/ prehistorical earthquakes on the identified faults.
Hot springs	3	Hot springs inform on regions where water circulates deep and fast in the crust and their alignments across lithological boundaries are known to delineate major fracture zones, some of them going down to Moho depth. Their correlation with recent seismic activity is questionable, but such alignments are important for large-scale zoning because they point to crustal fractures, i.e. weak contacts prone to eventual reactivation. Dhansey et al., (2017) identified that anomalous heat flow and underpinning tectonic influences are also evident with the occurrence of hot springs and higher number of natural on-craton seismic events around these structures. In general, seismicity related to these deep cratonic discontinuities highlight reactivation associated with a more recent northeast to southwest oriented extension, which is in agreement with the present-day stress state seen in much of South Africa. In addition, they do not yield a complete set of major fracture zones; other fracture zones, devoid of hot springs and water circulation, may exist.
Vertical movements, geodetic data, strain data	2	Geodetic data help in defining broad regional patterns, unless specific and detailed measurements for individual faults exist, which is not the case in South Africa. Yet, this information indicates seismic potential. However, as mentioned by Stamps et al. (2018), the African region is under studied in terms of geodetic measurements. In South Africa and in neighbouring areas, strain rates are homogeneous and overall very low (1 nanostrain per year or less), consistent with GPS measurements. Movement of the order of 1mm/yr have been observed from GPS data analysis (Calais et al., 2006; Jestin et al., 1994; Malservisi et al., 2013). Vertical movements are too small to distinguish isostatic response due to post-glacial rebound from tectonic signals.
Faults	1	Numerous faults are identified on geological maps at all scales, which reveal an equal potential for earthquakes almost everywhere. In the literature, there is very little convincing evidence for Quaternary movements that have offset topography and post-glacial features (e.g. Tankard et al. 1982; Manzunzu et al., 2019).
Shallow seismic profile	2	Seismic lines help in constraining the deformation ages if no signs of disturbance in the youngest sediments are seen. However, the information available is fragmented and incomplete and might give a statistically biased view.
In situ stress measurements	2	Few data measured in mines are available and reasonably consistent with focal mechanisms. They show that the uppermost continental crust of Witwatersrand basin presently is mostly under nearly N–S extension (Stacey and Wessloo, 1998; Bird *et al.*, 2006). A broad stress field is consistent across the entire region, but different regions are dominated by different stress orientations (Figure 1.5).
Deep seismic profiles, P- and S-wave velocity structure	3	The regional velocity structure may identify areas of potential deep activity. From tomographic studies and reflection/ refraction seismology, a good knowledge of P-wave velocities down to the Moho exists (Kgaswane et al., 2012; Wright et al., 2002). The S-wave velocity structure, however, is largely unknown. In addition, it is not clear how these velocities relate to seismic potential, because ruptures can cut across velocity transients.
Potential fields (Gravimetry, Magnetism)	3	Potential fields provide regional, large-scale information. Their relevance for zonation is limited because the link between seismic hazard and potential fields is not clear.

The seismological, geological as well as tectonic data compiled were synthesized to identify potential seismic sources. From this classification, the synthesized data is shown in Figure 5-10. The available information shows that the seismicity in southern Africa is driven by regional stresses originating from large-scale features that include intra-continental rifts, large-scale topographic elevations, and the network of surrounding mid-oceanic ridges.

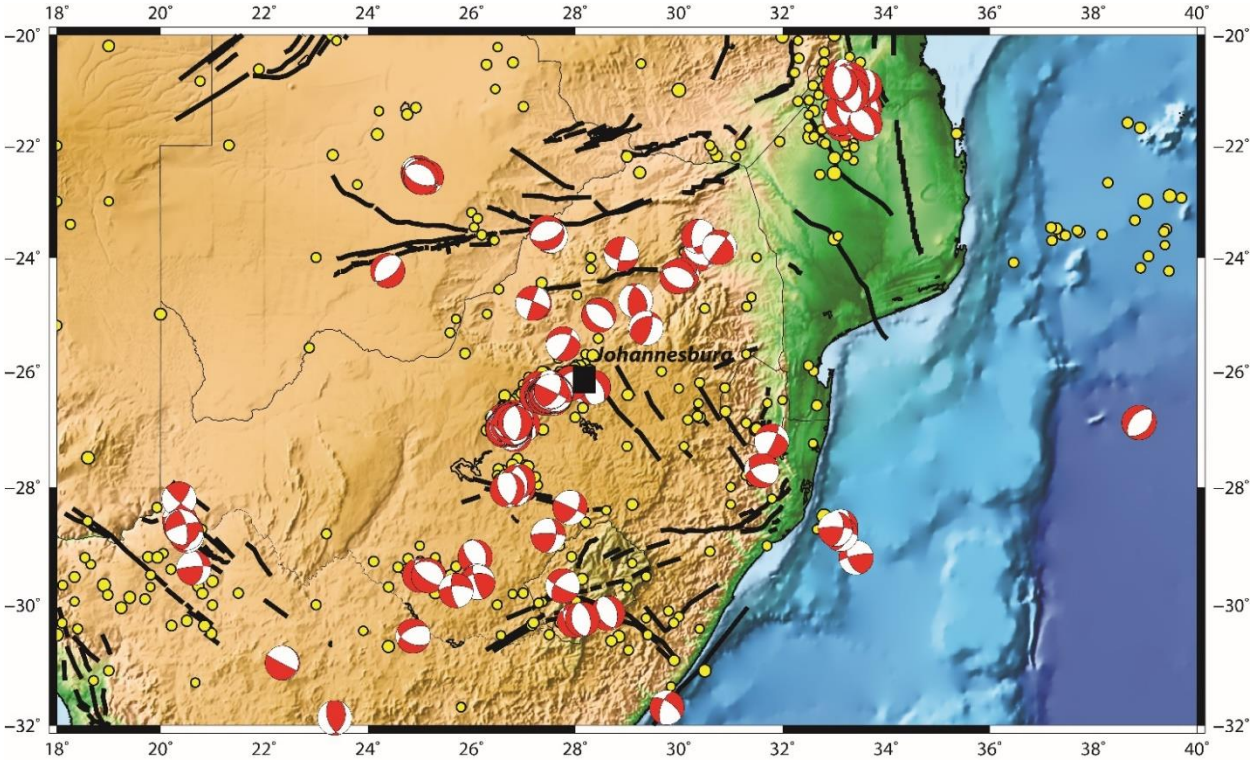


Figure 5-10: Seismotectonic map for Johannesburg and surrounding region used to delineate potential seismic sources (Faults were extracted from Manzunzu et al., 2019; background topography was extracted from Amante et al., 2009).

5.6. Delineation of seismic source zones

The seismotectonic model includes all seismic sources deemed capable of contributing to the ground-motion hazard for Johannesburg. The development criteria for seismic source zones identifies unique zones that account for distinct differences in:

1. Earthquake spatial distribution and recurrence rate.
2. Expected maximum earthquake magnitude (M_{max}).
3. Expected future earthquake characteristics (*e.g.*, style of faulting, rupture orientation, seismogenic thickness).
4. Probability that a fault is seismogenic.

By "differences," it is meant that a given potential seismic source would differ significantly in one or more of these criteria from its neighbour such that identifying a unique seismic source is justified (Coppersmith et al., 2009). For example, observed differences in the spatial distribution and density (number of events per unit area) from one region to another. Identification of potential seismic source zones using seismicity data assumes that the pattern of past earthquakes will remain the same in future (e.g. Kafka, 2007). However, in South Africa records of past seismicity are relatively short compared

to the recurrence intervals for large-magnitude earthquakes (Bommer et al., 2018). Despite this shortcoming, it is assumed that the spatial distribution of observed smaller-magnitude earthquakes constrains the spatial distribution of larger-magnitude earthquakes (Kijko and Singh, 2011).

5.6.1. Criteria for defining seismic sources

Due to lack of enough information to characterize individual faults, areal source zones were identified and delineated and it is presumed that seismicity is homogeneous in character within the zones. The earthquake locations determined by the SANSN resulted in large errors (about 10km). As a result, it was not possible to conclusively identify active faults that could be used as linear sources in the hazard assessment. Instead, area source zones were created using the seismicity locations and tectonic information. The detailed geometry of the zones reflects both geological features, where these seem to be relevant and the seismicity itself. Previous seismotectonic studies were also taken into consideration during the delineation process. Since the hypotheses by the proponent experts (Hartnady, 1996; Du Plessis, 1996; Partridge, 1995) had been put forward, the diffuse seismicity has become more populated with new more accurate seismicity data. However, even with the updated earthquake catalogue there is no significant deviation from these models with respect to delineation of capable faults, hence the decision to rely on previous models for the delineation of seismic sources in this study. This current information help in constraining the current seismotectonic models while previous studies are used in supporting the delineated sources. The source zones delineated include twenty area source zones (

Figure **5-11**). Both tectonic and mining related seismic sources were identified. We used the seismicity located by the dense network of stations to define the boundaries of the zones in mines. Where possible, boundaries of mines were used to decide on boundaries of zones bearing in mind that some of the faults in the mining regions might extend outside the mine boundaries. Background seismicity was also delineated as its own zones.

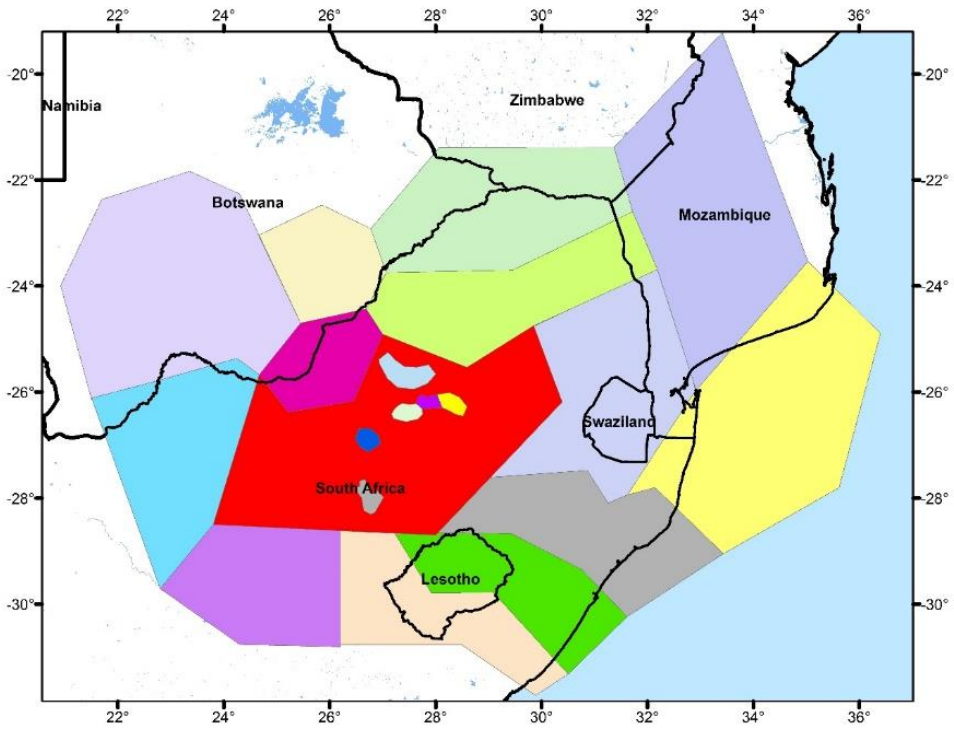


Figure 5-11: Seismic source zones identified for this study. The smaller zones found within the red zone are the mining-related zones.

5.6.2. Seismotectonic sources from tectonic regions

These are broad geological units mainly defined by either changes in fault orientation or seismicity density. In most cases, these zones are associated with a system of faults oriented in some direction and stress orientations as determined in section 5.3.

CEDAR (Cedarville): East of the Koffiefontein cluster of seismicity is a broad zone of seismicity demarcated here as the Cedarville zone, which coincides with the active Cedarville fault as well as a major cluster of events in Lesotho. The zone forms the eastern part of the Namaqua-Natal belt. Though very active, the zone is characterized by events of small to moderate magnitude with the largest observed earthquake having a magnitude of M_W5.2. Faulting is mainly normal on E-W trending faults. Previous models have always combined this zone with the Koffiefontein but due to the change in fault orientation, we decided to split them into two independent zones. More than 200 seismic events are located in this zone.

KHEIS (Kheis mobile belt): This zone is entirely located within the Kheis mobile belt, whose seismicity is made up mainly of small-scattered earthquakes. According to Cornell *et al.* (2011), the Kheis Belt could be either an orogenic belt (~ 1800 Ma) or a northern branch of the Namaqua-Natal Belt (~ 1200 Ma). It is described as a thin-skinned region with east-verging thrust belt characteristics.

This zone is bounded by the Kaapvaal Craton to the east. The largest magnitude earthquake in this zone is M3.7. There are no faults that have been identified as active in this zone.

KOFFIE (Koffiefontein): The Koffiefontein zone was previously defined by du Plessis (1996) and Singh *et al.* (2011). It coincides with a cluster of events of normal faulting located near Koffiefontein. One of the largest earthquakes in South Africa occurred in this zone in 1912 with a magnitude of M_W 6.2 followed by another in 1976 (M_L 5.8), which they were felt widely in southern Africa. However, no information is currently available to link the seismicity in this region to known active faults. Hartnady (1996) and Partridge (1995) combined this zone with the Cedarville and Okiep region. However, in this study it was decided to keep it as a separate unique zone due to the occurrence of a number of moderately sized events, of which there is currently no evidence that they can equally occur in Cedarville or Okiep.

KVAAL (Kaapvaal Craton): The zone approximately bound by the boundaries of the Kaapvaal Craton and is characterised by diffuse background seismicity. Seismicity in the Kaapvaal region is mainly associated with mining activities and a few outliers from the mining boundaries are represented in this seismic zone. The Rietfontein fault system is prominent in this zone although its activity in questionable (Manzunzu *et al*., 2019). Generally NW-SE trending structures are dominant. Du Plessis (1996) considered the whole region as central South Africa while Hartnady (1996) split it into a number of smaller zones. Seismicity is moderate with the largest event having a magnitude M_L4.8. Faults that have been identified to be active are being reactivated by fluid either induced or mining operations.

LIMPOPO (Limpopo Mobile Belt): This zone is confined within the Limpopo Mobile Belt. The largest observed earthquake had a magnitude of M_L 5.2. Structures in the zone generally trend in ENE-WSW direction. Geological investigations (Holland, 2011) have shown normal faulting along most of the structures, with displacement of aeolian sands along major faults (Bosbokpoort and Melinda faults) and fault scarps ranging from 2 to 10 m in height. The characterization of these faults is difficult due to lack of information. Partridge (1995) also identified this zone as active.

LESOTHO: The Lesotho zone is made of NE-SW trending faults oriented at an angle to those in the CEDAR zone. Though it appears to be very active, most of the events are of a different type to those in the CEDAR and TUGELA zones, which are mostly made of seismicity linked to large dams in Lesotho. The association of the events to active faults is unknown. Largest observed magnitude is M_W5.3.

MDSN (Mpumalanga-Drakensberg-Swaziland-Natal): The MDSN zone is made up of a combination of NE-SW and N-S trending faults of normal faulting. The zone is characterised by

diffuse seismicity, though a number of moderate events have occurred in the past. All the three previous seismotectonic models (i.e. du Plessis, 1996; Partridge, 1995; Hartnady, 1996) also identified this zone although the extent varies. The zone is bound to the west by the Kaapvaal Craton and the Mozambique Channel zone to the east. Its northern end is marked by the change in orientation of structures to a predominantly E-W direction. Seismicity in this zone rarely reaches magnitude 5 with the largest earthquake having a magnitude of M_W5.0.

MOZA (Southern parts of Mozambique): This zone is where the 2006 Machaze earthquake (M_w = 7.0) occurred. It is believed to be part of the southern limit of the EARS. A few faults have been mapped in the region but were not characterised. Due to poor station coverage in Mozambique, it is very difficult to associate the seismicity to the faults in the area. Most earthquakes are located by regional and teleseismic stations. Major faults in the area include the Machaze fault, which was the source of the 2006 earthquake. The faults are predominantly NW – SE oriented.

MOZCHAN (Mozambique Channel): In his study, Hartnady (1985) proposed a hotspot 'pre-weakening' model to explain the seismicity from Mozambique (ca 60Ma) through St Lucia (ca 10Ma) to Cedarville near Lesotho. He also suggested that this might be the point where the EARS will extend to in the future. Part of this track is demarcated as a zone independent from the nearby east – west trending zones that have faults oriented in either NE-SW or E-W. The zone is characterized by diffuse seismicity, though a number of moderate events have occurred in the past. Singh *et al*., (2011) identified the Port Dunford-Mozambique coastal (PDMOZ) fault as active in this region although it was not characterized.

NWEST (North West province): This zone sits in the Bushveld Igneous Complex which is a geological structure that intrudes the Kaapvaal craton. Although there are several faults in this zone, most seismicity recorded are of small magnitude and shallow depth suggesting they might be related to platinum mining activities taking place in the region. The observed magnitudes are also currently below M_L 5.0 with the largest observed magnitude being M_W4.8.

TUGELA: The zone is made up of the boundary between the Kaapvaal Craton and the Namaqua-Natal mobile belt represented in the region by the Tugela fault zone. The area is also defined by diffuse seismicity, some of which appears to be associated with the fault. The eastern extend of the zone is represented by the location of the large M_W6.3 St Lucia earthquake of December 1932 (Krige and Venter, 1933). Some hot springs in the KwaZulu Natal area have also been identified in this zone.

WBOTS (South Western Botswana region): This zone is characterised by some clusters of seismicity, which might be associated with mining activities in the region. A magnitude of M_W 5.2

earthquake was reported to have occurred in the zone in 2011. However, given that there are no known faults near the location of this event, further investigations of this event need to be carried out. The zone is bound to the south by the northern boundary of the Kheis province, the Damara belt to the north and western extent of identified major faults in the east.

ZEBED (Zebediela region): The ZEBED source zone is characterised by the Thabazimbi Murchinson Lineaments and dominated by the NE-SW trending Zebediela and Thabazimbi faults, which appear to be active, but without enough information to be implemented in the study as linear sources. A few moderate earthquakes can clearly be associated with the same faults (Figure 13). In recent investigations (Brandt and Saunders, 2011; Singh et al., 2009, 2011), it was shown that faulting in the region is mainly normal with a strike-slip component. The 2013 Bela Bela earthquake occurred in this zone (Midzi et al., 2015; Mello, 2017). The largest recorded event is of magnitude M_W5.0.

ZOET (Zoetfontein fault region): This zone is in a region located immediately west of the Limpopo mobile belt. The main fault in the region is the Zoetfontein fault which has branches trending in a ENE-WSW and some in a NW-SE direction. The Zoetfontein fault roughly delineates the boundary between the Limpopo Mobile Belt and the Transvaal basins. Several moderately sized earthquakes can be associated with the fault. According to Jelsma et al. (2009), the fault was reactivated in the late Archaean and continues reactivating to the present. The 2017 Botswana earthquake (M6.5) occurred in this zone (Midzi et al., 2017; Gardonia et al., 2018; Mulabisana et al., 2021).

5.6.3. Seismic source zones from mining regions

Mine zones were mainly delineated using boundaries of the mines and changes in seismicity density. The actual location of mine boundaries with the exact extend of the tunnels is difficult to know especially for the old mines in the Witwatersrand basin. Mining has been stopped in most parts of the basin hence current seismicity might be due to fluid induced. In the Witwatersrand basin, reactivation of dormant faults might be possible due to anthropogenic stress changes from mining. Most of the seismicity is below M_W5.0.

CRAND (Central Rand Gold Mines): The zone constitutes mines located in the central part of Johannesburg. Most mines in this zone have ceased operations and water ingress is predominant. Seismicity is below M_W 5.0 although several of these events have been felt which have occasionally raised concerns over the safely of structures in the city of Johannesburg (e.g. Midzi *et al*., 2015b). Seismicity is diffuse and not as much as other gold mining regions. E-W trending faults of the Rietfontein system characterise this zone.

ERAND (East Rand Gold Mines): this zone covers the gold mining region to the east of Johannesburg, which include Benoni, Germiston and Boksburg. The mining-related events observed within this zone are all smaller than M_W 5.0, although a few events in the past have been located in this region. Given the activity observed in the region, it is possible that earthquakes of magnitude greater than M_L 5.0 can occur in the future. Therefore, it was decided to include this source in the hazard calculations. There are shallow mapped faults mostly trending E-W located in the mining horizons. The largest has a magnitude M_W4.9.

KOSH (Klerksdorp – Orkney – Stilfontein – Hartbeesfontein region): The area around KOSH has shown to be active in terms of seismicity, producing some of the largest mining related events to have affected South Africa. It is not obvious why this is so unless stress concentrations and complex faulting play a major role. The largest recorded mining related earthquake in South Africa occurred in the KOSH area on 5 August 2014 with a magnitude of M_W 5.5 (Midzi *et al*., 2015; Manzunzu *et al*., 2017). The aftershock analysis done by Manzunzu *et al.* (2017) revealed the area is predominantly experiencing extensional stress, though the 5 August 2014 earthquake was caused by strike slip faulting. Prior to this event, another moderately large event occurred in the same area in 2005 and it had a magnitude of M_W 5.3. The event resulted in structural damage worth millions of rands both underground in the mines and on the surface especially in the town of Stilfontein (Durrheim *et al.*, 2006).

PLATINUM (Platinum mines in the North West province): This zone sits in the Bushveld Igneous Complex which is a geological structure that intrudes the Kaapvaal craton. Although there are several faults in this zone, most seismicity recorded are of small magnitude and shallow depth suggesting they might be related to platinum mining activities taking place in the region. The level of seismicity in the platinum mines is currently low compared to the gold mines in the Wits basin. The observed magnitudes are also currently below M_L 5.0.

WELKOM (Welkom gold mining region): This zone is characterised by many earthquakes associated with mining activity and is marked by N-S and NW-SE trending faults. Some evidence of fault activity have been identified on some of the faults in this zone. Dor *et al.* (2001) list moderately sized earthquakes in the Welkom region since 1972 with magnitude values ranging between M_L 4.7 and 5.2. Marshall (1987) undertook a morphotectonic analysis of the Wesselsbron panveld in which she presented convincing evidence for uplift of a granitic dome to the south-west of Wesselsbron. This, in turn, led to the reactivation of a number of NNW-SSE trending located on the eastern flank of the dome. The largest earthquake has a magnitude M_W5.6.

WRAND (West Rand Gold Mines): The level of seismicity in this zone is higher than for the East Rand. As with the East Rand, events in this zone have remained below M_L 5.0 in size, though more than 50 earthquakes of magnitude greater than or equal M_L 4 were located in the region. NE-SW trending faults have also been mapped in the mining horizons. Manzi *et al.* (2012) suggested that the Bank fault (oriented N-S) is active but no information on its activity rates is available.

FWRAND (Far West Rand Gold Mines): The FWRAND zone is by far the most active of the zones in the mining districts in and around Johannesburg, with a total of about 12 400 events between 1983 and 2018. However, the events in this zone are generally small in size with largest having a magnitude of M_W4.7.

5.7. Uncertainties in seismotectonic modelling

For the purposes of seismic hazard analysis, selected seismic source zones may be similar to or different from the actual source depending on the accuracy and the geometry of the source and the relative location of the site of interest as well as available information. A single standard procedure does not exist by which seismic source zones can be unambiguously drawn, hence the source zones do not have clearly defined boundaries (Coppersmith et al., 2009). The location of the boundary is however of great importance for seismic hazard analysis, especially at sites close to the boundary.
Due to the uncertainty in the stress origins as well as the geological uncertainties, it is very difficult to associate sources of seismic events to the geological structures within the study region. The absence of clearly identified active faults also adds up to this uncertain scenario. South Africa is said to be located in a stable continental region (Johnston 1996; Calais et al., 2016) that is characterized by low strain rates and long recurrence rates (Malservisi et al., 2003; Stamps et al., 2018). Movement of faults is very slow which results in difficulties in associating seismicity to individual faults.

Different interpretation of the present data is possible which will result in different models. It has been observed even in large PSHA project (e.g. PEGASOS, ESKOM) that different experts will give different seismic source zones even from the same datasets. It is therefore important to know if it is necessary to have complex seismic sources, which will result in computationally complex calculations or simple and conservative hazard results. In this study, the uncertainty associated with the development of the source models was taken into account by considering the three models described in section 5.2 and the fourth model develop in this study (section 5-6) for sensitivity analysis (Figure 5-12). Although these models were developed using different data sets, they highlight several common seismic zones known to have caused moderate to large earthquakes in South Africa.

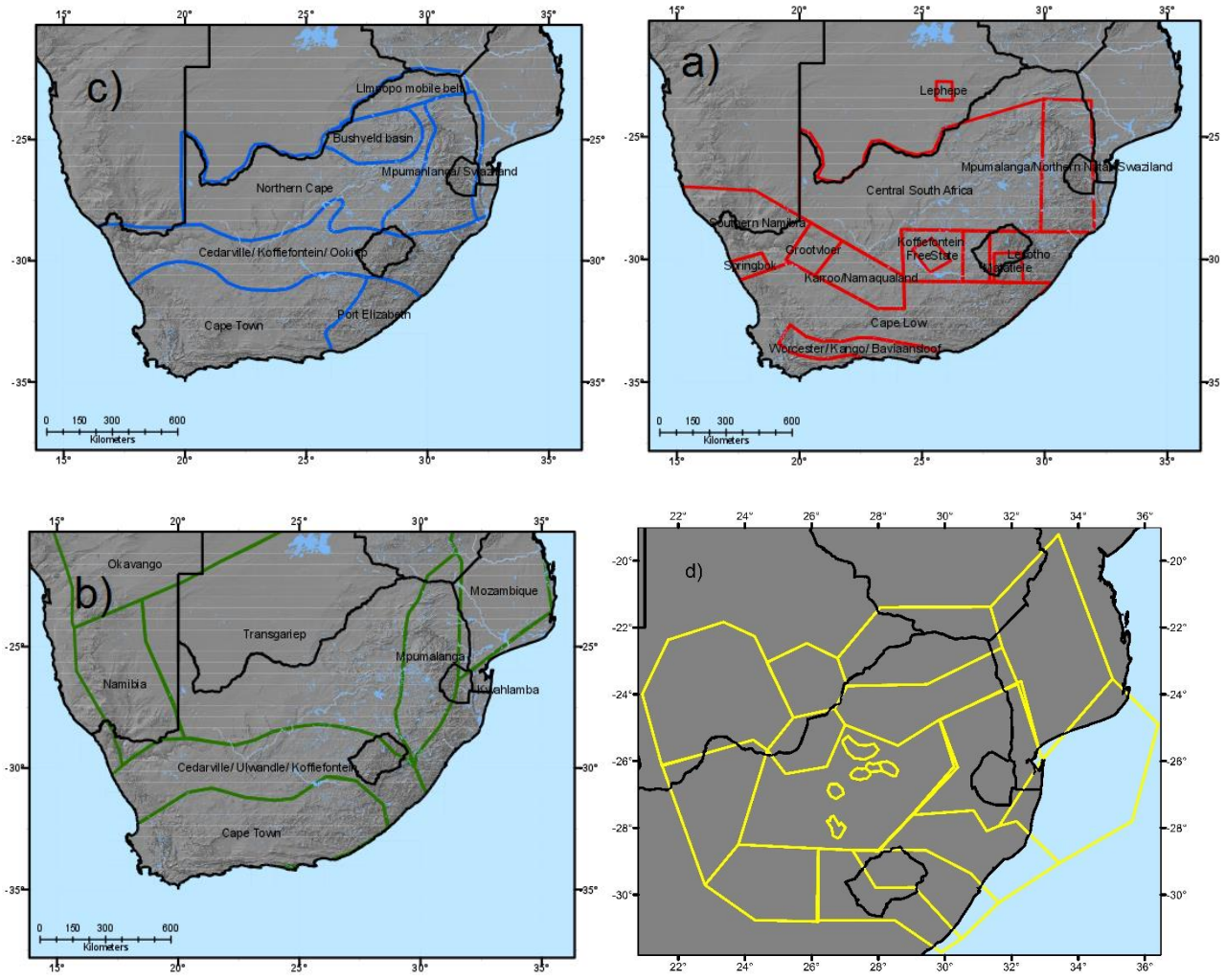


Figure 5-12: The seismotectonic models used in this study for sensitivity analysis used in this study. (a) du Plessis (1995) (b) Partridge (1995) (c) Hartnady (1996) (d) model developed in this study.

5.8. Conclusions

The seismological, geological as well as tectonic data compiled were synthesized to identify potential seismic sources for the analysis of seismic zones for Johannesburg. A seismotectonic map was derived through the analysis of structural, neotectonic and seismological data to establish links between seismicity and current deformation mechanisms with the ultimate goal to individualize and delimit the different seismotectonic units (

Figure **5-11**). Focal mechanism solutions were used in conforming the orientation of the major faults identified. A major task was to associate the seismicity to some geological phenomena. Though this was possible in general, the scatter in seismicity associated with poor locations especially of small events, makes this a difficult task. The sparsity of the South African National Seismograph Network (SANSN) resulted in such large errors (about 10 km). As a result, it was not possible to conclusively

identify active faults that could be used as linear sources in the hazard assessment. Instead, area source zones were created using the seismicity locations and tectonic information.

Many of the events were observed to occur within the mining regions. Several seismic clusters were observed which were identified as possible seismic sources. Since the hypotheses by the previous proponent experts had been put forward, the diffuse seismicity has become more populated with new seismicity data. More information have emerged which have been used in this study to characterise the seismic sources. New evidence has made it possible to split the Namaqua-Natal-Hotspot- Track (Hartnady, 1996; 2000) into several smaller seismic zones. The sources identified in this chapter will be characterised (Chapter 6) and used in the hazard calculations (Chapter 8). To account for uncertainty, the four seismic source models discussed here will be be used for sensitivity analysis.

CHAPTER 6: MODELLING RECURRENCE PARAMETERS

6.1. Introduction

In order to assess the seismic hazard of a region, identified seismic zones need to be characterised in terms of the relative frequency of occurrence of earthquakes with different sizes (activity rate and *b*-value), as well as the maximum expected earthquake magnitude (M_{max}) for each source (Cornell and Van Marke, 1969; Sokolov and Ismael-Zadeh, 2015). Computations of the activity rate, *b*-value and M_{max} for each source zone defined in Chapter 5 were performed and are presented in this chapter. The available information on local tectonic conditions, such as the geology, buried faults and tectonic stresses do not provide reliable information on potential movement along identified faults during the recent geological past (from the start of the Quaternary Period at ca. 2.6 Ma to the present day). Therefore, the assessment of the seismic recurrence parameters is entirely based on the knowledge of historical and instrumental seismicity. In this study, only area sources were identified (Chapter 5) and characterised using the frequency magnitude distribution model as there is insufficient information to allow fault sources to be characterised. The model assumes that the seismic catalogue for each area source zone has a truncated exponential distribution (Gutenberg and Richter, 1944) characterised by the following parameters:

- The M_{max} value, defined as the maximum possible earthquake magnitude for each source zone.
- The *b*-value, which is given by the slope of the Gutenberg-Richter relation, and represents the relative frequency of occurrence of earthquakes of different magnitudes.
- The activity rate, *a*, which is the intercept of the Gutenberg-Richter relation and represents the number of earthquakes greater or equal to M_0 that occur each year.

Ideally, all three parameters characterising the recurrence relations are determined jointly. However, in the present study, the data is too sparse in some areas to allow a good level of constraint on M_{max} values. Hence, this parameter was assessed separately for each seismic zone. To compute statistically reliable recurrence parameters for each source zone, a minimum of 100 seismic events is required (Musson and Sergeant, 2007). If the seismic events are few within a zone, the recurrence parameters are poorly constrained or even indeterminable. In this case, earthquakes from neighboring source zones with similar characteristics were added to help in the computation.

In this study, twelve (12) catalogues were generated from the uncertainties considered (presented in Chapter 4) and for each catalogue, recurrence parameters were computed. The recurrence parameters

calculated here will be used in the seismic hazard sensitivity analysis. In computing the recurrence parameters, three models were applied on each catalogue as follows:

1) Constant *b*-value and variable *a*-value determined on the entire observation period. The *b*-value is computed using the maximum likelihood method as implemented in the BVALUE program in SEISAN (Ottemöller et al., 2018). This model has one free parameter, the *a*-value.
2) Variable *b* and *a*: Here we determine both the best fitting *a*- and *b*-value; hence the model has two free parameters. This is the model assumption in the ZMAP software (Wiemer, 2001).
3) The maximum likelihood procedure developed by Kijko (2004; 2012) and Kijko et al. (2016) which accounts for uncertainties in earthquake magnitude determination and the applied earthquake occurrence model using compound distributions (Kijko 2012; Kijko and Singh 2011).

6.2. *b*-value estimation

Estimation of the *b*-value is also dependent on having a sufficient number of earthquakes to calculate robust statistics. In some cases, source zones in low-seismicity regions have few earthquakes making it difficult to calculate reliable *b*-values. Theoretically, the *b*-value is expected to be regionally stable with variations less than the uncertainty limits, while the activity rate is liable to vary substantially from one seismic source zone to another. Values for *b*-values can be split into two classes: those from tectonic areas and those from mining-related source areas. Tectonic sources had *b*-values close to 1 (from 0.84 to 1.2) while mining-related sources had values between 1.2 and 1.5. there are variations observed from the methods used to determine the b-values with the Zmap giving slightly higher values while the Kijko method are slightly lower. Within each source, the b-values seem to be relatively constant with ±0.15 varioation. Different declustering methods show insignificant variation in the b-values.

Table 6-1: *b*–value estimations for the source areas determined in this study. For each source area, different catalogues were created during the catalogue processing step, and for each catalogue, recurrence parameters were calculated to represent the uncertainties associated with each step. Cat 1= Homogenised using M_w-M_L relations developed in this study. Cat 2 = Homogenized using global relations. Cat 3 = post 1970 catalogue. Cat 4 = All events. Cat 5 = Gardner & Knopoff (1974), Cat 6 = Grünthal et al (1985) and Cat 7 = Cluster (Seisan). The three methods used to compute the b-values are ZMAP, SEISAN aand Kijko.

ZONE	Homogenisation	Temporal	Declustering	Zmap	Seisan	Kijko	Average b-value	standard deviation
CEDAR	Cat 1	Cat 3	Cat 5	1.05	1	0.9	0.98	0.08
			Cat 6	0.98	1.01	0.96	0.98	0.03
			Cat 7	0.94	1.02	1	0.99	0.04
		Cat 4	Cat 5	0.95	1.01	0.98	0.98	0.03
			Cat 6	0.81	0.94	0.93	0.89	0.07
			Cat 7	0.85	0.88	0.87	0.87	0.02

	Cat 2	Cat 3	Cat 5	1.2	1.06	1.1	1.12	0.07
			Cat 6	1.16	0.94	1.03	1.04	0.11
			Cat 7	1.14	0.81	0.94	0.96	0.17
		Cat 4	Cat 5	0.97	1.05	1.2	1.07	0.12
			Cat 6	0.96	1	1.13	1.03	0.09
			Cat 7	0.93	0.93	0.91	0.92	0.01
CRAND	Cat 1	Cat 3	Cat 5	1.54	1.54	1.48	1.52	0.03
			Cat 6	1.48	1.4	1.43	1.44	0.04
			Cat 7	1.46	1.34	1.24	1.35	0.11
		Cat 4	Cat 5	1.32	1.3	1.33	1.32	0.02
			Cat 6	1.31	1.29	1.31	1.30	0.01
			Cat 7	1.29	1.27	1.19	1.25	0.05
	Cat 2	Cat 3	Cat 5	1.43	1.47	1.29	1.40	0.09
			Cat 6	1.4	1.44	1.3	1.38	0.07
			Cat 7	1.38	1.4	1.2	1.33	0.11
		Cat 4	Cat 5	1.33	1.46	1.42	1.40	0.07
			Cat 6	1.3	1.44	1.31	1.35	0.08
			Cat 7	1.29	1.43	1.34	1.35	0.07
ERAND	Cat 1	Cat 3	Cat 5	1.45	1.48	1.33	1.42	0.08
			Cat 6	1.4	1.37	1.31	1.36	0.05
			Cat 7	1.35	1.2	1.26	1.27	0.08
		Cat 4	Cat 5	1.32	1.27	1.28	1.29	0.03
			Cat 6	1.23	1.16	1.25	1.21	0.05
			Cat 7	1.19	1.08	1.12	1.13	0.06
	Cat 2	Cat 3	Cat 5	1.53	1.38	1.2	1.37	0.17
			Cat 6	1.48	1.27	1.22	1.32	0.14
			Cat 7	1.34	1.11	1.21	1.22	0.12
		Cat 4	Cat 5	1.35	1.35	1.3	1.33	0.03
			Cat 6	1.3	1.28	1.21	1.26	0.05
			Cat 7	1.22	1.25	1.16	1.21	0.05
KHEIS	Cat 1	Cat 3	Cat 5	1.69	1.52	1.42	1.54	0.14
			Cat 6	1.56	1.47	1.38	1.47	0.09
			Cat 7	1.62	1.47	1.43	1.51	0.10
		Cat 4	Cat 5	1.6	1.2	1.23	1.34	0.22
			Cat 6	1.44	1.38	1.21	1.34	0.12
			Cat 7	1.31	1.24	1.08	1.21	0.12
	Cat 2	Cat 3	Cat 5	1.44	1.52	1.36	1.44	0.08
			Cat 6	1.36	1.5	1.41	1.42	0.07
			Cat 7	1.33	1.45	1.43	1.40	0.06
		Cat 4	Cat 5	1.42	1.43	1.29	1.38	0.08
			Cat 6	1.34	1.28	1.27	1.30	0.04
			Cat 7	1.23	1.08	1.25	1.19	0.09
KOFFIE	Cat 1	Cat 3	Cat 5	1.03	0.97	0.87	0.96	0.08
			Cat 6	0.94	0.86	0.82	0.87	0.06

			Cat 7	0.8	0.81	0.76	0.79	0.03
		Cat 4	Cat 5	0.78	0.74	0.7	0.74	0.04
			Cat 6	0.73	0.71	0.72	0.72	0.01
			Cat 7	0.71	0.69	0.66	0.69	0.03
	Cat 2	Cat 3	Cat 5	0.92	0.84	0.81	0.86	0.06
			Cat 6	0.87	0.84	0.86	0.86	0.02
			Cat 7	0.77	0.81	0.9	0.83	0.07
		Cat 4	Cat 5	0.81	0.92	0.86	0.86	0.06
			Cat 6	0.83	0.91	0.86	0.87	0.04
			Cat 7	0.84	0.89	0.85	0.86	0.03
KOSH	Cat 1	Cat 3	Cat 5	1.32	1.29	1.29	1.30	0.02
			Cat 6	1.27	1.24	1.21	1.24	0.03
			Cat 7	1.23	1.22	1.16	1.20	0.04
		Cat 4	Cat 5	1.4	1.22	1.18	1.27	0.12
			Cat 6	1.39	1.17	1.15	1.24	0.13
			Cat 7	1.37	1.01	1.04	1.14	0.20
	Cat 2	Cat 3	Cat 5	1.45	1.39	1.27	1.37	0.09
			Cat 6	1.37	1.23	1.14	1.25	0.12
			Cat 7	1.35	1.19	1.13	1.22	0.11
		Cat 4	Cat 5	1.28	1.24	1.21	1.24	0.04
			Cat 6	1.24	1.2	1.18	1.21	0.03
			Cat 7	1.24	1.13	1.16	1.18	0.06
KVAAL	Cat 1	Cat 3	Cat 5	1.33	1.31	1.38	1.34	0.04
			Cat 6	1.27	1.23	1.34	1.28	0.06
			Cat 7	1.22	1.34	1.27	1.28	0.06
		Cat 4	Cat 5	1.43	1.32	1.27	1.34	0.08
			Cat 6	1.34	1.32	1.21	1.29	0.07
			Cat 7	1.27	1.33	1.24	1.28	0.05
	Cat 2	Cat 3	Cat 5	1.59	1.28	1.27	1.38	0.18
			Cat 6	1.43	1.25	1.24	1.31	0.11
			Cat 7	1.11	1.24	1.23	1.19	0.07
		Cat 4	Cat 5	1.38	1.27	1.29	1.31	0.06
			Cat 6	1.31	1.26	1.23	1.27	0.04
			Cat 7	1.23	1.09	1.1	1.14	0.08
LESOTHO	Cat 1	Cat 3	Cat 5	1.12	1.21	0.97	1.10	0.12
			Cat 6	1.13	1.16	0.99	1.09	0.09
			Cat 7	1.11	1.01	1.07	1.06	0.05
		Cat 4	Cat 5	0.82	0.79	0.82	0.81	0.02
			Cat 6	0.79	0.82	0.76	0.79	0.03
			Cat 7	0.72	0.74	0.79	0.75	0.04
	Cat 2	Cat 3	Cat 5	1.31	0.95	0.97	1.08	0.20
			Cat 6	1.23	0.91	0.87	1.00	0.20
			Cat 7	1.11	0.82	0.88	0.94	0.15
		Cat 4	Cat 5	1.05	1.21	1.16	1.14	0.08

			Cat 6	1	0.93	0.99	0.97	0.04
			Cat 7	0.96	0.86	0.85	0.89	0.06
LIMPOPO	Cat 1	Cat 3	Cat 5	0.82	1.18	1.08	1.03	0.19
			Cat 6	0.75	1.12	1.01	0.96	0.19
			Cat 7	0.71	1.09	1.13	0.98	0.23
		Cat 4	Cat 5	1.25	1.24	1.34	1.28	0.06
			Cat 6	0.97	1.19	1.23	1.13	0.14
			Cat 7	0.92	1.12	1.21	1.08	0.15
	Cat 2	Cat 3	Cat 5	1.4	0.94	0.94	1.09	0.27
			Cat 6	1.21	0.89	0.91	1.00	0.18
			Cat 7	0.92	0.82	0.92	0.89	0.06
		Cat 4	Cat 5	1.24	1.25	1.06	1.18	0.11
			Cat 6	1.23	1.15	1.07	1.15	0.08
			Cat 7	1.12	1.03	1.03	1.06	0.05
MDSN	Cat 1	Cat 3	Cat 5	1.21	1.11	0.93	1.08	0.14
			Cat 6	1.1	1.12	0.93	1.05	0.10
			Cat 7	1.03	1.09	0.91	1.01	0.09
		Cat 4	Cat 5	1.13	0.92	1.3	1.12	0.19
			Cat 6	0.98	0.84	1.2	1.01	0.18
			Cat 7	0.65	0.79	0.99	0.81	0.17
	Cat 2	Cat 3	Cat 5	1.13	1.01	0.96	1.03	0.09
			Cat 6	1.07	0.92	0.93	0.97	0.08
			Cat 7	0.98	0.87	0.93	0.93	0.06
		Cat 4	Cat 5	0.92	0.98	1.03	0.98	0.06
			Cat 6	0.83	0.89	0.86	0.86	0.03
			Cat 7	0.79	0.88	0.84	0.84	0.05
MOZA	Cat 1	Cat 3	Cat 5	1.03	1.2	1.11	1.11	0.09
			Cat 6	1.07	1.04	1.13	1.08	0.05
			Cat 7	1.13	0.98	1.2	1.10	0.11
		Cat 4	Cat 5	0.86	0.91	1.05	0.94	0.10
			Cat 6	0.82	0.89	1.04	0.92	0.11
			Cat 7	0.81	0.84	0.99	0.88	0.10
	Cat 2	Cat 3	Cat 5	0.93	0.9	1.15	0.99	0.14
			Cat 6	0.95	0.98	1.03	0.99	0.04
			Cat 7	0.98	1.04	0.91	0.98	0.07
		Cat 4	Cat 5	1.11	1.2	1.07	1.13	0.07
			Cat 6	1.04	1.16	1.02	1.07	0.08
			Cat 7	0.95	1.06	0.98	1.00	0.06
MOZCHAN	Cat 1	Cat 3	Cat 5	0.79	0.85	0.7	0.78	0.08
			Cat 6	0.88	0.91	0.79	0.86	0.06
			Cat 7	0.93	1.08	0.84	0.95	0.12
		Cat 4	Cat 5	0.94	0.98	0.92	0.95	0.03
			Cat 6	0.89	0.94	0.88	0.90	0.03
			Cat 7	0.83	0.89	0.85	0.86	0.03

	Cat 2	Cat 3	Cat 5	0.82	0.74	0.77	0.78	0.04
			Cat 6	0.87	0.92	0.84	0.88	0.04
			Cat 7	0.91	1.03	0.99	0.98	0.06
		Cat 4	Cat 5	0.7	0.84	0.93	0.82	0.12
			Cat 6	0.86	0.91	1.02	0.93	0.08
			Cat 7	1.02	1.2	1.06	1.09	0.09
NWEST	Cat 1	Cat 3	Cat 5	1.13	0.99	1.23	1.12	0.12
			Cat 6	1.03	0.92	1.17	1.04	0.13
			Cat 7	0.92	0.86	1.16	0.98	0.16
		Cat 4	Cat 5	0.95	1.3	1.02	1.09	0.19
			Cat 6	0.87	1.28	1.06	1.07	0.21
			Cat 7	0.84	1.21	1.15	1.07	0.20
	Cat 2	Cat 3	Cat 5	1.2	1.17	1.28	1.22	0.06
			Cat 6	1	0.97	1.11	1.03	0.07
			Cat 7	1.14	1.02	0.97	1.04	0.09
		Cat 4	Cat 5	1.23	1.2	1.24	1.22	0.02
			Cat 6	1.14	0.94	1.03	1.04	0.10
			Cat 7	0.99	1.19	1.17	1.12	0.11
PLATINUM	Cat 1	Cat 3	Cat 5	0.92	0.86	1.16	0.98	0.16
			Cat 6	0.84	0.81	0.94	0.86	0.07
			Cat 7	0.78	0.82	1.06	0.89	0.15
		Cat 4	Cat 5	0.95	0.95	0.98	0.96	0.02
			Cat 6	1.01	0.94	0.96	0.97	0.04
			Cat 7	1.3	0.88	0.89	1.02	0.24
	Cat 2	Cat 3	Cat 5	1	0.84	1.04	0.96	0.11
			Cat 6	0.93	0.81	0.86	0.87	0.06
			Cat 7	0.88	0.79	0.91	0.86	0.06
		Cat 4	Cat 5	1.16	1.2	1.24	1.20	0.04
			Cat 6	1.23	1.17	1.2	1.20	0.03
			Cat 7	1.35	1.32	1.3	1.32	0.03
TUGELA	Cat 1	Cat 3	Cat 5	0.98	0.93	0.91	0.94	0.04
			Cat 6	0.94	0.86	0.87	0.89	0.04
			Cat 7	0.95	0.81	0.84	0.87	0.07
		Cat 4	Cat 5	1.02	1.06	0.85	0.98	0.11
			Cat 6	0.97	0.91	0.88	0.92	0.05
			Cat 7	1.17	0.83	0.88	0.96	0.18
	Cat 2	Cat 3	Cat 5	0.85	0.88	1.02	0.92	0.09
			Cat 6	0.83	0.86	0.81	0.83	0.03
			Cat 7	0.8	0.73	0.79	0.77	0.04
		Cat 4	Cat 5	1.13	1.17	0.88	1.06	0.16
			Cat 6	0.98	1.03	0.8	0.94	0.12
			Cat 7	0.95	0.83	0.81	0.86	0.08
WBOTS	Cat 1	Cat 3	Cat 5	1.23	0.8	1.21	1.08	0.24
			Cat 6	0.91	0.77	1.14	0.94	0.19

			Cat 7	1.18	0.76	1.12	1.02	0.23
		Cat 4	Cat 5	1.22	1.32	1.33	1.29	0.06
			Cat 6	1.16	1.25	1.27	1.23	0.06
			Cat 7	1.08	1.24	1.24	1.19	0.09
	Cat 2	Cat 3	Cat 5	1.04	0.99	1.19	1.07	0.10
			Cat 6	0.94	0.96	1.13	1.01	0.10
			Cat 7	0.9	0.95	1.16	1.00	0.14
		Cat 4	Cat 5	0.94	0.97	1.2	1.04	0.14
			Cat 6	0.91	0.92	1.16	1.00	0.14
			Cat 7	0.83	0.87	1.16	0.95	0.18
WELKOM	Cat 1	Cat 3	Cat 5	1.3	1.28	1.28	1.29	0.01
			Cat 6	1.3	1.21	1.19	1.23	0.06
			Cat 7	1.32	1.18	1.15	1.22	0.09
		Cat 4	Cat 5	1.32	1.34	1.24	1.30	0.05
			Cat 6	1.27	1.32	1.22	1.27	0.05
			Cat 7	1.23	1.3	1.22	1.25	0.04
	Cat 2	Cat 3	Cat 5	1.33	1.32	1.29	1.31	0.02
			Cat 6	1.28	1.31	1.22	1.27	0.05
			Cat 7	1.25	1.32	1.22	1.26	0.05
		Cat 4	Cat 5	1.45	1.23	1.18	1.29	0.14
			Cat 6	1.41	1.22	1.16	1.26	0.13
			Cat 7	1.36	1.21	1.1	1.22	0.13
WRAND	Cat 1	Cat 3	Cat 5	1.65	1.45	1.34	1.48	0.16
			Cat 6	1.57	1.41	1.32	1.43	0.13
			Cat 7	1.52	1.33	1.23	1.36	0.15
		Cat 4	Cat 5	1.52	1.43	1.31	1.42	0.11
			Cat 6	1.39	1.4	1.32	1.37	0.04
			Cat 7	1.31	1.33	1.33	1.32	0.01
	Cat 2	Cat 3	Cat 5	1.11	1.56	1.32	1.33	0.23
			Cat 6	1.13	1.46	1.24	1.28	0.17
			Cat 7	1.09	1.44	1.11	1.21	0.20
		Cat 4	Cat 5	1.45	1.32	1.3	1.36	0.08
			Cat 6	1.37	1.28	1.13	1.26	0.12
			Cat 7	1.31	1.16	1.07	1.18	0.12
ZEBED	Cat 1	Cat 3	Cat 5	1.2	0.98	1.28	1.15	0.16
			Cat 6	1.04	0.91	0.95	0.97	0.07
			Cat 7	0.96	0.88	0.91	0.92	0.04
		Cat 4	Cat 5	1.3	1.34	1.22	1.29	0.06
			Cat 6	1.24	1.21	1.15	1.20	0.05
			Cat 7	1.28	1.16	1.08	1.17	0.10
	Cat 2	Cat 3	Cat 5	1.17	1.23	1.16	1.19	0.04
			Cat 6	1.09	0.93	1.12	1.05	0.10
			Cat 7	1.02	0.86	1.11	1.00	0.13
		Cat 4	Cat 5	1.28	1.35	1.3	1.31	0.04

			Cat 6	1.15	1.21	1.26	1.21	0.06
			Cat 7	1.11	0.96	1.13	1.07	0.09
ZOET	Cat 1	Cat 3	Cat 5	0.98	1.02	0.95	0.98	0.04
			Cat 6	0.94	0.97	0.88	0.93	0.05
			Cat 7	0.93	0.86	0.76	0.85	0.09
		Cat 4	Cat 5	1.2	1.06	0.92	1.06	0.14
			Cat 6	0.93	0.95	0.87	0.92	0.04
			Cat 7	0.9	0.85	0.84	0.86	0.03
	Cat 2	Cat 3	Cat 5	1.13	1.09	1.1	1.11	0.02
			Cat 6	1.08	1.03	0.97	1.03	0.06
			Cat 7	0.92	0.91	0.73	0.85	0.11
		Cat 4	Cat 5	0.95	0.96	0.95	0.95	0.01
			Cat 6	0.92	0.84	0.91	0.89	0.04
			Cat 7	0.87	0.83	0.91	0.87	0.04

6.3. Earthquake *a*-value estimation

Estimation of the *a*-value is sensitive to the number of events in the catalogue and the *b*-value. Epistemic uncertainty in the estimation of the *a*-value is assessed by determining them using three methods as implemented in SEISAN software (BVALUE program; Ottermöller et al., 2018), HA3 (Kijko, 2014) and ZMAP program (Wiemer, 2001) for each seismic source zone. A total of 36 *a*-values were obtained for each source zone (Table 6-2). The three techniques produced significantly different results with values ranging from 1.63 to 6.44. Tectonic sources have lower *a*-value compared to sources from the mining region. This mainly because a lot seismic events with lower magnitudes are located in the mining regions. Results of the *a*-values do not show any systematic change. Of note are high value obtained using the Gardner and Knoppoff catalogue ompared to the other declustering methods at most sites. These parameters will be tested if they produce significant differences in the hazard.

Table 6-2: *a*-values for the Sources determined in this study. For each source, different catalogues were created during the catalogue processing and for each catalogue recurrence parameters were calculated to represent the sources of uncertainties. Cat 1= Homogenised using M_W-M_L relations developed in this study. Cat 2 = Homogenised using global relations. Cat 3 = post 1970 catalogue. Cat 4 = All events. Cat 5, Cat 6 and Cat 7 were declustered using the Gardner and Knopoff (1974), Grunthal *et al.* (1985) and Cluster (SEISAN) techniques respectively.

Zone	**Homogenisation**	**Temporal**	**Declustering**	Zmap	Seisan	Kijko	Average a-value	standard deviation
CEDAR	Cat 1	Cat 3	Cat 5	3.64	3.51	3.01	3.39	0.33
			Cat 6	3.31	3.74	3.6	3.55	0.22
			Cat 7	2.78	3.63	3.29	3.23	0.43
		Cat 4	Cat 5	3.2	3.71	3.46	3.46	0.26
			Cat 6	3.43	3.64	3.34	3.47	0.15

			Cat 7	3.04	3.59	3.26	3.30	0.28
	Cat 2	Cat 3	Cat 5	3.5	3.84	3.63	3.66	0.17
			Cat 6	3.01	3.33	3.82	3.39	0.41
			Cat 7	3.22	3.64	3.7	3.52	0.26
		Cat 4	Cat 5	3.34	3.34	3.5	3.39	0.09
			Cat 6	3.81	3.8	3.84	3.82	0.02
			Cat 7	2.83	3.09	3.28	3.07	0.23
CRAND	Cat 1	Cat 3	Cat 5	5.14	5.14	4.13	4.80	0.58
			Cat 6	5.36	5.03	4.1	4.83	0.65
			Cat 7	5.49	4.96	3.97	4.81	0.77
		Cat 4	Cat 5	4.1	4.54	4.31	4.32	0.22
			Cat 6	4.07	4.37	4.47	4.30	0.21
			Cat 7	4.04	4.23	3.79	4.02	0.22
	Cat 2	Cat 3	Cat 5	4.41	4.19	3.86	4.15	0.28
			Cat 6	4.2	4.68	3.95	4.28	0.37
			Cat 7	5.03	4.73	4.92	4.89	0.15
		Cat 4	Cat 5	4.13	3.97	4.2	4.10	0.12
			Cat 6	4.05	3.61	4.1	3.92	0.27
			Cat 7	4.68	4.48	4.43	4.53	0.13
ERAND	Cat 1	Cat 3	Cat 5	5.47	5.49	4.22	5.06	0.73
			Cat 6	5.5	5.23	4.44	5.06	0.55
			Cat 7	5.39	5.16	4.6	5.05	0.41
		Cat 4	Cat 5	4.93	5.07	4.1	4.70	0.52
			Cat 6	4.96	4.18	4.37	4.50	0.41
			Cat 7	4.69	4.13	4.25	4.36	0.29
	Cat 2	Cat 3	Cat 5	5.21	5.37	5.01	5.20	0.18
			Cat 6	4.04	4.83	4.51	4.46	0.40
			Cat 7	4.56	4.32	4.28	4.39	0.15
		Cat 4	Cat 5	4.22	4.44	4.36	4.34	0.11
			Cat 6	4.16	4.31	4.19	4.22	0.08
			Cat 7	4.54	4.88	4.19	4.54	0.35
KHEIS	Cat 1	Cat 3	Cat 5	3.91	3.7	3.89	3.83	0.12
			Cat 6	3.02	3.7	3.62	3.45	0.37
			Cat 7	3.17	3.38	3.8	3.45	0.32
		Cat 4	Cat 5	4.4	4.87	3.86	4.38	0.51
			Cat 6	3	3.82	3.71	3.51	0.45
			Cat 7	3.2	4.1	4.17	3.82	0.54
	Cat 2	Cat 3	Cat 5	4	4.69	4.21	4.30	0.35
			Cat 6	4.2	3.11	3.73	3.68	0.55
			Cat 7	4.8	4.21	4.03	4.35	0.40
		Cat 4	Cat 5	3.89	3.8	3.76	3.82	0.07
			Cat 6	3.21	3.5	2.97	3.23	0.27
			Cat 7	3	4.21	4	3.74	0.65
KOFFIE	Cat 1	Cat 3	Cat 5	3.1	3.09	3.01	3.07	0.05

			Cat 6	2.65	2.51	2.73	2.63	0.11
			Cat 7	2.87	3	2.89	2.92	0.07
		Cat 4	Cat 5	2.81	2.74	2.92	2.82	0.09
			Cat 6	2.31	2.28	2.36	2.32	0.04
			Cat 7	2.44	2.56	2.43	2.48	0.07
	Cat 2	Cat 3	Cat 5	3.48	2.69	3.1	3.09	0.40
			Cat 6	3.26	2.61	3.31	3.06	0.39
			Cat 7	2.83	2.64	3.01	2.83	0.19
		Cat 4	Cat 5	3.01	2.89	2.94	2.95	0.06
			Cat 6	2.84	2.73	3.05	2.87	0.16
			Cat 7	3.36	2.96	3.12	3.15	0.20
KOSH	Cat 1	Cat 3	Cat 5	5.52	5.48	5.74	5.58	0.14
			Cat 6	5.26	5.13	5.47	5.29	0.17
			Cat 7	5.43	5.36	5.69	5.49	0.17
		Cat 4	Cat 5	5.03	4.89	5.41	5.11	0.27
			Cat 6	4.73	4.65	5.21	4.86	0.30
			Cat 7	5.61	5.46	5.46	5.51	0.09
	Cat 2	Cat 3	Cat 5	5.2	5.33	5.34	5.29	0.08
			Cat 6	4.32	4.92	4.49	4.58	0.31
			Cat 7	4.36	5.07	4.83	4.75	0.36
		Cat 4	Cat 5	5.74	5.69	5.06	5.50	0.38
			Cat 6	5.01	5.38	4.84	5.08	0.28
			Cat 7	6.34	6.48	6.44	6.42	0.07
KVAAL	Cat 1	Cat 3	Cat 5	4.51	4.3	4.23	4.35	0.15
			Cat 6	3.88	3.64	4.21	3.91	0.29
			Cat 7	4	3.98	4.66	4.21	0.39
		Cat 4	Cat 5	4.42	4.21	3.92	4.18	0.25
			Cat 6	4.01	4.16	4.15	4.11	0.08
			Cat 7	4.76	4.67	4.41	4.61	0.18
	Cat 2	Cat 3	Cat 5	4.36	4.4	4.27	4.34	0.07
			Cat 6	3.91	4.08	4.23	4.07	0.16
			Cat 7	4.62	4.9	4.38	4.63	0.26
		Cat 4	Cat 5	4.23	4.66	4.53	4.47	0.22
			Cat 6	3.68	3.74	3.71	3.71	0.03
			Cat 7	3.77	3.94	3.82	3.84	0.09
LESOTHO	Cat 1	Cat 3	Cat 5	3.52	2.83	3.05	3.13	0.35
			Cat 6	2.73	2.69	2.81	2.74	0.06
			Cat 7	3.01	2.97	2.93	2.97	0.04
		Cat 4	Cat 5	3	2.5	2.87	2.79	0.26
			Cat 6	2.61	2.53	2.77	2.64	0.12
			Cat 7	2.79	3.34	3.12	3.08	0.28
	Cat 2	Cat 3	Cat 5	2.91	2.86	2.82	2.86	0.05
			Cat 6	2.69	2.73	2.53	2.65	0.11
			Cat 7	3.37	3.1	2.91	3.13	0.23

		Cat 4	Cat 5	3.05	2.93	3.02	3.00	0.06
			Cat 6	2.64	2.76	2.72	2.71	0.06
			Cat 7	2.8	2.85	2.98	2.88	0.09
LIMPOPO	Cat 1	Cat 3	Cat 5	1.34	1.9	1.95	1.73	0.34
			Cat 6	1.4	1.88	2.31	1.86	0.46
			Cat 7	1.48	2.15	2.78	2.14	0.65
		Cat 4	Cat 5	2.09	3.15	2.86	2.70	0.55
			Cat 6	1.83	2.76	2.64	2.41	0.51
			Cat 7	2.24	2.79	2.1	2.38	0.36
	Cat 2	Cat 3	Cat 5	3.32	3.06	2.56	2.98	0.39
			Cat 6	2.3	2.78	2.21	2.43	0.31
			Cat 7	2.86	3.33	2.32	2.84	0.51
		Cat 4	Cat 5	1.95	2.78	2.68	2.47	0.45
			Cat 6	1.63	1.97	2.36	1.99	0.37
			Cat 7	3.75	3.6	2.99	3.45	0.40
MDSN	Cat 1	Cat 3	Cat 5	3.85	3.92	4.32	4.03	0.25
			Cat 6	3.23	3.08	3.64	3.32	0.29
			Cat 7	3.35	3.15	3.75	3.42	0.31
		Cat 4	Cat 5	2.06	2.41	3.55	2.67	0.78
			Cat 6	2.41	2.29	2.34	2.35	0.06
			Cat 7	2.72	2.87	3.97	3.19	0.68
	Cat 2	Cat 3	Cat 5	2.96	3.14	3.24	3.11	0.14
			Cat 6	2.78	2.64	2.81	2.74	0.09
			Cat 7	3.03	2.96	3	3.00	0.04
		Cat 4	Cat 5	4.32	3.75	3.3	3.79	0.51
			Cat 6	3.41	3.05	3.24	3.23	0.18
			Cat 7	3.55	3	3.43	3.33	0.29
MOZA	Cat 1	Cat 3	Cat 5	4.5	4.68	4.05	4.41	0.32
			Cat 6	4.2	4.46	4.33	4.33	0.13
			Cat 7	4.32	4.86	4.45	4.54	0.28
		Cat 4	Cat 5	4.01	4.25	4.51	4.26	0.25
			Cat 6	4.19	4.19	4.3	4.23	0.06
			Cat 7	4.53	3.99	4.42	4.31	0.29
	Cat 2	Cat 3	Cat 5	5.2	5.02	4.29	4.84	0.48
			Cat 6	4	4.43	4.17	4.20	0.22
			Cat 7	3.8	3.6	3.72	3.71	0.10
		Cat 4	Cat 5	4.05	4.45	4.39	4.30	0.22
			Cat 6	4.23	4.31	4.19	4.24	0.06
			Cat 7	4.49	4.6	4.56	4.55	0.06
MOZACHAN	Cat 1	Cat 3	Cat 5	3.76	3.3	2.67	3.24	0.55
			Cat 6	2.31	2.49	3.06	2.62	0.39
			Cat 7	2.28	3.66	3.2	3.05	0.70
		Cat 4	Cat 5	3.76	3.02	3.08	3.29	0.41
			Cat 6	2.93	2.78	2.82	2.84	0.08

			Cat 7	3.3	2.87	2.74	2.97	0.29
	Cat 2	Cat 3	Cat 5	3.71	3.68	2.95	3.45	0.43
			Cat 6	3.38	3.49	3.41	3.43	0.06
			Cat 7	3.77	3.81	3.12	3.57	0.39
		Cat 4	Cat 5	2.67	3.2	2.65	2.84	0.31
			Cat 6	2.73	2.79	2.84	2.79	0.06
			Cat 7	2.95	2.15	2.83	2.64	0.43
NWEST	Cat 1	Cat 3	Cat 5	1.98	1.99	2.81	2.26	0.48
			Cat 6	1.63	1.59	2.61	1.94	0.58
			Cat 7	1.76	1.73	2.61	2.03	0.50
		Cat 4	Cat 5	2.21	1.89	2.33	2.14	0.23
			Cat 6	2.01	1.75	1.95	1.90	0.14
			Cat 7	2.47	2.1	2.09	2.22	0.22
	Cat 2	Cat 3	Cat 5	1.98	2.18	2.12	2.09	0.10
			Cat 6	1.69	1.72	1.43	1.61	0.16
			Cat 7	3.46	2.48	3	2.98	0.49
		Cat 4	Cat 5	2.81	2.61	2.35	2.59	0.23
			Cat 6	1.75	1.69	1.57	1.67	0.09
			Cat 7	2.64	2.43	2.15	2.41	0.25
PLATINUM	Cat 1	Cat 3	Cat 5	1.98	1.99	2.81	2.26	0.48
			Cat 6	2.23	1.87	1.9	2.00	0.20
			Cat 7	2.7	2.88	3.23	2.94	0.27
		Cat 4	Cat 5	2.21	3.52	3.06	2.93	0.66
			Cat 6	1.99	2.36	2.4	2.25	0.23
			Cat 7	2.47	2.73	2.33	2.51	0.20
	Cat 2	Cat 3	Cat 5	2.43	2.56	2.89	2.63	0.24
			Cat 6	1.98	1.73	1.86	1.86	0.13
			Cat 7	3.46	2.69	2.81	2.99	0.41
		Cat 4	Cat 5	2.81	3.23	3.11	3.05	0.22
			Cat 6	2.63	2.87	2.74	2.75	0.12
			Cat 7	2.76	3.01	2.83	2.87	0.13
TUGELA	Cat 1	Cat 3	Cat 5	2.94	3.31	3.52	3.26	0.29
			Cat 6	2.36	2.85	2.34	2.52	0.29
			Cat 7	2.43	3.32	2.25	2.67	0.57
		Cat 4	Cat 5	2.76	2.18	2.4	2.45	0.29
			Cat 6	1.95	1.83	2	1.93	0.09
			Cat 7	2.88	2.46	2.67	2.67	0.21
	Cat 2	Cat 3	Cat 5	3.18	2.59	3	2.92	0.30
			Cat 6	2.41	2.56	2.37	2.45	0.10
			Cat 7	2.99	2.4	2.49	2.63	0.32
		Cat 4	Cat 5	3.52	2.25	3.06	2.94	0.64
			Cat 6	1.99	1.63	2.01	1.88	0.21
			Cat 7	2.41	1.87	2.19	2.16	0.27
WBOTS	Cat 1	Cat 3	Cat 5	2.24	2.13	3.04	2.47	0.50

			Cat 6	1.82	1.94	2.43	2.06	0.32
			Cat 7	2.64	1.89	2.81	2.45	0.49
		Cat 4	Cat 5	2.54	2.43	2.39	2.45	0.08
			Cat 6	2.44	2.39	2.21	2.35	0.12
			Cat 7	2.67	2.98	2.46	2.70	0.26
	Cat 2	Cat 3	Cat 5	2.03	1.88	2.4	2.10	0.27
			Cat 6	1.76	1.94	1.63	1.78	0.16
			Cat 7	1.9	2.26	2.73	2.30	0.42
		Cat 4	Cat 5	3.04	2.81	2.96	2.94	0.12
			Cat 6	2.53	2.48	2.36	2.46	0.09
			Cat 7	2.86	2.73	2.79	2.79	0.07
WELKOM	Cat 1	Cat 3	Cat 5	5.22	5.31	4.96	5.16	0.18
			Cat 6	4.95	5.03	4.84	4.94	0.10
			Cat 7	5.16	5.29	5.24	5.23	0.07
		Cat 4	Cat 5	5.18	5.04	4.85	5.02	0.17
			Cat 6	4.91	4.78	4.62	4.77	0.15
			Cat 7	5.37	4.77	4.79	4.98	0.34
	Cat 2	Cat 3	Cat 5	5.18	5.23	5.21	5.21	0.03
			Cat 6	4.93	4.81	5.06	4.93	0.13
			Cat 7	5.28	5.31	5	5.20	0.17
		Cat 4	Cat 5	4.96	5.24	5.13	5.11	0.14
			Cat 6	4.89	4.76	5.02	4.89	0.13
			Cat 7	5.4	4.83	5.32	5.18	0.31
WRAND	Cat 1	Cat 3	Cat 5	6.93	6.82	6.53	6.76	0.21
			Cat 6	6.33	6.51	6.19	6.34	0.16
			Cat 7	6.98	6.72	6.31	6.67	0.34
		Cat 4	Cat 5	6.88	6.63	6.23	6.58	0.33
			Cat 6	5.52	5.76	5.59	5.62	0.12
			Cat 7	6.44	6.29	6.19	6.31	0.13
	Cat 2	Cat 3	Cat 5	6.45	6.51	6.47	6.48	0.03
			Cat 6	5.83	5.98	5.74	5.85	0.12
			Cat 7	6.21	6.43	6.37	6.34	0.11
		Cat 4	Cat 5	6.53	6.31	6.4	6.41	0.11
			Cat 6	6.28	6.11	6.06	6.15	0.12
			Cat 7	6.73	6.5	6.51	6.58	0.13
ZEBED	Cat 1	Cat 3	Cat 5	2.86	2.79	3.88	3.18	0.61
			Cat 6	2.79	2.61	2.73	2.71	0.09
			Cat 7	2.94	3.01	3.65	3.20	0.39
		Cat 4	Cat 5	3.62	3.49	3.58	3.56	0.07
			Cat 6	2.84	2.86	2.61	2.77	0.14
			Cat 7	3.43	3.93	2.84	3.40	0.55
	Cat 2	Cat 3	Cat 5	4.38	3.49	3.08	3.65	0.66
			Cat 6	3.96	3.41	3.23	3.53	0.38
			Cat 7	4.19	3.94	3.72	3.95	0.24

		Cat 4	Cat 5	3.88	3.65	3.49	3.67	0.20
			Cat 6	3.64	3.42	3.37	3.48	0.14
			Cat 7	3	3.09	2.98	3.02	0.06
ZOET	Cat 1	Cat 3	Cat 5	2.92	2.72	2.91	2.85	0.11
			Cat 6	2.46	2.34	2.85	2.55	0.27
			Cat 7	2.31	2.51	2.73	2.52	0.21
		Cat 4	Cat 5	2.8	3.1	2.84	2.91	0.16
			Cat 6	2.64	2.69	2.52	2.62	0.09
			Cat 7	2.98	2.76	2.44	2.73	0.27
	Cat 2	Cat 3	Cat 5	2.74	2.81	2.7	2.75	0.06
			Cat 6	2.53	2.76	2.61	2.63	0.12
			Cat 7	2.74	2.9	2.81	2.82	0.08
		Cat 4	Cat 5	2.91	2.73	2.76	2.80	0.10
			Cat 6	2.44	2.36	2.73	2.51	0.19
			Cat 7	2.83	2.44	2.93	2.73	0.26

6.4. Maximum magnitude M_{max} calculation

The determination of M_{max} for regions of low seismicity like South Africa is a very contentious issue since there is little information to go by. Due to lack of paleoseismic and fault rupture information, M_{max} is mainly calculated using seismic data, except for those source zones where faults that are assumed to be active have known dimensions. Assessment of M_{max} for seismic source zones has been designed to incorporate the uncertainties in both the conceptual models and the parameter values associated with each model. Procedures for estimating M_{max} using seismic catalogue only are commonly used in many regions and has been well documented (Kijko, 2004). The approach is part of a family of approaches that uses the observed earthquakes within a seismic source to estimate M_{max}. The maximum observed earthquake magnitude ($M_{max\text{-}obs}$) is a very important parameter for determining M_{max} according to these techniques. For source zones with identified active faults, an M_{max} value was estimated using the Wells and Coppersmith (1994) equation that links magnitude size to surface rupture length. Faults identified as active in each zone were used in this calculation with the length measured from segments that are associated with earthquake locations. An assumption was made that the largest possible earthquake is that which occurs when the all identified segments of the fault rupture in one go. Thus, large M_{max} values were obtained using this technique producing upper bound estimates. In addition, the traditional method of adding 0.5 to the maximum observed magnitude was also included.

Overall, the largest $M_{max\text{-}obs}$ in this study comes from the Mozambique zone. A magnitude M_W7.2 earthquake occurred in the Manica province in Mozambique on 22 February 2006. Other zones where

large earthquakes have occurred are KOFFIE, TUGELA and ZOET *viz.* the 20 February 1912 (M_W 6.2), 31 December 1932 (M_W 6.3) and 3 April 2017 (M_W 6.5) earthquakes, respectively. In all other zones, the largest earthquake is less than M_W 6.0. The famous Ceres-Tulbagh earthquake falls outside the boundaries of the study area hence it was not considered. In the mining regions, the largest observed event was a M_W 5.5 earthquake that occurred in the KOSH zone on 5 August 2014 near Orkney. To assess the uncertainty associated with the M_{max} values, three methods (Tate-Pisarenko, Tate-Pisarenko-Bayes, and Kijko-Sellevoll-Bayes) implemented in the HA3 program by Kijko (2014) were used to compute M_{max} values for each source. Another method implemented in this study is to add 0.5 magnitude unit to the maximum observed magnitude. For those sources with known fault length, the Wells and Coppersmith (1994) method was also implemented in computing M_{max}. Some zones have large variations (e.g. WBOTS, KHEIS, LIMPOPO and KVAAL) showing how unreliable their solutions are; this might be because few events were used in the computation.Kijko and Singh (2011) also stated these sentiments in which they recommended that M_{max} need to be computed by combining both seismicity and geological information. For seismic hazard analysis M_{max} determination will remain a major source of uncertainty hence no one method can be singled out to be the best to use.

Table 6-3: M_{max} values calculated for identified seismic sources determined using different methods. For some source zones where there are identified faults, the Wells and Coppersmith (1994) method was also used to compute M_{max}. M_{max_obs} is the maximum observed magnitude for the source. The five methods used to compute M_{max} are illustrated.

Zone	**$M_{max\text{-}obs}$**	**M_{obs} + 0.5**	**Tate-Pisarenko**	**Tate-Pisarenko-Bayes**	**Kijko-Sellevoll-Bayes**	**Wells and Coppersmith (1994)**		**Number of events**
						Fault length (km)	**Magnitude**	
CEDAR	5.2	5.7	5.5	5.7	5.8			56
CRAND	4.1	4.9	4.8	4.6	5.2	11.8	6.0	1820
ERAND	4.9	5.4	5.5	5.2	5.4	18.7	6.3	3417
KHEIS	3.7	4.2	4.8	5.3	5.2			48
KOFFIE	6.2	6.7	6.9	6.9	6.4			247
KOSH	5.5	6.0	6.0	6.0	5.7			8736
KVAAL	5.7	5.2	4.9	5.3	5.9	30	6.7	102
LESOTHO	5.3	5.8	5.8	5.9	5.5			176
LIMPOPO	6.5	5.5	6.8	5.3	5.5			118
MDSN	5.0	5.5	5.3	5.3	5.2			468
MOZA	7.2	7.7	7.7	7.7	7.5	40	7.2	553
MOZCHAN	6.3	6.8	6.8	6.5	7.3			125
NWEST	4.8	5.3	4.8	5.2	5.4			148
PLATINUM	5.0	5.5	6.1	5.2	5.7			173
TUGELA	6.3	6.5	6.5	6.6	6.5	30	6.6	125
WBOTS	5.2	5.7	6.3	5.6	6.1			92
WELKOM	5.6	6.1	6.1	6.5	6.2			4143
WRAND	4.8	5.3	4.9	5.4	5.9	20	6.3	24456
ZEBED	5.0	5.5	6.0	5.5	5.9	75.5	7.2	566
ZOET	6.5	7.0	7.2	7.1	7.0	25	6.5	56

6.5. Conclusion

In this chapter, the *a*- and b-value recurrence parameters were computed from different catalogues that were developed in Chapter 4. Different statistical methods were used to compute M_{max} and recurrence parameters values. For each source zone, 36 *a* - and *b*-values were computed and these were used in the sensitivity analysis. Recurrence parameters for tectonic sources are lower than those for mining related sources. Slight variations in the recurrence parameters (especially M_{max}) were observed. These might be improved by re-evaluating pre and early instrumental seismicity, which will increase the number of events in our catalogue as well as better constrain our $M_{max\text{-}obs}$. It is very important to use the correct catalogue and method for computing recurrence parameters. The computation of M_{max} was mainly done using seismological data (i.e. the earthquake catalogue) since geological information is only available for a few sources. It is important to look for more information on fault rupture properties through paleoseismic studies in order to improve on our estimation of recurrence parameters (e.g. M_{max}). There is a need to put more efforts in determining the best method that suites our local datasets for both recurrence parameters and M_{max} values. We recommend that for recurrence parameters, the ZMAP methods should be used, while for M_{max} more than one method can be used simultaneously to cater for uncertainties.

CHAPTER 7: GROUND MOTION MODEL

7.1. Introduction

The ground motion model predicts the distribution of expected ground-motions conditional on the occurrence of a given earthquake scenario. The choice of a ground motion model is an important factor in seismic hazard analysis (SHA). Ground-motion prediction equations (GMPEs) relate a ground-motion parameter (e.g. peak ground acceleration (PGA), peak ground velocity (PGV), peak ground displacement (PGD)) to a set of explanatory variables describing the earthquake source, wave propagation path and local soil conditions (Douglas, 2003; Stewart et al., 2015; Akkar et al., 2014). These independent variables include magnitude, source-to-site distance, local site conditions and often style-of-faulting. Some recent models go further to account for other factors affecting earthquake ground motions such as hanging wall effects and directivity (e.g. Boore et al., 2014). Each SHA study needs to incorporate a GMPE which models the propagation of ground motion from the source to the site.

Ideally, it is preferable to use a GMPE relation derived from local data, but this is seldom possible except in regions of dense station coverage and high seismicity such as Japan or California (Douglas et al., 2011; Bommer et al., 2015a). In South Africa, the only accelerometric stations installed are in the cluster networks in the mining regions. These stations were deployed recently (from 2012), and the existing ground motion record dataset does not allow users to derive such a model, due to the lack of strong motion earthquakes (Groobelaar et al., 2017). In this regard, models from other regions are carefully selected and tested to determine if they fit appropriately to the local data. In actual use in hazard analysis, a ground motion model will be called upon to predict accelerations from the complete range of magnitude and distance (Shoja-Taheri et al., 2010; Stewart et al., 2015; Midzi et al., 2020). A model that is derived from a dataset that does not cover this full range may not be reliable. This is particularly a problem because the datasets frequently tend to be biased towards small earthquakes at short distances and large earthquakes at long distances (Musson and Sargeant, 2007). This can lead to scaling problems when ground motions must be calculated for parts of the magnitude-distance domain not well represented in the dataset. Otherwise, one must adopt either a relationship in which local data is augmented with data from a broader region, or a relationship from anywhere in the world that is considered to be tectonically similar (Cotton et al., 2006; Bommer et al., 2015a; Midzi et al., 2020). Given that hundreds of equations have been published in recent times, it is a daunting task to identify a suitable model for a given project (Stewart et al., 2015; Douglas, 2016).

The procedure for the selection of the appropriate GMPEs for use in the seismic hazard assessment has been well documented by a number of authors (Cotton et al., 2006; Scherbaum et al., 2009; Bommer et al., 2010). This process should result in the smallest set of independent models that capture the expected range of possible ground-motions in the target region (Cotton et al., 2006). This smallest set of GMPEs will be compared with local data to verify if they really capture the uncertainty in the local data. Many studies have been devoted in recent years to evaluating the performance and reliability of the GMPEs (Cotton et al., 2006; 2008; Shoja-Taheri et al., 2010; Bommer et al., 2003; 2011). Among them, Cotton et al. (2008) investigated the consequences of using them outside their range of validity. It is often the case of the prediction of the spectral ordinates from earthquake of small-to-moderate magnitude, for which the observed spectral values are systematically smaller. The problem arises because of the scarcity of strong motion data that are needed to definitively resolve the shape of the attenuation curve. The uncertainty in the selection process is represented in the branches of the logic tree and weighted according to the relative confidence (Bommer *et al*., 2005) or degree of belief by the analyst using available information.

7.2. Identification and testing of suitable ground motion prediction equations for Johannesburg

In view of its position relative to plate boundaries, relatively low earthquake activity and the slow rates of crustal deformation, South Africa is generally considered a Stable Continental Region (SCR). According to Malservisi et al. (2013) and Stamps et al. (2018) deformation rates for South Africa are less than 1mm per year. In another study, using GPS array (Nocquet and Calais, 2003) it was found that actual convergence rate is even lower. Therefore, it is considered that an analogy for this region would be a SCR such as the Eastern North America (ENA) and Australia, for which a number of ground-motion models are available.

Unlike ENA, however, the current tectonic regime of the southern African region (mainly along the eastern parts) shows evidence of extensional tectonic stresses with dominant normal faulting (Hartnady, 2002; Stamps et al., 2018; Manzunzu et al., 2019; Midzi et al., 2020; Mulabisana et al., 2021). Studies such as that by Johnston et al. (1994) show that extensional tectonic stresses are uncommon within SCRs, for which reason alternative GMPEs from active shallows crust were selected.

In the current South African seismic catalogue, 90% of seismic events comes from the mining regions; therefore, it is more appropriate to represent the ground motion using proper GMPEs derived from induced seismicity. Ground motions from induced seismicity are characterised by high

frequencies which tend to attenuate faster than natural tectonic events (McGarr and Fletcher, 2005; Manzunzu et al., 2017; Zulu, 2018). Locally derived GMPEs are important because the correctly model the local geological variations which in most cases vary significantly which alters the frequent content of the ground motion (Camelbeeck and Meghraoui, 1998; Camelbeeck et al., 2004; Camelbeeck et al., 2014). In most GMPEs, local site conditions are modelled by the Vs30 parameter (e.g. the Next Generation of Attenuation project) however this value has been observed not to be accurately modelled especially in areas where bedrock depth are more than 30 metres (Camelbeeck, 2004). There are several GMPEs derived from induced seismic events; however, only one (the relation by McGarr and Fletcher, 2005) is specifically derived from mining related events. Most of the other GMPEs were derived either from geothermal events or from fracking events. However, the McGarr and Fletcher (2005) relation has been observed to grossly under predict events of $M_W > 5.0$ and distances larger than 10 km (Zulu, 2018). Most of these GMPEs from induced seismicity failed the selection criteria in that they were derived only for PGA, not for the other spectral periods, hence were not tested in this study. The only GMPE from induced seismicity applied in this study is by Atkinson (2015) which was developed for geothermal sources for spectral periods up to 2 seconds.

Ten pre-selected GMPEs from the three tectonic regions mentioned above were tested on how suitable they predict ground motion in South Africa using local data for different spectral periods. The information for each GMPE is shown in Table 7.1 below.

Table 7-1: GMPEs preselected from different tectonic settings to be used in this study, including the regions for which they were developed. SCR represents stable continental regions, SAC represents shallow active crusts and ISR represents induced seismicity regions.

	GMPE	**Tectonic region**	**Magnitude range (M_w)**	**Distance range (km)**
1	Boore and Atkinson (2008) as modified by Atkinson and Boore (2011)	Referenced empirical model for eastern North America (SAC)	5 - 8	0 - 400
2	Atkinson and Boore (2006) as modified by Atkinson and Boore (2011)	Extended stochastic model for eastern America (SCR)	3.5-8	1-1000
3	Campbell (2003)	Hybrid model for eastern North America (SCR)	5-8.2	1-1000
4	Rietbrock et al., (2013)	Stochastic model for United Kingdom (SCR)	4.5 – 7.5	1 - 1000
5	Frankel et al. (1996) as parameterized by EPRI (2004)	Stochastic model for eastern North America	5 - 8	1 - 300
6	Akkar et al., (2014)	Europe and Middle East (SAC)	4-8	1 - 300
7	Silva et al. (2002)	Stochastic model for eastern North America (SCR)	4.5 – 8.5	1 - 400
8	Pezeshk *et al.* (2011)	Hybrid model for eastern North America (SCR)	5-8	1-1000

9	Toro et al. (1997) modified by Toro (2002)	Stochastic model for eastern North America (SCR)	5 - 8	1 - 100
10	Atkinson (2015)	Small to medium events at short distance (ISR)	3 - 6	5 - 40

7.3. GMPE Parameter adjustments

It is important that equations used in seismic hazard calculations are consistent in terms of the variables considered. Therefore, where there are differences in terms of the definitions employed for the variables used in the parameterisation of the equation, adjustment factors need to be applied (Bommer et al., 2003). The parameters that needs to be considered for adjustment are those discussed below.

7.3.1. Horizontal component definition

Ground motions calculated in seismic hazard analysis are usually for the geometric mean of the two horizontal components of motion. The geometric mean takes into account the compounding that occurs from period to period, which dampens the effects of the outliers. No adjustment is necessary for the selected GMPEs because they both use a geometric mean of the two horizontal components of motion.

7.3.2. Magnitude

The seismic catalogue used in this study was homogenised to M_w as described in Chapter 4. The GMPEs adopted for the hazard calculations use M_w. Thus, no adjustment is necessary.

7.3.3. Distance

The different equations used different distance metrics however, no adjustment for this parameter is necessary since the software used in the hazard calculation (OPENQUAKE) computes the appropriate distance for each model.

7.3.4. Style-of-faulting

Although the GMPEs used in the hazard calculations have been selected in order to be compatible with the tectonic setting of South Africa, the composition of the underlying dataset in terms of style-of-faulting (SOF) is not always consistent with the predominantly normal faulting mechanisms of South Africa tectonic earthquakes. However, the GMPE models do not require adjustment, because in the hazard calculation software, OPENQUAKE, it is possible to explicitly select the appropriate style of faulting. Thus, no adjustment was required for either equation. Most of the GMPE models do

not require adjustment, because either they are stochastic (simulated) models or they allow for the selection of the style of faulting during the hazard calculation.

7.4. Identified testing data

The method of Scherbaum et al. (2004) was applied in order to rank 10 GMPEs selected in this study. This method is based on a transparent and data-driven process that quantifies the model fit and measures how well the underlying model assumptions are met. A database of 61 seismic events (Figure 7-1) was compiled from the South African mining Cluster Networks for use in the testing of the GMPEs. Because the cluster networks are installed in mining regions to record ground motion mostly due to mining induced seismicity, our dataset is mainly composed of mining related events. However, according to Douglas et al. (2013) and Atkinson (2015), ground motion from natural and induced sources are indistinguishable. Therefore, we compared our datasets to the selected GMPEs.

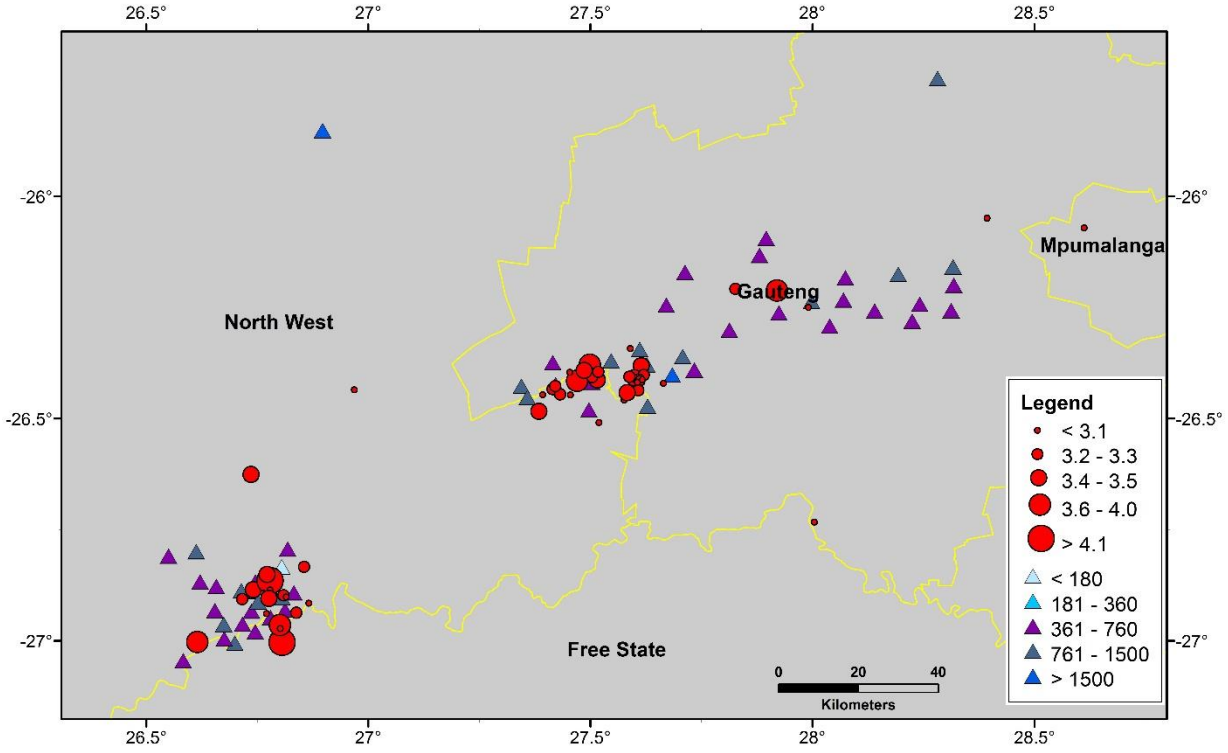


Figure 7-1: Location of earthquakes used in the testing of GMPEs. The figure shows the spatial distribution of the seismic events and the stations. Triangles represent the stations recording the events with each station having a V_{s30} value indicated with the color; circles are the seismic events.

Only events with good waveform data in terms of signal to noise ratio and recorded by at least five stations, were included. These contributed 2 018 two-component horizontal acceleration time series within a hypocentral distance range of 1.2 km to 350 km. The magnitude of the events ranged from 3.0 to 5.5. The various magnitude ranges of the events and number of records associated with each listed magnitude value are presented in Table 7-2. Hypocentral distance was taken as the distance

metric for all comparisons in place of rupture distance. Due to the moderate magnitudes of all earthquakes and shallow depth, the assumption of equality between hypocentral and rupture distance is inferred (Gupta, 2006).

Table 7-2: Number of events and recordings in different magnitude range showing the distance range of the recording stations.

Magnitude	**3.0**	**3.1**	**3.2**	**3.3**	**3.4**	**3.5**	**3.6**	**3.9**	**4.6**	**5.5**
No. of events	11	13	11	7	3	6	3	1	1	1
No. of recordings	284	424	405	265	130	220	137	41	40	38
Hypocentral Distance (km)	1.4 - 349	0.1 - 284	0.7 - 232	1.8 - 337	0.9 - 218	1.2 - 231	2.4 - 218	4.3 - 117	4.2 - 195	4.8 - 177

An effort was also made to classify the site conditions at each of the seismic stations that recorded the earthquakes in this investigation. Given the lack of detailed geological information at all the seismic stations, five site classes based on the National Earthquake Hazards Reduction Program (NEHRP) (FEMA, 2003) site classification were used. The NEHRP site classification forms one of the standard site classifications used in GMPEs (Table 7-3).

Table 7-3: NEHRP site classification scheme (FEMA, 2003). V_{S30} is the shear-wave velocity averaged over the uppermost 30m.

Site Class	**Geologic Description**	**V_{S30} (m/s)**
A	Hard Rock	$V_{S30} > 1500$
B	Soft Rock	$760 < V_{S30} \leq 1500$
C	Stiff soil	$360 < V_{S30} \leq 760$
D	Soft soil	$180 < V_{S30} \leq 360$
E	Very soft soil	$V_{S30} \leq 180$

Most of the stations are located on soft rock (Site Class B), followed by stiff rock (site class C). This is illustrated clearly in Figure 7-2, which shows the distribution of earthquake magnitude with hypocentral distance, where each record is linked to the appropriate site conditions.

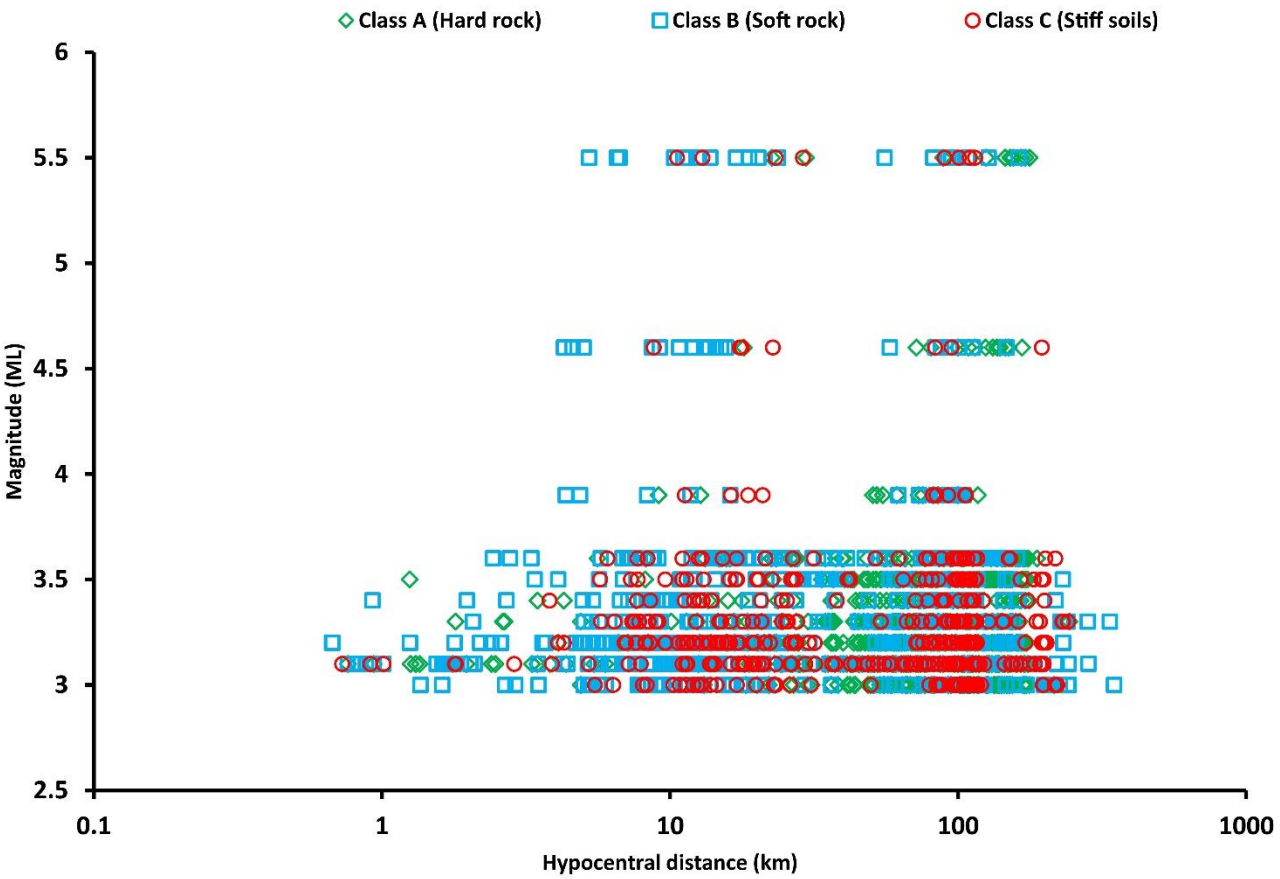


Figure 7-2: Illustration of site classification of the seismic station records representing different site classes based on NEHRP site classification.

7.4.1. Results of Comparisons

The comparison of observed and calculated ground motion is carried out by calculating residuals. Residuals are generally defined as the difference between the natural logarithm of the observed parameter (Y_{ij}) and the mean calculated parameters ($\hat{Y}$) for a given GMPE (equation 7.1; Shoja-Taheri et al., 2010; Skarlatoudis, 2017). For each observed waveform, the ground motion parameter are extracted at differentspectral periods. Each ground motion parameter is compared with each individual GMPE at different spectral periods to compute the required residuals.

$$\boldsymbol{r_{ij} = lnY_{ij} - ln\,\hat{Y}} \qquad (7.1)$$

where lnY_{ij} is the value of the j^{th} record at the i^{th} event and $ln\hat{Y}$ is the mean value of lnY computed using a particular GMPE. The results of the comparison were presented by considering intra-event and inter-event residuals, which are all usually close to zero and represent the residuals related to each individual source and to combined sources respectively. The intra-event terms presented here were obtained using the whole database of events for all available hypocentral distances in a similar

way as reported by Graves et al. (2008). The two residuals are given by the following equations, 7.2 and 7.3.

$$\boldsymbol{r_{ij}^{intra} = r_{ij} - \eta_i} \quad (7.2)$$

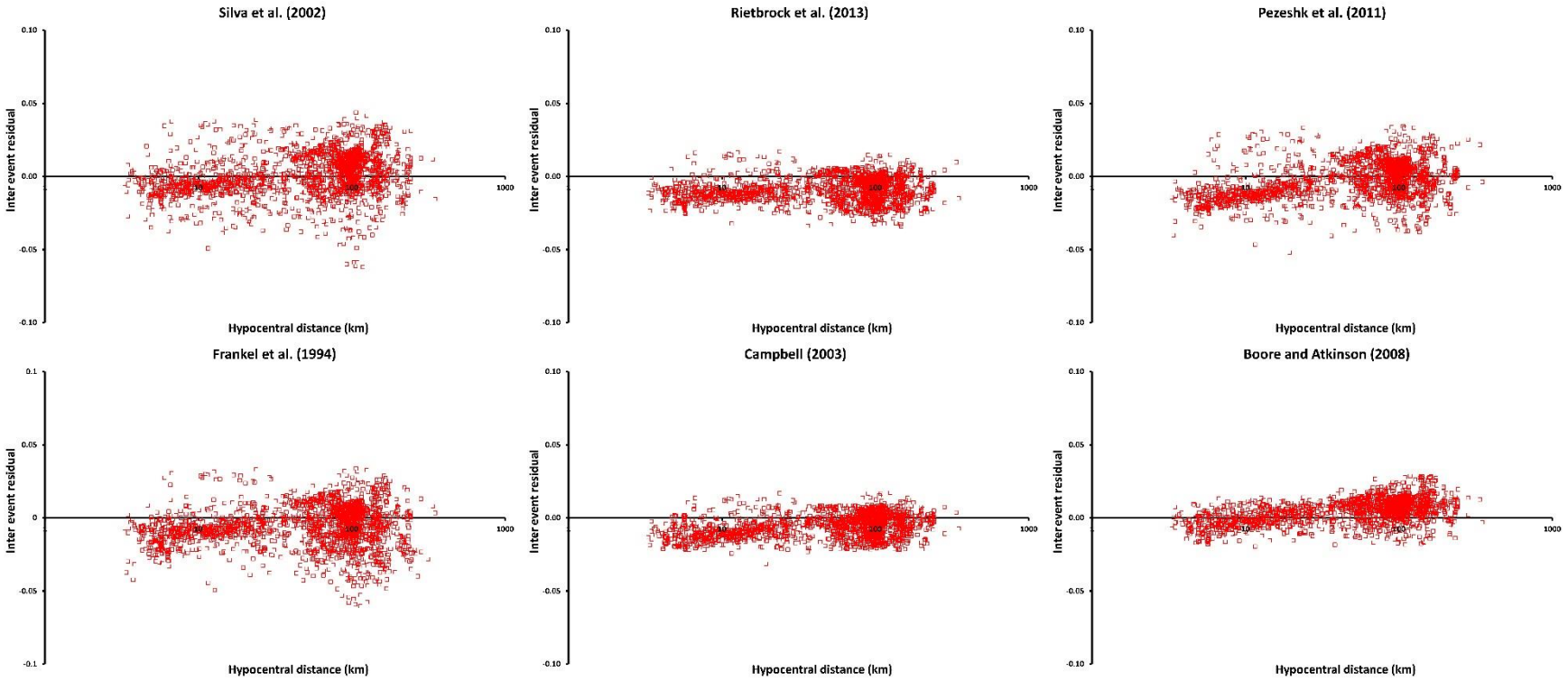
$$\boldsymbol{r_i^{inter} = \eta_i - \frac{1}{N_e}\sum_{i=1}^{N_i}\eta_i} \quad (7.3)$$

where N_e is the total number of events and the mean of the residuals for the i^{th} event with N_i records is defined as in equation 7.4:

$$\eta_i = \frac{1}{N_i}\sum_{j=1}^{N_i} r_{ij} \quad (7.4)$$

For each GMPE, the residuals were calculated for 5% damped pseudo spectral acceleration for periods 0.0s (PGA), 0.1s and 2.0s. In the following section, the results are presented by considering the figures related to the residuals (equation 7-2 and 7-3). Figure **7-3**, Figure **7-4** and Figure **7-5** shows inter-event residuals for the GMPEs that were preselected (Table 7-1) and tested with observed data in this investigation for the three spectral periods (PGA, PSA = 0.15s and PSA = 2.0s.

The inter-event terms show similar variation with distance for most of the equations. For most of the GMPEs the residuals are negative with the lowest at about -0.01 and smaller at long periods, where residuals are less than -0.005 (and 0.005 where positive) for periods greater than 1.0 seconds. The notable trend of the data in this figure at all periods is its linear nature. The inter event residuals distribution implies that most of models (in particular, Rietbrock et al. (2013); Campbell (2003); Atkinson (2015) and Toro (2002)) overestimate the observed ground motion. The residuals for PGA are large for Silva et al. (2003), Pezeshk et al. (2011), Frankel et al. (1994) and Atkinson and Boore (2006) GMPEs (Figure 7-3). For spectral period T = 0.15s, the Atkinson (2015), Akkar et al. (2014), Campbell (2003), Rietbrock et al. (2013 and Pezeshk et al. (2011) GMPEs have negative residual values while Boore and Atkinson (2008) and Atkinson and Boore (2006) have positive values (Figure 7-4). All GMPEs are evenly distributed around the zero residual line for the T = 2.0s spectral period (Figure 7-5).


Silva et al. (2002)
Rietbrock et al. (2013)
Pezeshk et al. (2011)
Frankel et al. (1994)
Campbell (2003)
Boore and Atkinson (2008)
Inter event residual
Hypocentral distance (km)

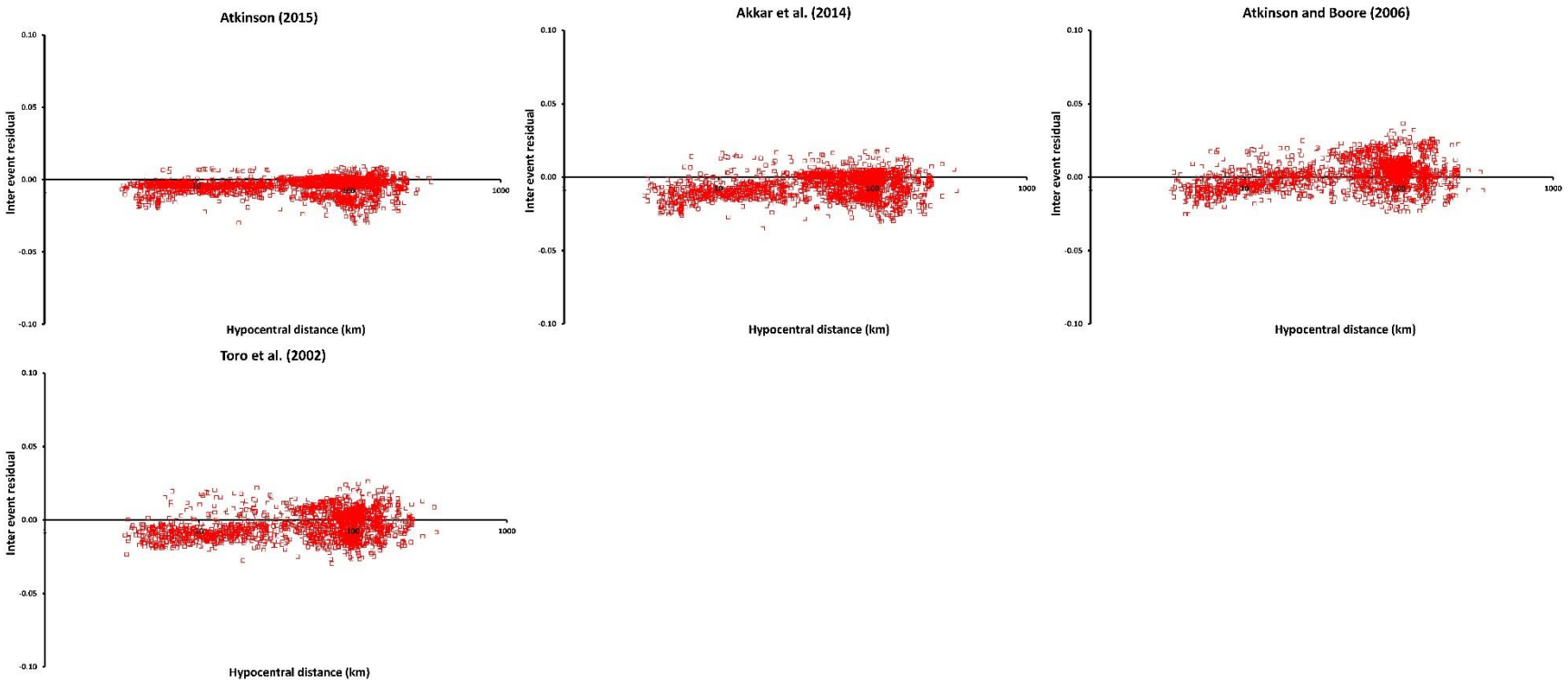
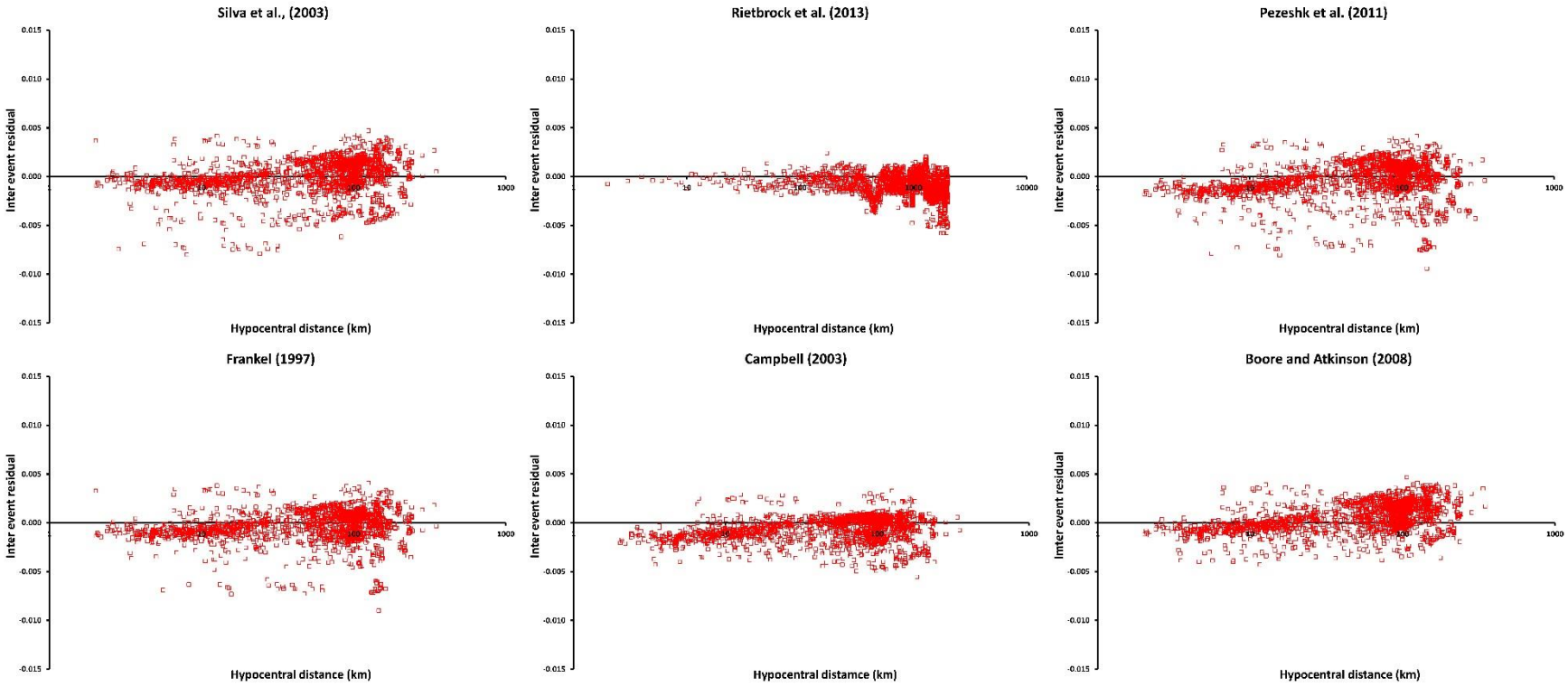


Figure 7-3: The inter-event residuals of all GMPEs for PGA (T = 0.01s) spectral acceleration versus hypocentral distance.


Silva et al., (2003)
Rietbrock et al. (2013)
Pezeshk et al. (2011)
Frankel (1997)
Campbell (2003)
Boore and Atkinson (2008)
Inter event residual
Imter event residual
Hypocentral distance (km)
Hypocentral distamce (km)

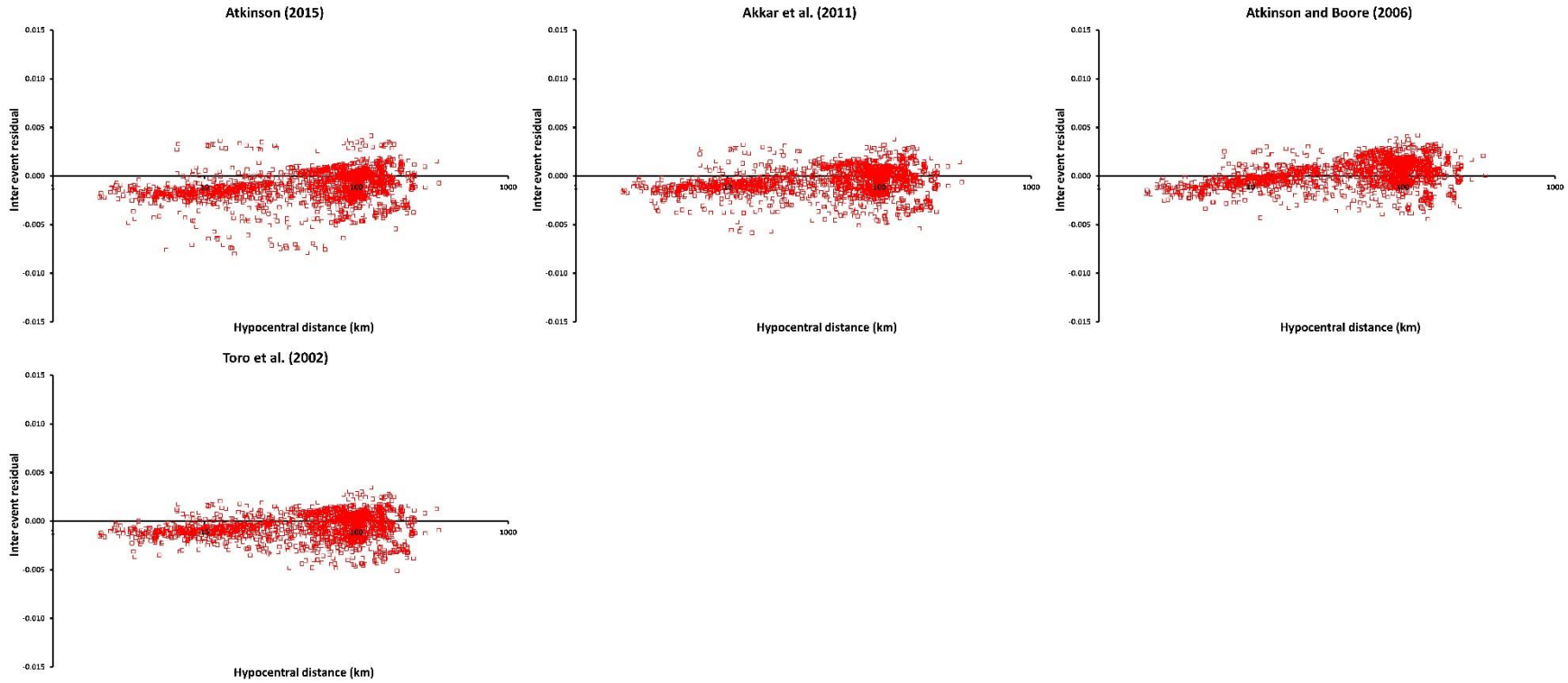
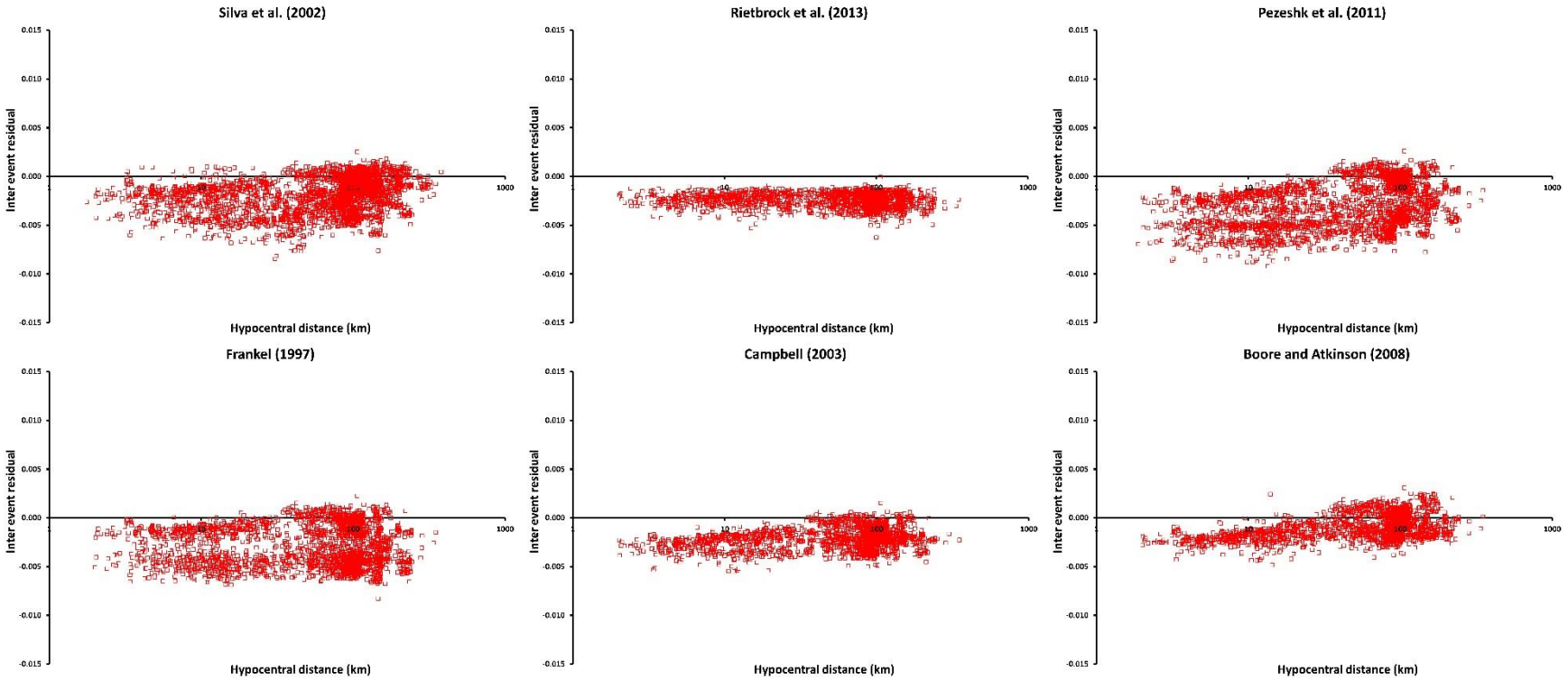


Figure 7-4: The inter-event residuals of all GMPEs for PSA (T = 0.15s) versus hypocentral distance.


Silva et al. (2002)
Rietbrock et al. (2013)
Pezeshk et al. (2011)
Frankel (1997)
Campbell (2003)
Boore and Atkinson (2008)
Inter event residual
Hypocentral distance (km)
0.015
0.010
0.005
0.000
-0.005
-0.010
-0.015
10
100
1000

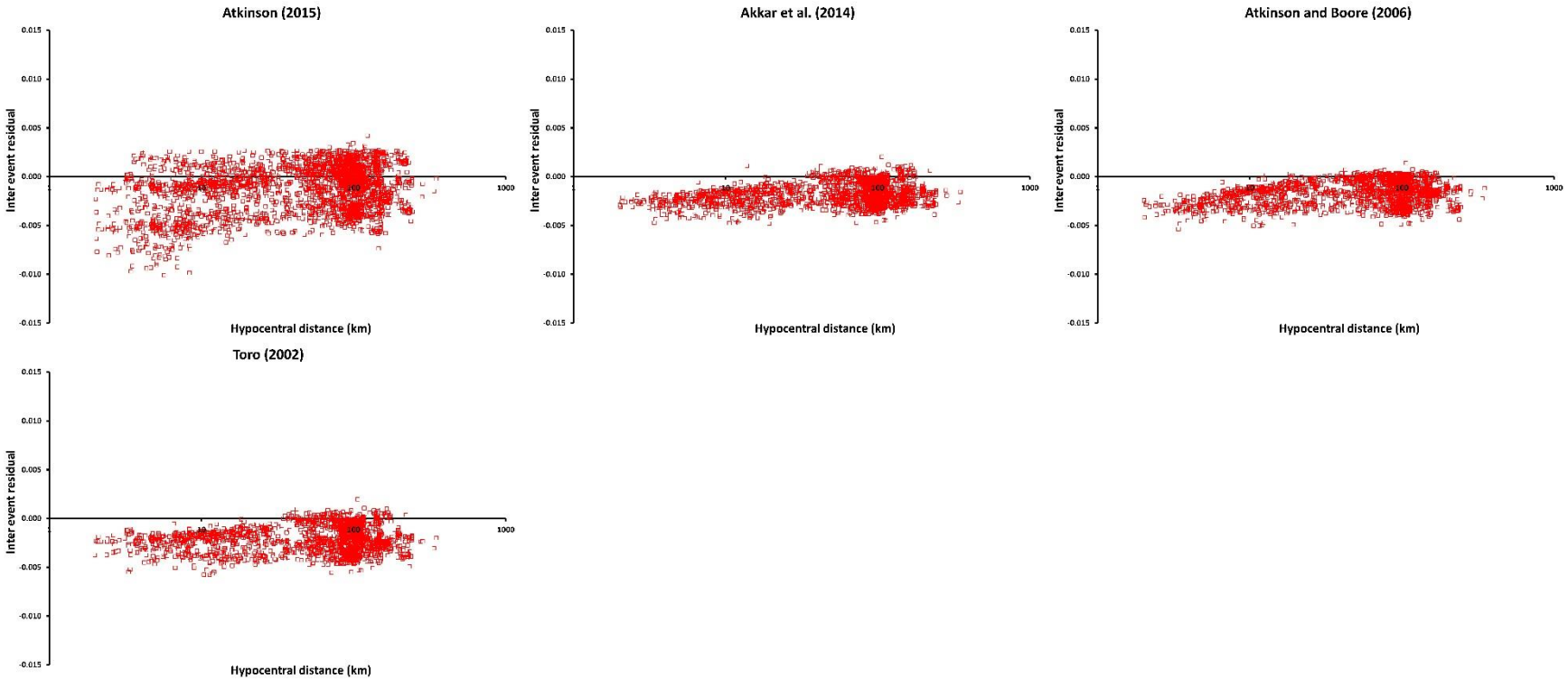
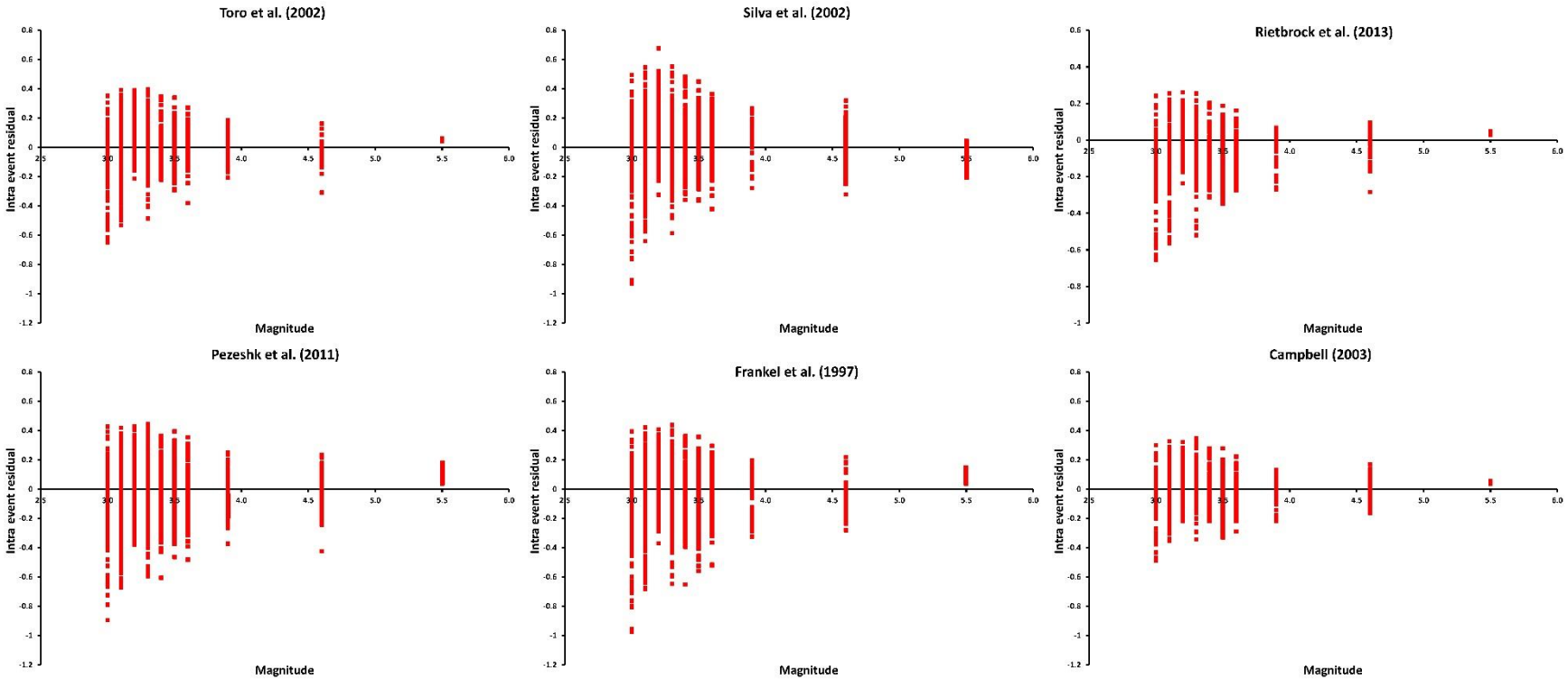


Figure 7-5: The inter-event residuals of all GMPEs for PGA (T = 2.0s) versus hypocentral distance.

Analysis of intra-event residual shows larger residuals (between -0.2 to 0.2) compared to inter event residual (Figure 7-6, Figure 7-7 and Figure 7-8). High scattering at low magnitudes is consistently observed for all the spectral periods. The scattering improves at high magnitudes but changes from positive to negative residuals with increasing periods. Large residual values seen in Figure 7-6 and Figure 7-7 might be due to the use of GMPEs outside their range of applicability. Silva et al. (2003); Rietbrock et al. (2013); Frankel et al. (1994) and Atkinson (2015) have large scatter for PGA compared to other GMPEs. The scatter is more significant for small magnitude events than for the moderate ones. For spectral period T= 0.15s, all the GMPEs have residuals less than 0.1 although they seem to follow the trend as that of PGA. At spectral period 2.0s, the residuals are lower than ± 0.05 although they seem to be more negative.


Toro et al. (2002)
Silva et al. (2002)
Rietbrock et al. (2013)
Pezeshk et al. (2011)
Frankel et al. (1997)
Campbell (2003)
Intra event residual
Magnitude

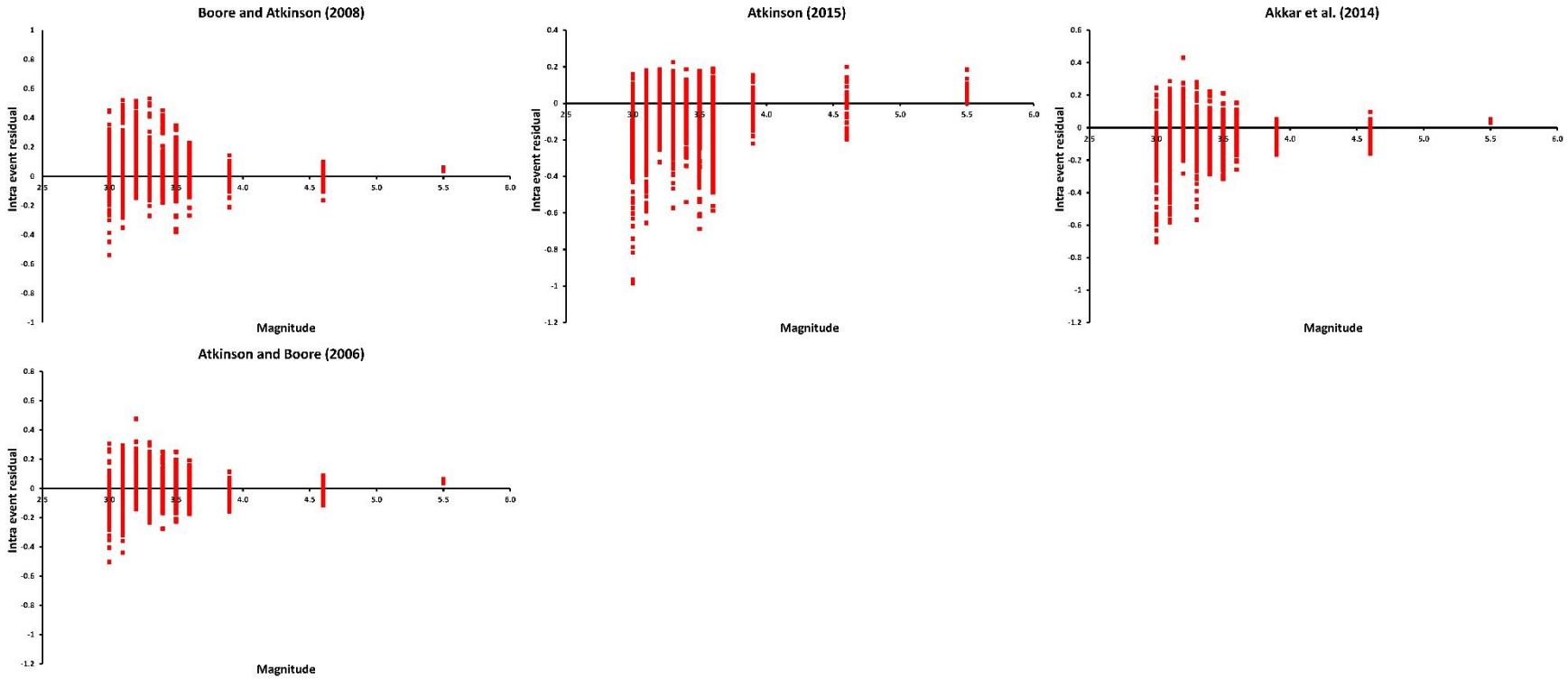
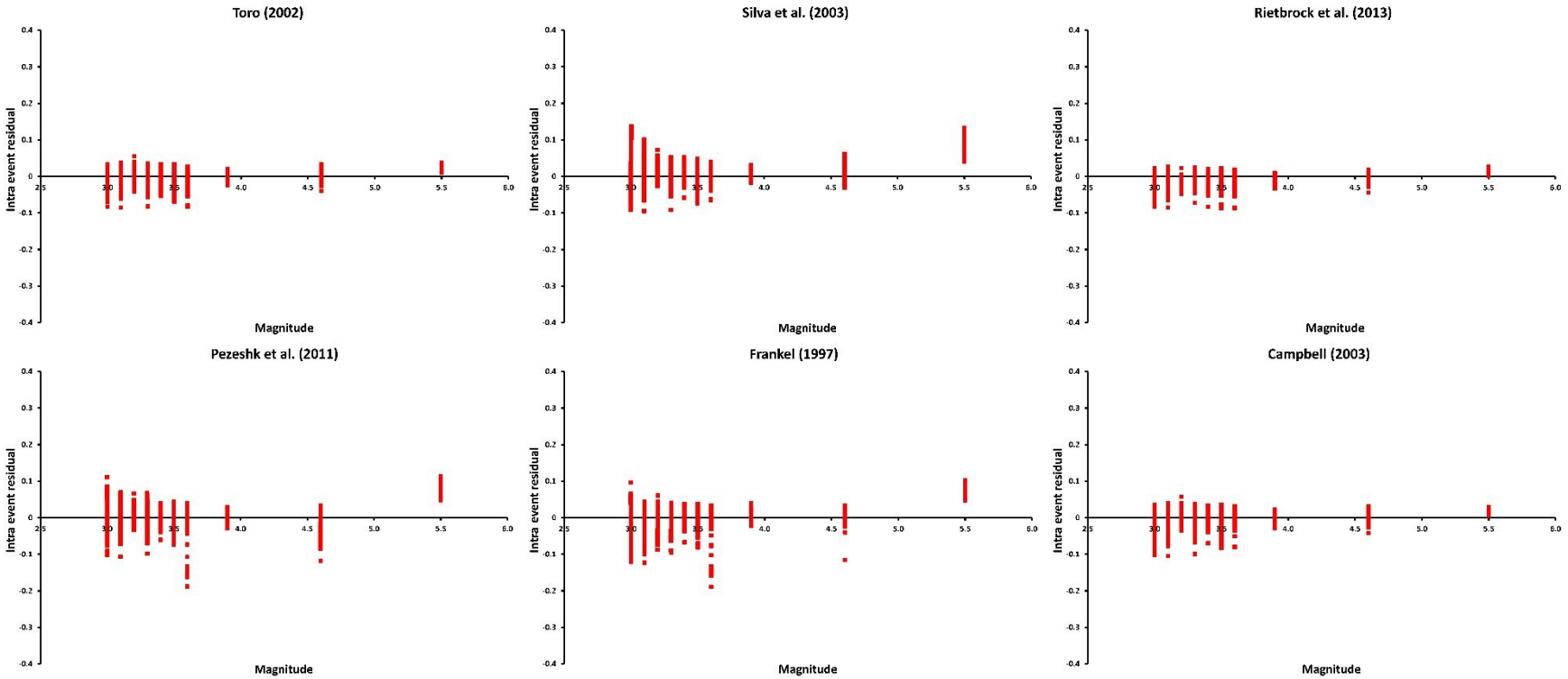


Figure 7-6: Intra-event terms, also referred to as the mean residual, for the 10 GMPEs for PGA.


Toro (2002)
Silva et al. (2003)
Rietbrock et al. (2013)
Pezeshk et al. (2011)
Frankel (1997)
Campbell (2003)
Intra event residual
Magnitude

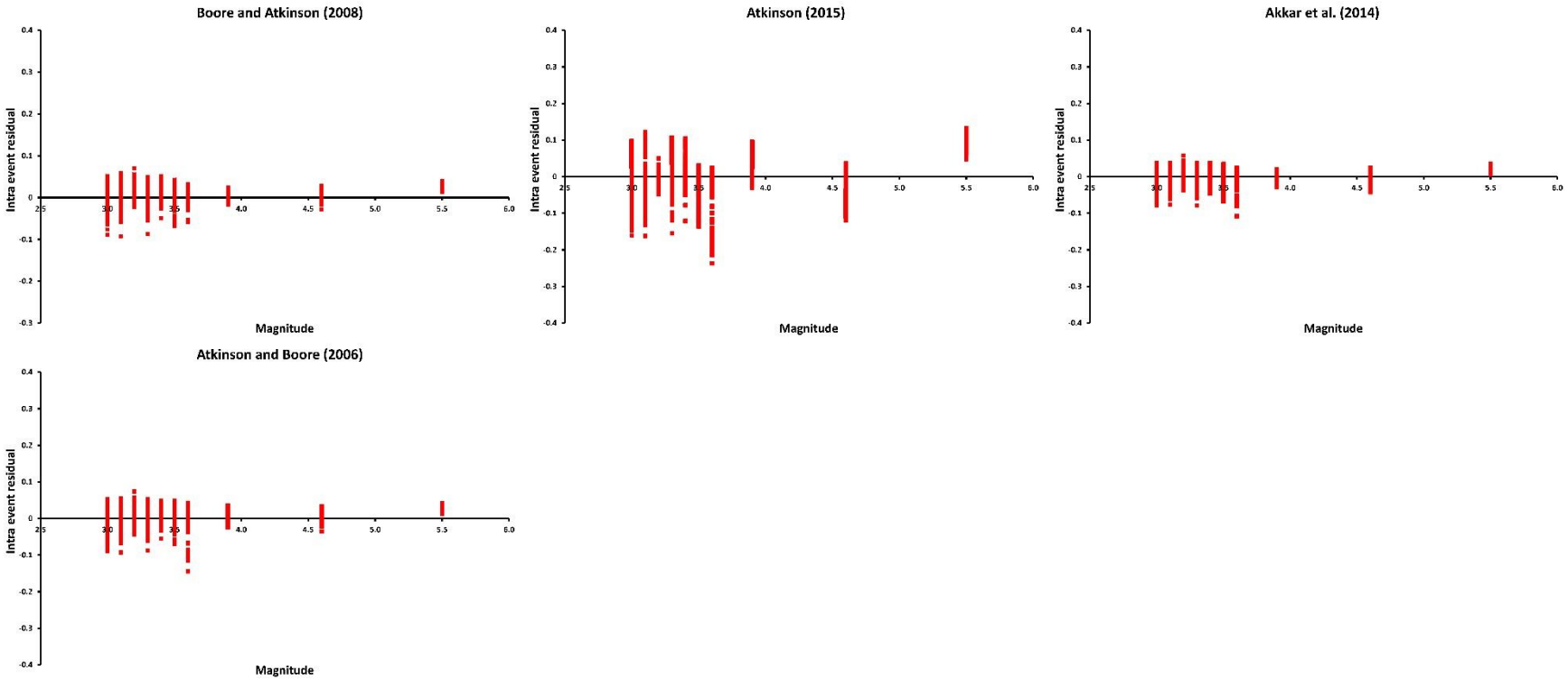
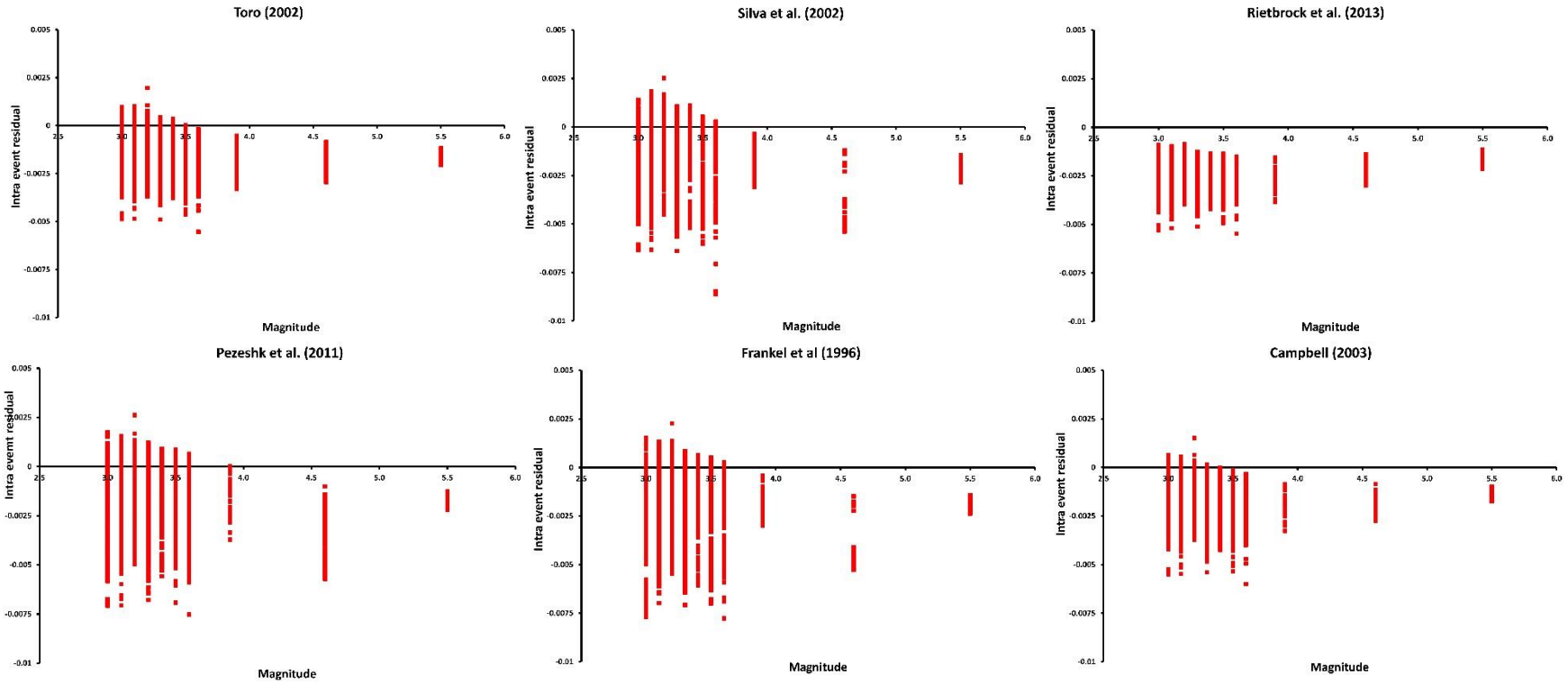


Figure 7-7: Intra-event terms, also referred to as the mean residual, for the 10 GMPEs T=0.15s spectral period.


Toro (2002)
Silva et al. (2002)
Rietbrock et al. (2013)
Pezeshk et al. (2011)
Frankel et al (1996)
Campbell (2003)
Intra event residual
Intra evemt residual
Magnitude
0.005
0.0025
0
-0.0025
-0.005
-0.0075
-0.01
2.5
3.0
3.5
4.0
4.5
5.0
5.5
6.0

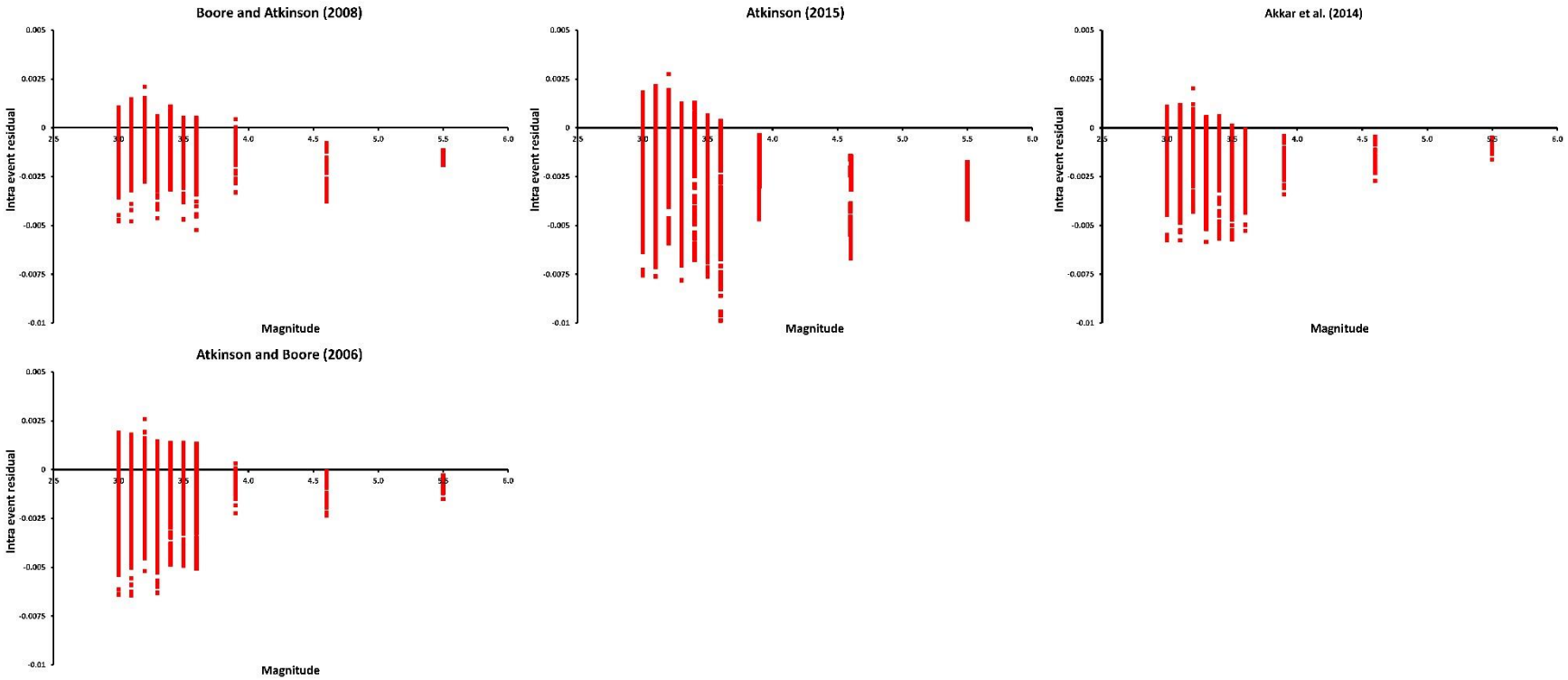


Figure 7-8: Intra-event terms, also referred to as the mean residual, for the 10 GMPEs for T= 2.0s spectral period.

Negative residuals means the GMPEs overestimates while positive means it underestimates. In general all the GMPEs over estimates the ground motion parameters. The use of these GMPEs will result in hazard values that are slightly higher. However, since these are mean hazard values, therefore GMPE selection is one of the critical parameters that is difficult to estimate for our region.

Much of the scatter is at lower magnitudes and larger distances meaning small events recorded at longer hypocentral distances gave large errors. The fact that mining related seismicity attenuates fast with increasing hypocentral distance can also be a contributing factor. The selected GMPEs cover a large spectrum and will represent the uncertainty in the selection of GMPEs for our region.

The large variation of the Atkinson and Boore (2006) model seen above where it appears to underestimate ground motion at short period, but overestimates at long period at all distances. Considering the trends observed the Campbell (2003); Toro et al. (2002); Boore and Atkinson (2008); Akkar et al. (2014); Rietbrock et al., (2013); Atkinson and Boore (2006) models consistently appear to match observed data better than the other GMPEs. Akkar et al (2014) over predicts for all spectral periods. Pezeshk et al., (2011) over predicts for short periods and under predicts for long periods. Variations in residuals might be due to the GMPEs used outside their derived magnitude range since most the events used in this study falls outside the range of applicability of most of the GMPEs. The Atkinson (2015) model for induced seismicity was derived for short distances (less than 40 km) and can only be used for induced seismic sources.

7.5. Comparison of the Orkney earthquake strong-motion data with pre-selected GMPEs

The strike-slip M_W 5.5 Orkney earthquake of 5 August 2014, which occurred in the North West Province, South Africa at about 10:22 GMT was recorded by the SANSN as well as the cluster network in the mining regions. Data from the cluster network stations was used to compare the observed ground motion to the GMPE models. Figure 7-9 compare the predictions of the ten GMPEs selected in this study with the observations from the 2014 Orkney earthquake (Mw = 5.5). Rietbrock et al., (2013) and Akkar et al. (2014) fits the data on all the spectral periods analyzed while the Atkinson (2015) over predicts on all the spectral periods. Due to its short distance of applicability, the Atkinson (2015) model was not used for further analysis. Toro et al. (2002) and Campbell (2003) mainly overestimate for most of the spectral periods whilst

fitting well on others. Silva et al. (2002) and Pezeshk et al. (2011) mainly underestimates although they sometimes overestimates the ground motion. Atkinson and Boore (2006) sometimes overestimates (lower spectral periods <0.1 sec) and sometimes fits well the hazard (high spectral periods > 0.1 sec). Boore and Atkinson (2008) fits well up to spectral periods of 0.5 seconds then it overestimates. For PGA most of the GMPEs overestimates the hazard except for Rietbrock et al. (2013) and Akkar et al. (2014) that fits well to the data, while the Pezeshk et al. (2011) predicts lower values. For 0.05 seconds, Rietbrock et al. (2013), Akkar et al. (2013), Boore and Atkinson (2008) fits the data while rest of the GMPEs over predicts.

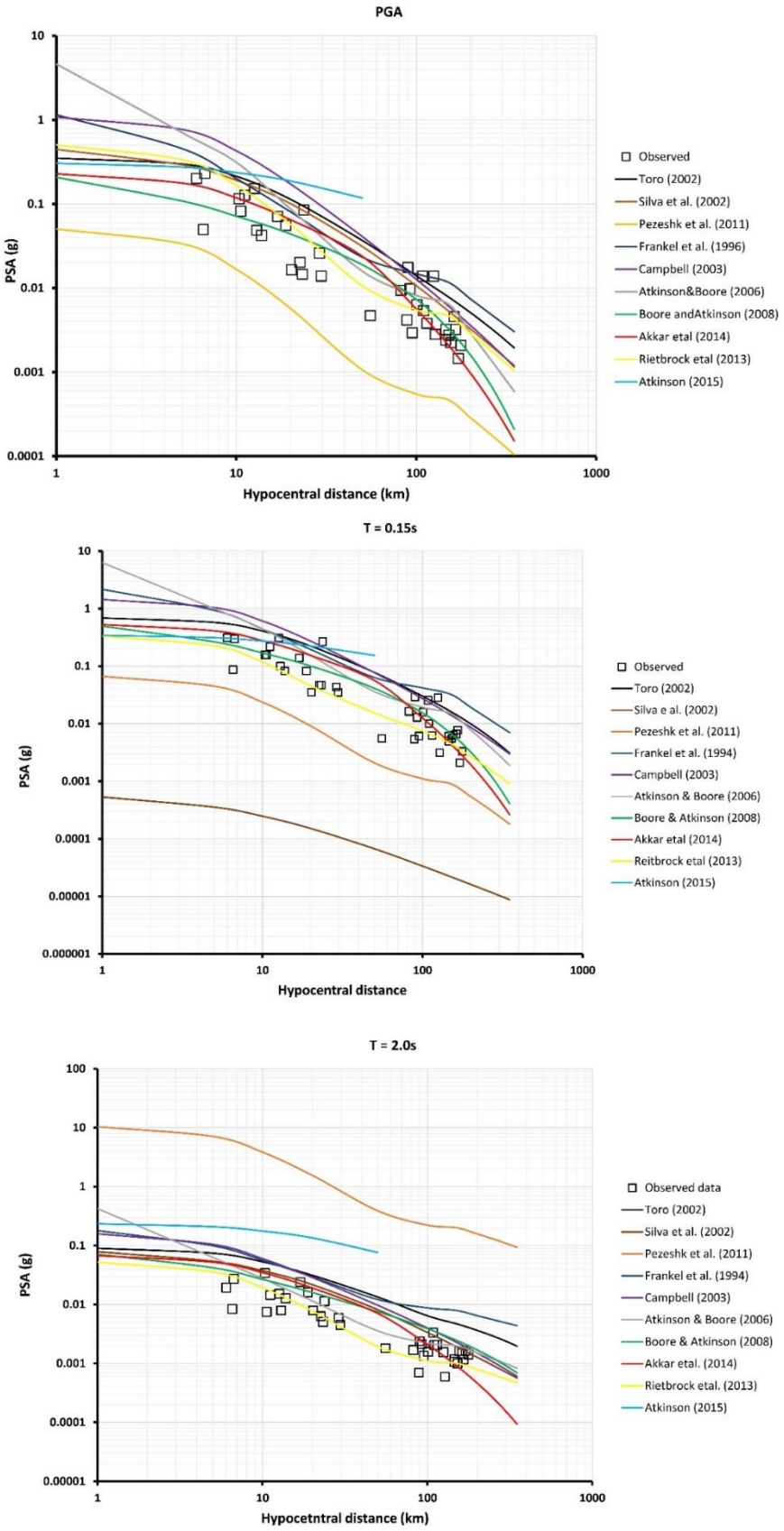


Figure 7-9. Comparison between the spectral accelerations at three spectral periods recorded during the 2014 Orkney earthquake of magnitude *Mw* = 5.5 and the predictions obtained with ten preselected GMPEs.

It is apparent from these results, that the shape of attenuation curves of only one model cannot capture the real behaviour of the data. Therefore, six GMPEs were selected to cover the lower (Toro et al., 2002; Boore and Atkinson, 2008), median (Akkar et al., 2014; Rietbrock et al., 2013) and upper range (Campbell, 2003; Atkinson and Boore 2006) of the ground motion in order to capture the uncertainty associated with GMPE selection. These six GMPEs were then used for sensitivity analysis.

7.6. Conclusions

Due to the complexity of the seismotectonic setting around the study area, GMPEs from different tectonic regimes were selected for use in seismic hazard analysis. Ten GMPEs were compared with local dataset to select a suit of GMPEs that represents well our local data. Of these, six (Boore and Atkinson, 2008; Campbell, 2003; Akkar et al., 2014; Toro et al., 2002; Rietbrock et al., 2013 and Atkinson and Boore, 2006) were selected to represent the epistemic uncertainty in the selection process. The selected GMPEs have shown to compute ground motion values which are within the uncertainty range of our local data. Sensitivity analysis will also be performed to assess the influence of the GMPE selection process to the final hazard. GMPEs from induced seismicity could not be used because they did not satisfy the selection criteria as defined by Bommer et al., (2010). Most of these were only developed for PGA only without other spectral periods. The Atkinson (2015) equation was not used because it is valid for small magnitude ranges while seismic hazard analysis is corncerned with events of moderate to large magnitudes that can generate hround motions capable of affecting building structures. The comparisons show that when the attenuation models are based on a well assembled database and they are used within their range of validity they can correctly predict the ground motion parameters, in particular for short and intermediate structural periods.

CHAPTER 8: SENSITIVITY ANALYSIS OF SEISMIC HAZARD OF JOHANNESBURG

8.1. Introduction

In seismic hazard analysis, uncertainties associated with different models and parameters are usually implemented in the analysis using logic trees, which may include a large number of branches. Probabilistic Seismic Hazard Analysis is computationally intense. A typical application running on a Windows core i7 with 64GB RAM on a 64-bit processor may take three days to run just one branch of the logic tree. However, some of the branches may have little impact on the calculated seismic hazard. Therefore, it is desirable to 'prune' them. Branches with little significance are identified by a sensitivity analysis (SA), which is a method that quantifies the impact of the parameters and models on the hazard calculation. This type of analysis can identify critical inputs, provide insight to model behaviour, and help understand underlying mechanisms (Crowley et al., 2005; Barani et al., 2007; Rohmer et al., 2014; Kowsari et al., 2017). Thus it is important to perform a SA at the early stage of a PSHA, where essential modelling decisions have to be made in order to identify the contribution of each input to the seismic hazard.

The Senior Seismic Hazard Advisory Committee (SSHAC) report (Budnitz et al., 1997a; b) emphasised that SA for PSHA is crucial, both during the modelling process (for preliminary hazard calculations) and for understanding the final hazard results that are obtained. In other words, SA provides knowledge on how the uncertainty in the output can be allocated to different sources of uncertainty in the model input parameters (Cramer et al., 1996; Budnitz et al., 1997a; b; Saltelli et al., 2000; Giner et al., 2002). SA results are useful to determine which parameters contribute the most to the hazard and its uncertainty and can be used as a preliminary step for the construction of final logic trees consisting of those parameters found to be most sensitive. This also allows analysts to decide which parameters require more attention during the analysis.

The purpose of SA is to identify the parameters that have the largest effect on the seismic hazard assessment for Johannesburg. SA was performed by analysing one parameter at a time to assess its influence on the total hazard, as suggested and implemented by many other authors (e.g. Atkinson and Charlwood, 1983; Grünthal and Wahlström, 2001; Tavakoli, 2002; Beauval and Scotti, 2004). This approach assumes that these parameters are independent.

Parameters that contribute to the uncertainty in the output for seismic hazard analysis can be classified into two groups, namely, global and local variables. Global variables are those that have similar influence on all the seismic sources (all area sources, as well as any fault sources), while local variables only affect individual sources. In other words, varying global variables will affect the entire hazard analysis, while local parameter is only limited to specific sources. Although they only affect local sources, local parameters can have large impact on the final hazard and therefore need to be carefully assessed (e.g. Cramer, 2002; Wiemer et al., 2009; Bommer et al., 2015a). Thus for the SA in this study, global variables were assessed using the entire seismic source model, while local variables were assessed for each and every source.

8.2. Sensitivity analysis method

Extensive SA was performed in order to assess the role and impact of declustering, temporal stationarity of the catalogue, method of computing reccurence parameters, magnitude homogenisation, bedrock velocity, seismic source modelling, activity rate, *b*-value, M_{min}, M_{max}, and the selection of GMPEs. The sensitivity of the output to variations in the input parameters is quantified using the Coefficient of Variation (COV), where COV is a measure of relative variability, and is related to both the standard deviation (σ) and the mean (μ) through the relation by Cramer (2001a; 2001b; 2002).

$$\mathbf{COV} = \frac{\boldsymbol{\sigma}}{\boldsymbol{\mu}} \qquad 8\text{-}1$$

COV is a standardized, unitless measure that allows you to compare variability between dissimilar groups and characteristics. A small COV value indicates that variation in the related parameter does not show large variation in output, while a large COV indicates that the output is very sensitive to variations in the parameter under investigation (Gomez and Gomez, 1984; Cramer, 2002; Campbell et al., 2010). The advantage of using the COV is that it can relate across different variables as they are measured on the same relative scale. COV is computed by allowing one parameter to vary while the other parameters are fixed to mean values. This will allow the COV to vary about the mean ground motion hazard while helping in identifying parameters have the greatest impact on the results (Cramer et al., 1996).

The bedrock ground motion was computed at sites distributed evenly in the Municipality of Johannesburg. OPENQUAKE software developed by the Global Earthquake Model (GEM)

team was implemented to compute the hazard. The seismic hazard was computed as spectral acceleration values (PGA, PSA = 0.15s and 2.0s) for a 475 year return period. The computations were made for 217 points distributed on a grid at approximately 3.5 km intervals. This essentially defines the spatial resolution of the maps. For each parameter or model considered in the sensitivity analysis, the hazard was computed at each grid site. The hazard values calculated for each parameter were then used to compute the mean and standard deviation at each point on the grid, which were then used to compute the COV using equation 8-1. COV values were determined for the three spectral periods to observe impact of each parameter at these periods. The contour maps were generated using a regularised spline technique based on twelve-point samples. This was chosen to avoid smoothing away peaks in the hazard. Variation in COV reflects the influence of the input parameter to the final hazard. In seismic hazard analysis, a COV of about 0.1 (10%) is considered the threshold of significance, depending on the actual level of ground motion (Cramer et al., 1996; Cramer 2002). Parameters that have large COV values (> 0.1) imply that a change in the input produces large variations in the output, which means that changes to the parameter may influence the hazard results significantly, and therefore needs to be carefully determined.

A baseline hazard was computed using the mean values for the different parameters under study to test the results of our sensitivity analysis (Figure 8-1). GMPEs by Akkar et al. (2014) and Boore and Atkinson (2008) were implemented in the baseline study since these were used in the PSHA study for South Africa (Midzi et al., 2020b). For all the seismic source zones developed in this study, recurrence parameters determined from the full catalogue declustered using the Gardner and Knoppoff (1975) method and computed using the SEISAN method were used to compute the baseline study. Seismic hazard values shows that for most of Johannesburg Metropolitan, the hazard is low (less than 0.15 g for PGA, less than 0.30g for PSA = 0.15 and less than 0.02 for PSA = 2.0s), the only exceptions being the Johannesburg CBD and southwestern areas around Soweto where acceleration values are high. These high hazard values to the western side is attributed to the strong influence of the KOSH and WRAND seismic source zones, which have high activity rates compared to the other nearby sources as was also observed in Midzi et al. (2020b). Identification of areas with high ground motion helps in deciding the level of PSHA results shows that major roads in and around Johannesburg will experience low to moderate ground motion compared to the residential suburbs of Soweto. The hazard computations in this study can be taken as inputs to microzonation and building codes formulation. These critical studies can assist both the structural engineers and town

planners in deciding which areas to built different types of structures. The difference in the hazard values for the three spectral periods defines the hazard curve at each site. It is generally expected by the nature of the response curve to have hazard values high for shorter periods like PSA = 0.15s as compared to PGA and PSA = 2.0s.

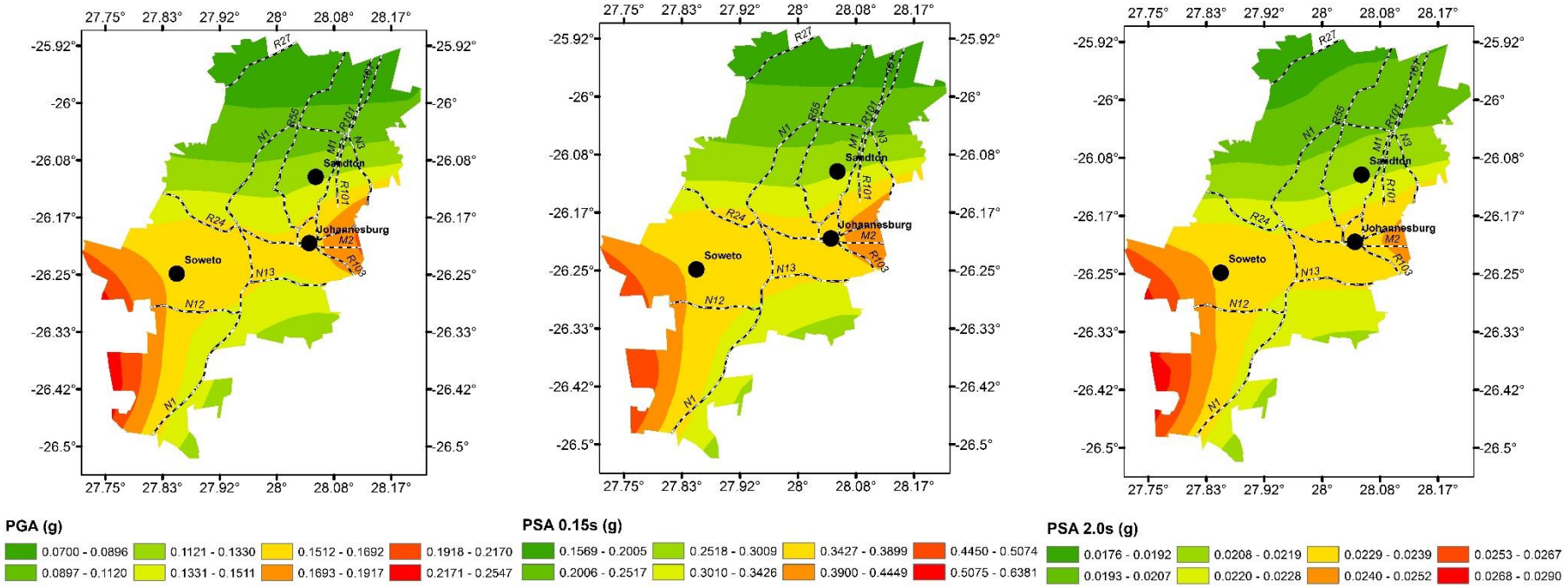


Figure 8-1: Mean 10% probability of exceedance in 50 year seismic hazard maps for Johannesburg computed for the three spectral periods PGA, PSA = 0.15s and PSA = 2.0s.

8.3. Sensitivity analysis related to global variables

Global variables affect more than one seismic source, hence their impact cannot be assessed on a single source. The main global variables in this study are the GMPEs, the earthquake catalogue and the seismotectonic model of the area. A critical issue to be addressed before any scientific analysis is to assess the quality, consistency and homogeneity of the seismic catalogue to be used for hazard analysis. Although the geology surrounding the study area is known and some of the faults are known, very little information exists on the seismogenic nature of the faults (Manzunzu et al., 2019). In this regard, seismic source zones are delineated according to areal zones related to seismicity distribution (see Chapter 5). Consequently, an effort was made to assess the impact of the processes that were followed in the preparation of an earthquake catalogue used in the seismic hazard analysis for Johannesburg. Generally where mean hazard is high we can expect low COV values however if the standard deviation is also high the the OCV becomes high. This would mean the the variation in the output hazard have large scatter for a given parameter being considered. For most global parameters, high COV values were observed in areas where the mean hazard was low for PSA = 0.15s while for PGA and PSA=2.0s low COV values were in high mean hazard regions.

8.3.1. Earthquake Catalogue Magnitude homogenisation process

The process of homogenising the earthquake catalogue for South Africa is complicated because several local magnitude relations have been used in computing magnitude values over the years (see section 4.7.1.1). In trying to homogenise the catalogue earthquake magnitude into M_W, most of the PSHA studies carried out in South Africa assumed that all the M_L relations previously used in South Africa are equivalent. Therefore, a single M_L-M_W relation adopted from global relations was used (e.g. Kijko et al., 2003; Bommer et al., 2015a; Midzi et al., 2020b). However, it was noted that there are significant differences in the three M_L relations that have been used in South Africa over the years (Manzunzu et al., 2020). Hence, in this study, we derived three different M_L-M_W relations to homogenise our catalogue as described in Chapter 4. The three relations were derived using seismic events for which both M_W and M_L were computed and each relation is only valid during its time of use in the SANSN (Manzunzu et al., 2020).

In this investigation, we test if the selection of conversion relations has an impact on the seismic hazard results. To assess uncertainty in the process of homogenisation, two catalogues were produced. One catalogue was produced after magnitude homogenisation using the three determined relations.

The second catalogue was created by assuming that $M_L \approx M_W$ as suggested by Deichmann (2006). This assumption was applied in several studies in South Africa (e.g. Kijko et al., 2003; Mulabisana, 2016; Midzi et al., 2020b).

It was observed that the process of homogenisation produced catalogues that have significantly different Gutenberg- Richter frequency-magntidue relationships (Figure 8-2). These would certainly result in different recurrence parameters and perhaps M_{max} values, which could influence the hazard process. Hazard computations were performed using the recurrence parameters from the two catalogues. The results were used in computing the mean and standard deviation that was then used for calculating the COV.

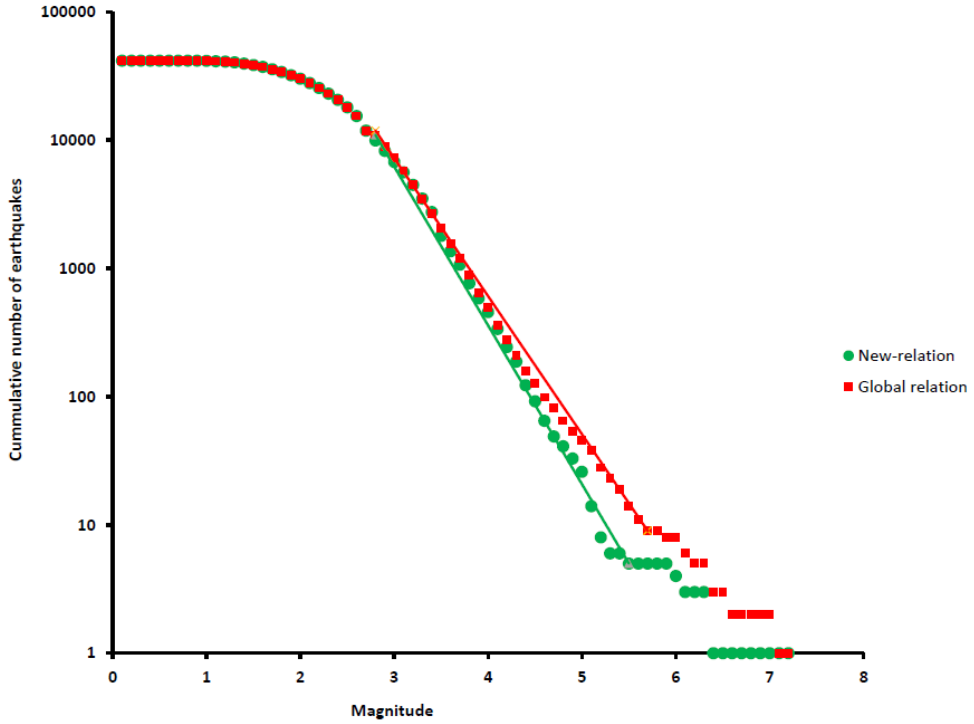


Figure 8-2: G-R curves for the two catalogues used for sensitivity analysis for the homogenisation process. New relation refers to the homogenisation relations developed by Manzunzu et al. (2020) as applied while Global relation refers to the Deichmann (2006) magnitude homogenisation relation.

For each catalogue, recurrence parameters and M_{max} were determined for all zones using the two catalogues. Variation in the hazard results was then compared using COV. The results show that the homogenisation process is a critical aspect of preparing the earthquake catalogue and should be handled carefully and properly as done in Chapter 4 of this study. COV values from the sensitivity analysis shows significant variation in hazard at all spectral periods, but with higher values at 0.15s and 2.0s (Figure 8-3). The values are significantly higher than the threshold of 0.1 with values as high as 0.21 for PGA; while PSA 0.15 and 2.0s have values of 0.92 and 0.32, respectively. COV values vary at each site and at the different spectral periods. For PGA and PSA= 2.0s, high COV are observed in the north and they decrease going to the south, while for PSA = 0.15s high COV values are in the

western side. Relatively higher COV values were observed for PSA = 0.15s spectral period at all sites, therefore the homogenisation process is more sensitive for PSA = 0.15s at all sites. This means this parameter is more sensitive for PSA = 0.15s than for PGA and PSA = 2.0s. COV values for PGA are low at most sites except to the far north of Sandton. In areas where the hazard is high (see Figure 8-1) the COV is low for PGA. For PSA = 0.15s, distinctly high COV values are observed in the western parts of Soweto. Since the hazard is already higih in this area, it implies that the standard deviation is also high meaning there is larger variations in the output hazard values from the different input values. For PSA = 2.0s, the southwestern parts of the study area have the lowest COV values while the northern and central parts have high values.

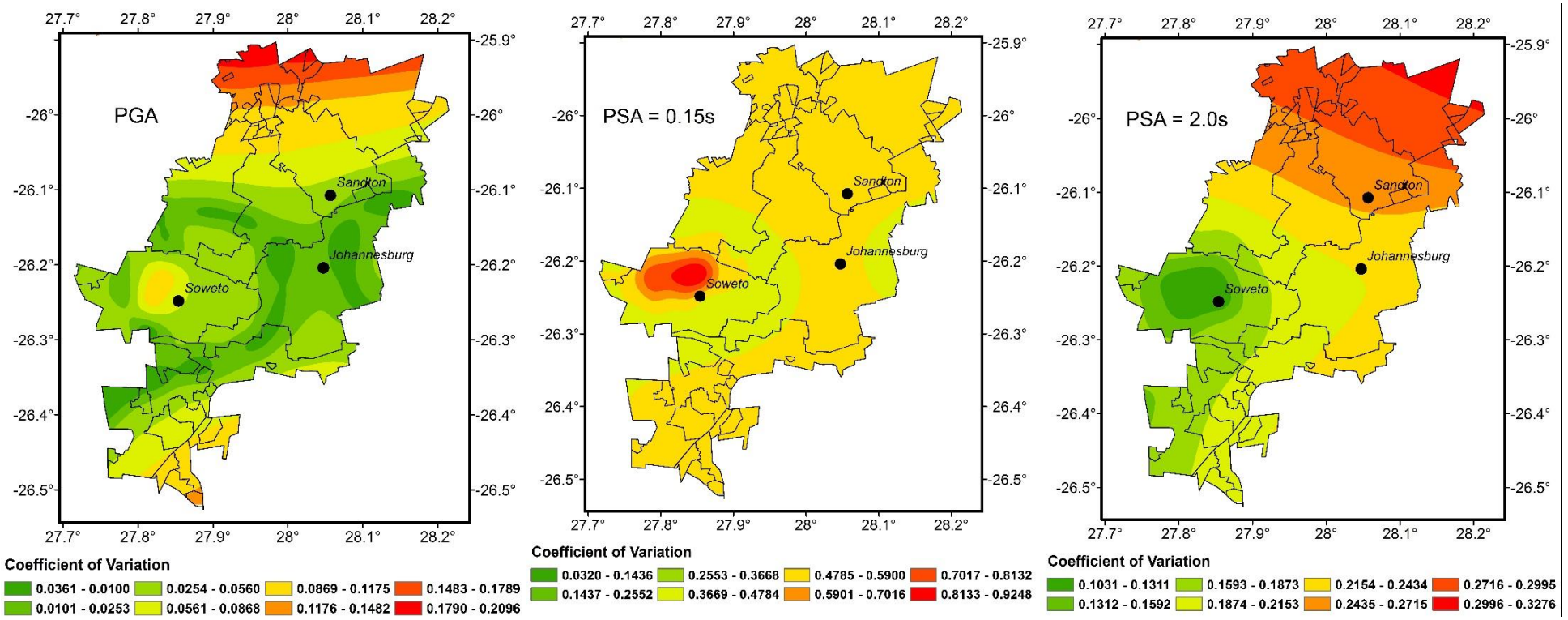


Figure 8-3: COV results for earthquake magnitude homogenisation process.

8.3.2. Temporal stationarity of the catalogue

There is significant temporal variations in the catalogue for Johannesburg. Three distinct periods can be identified, which have potential to influence our seismic hazard parameters. The period before 1970 is characterised by seismicity mainly determined from macroseismic information with a few large events recorded by early instruments. This period has a high value for the magnitude of completeness and very few events (see section 4.12.3). It is also associated with high uncertainties in location and magnitude values. The period between 1970 and 2010 has instrumentally- recorded seismicity by the SANSN (see section 4.6.3). Location errors reduced with time as monitoring improved with more stations added in the analysis of seismic data. The period after 2010 has seen the installation of cluster networks in the mining region as well as a marked increase in the number of seismic stations for the national network. With these improvements, earthquake location has significantly improved and more small magnitude earthquakes have been recorded.

For recurrence rate calculation, it was observed that the pre-instrumental catalogue (pre 1970) had few events with large uncertainties and hence would probably influence recurrence rates. However, these pre-instrumental events are necessary in M_{max} computation as they help increase the catalogue length (i.e. longer time covered). The longer the catalogue, the more accurate the M_{max} (Kijko, 2004) and the more information available to help understand the history of seismicity in the region covered. The potential for a change in seismicity rate at about 1970 was explicitly incorporated as an alternative conceptual model in the recurrence parameter estimates.

Although there are marked changes in the recorded seismicity around 2010 due to the improved recording of seismicity in the mining regions (see section 4.2.2), these changes are mostly for small magnitude earthquakes, which rarely affect our seismic hazard parameters. Therefore, the catalogue between 2010 and 2016 poorly represents the long-term recurrence rates needed for hazard computation and was not considered as a source of uncertainty in this study. It was, however, merged with the 1970 to 2010 catalogue for recurrence parameter computation. The second alternative catalogue was based on events from the entire investigation period, including pre-1970 events. Results show slight changes in the Gutenberg-Richter plot showing the significance of the temporal variation in the seismic catalogue that were then used to estimate recurrence parameters and M_{max} values for each source (Figure 8-4). The G-R plot show how the two catalogues vary and would affect in the computation of recurrence parameters.

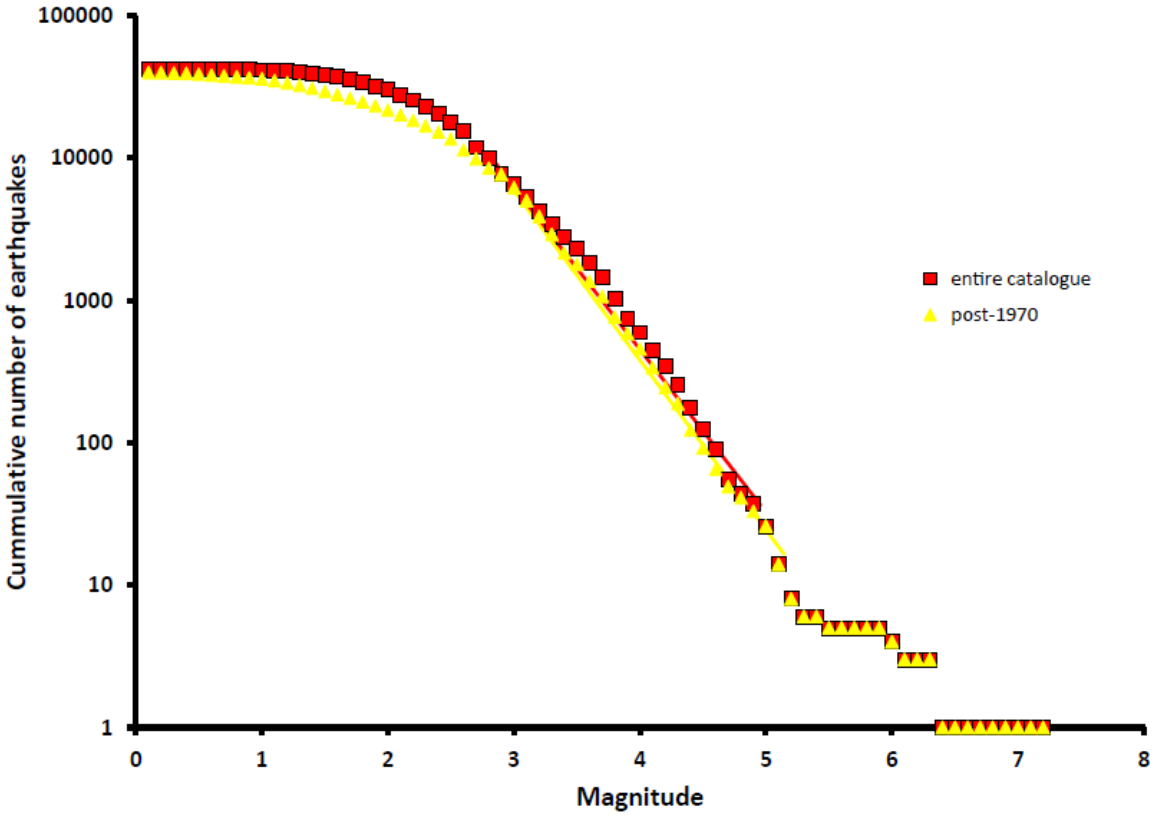


Figure 8-4: G-R curves for the two catalogues used in the assessment of the temporal stationarity of the catalogue. The entire catalogue starts from 1620 to 2016 while the post 1970 catalgogue is from 1970 to 2016.

The two sets of parameters were used in hazard calculation to produce the COV maps shown in Figure 8-5. COV values from the sensitivity analysis shows significant variation in values at all spectral periods (Figure 8-5). Because the full catalogue truly represents the long term seismicity of the region, especially for moderate magnitude events the effects of temporal variation are more pronounced in longer spectral periods (in PSA = 2.0s). COV values are high on almost all sites for PSA = 2.0s although the other spectral periods also show significantly high COV values.The values are significantly higher than our threshold of 0.1 with values as high as 0.36 for PGA and PSA = 0.15s while for PSA = 2.0s the highest value is around 0.32. High COV values are observed on the western side in Soweto for PSA = 2.0s and they decrease going eastwards. For PGA and PSA=0.15s, low COV values were obtained in areas where the mean hazard was high in the western side. These high COV values indicate the strong significance of the temporal variations in the catalogue, while the Johannesburg CBD has high COV. The results indicate the importance of historical seismicity in seismic hazard analysis. Improvements in both the location and number of events in the pre-1970 period (e.g. Manzunzu et al., In press.) is therefore of importance for our hazard computation.

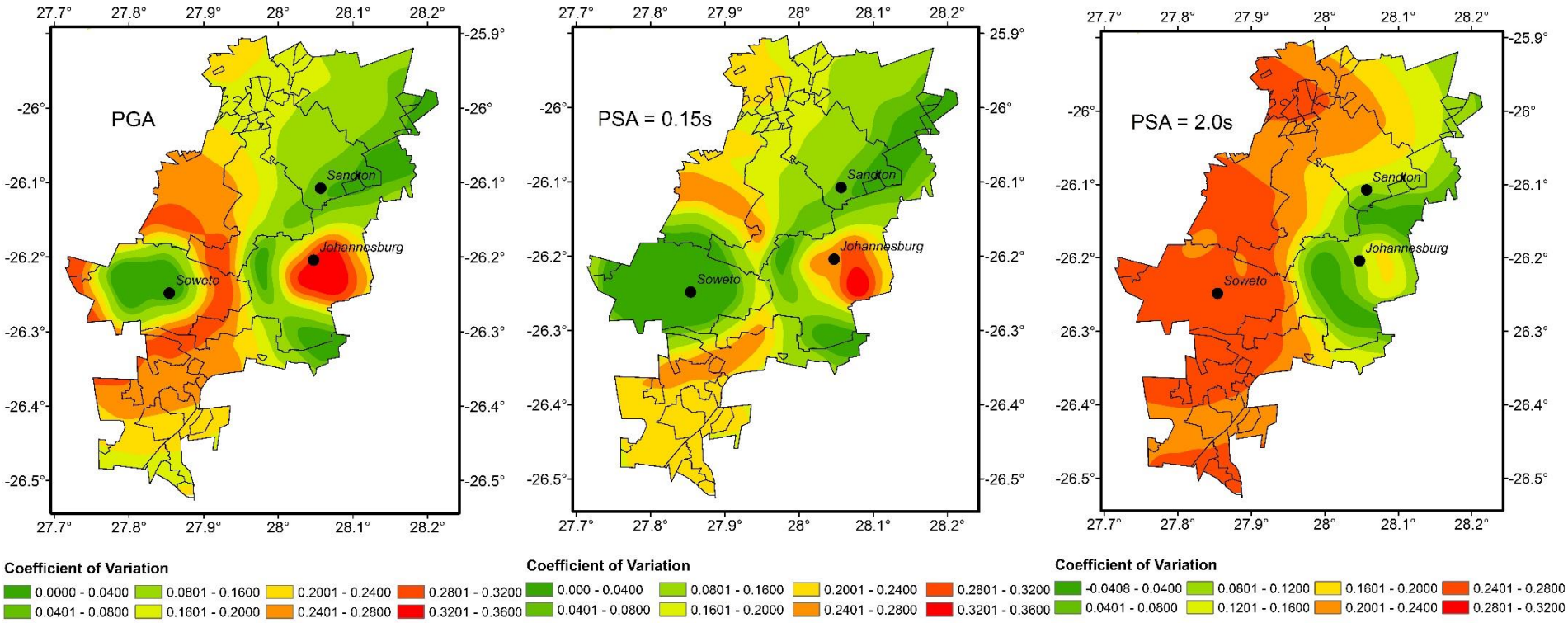


Figure 8-5: COV results for length of catalogue (full catalogue and post 1970 catalogue).

8.3.3. Declustering process

This branch expresses the uncertainty of different declustering approaches. Declustering is necessary, because the assumption of a stationary Poissonian process made in the subsequent hazard computations is not fulfilled if the catalogue contains dependent events. No unique and generally accepted approach to declustering exists and to express the epistemic uncertainty of alternative approaches, the three catalogues which were accepted by the statistical test were applied (see Chapter 4). The three declustering techniques used were Gardner and Knoppoff (1974), Gruenthal (1985) and CLUSTER as implemented in SEISAN. The G-R relation was used for the analysis (Figure 8-6). Catalogues obtained using the Gruenthal et al. (1985) and the Gadner and Knoppoff (1974) techniques were similar thus the G-R relation are very similar while the SEISAN catalogue had slightly more events (Figure 8-6).

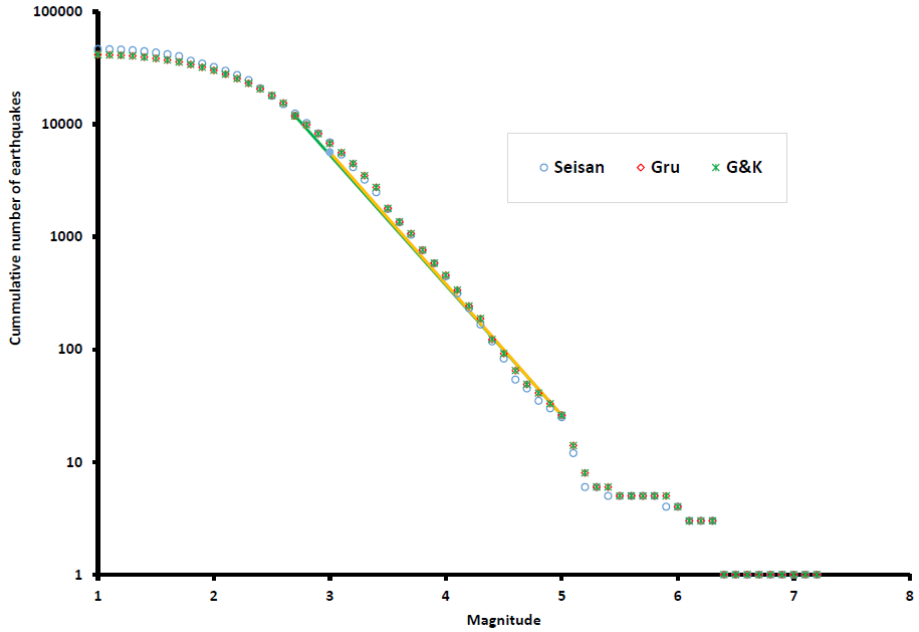


Figure 8-6: The G-R distribution for the three declustered catalogues used for sensitivity analysis. Seisan is from the CLUSTER program in SEISAN, Gru is the catalogue declustered with the Grunthal (1985) and G&K is from the Gardner and Knoppoff (1975) catalogue.

The sensitivity feedback demonstrated that the effect of the declustering on the final earthquake rate forecast is insignificant (Figure 8-7). Seismic hazard results showed slight variation in the hazard across the three methods. This is mainly because the declustering methods used were carefully selected taking into account their ability to meet the Poissonian distribution. Thus the significant COV variations are seen for PGA and PSA = 2.0s spectral periods. The values are slightly higher than our threshold of 0.1 with PGA values as high as 0.18 for PGA and PSA = 0.15, while PSA = 2.0s has values of 0.20. Distribution of COV values for PGA is increasing from the east going towards the

west side of the study area. PSA = 2.0s has similar distribution but with slightly larger values than for PGA. COV values for PSA = 0.15s show a significantly different distribution, with low COV values on the western side, increasing towards the east. This means declustering needs to be considered carefully as well, especially where spectral hazard maps are going to be produced (Figure 8-7). Although the catalogues assessed in this section all met the Poissonian criteria (see section 4.11), they show significant variation in the output hazard as depicted by high COV values at all spectral periods, implying there is need to carefully select the declustering algorithm to use in the region.

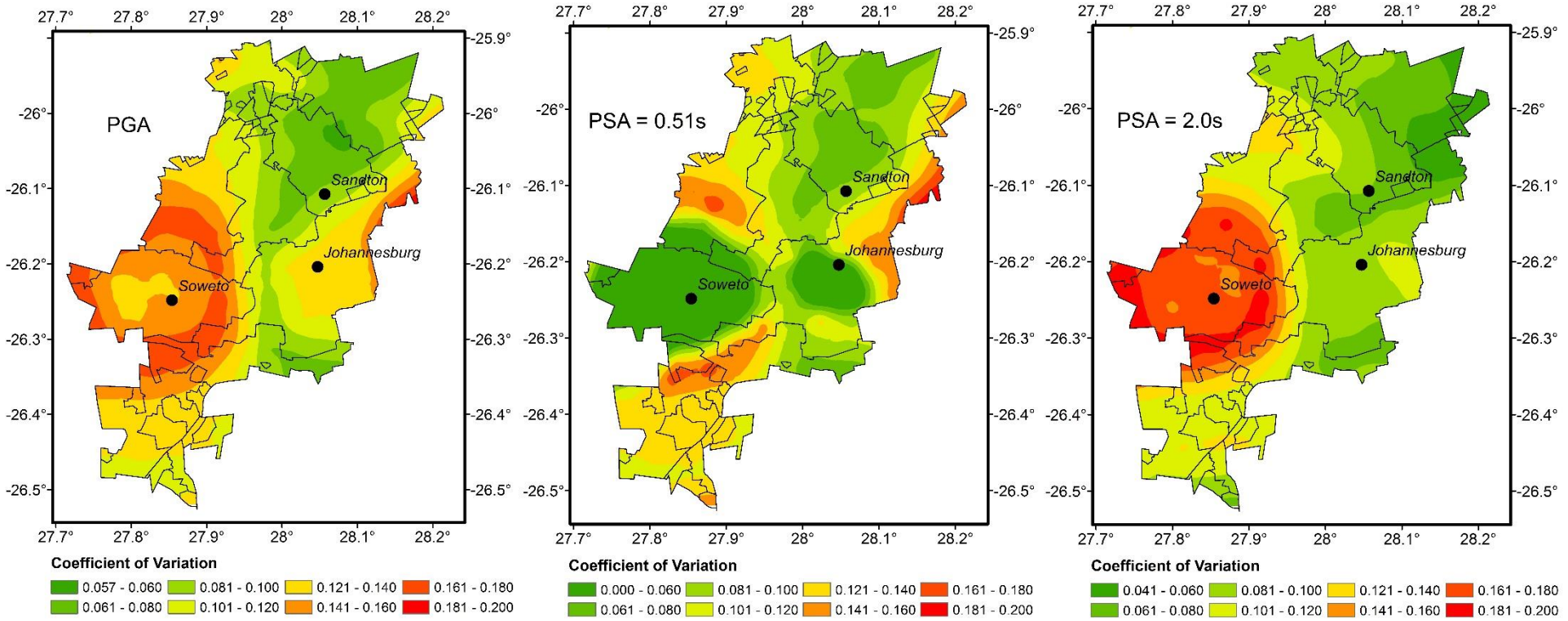


Figure 8-7: COV results for the sensitivity analysis for declustering for the three spectral periods analysed.

8.3.4. Method of computing recurrence parameters

Recurrence parameter estimation is one of the main sources of uncertainty in PSHA. In low seismicity regions, seismic events recorded especially historically are very few rendering the catalogue length to be short resulting in the computations of recurrence parameters having large uncertainties. The three methods (SEISAN, Kijko and ZMAP) used to compute recurrence parameters were compared. The three methods represents different models of computing reccurence parameters. For each method, recurrence parameters were computed (see section 6.2 and section 6.3) and were used to compute the hazard. COV values were computed from the hazard results. Sensitivity results show high COV values of 0.3 (Figure 8-8) indicating that selection of the right method is a significant part of the process and should be carefully done and/or taken into consideration in the hazard computation. Spatial distribution of COV is different for the three spectral periods however the values are generally high showing significant influence to the hazard computation. High COV values are observed in the western side which decreases going to the east for PGA and PSA=2.0s spectral periods while for PSA=0.15s low COV values are in the west. In Johannesburg CBD, high values are observed for PGA and PSA = 0.15s while PSA = 2.0s have low COV values (less than 0.1).

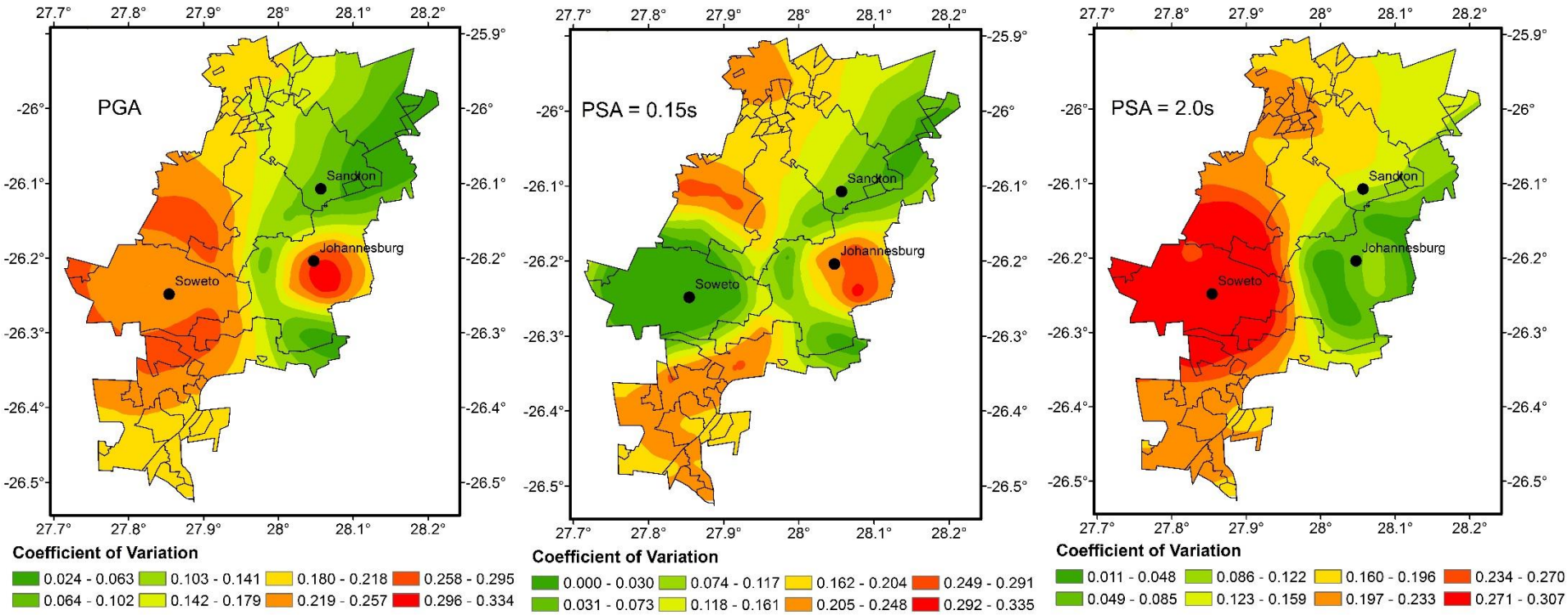


Figure 8-8: COV results for the sensitivity analysis for methods of computing recurrence parameters.

8.3.5. Assessment of seismic source models

Investigations carried out and presented in this section considered the possible influence of seismic source zonation on the total seismic hazard results of Johannesburg. The seismic source model developed for this study (see section 5.7 and Figure 5-12) was compared to previously developed models by du Plessis (1995), Partridge (1995) and Hartnady (1996). The four source models represent the uncertainty in seismic source modelling. Recurrence parameters for each model were computed using the catalogue of earthquakes discussed in Chapter 4 obtained using the homogenised process developed in this study and declustered using the Gardner and Knoppoff (1974) technique. The recurrence parameters for the different source models are shown in Table 8-1, Table 8-2, Table 8-3 and Table 8-4. Source zones from the mining regions (CRAND, ERAND, WRAND, KOSH, WELKOM) were added to all the models because the models by du Plessis (1995), Partridge (1995) and Hartnady (1996) were mainly concerned with tectonic seismicity.

Table 8-1: Recurrence parameters for the sources in the du Plessis (1995) model.

Zone	***b* value**	***a* value**	**M_{obs}**	**M_{max} (Kijko, 2004)**
LESOTHO	0.93	3.31	5.3	5.5
ERAND	1.48	5.72	4.8	5.37
CRAND	1.47	4.9	4	5.99
KOFFIEFONTEIN	0.78	2.81	6.2	6.94
KOSH	1.21	5.2	5.5	5.83
GROOTVLOER	1.49	4.65	4.9	6.84
MPUMALANGA	0.65	1.97	4.8	6.91
KARROO	1.45	3.82	5.1	5.44
WELKOM	1.29	5.31	5.2	5.28
WRAND	1.42	6.2	4.9	4.85
MATATIELE	1.29	4.25	6.2	6.73
LEPHEPE	0.88	2.76	6.5	6.94
CENTRAL SOUTH AFRICA	1.1	3.77	5.5	6.2

Table 8-2: Recurrence parameters for the sources determined by Hartnady (1996).

Zone	***b* value**	***a* value**	**M_{obs}**	**M_{max} (Kijko, 2004)**
CEDAR/LWANDE/KOFFIE	1.06	3.64	6.2	6.8
ERAND	1.27	4.15	4.9	5.3
CRAND	1.3	4.04	4.1	4.43
KOSH	1.4	6.34	5.5	6.01
MPUMALANGA	0.65	1.97	4.8	6.91

WELKOM	1.31	4.79	5.2	5.28
WRAND	1.32	5.64	4.9	6.34
TRANSGARIEP	1.99	7.41	6.5	6.74
KWAHLAMBA	0.85	3.31	6.2	7.1
MOZAMBIQUE	0.97	4.68	7.2	7.82

Table 8-3: Recurrence parameters for the sources determined by Partridge (1995).

Zone	***b* value**	***a* value**	**M_{obs}**	**M_{max} (Kijko, 2004)**
ERAND	1.45	5.47	4.9	5.3
CRAND	1.54	5.14	4.1	4.23
CEDAR/KOFFIE/OOKIE	0.84	3.01	6.2	6.94
KOSH	1.23	5.42	5.5	5.24
LIMPOPO	0.62	1.34	5.0	6.84
MPUMALANGA	0.79	2.56	4.8	6.91
BUSHVELD	0.87	1.92	4.2	4.77
WELKOM	1.29	5.22	5.2	5.28
WRAND	1.65	6.93	4.9	4.64
NORTHENR CAPE	1.35	4.52	5.5	5.9

Table 8-4: Recurrence parameters for the sources determined in this study.

Zone	***b*-value**	***a*-value**	**M_{max}**
CRAND	1.62	5	5.5
ERAND	1.34	4.85	5.2
FWRAND	1.27	4.68	5.5
KOSH	1.29	5.38	6
KVAAL	1.34	4.41	5.3
MOZA	0.85	3.6	7.7
WRAND	1.38	4.42	5.2
CEDAR	0.93	3.22	5.5
KHEIS	1.39	3.36	5.1
KOFFIE	0.77	2.53	6.1
LESOTHO	0.84	2.23	6.1
LIMPOPO	0.76	1.9	6.1
MDSN	0.95	3.16	6.1
MOZCHAN	0.76	2.4	6.1
NWEST	1.11	2.95	6.1
TUGELA	0.82	2.14	5.2
WBOTS	1.03	2.68	6.3
WELKOM	1.25	3.92	6.1
ZEBED	0.97	2.8	6.1
ZOET	0.83	2.59	6

Seismic hazard analysis was computed using the recurrence parameters in the tables above for the different source models. Sensitivity analysis of the four models was performed to understand their effects on the hazard of Johannesburg. Variations in source zone delineation shows significant variation in the hazard output as indicated by the high COV results (up to 1.0) for all the spectral periods considered (Figure 8-9). High COV values might imply large standard deviation values which is a direct iindication of large variations in the hazard. Although there are high COV values observed for variation in source models, the general trends of COV is increasing from the east to the west for all spectral periods. In the eastern parts of Johannesburg central, low COV values are observed although moderate ground motion, values were observed in Figure 8-1. Delineation of seismic source zones is a multidisplinary study that needs to be performed thoroughly in order to have credible hazard results. New information that adds value, have to be sought and incorporated for the identification and delineation of seismic sources. The latest model developed in this study (Chapter 5) is used in further analysis going forward.

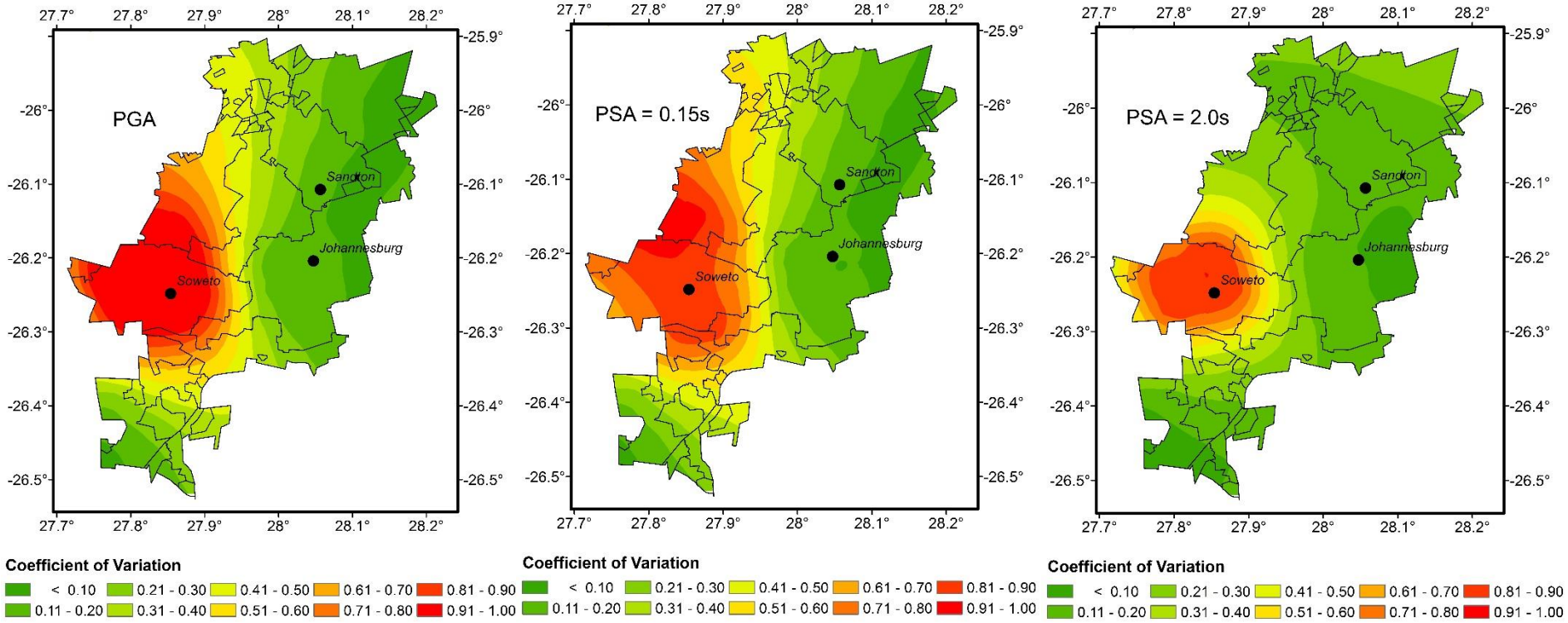
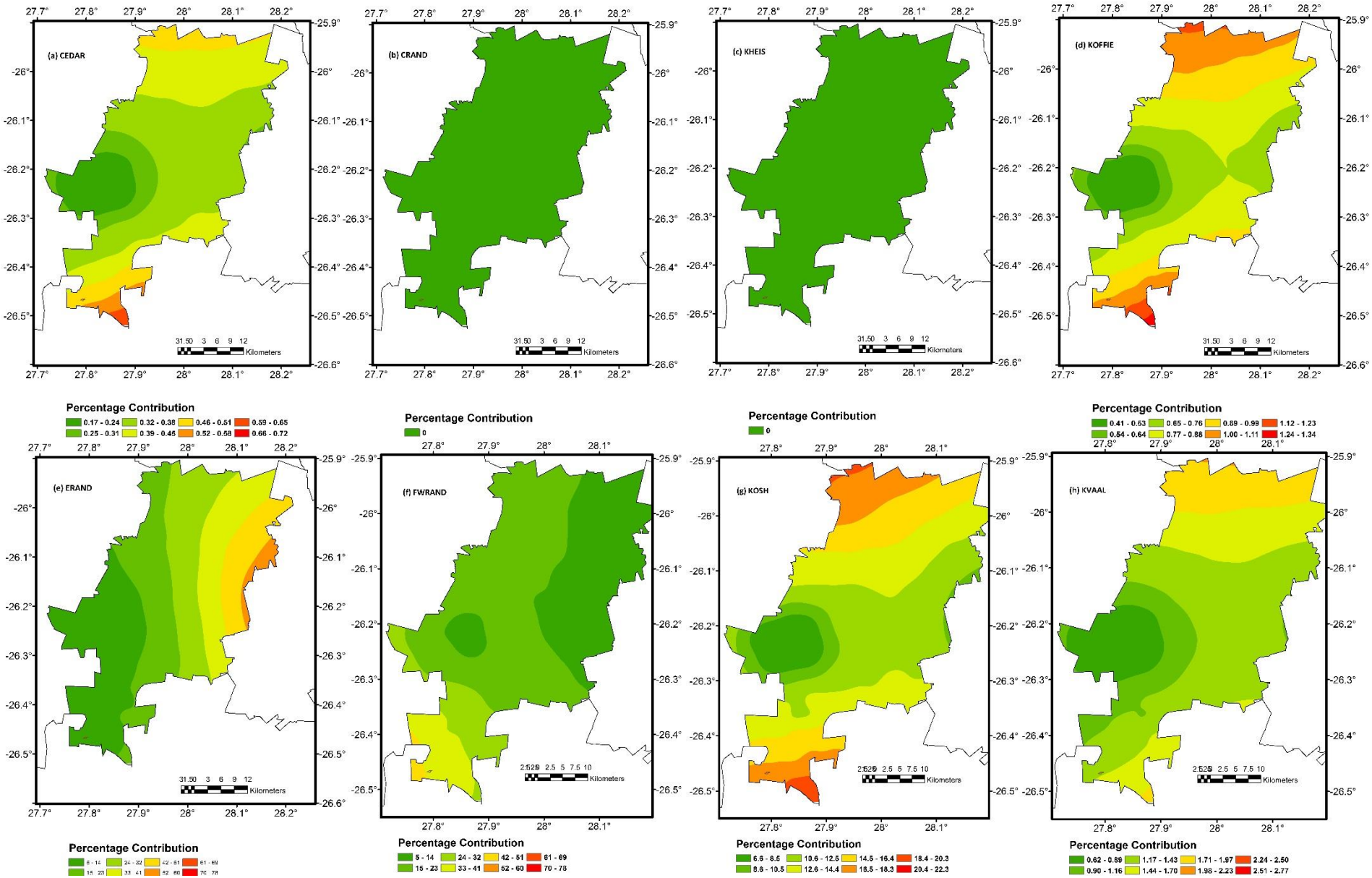


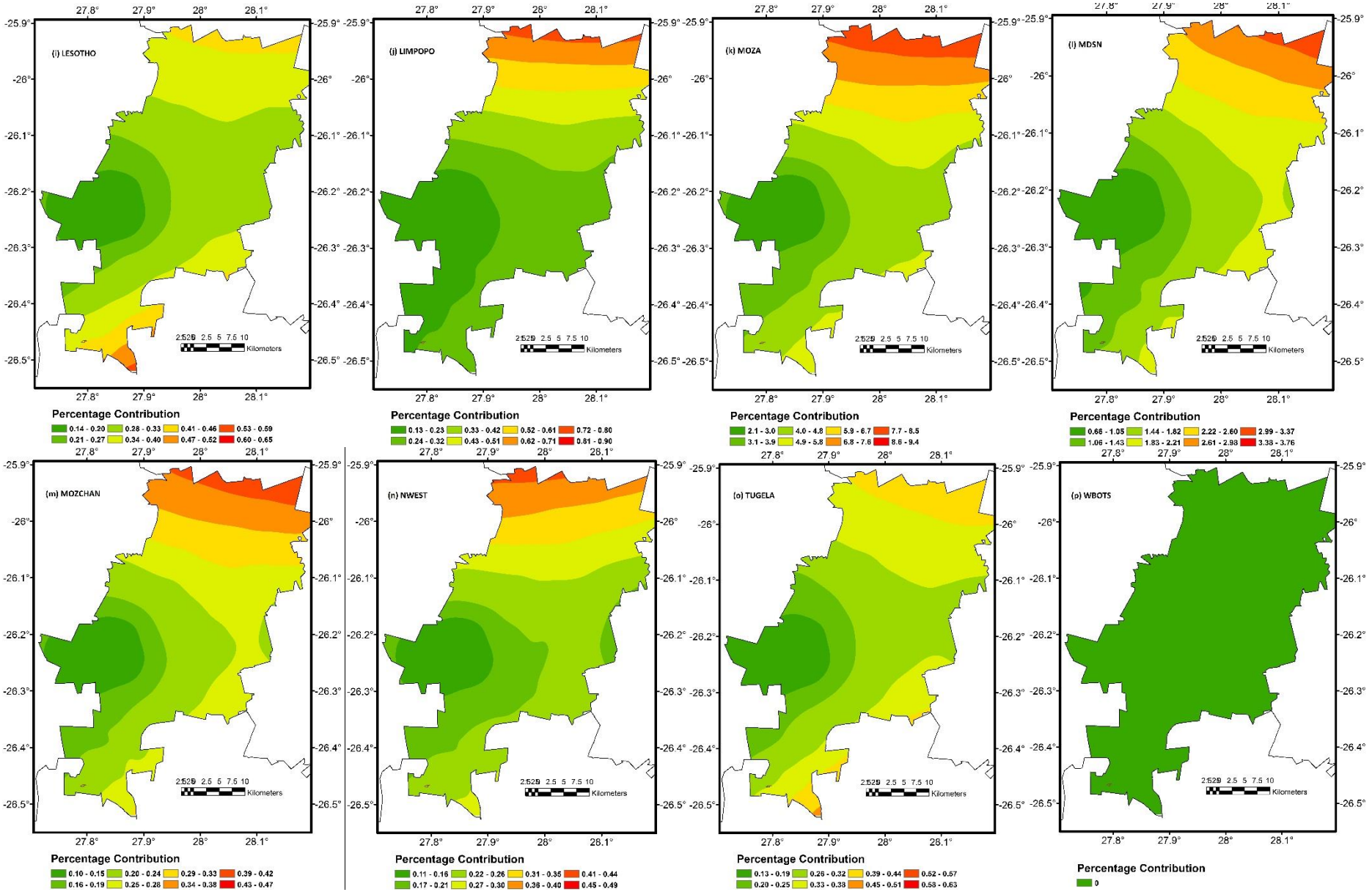
Figure 8-9: Results of different source models used in computing hazard for Johannesburg for the COV.

8.3.6. Effect of individual seismic source zones

To determine the influence of identified seismic source zones, the twenty sources for both mining and tectonic zones were used in the hazard computation. The reasons for the applied zoning and the justification for each zone are given and explained earlier in Chapter 5. Each of the sources were analysed to see how they influence the final hazard. Presented here are results obtained in assessing the impact of the delineated seismic zones (Figure 8-10, Figure 8-11 Figure 8-12). This parameter was assessed in terms of the percentage (%) contribution of each seismic source to the total hazard thus results shown in Figure 8-10, Figure 8-11 and Figure 8-12 reflect the % contribution of each source.

Most sources contributed between 2 and 20% to the total hazard, while a few did not contribute any hazard above 1% at all spectral periods. KOSH, MOZA and WRAND consistently contributed more than 5% of the total hazard at all spectral periods. KOFFIE, ZEBED, WELKOM and ZOET contributed hazard of more than 1% at a few sites, especially for lower spectral periods. CEDAR, LESOTHO, LIMPOPO, TUGELA, MOZCHAN, NWEST and CRAND sources contributed less than 1% of the hazard for all of the spectral periods. CRAND, which is located within Johannesburg, did not contribute any hazard at any of the spectral periods because it is characterised by very low seismicity with small magnitude earthquakes. Sources contributing less than 1% of the total hazard (i.e. CEDAR, KHEIS, LESOTHO, LIMPOPO, TUGELA, MOZCHAN, WBOTS, NWEST and CRAND) at all spectral periods were considered insignificant and therefore were not used for further analysis. Therefore, only 11 sources were considered in further sensitivity analysis.


(a) CEDAR
(b) CRAND
(c) KHEIS
(d) KOFFIE
(e) ERAND
(f) FWRAND
(g) KOSH
(h) KVAAL
Kilometers
Percentage Contribution
0.17 - 0.24
0.25 - 0.31
0.32 - 0.38
0.39 - 0.45
0.46 - 0.51
0.52 - 0.58
0.59 - 0.65
0.66 - 0.72
0
5 - 14
15 - 23
24 - 32
33 - 41
42 - 51
52 - 60
61 - 69
70 - 78
6.6 - 8.5
8.6 - 10.5
10.6 - 12.5
12.6 - 14.4
14.5 - 16.4
16.5 - 18.3
18.4 - 20.3
20.4 - 22.3
0.41 - 0.53
0.54 - 0.64
0.65 - 0.76
0.77 - 0.88
0.89 - 0.99
1.00 - 1.11
1.12 - 1.23
1.24 - 1.34
0.62 - 0.89
0.90 - 1.16
1.17 - 1.43
1.44 - 1.70
1.71 - 1.97
1.98 - 2.23
2.24 - 2.50
2.51 - 2.77


(i) LESOTHO
(j) LIMPOPO
(k) MOZA
(l) MDSN
(m) MOZCHAN
(n) NWEST
(o) TUGELA
(p) WBOTS
Percentage Contribution
0.14 - 0.20
0.21 - 0.27
0.28 - 0.33
0.34 - 0.40
0.41 - 0.46
0.47 - 0.52
0.53 - 0.59
0.60 - 0.65
0.13 - 0.23
0.24 - 0.32
0.33 - 0.42
0.43 - 0.51
0.52 - 0.61
0.62 - 0.71
0.72 - 0.80
0.81 - 0.90
2.1 - 3.0
3.1 - 3.9
4.0 - 4.8
4.9 - 5.8
5.9 - 6.7
6.8 - 7.6
7.7 - 8.5
8.6 - 9.4
0.66 - 1.05
1.06 - 1.43
1.44 - 1.82
1.83 - 2.21
2.22 - 2.60
2.61 - 2.98
2.99 - 3.37
3.38 - 3.76
0.10 - 0.15
0.16 - 0.19
0.20 - 0.24
0.25 - 0.28
0.29 - 0.33
0.34 - 0.38
0.39 - 0.42
0.43 - 0.47
0.11 - 0.16
0.17 - 0.21
0.22 - 0.26
0.27 - 0.30
0.31 - 0.35
0.36 - 0.40
0.41 - 0.44
0.45 - 0.49
0.13 - 0.19
0.20 - 0.25
0.26 - 0.32
0.33 - 0.38
0.39 - 0.44
0.45 - 0.51
0.52 - 0.57
0.58 - 0.63
0
2.5 0 2.5 5 7.5 10
Kilometers

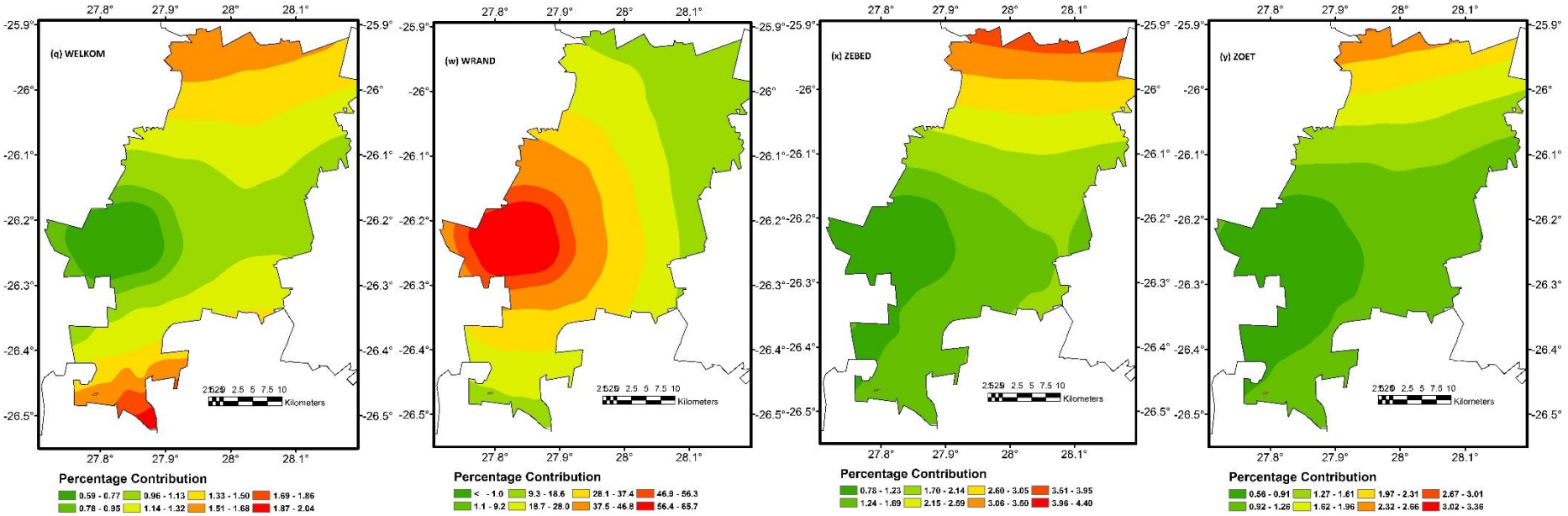
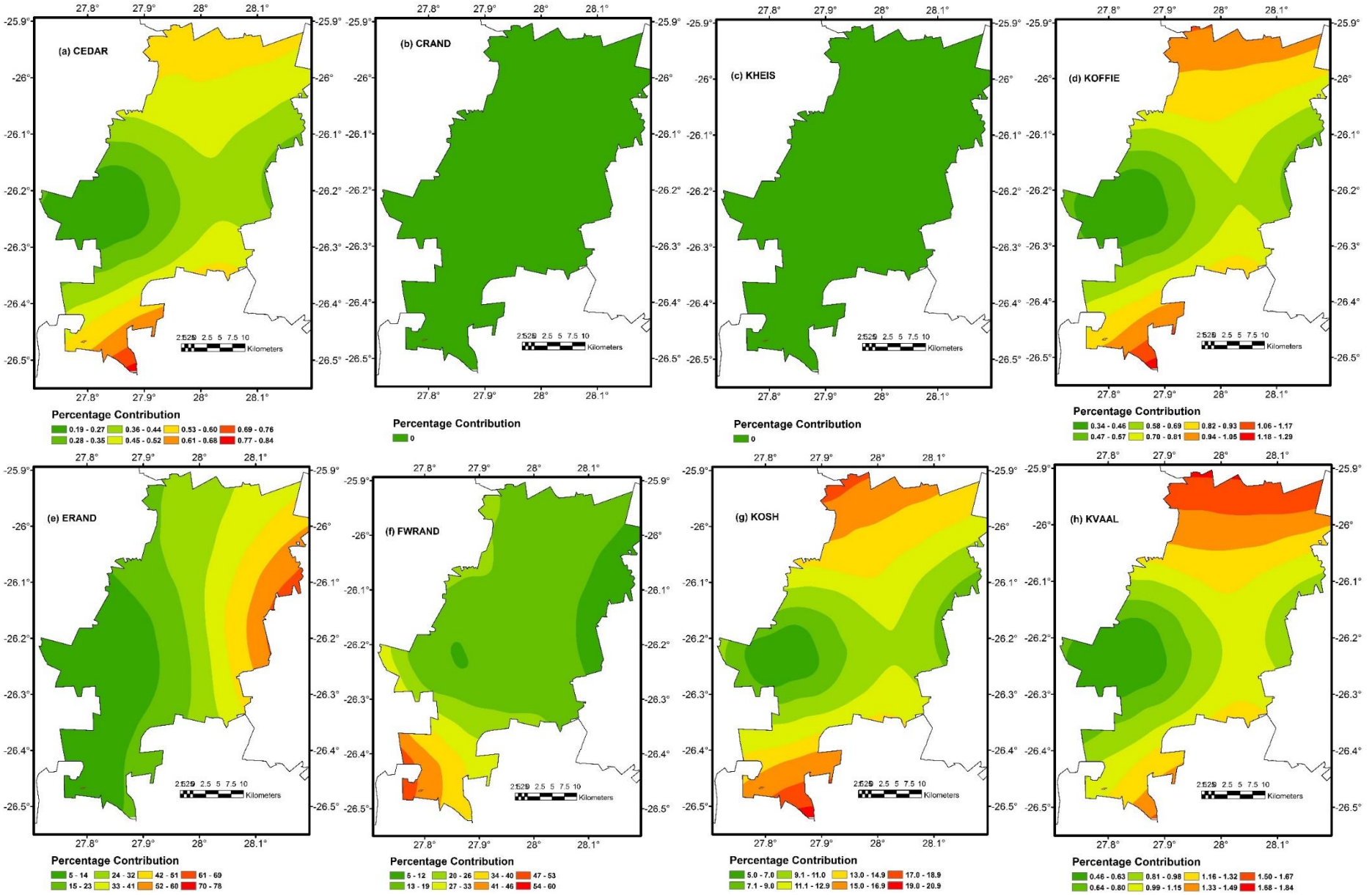
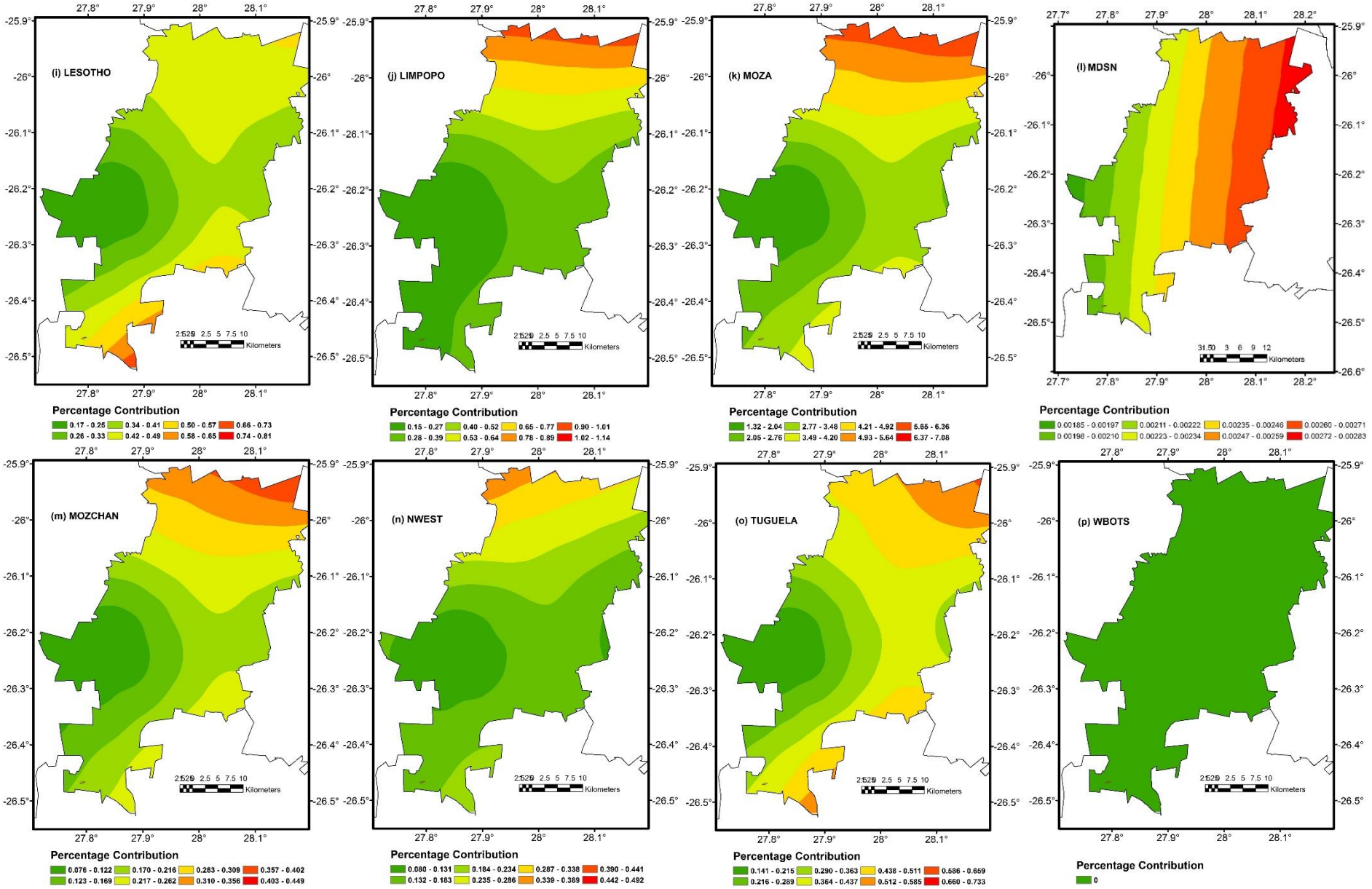


Figure 8-10: Maps showing the % contribution of the delineated zones to the total hazard for PGA for Johannesburg. Note the variation in the percentage value. Each map is scaled according to its own range of values.


(a) CEDAR
(b) CRAND
(c) KHEIS
(d) KOFFIE
(e) ERAND
(f) FWRAND
(g) KOSH
(h) KVAAL
27.8° 27.9° 28° 28.1°
25.9° 26° 26.1° 26.2° 26.3° 26.4° 26.5°
0 2.5 5 7.5 10
Kilometers
Percentage Contribution
0.19 - 0.27
0.28 - 0.35
0.36 - 0.44
0.45 - 0.52
0.53 - 0.60
0.61 - 0.68
0.69 - 0.76
0.77 - 0.84
Percentage Contribution
0
Percentage Contribution
0
Percentage Contribution
0.34 - 0.46
0.47 - 0.57
0.58 - 0.69
0.70 - 0.81
0.82 - 0.93
0.94 - 1.05
1.06 - 1.17
1.18 - 1.29
Percentage Contribution
5 - 14
15 - 23
24 - 32
33 - 41
42 - 51
52 - 60
61 - 69
70 - 78
Percentage Contribution
5 - 12
13 - 19
20 - 26
27 - 33
34 - 40
41 - 46
47 - 53
54 - 60
Percentage Contribution
5.0 - 7.0
7.1 - 9.0
9.1 - 11.0
11.1 - 12.9
13.0 - 14.9
15.0 - 16.9
17.0 - 18.9
19.0 - 20.9
Percentage Contribution
0.46 - 0.63
0.64 - 0.80
0.81 - 0.98
0.99 - 1.15
1.16 - 1.32
1.33 - 1.49
1.50 - 1.67
1.68 - 1.84


(i) LESOTHO
Percentage Contribution
0.17 - 0.25
0.26 - 0.33
0.34 - 0.41
0.42 - 0.49
0.50 - 0.57
0.58 - 0.65
0.66 - 0.73
0.74 - 0.81
(j) LIMPOPO
Percentage Contribution
0.15 - 0.27
0.28 - 0.39
0.40 - 0.52
0.53 - 0.64
0.65 - 0.77
0.78 - 0.89
0.90 - 1.01
1.02 - 1.14
(k) MOZA
Percentage Contribution
1.32 - 2.04
2.05 - 2.76
2.77 - 3.48
3.49 - 4.20
4.21 - 4.92
4.93 - 5.64
5.65 - 6.36
6.37 - 7.08
(l) MDSN
Percentage Contribution
0.00185 - 0.00197
0.00198 - 0.00210
0.00211 - 0.00222
0.00223 - 0.00234
0.00235 - 0.00246
0.00247 - 0.00259
0.00260 - 0.00271
0.00272 - 0.00283
(m) MOZCHAN
Percentage Contribution
0.076 - 0.122
0.123 - 0.169
0.170 - 0.216
0.217 - 0.262
0.263 - 0.309
0.310 - 0.356
0.357 - 0.402
0.403 - 0.449
(n) NWEST
Percentage Contribution
0.080 - 0.131
0.132 - 0.183
0.184 - 0.234
0.235 - 0.286
0.287 - 0.338
0.339 - 0.389
0.390 - 0.441
0.442 - 0.492
(o) TUGUELA
Percentage Contribution
0.141 - 0.215
0.216 - 0.289
0.290 - 0.363
0.364 - 0.437
0.438 - 0.511
0.512 - 0.585
0.586 - 0.659
0.660 - 0.733
(p) WBOTS
Percentage Contribution
0
Kilometers

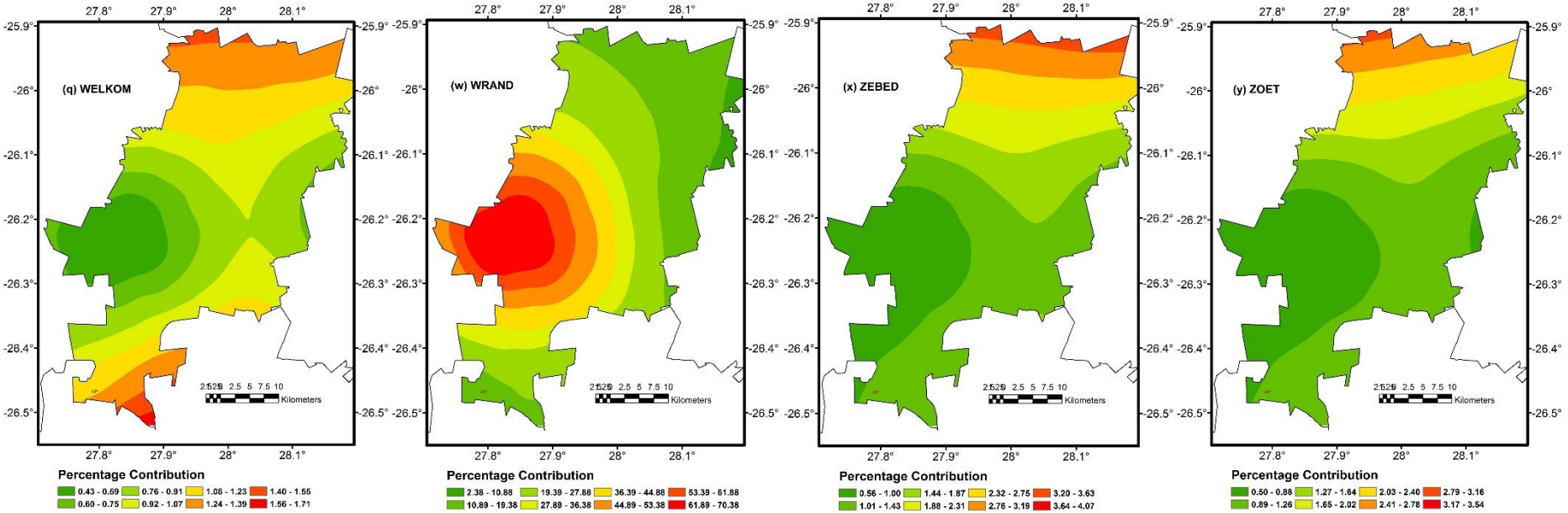
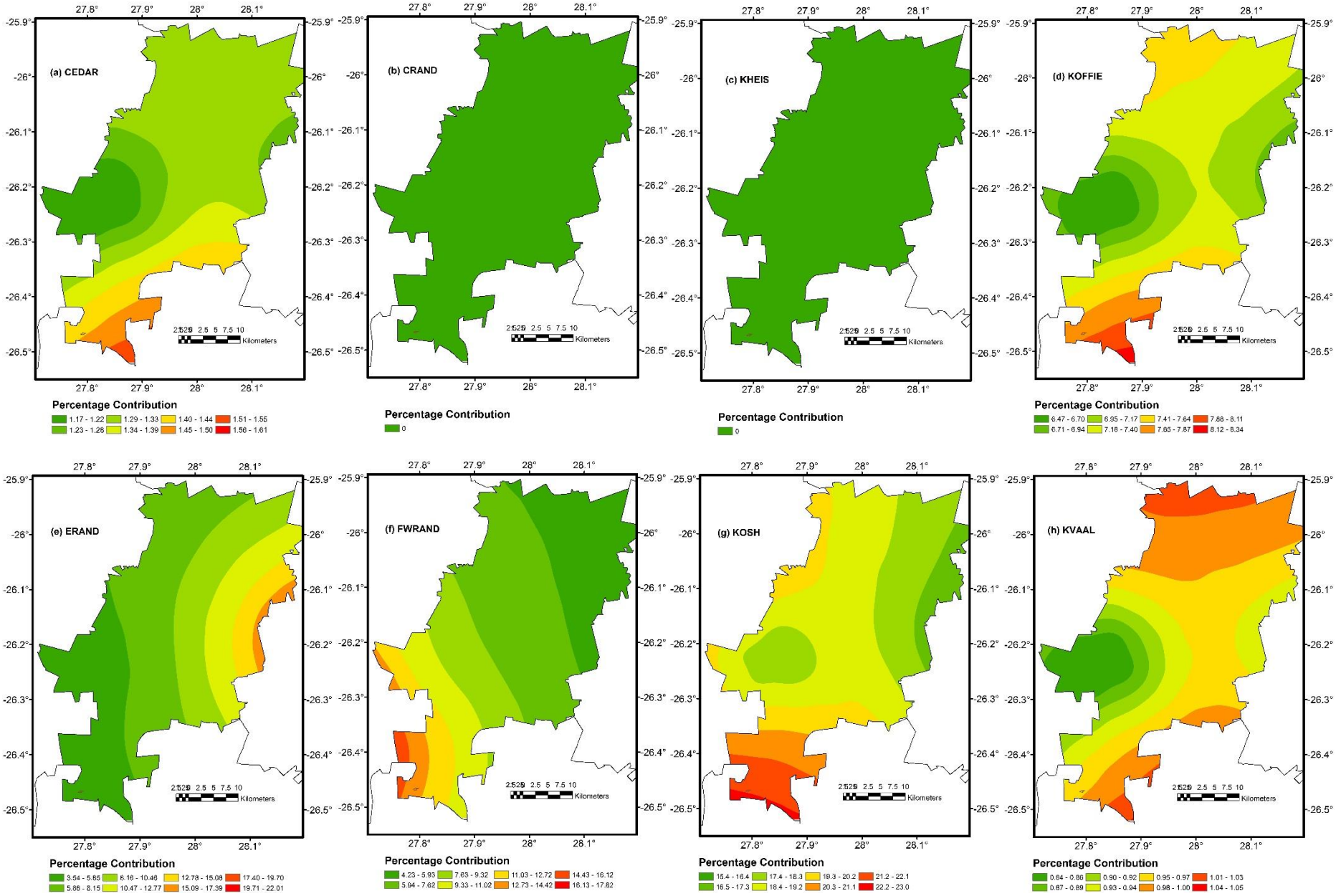
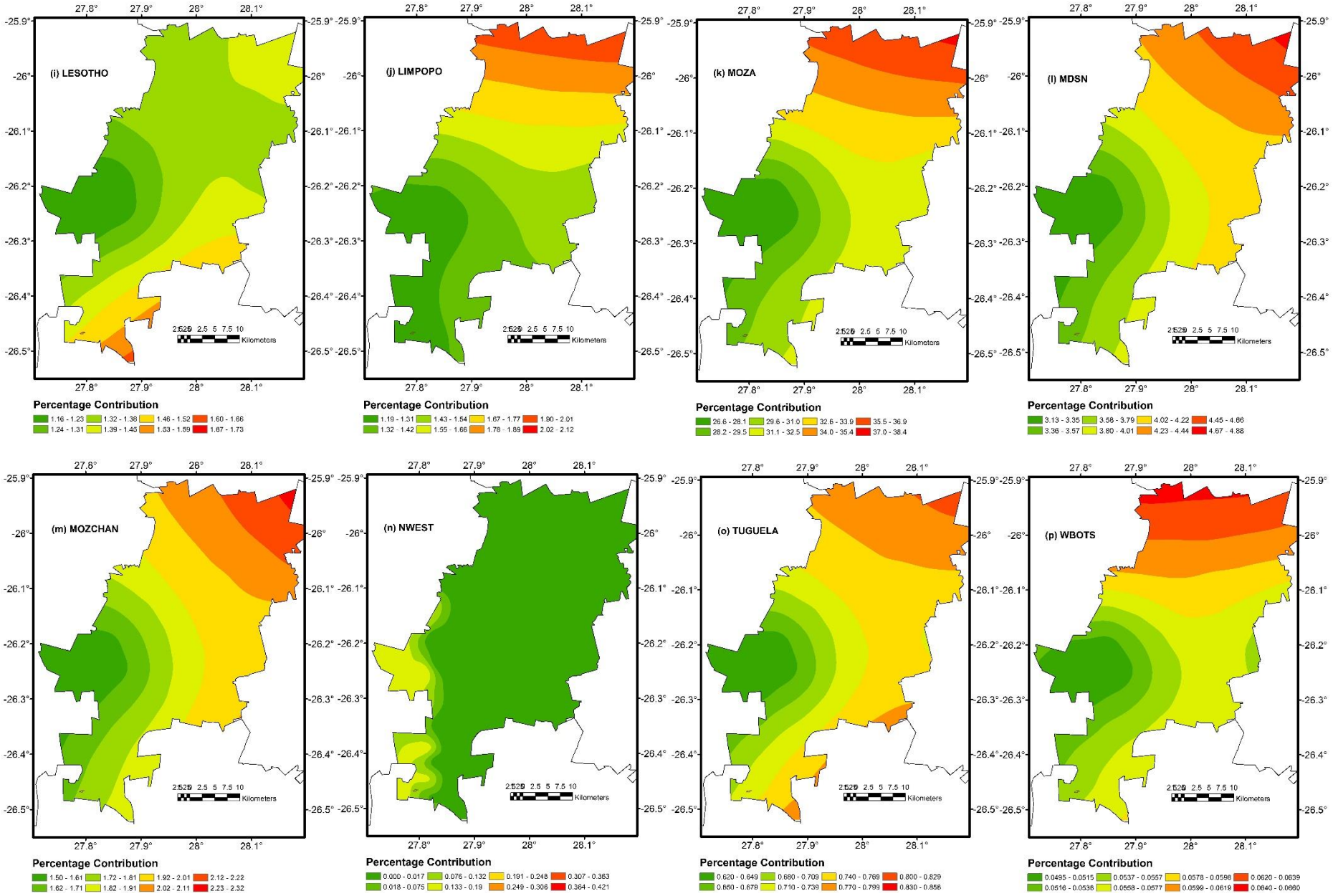


Figure 8-11: Maps showing the % contribution of the delineated zones to the total hazard for spectral period of 0.15s for Johannesburg. Note the variation in the percentage value. Each map is scaled according to its own range of values.


(a) CEDAR
(b) CRAND
(c) KHEIS
(d) KOFFIE
(e) ERAND
(f) FWRAND
(g) KOSH
(h) KVAAL
27.8° 27.9° 28° 28.1°
25.9° 26° 26.1° 26.2° 26.3° 26.4° 26.5°
2.5 5 7.5 10
Kilometers
Percentage Contribution
1.17 - 1.22
1.23 - 1.28
1.29 - 1.33
1.34 - 1.39
1.40 - 1.44
1.45 - 1.50
1.51 - 1.55
1.56 - 1.61
Percentage Contribution
0
Percentage Contribution
0
Percentage Contribution
6.47 - 6.70
6.71 - 6.94
6.95 - 7.17
7.18 - 7.40
7.41 - 7.64
7.65 - 7.87
7.88 - 8.11
8.12 - 8.34
Percentage Contribution
3.54 - 5.86
5.86 - 8.15
8.16 - 10.46
10.47 - 12.77
12.78 - 15.08
15.09 - 17.39
17.40 - 19.70
19.71 - 22.01
Percentage Contribution
4.23 - 5.93
5.94 - 7.62
7.63 - 9.32
9.33 - 11.02
11.03 - 12.72
12.73 - 14.42
14.43 - 16.12
16.13 - 17.82
Percentage Contribution
15.4 - 16.4
16.5 - 17.3
17.4 - 18.3
18.4 - 19.2
19.3 - 20.2
20.3 - 21.1
21.2 - 22.1
22.2 - 23.0
Percentage Contribution
0.84 - 0.86
0.87 - 0.89
0.90 - 0.92
0.93 - 0.94
0.95 - 0.97
0.98 - 1.00
1.01 - 1.03
1.04 - 1.05


(i) LESOTHO
(j) LIMPOPO
(k) MOZA
(l) MDSN
(m) MOZCHAN
(n) NWEST
(o) TUGUELA
(p) WBOTS
Kilometers
Percentage Contribution
1.16 - 1.23
1.24 - 1.31
1.32 - 1.38
1.39 - 1.45
1.46 - 1.52
1.53 - 1.59
1.60 - 1.66
1.67 - 1.73
1.19 - 1.31
1.32 - 1.42
1.43 - 1.54
1.55 - 1.66
1.67 - 1.77
1.78 - 1.89
1.90 - 2.01
2.02 - 2.12
26.6 - 28.1
28.2 - 29.5
29.6 - 31.0
31.1 - 32.5
32.6 - 33.9
34.0 - 35.4
35.5 - 36.9
37.0 - 38.4
3.13 - 3.35
3.36 - 3.57
3.58 - 3.79
3.80 - 4.01
4.02 - 4.22
4.23 - 4.44
4.45 - 4.66
4.67 - 4.88
1.50 - 1.61
1.62 - 1.71
1.72 - 1.81
1.82 - 1.91
1.92 - 2.01
2.02 - 2.11
2.12 - 2.22
2.23 - 2.32
0.000 - 0.017
0.018 - 0.075
0.076 - 0.132
0.133 - 0.19
0.191 - 0.248
0.249 - 0.306
0.307 - 0.363
0.364 - 0.421
0.620 - 0.649
0.650 - 0.679
0.680 - 0.709
0.710 - 0.739
0.740 - 0.769
0.770 - 0.799
0.800 - 0.829
0.830 - 0.858
0.0495 - 0.0515
0.0516 - 0.0536
0.0537 - 0.0557
0.0558 - 0.0577
0.0578 - 0.0598
0.0599 - 0.0619
0.0620 - 0.0639
0.0640 - 0.0660

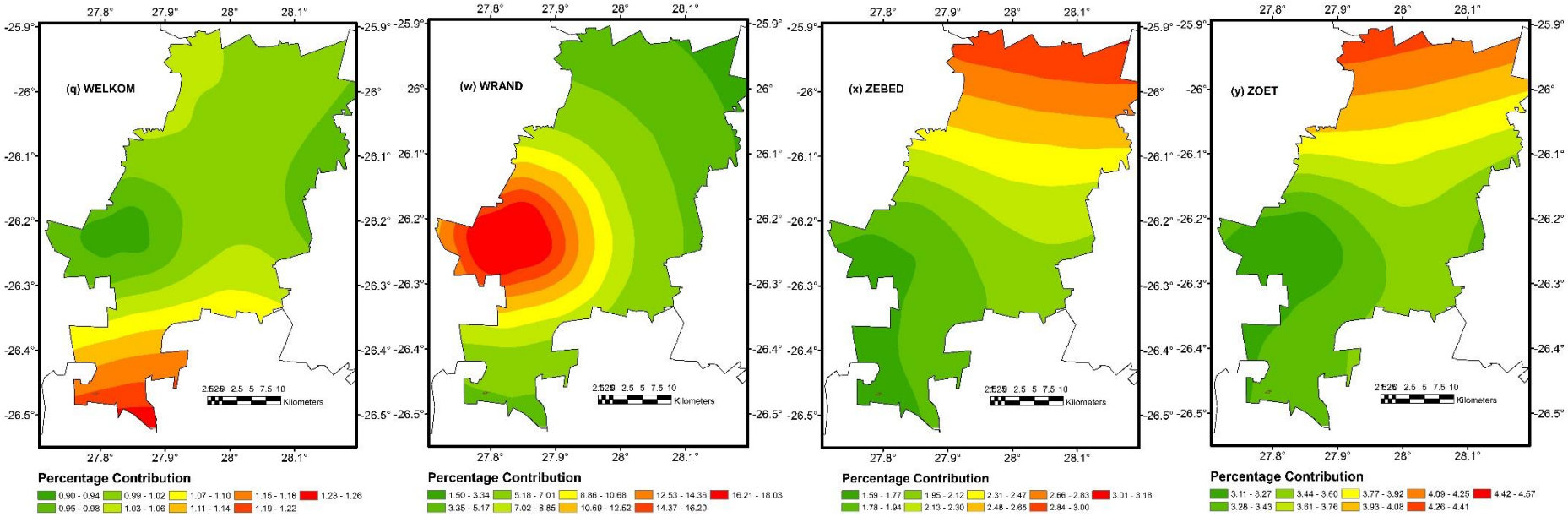


Figure 8-12: Maps showing the % contribution of the delineated zones to the total hazard for spectral period of 2.0s for Johannesburg. Note the variation in the percentage value. Each map is scaled according to its own range of values.

8.3.7. Local site effects

Site effects play a very important role in characterizing seismic ground motions because they may significantly amplify ground motions at a site. Therefore, they cannot be neglected in seismic hazard analysis. Variability in site conditions is caused by changes in local geology and topography. Thus, the diverse geology and topography under Johannesburg city is likely to contribute to spatially variable earthquake strong motions, manifested in part as localised differences in site effects. In seismic hazard analysis, local site effects are normally determined by carrying out a site response analysis that takes into account the site geophysical structure. However, this can be a difficult, expensive and time-consuming process. Thus in many cases, site conditions are represented by V_{s30} values, where V_{s30} is the average shear wave velocity to a depth of 30m below the earth's surface (NERHP, 2009; Mogren, 2020). In general, where site response analysis is not done and V_{s30} values are not available, hazard is calculated for bedrock site conditions defined by a bedrock shear wave velocity, V_S. However, the definition of bedrock can be tricky and introduces another uncertainty in the hazard calculation (see Mogren 2020). Different values of bedrock shear wave velocity have been suggested by different authors (e.g. a Vs value of 700 m/s was proposed by Miller et al., 1999; Santamarina et al., 2001; Ryden, 2004; Nath, 2007) while Ansal and Tonuk (2007) suggested a Vs Vs varying from 700 to 750 m/s, NEHRP (2009) and (Akin et al., 2013) proposed a value of 760 m/s). In this part of the study, four bedrock shear wave velocity values (i.e. 760 m/s, 900m/s, 1000m/s, 1500m/s) were used in calculating the hazard and the results compared.

The COV values estimated in the comparison of results for bedrock velocity ranges from 0.04 to 0.2 (Figure 8-13). COV values for PGA and PSA = 2.0s were higher than for PSA = 0.15s. The central and southern parts of the study area shows high COV values than the northern side for all spectral periods. COV variation for PGA and PSA = 2.0s exceed the threshold limi of 0.1 for most sites while for PSA = 0.15s all values are less than 0.1. Thus, unless for site specific studies where Vs values are critical, this parameter can be assigned an assumed value for bedrock. The tradition of picking a standard value for all sites (e.g. Vs = 760 m/s as in Midzi et al., 2020) has no significant implications to the hazard calculation. It is however necessary that geophysical investigations be carried out to determine experimentally the actual shear wave velocity of bedrock at the study area, as done for Johannesburg (Manzunzu et al., 2019).

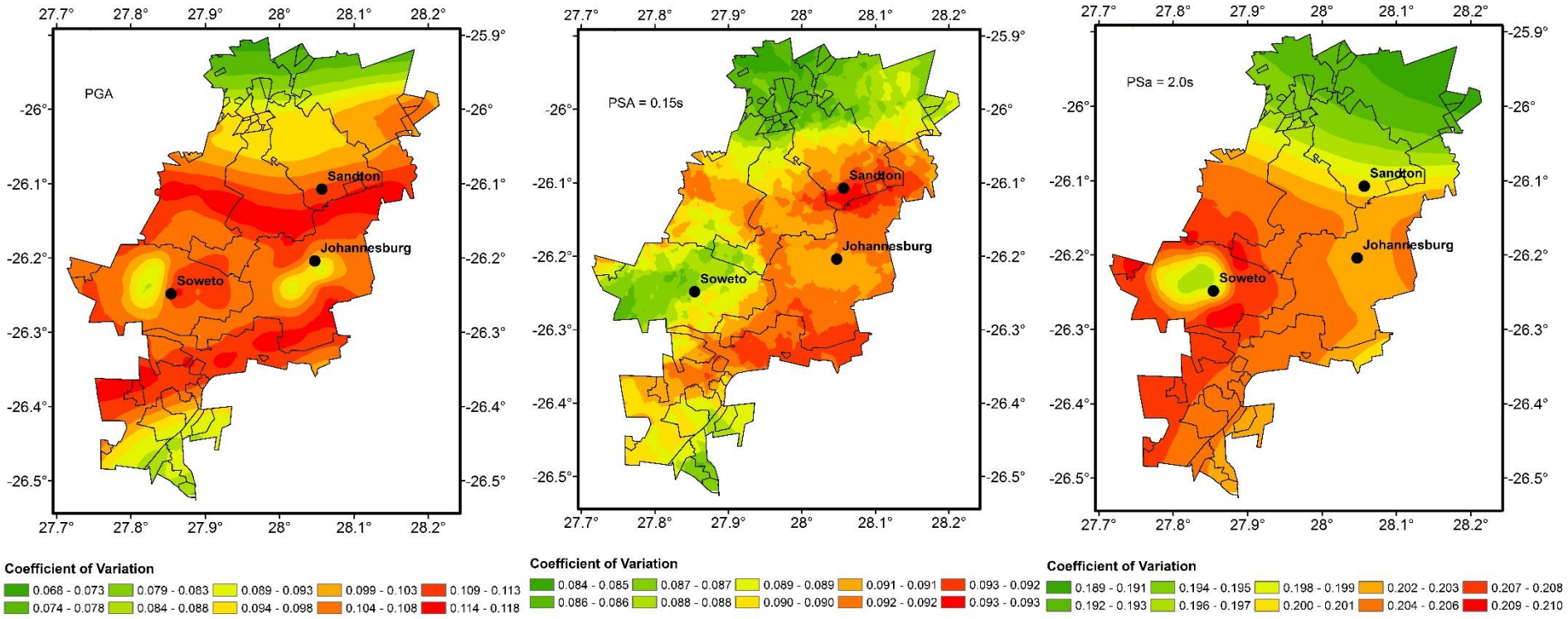


Figure 8-13: COV results for the sensitivity analysis for bedrock shearwave velocity Vs.

8.3.8. Minimum magnitude, M_{min}, for hazard calculation

In probabilistic seismic hazard analysis, probabilistic ground motions from all earthquakes within some magnitude range, $M_{min} < M < M_{max}$, are combined to estimate levels of peak ground acceleration that have a specified probability of being exceeded at a site during various time periods (Algermissen et al., 1982). Engineers have observed that high peak accelerations from small magnitude earthquakes ($M < 5$) may not cause significant damage to well-engineered structures (Bender and Campbell, 1989; Bommer and Crowley, 2017) and therefore, it is arguable whether ground motions from small-magnitude earthquakes should be included in seismic hazard calculations. There is no consensus among seismic hazard analysts as to an appropriate value of minimum magnitude to use in hazard calculations. Comparison of results obtained in some studies (e.g. Bernreuter et al., 1985 and EPRI, 1986), where seismic hazard was estimated for the same site using different M_{min} values, showed that differences in the minimum magnitude might significantly affect the ground motion estimates at some probability levels. Reflecting different opinions regarding the choice of M_{min} to use in seismic hazard analyses. It is therefore necessary to assess the possible impact of this parameter in the hazard estimates for Johannesburg. Most seismic hazard studies are computed for M_{min} of 5. However, Kramer (1996) noted that in most PSHAs, the lower threshold magnitude is set at values from about 4.0 to 5.0 since magnitudes smaller than that seldom cause significant damage. In this regard, we assessed the influence of this M_{min} to our hazard as a source of uncertainty. Here, the M_{min} values considered are 4.0, 4.5 and 5.0.

Spatial distribution of COV for PGA and PSA = 0.15 are almost similar. The PGA and 0.15s COV maps shown in Figure 8-14, shows that there is variation of greater than 0.1 across the region while for PSA = 2.0s they are all below 0.1. However, as expected the impact of lower M_{min} values is less at long period hazard maps as larger earthquakes with long period signals dominate. COV values increase from the west towards the east with highest values around Johannesburg CBD for all spectral periods. These results imply that this variation in M_{min} will result in significant variation in hazard in Johannesburg. Thus a decision has to be made on which value is suitable for use in seismic hazard assessment across South Africa. One issue that can guide this decision is the fact that most GMPEs, including those used in South Africa, are valid for earthquakes of magnitude greater than or equal to 5. Most GMPEs also do not behave properly when extrapolated down to lower magnitude values.

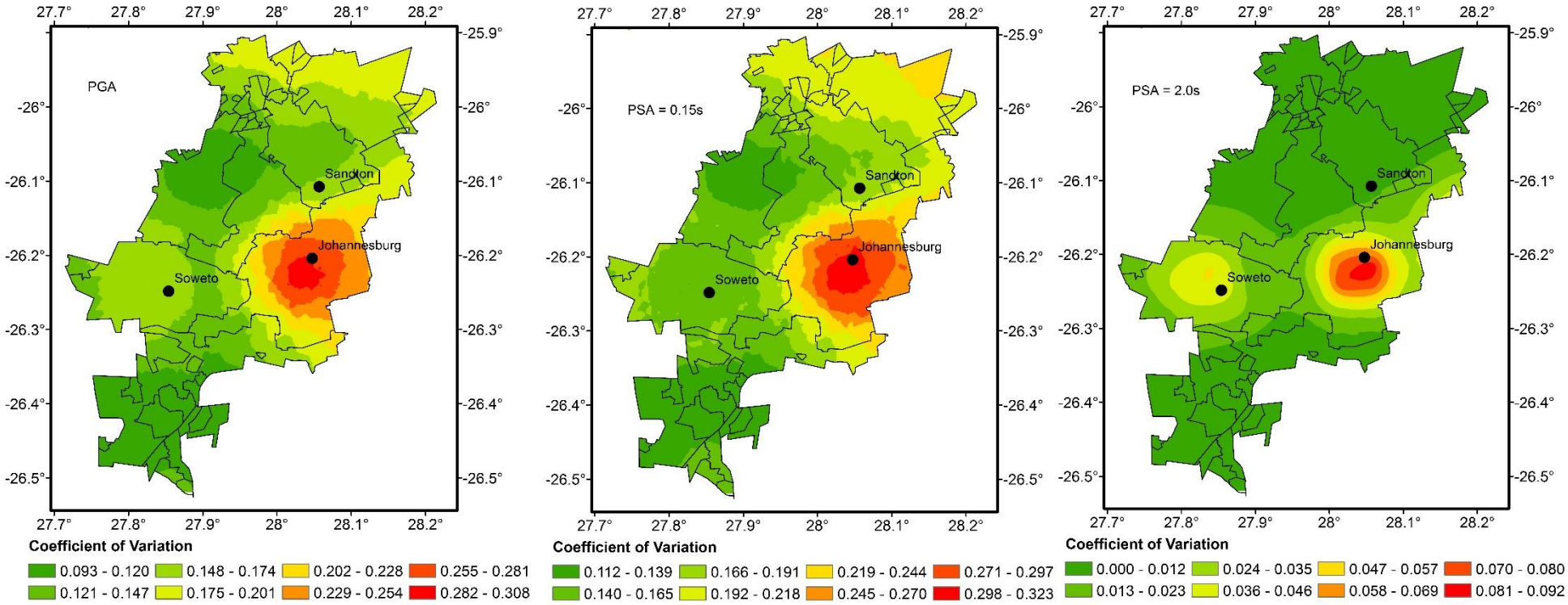


Figure 8-14: COV results for the sensitivity analysis for M_{min}.

8.3.9. Ground Motion Prediction Equations

The six GMPEs (AB06, BA08, AKETAL14,TO02, RIETAL13 AND CAM03) selected by comparing with local data were used in this study to demonstrate the effect of choice of model on the hazard results (see section 7.6). To show the effect of the selected GMPEs, the analyses are performed for six separate cases, where each case represents a different GMPE. The GMPEs were proposed in the GEM project as suitable for PSHA in shallow active crustal regions (Boore and Atkinson, 2008; Akkar et al., 2014) and in stable continental regions (Toro, 2002; Campbell, 2003; Atkinson and Boore, 2006; Rietbrock et al., 2013).

COV results show high values (>0.3) indicating large variability in the results (Figure 8-15). Spatial distribution of the COV values are significantly different for the three spectral periods. High COV values were observed in the central areas for PGA, which decreases north and southwards. For PSA=0.15s, high COV values are found in the eastern side around Johannesburg CBD while for PSA=2.0s they are on the west in Soweto. These high COV values for GMPEs show that this is an important parameter whose selection has significant influence on the hazard. The results support the comparisons made in Chapter 7. Given the uncertainty in the hazard linked to the GMPEs, it is necessary that a range of models that cover the epistemic uncertainty associated with the models be selected.

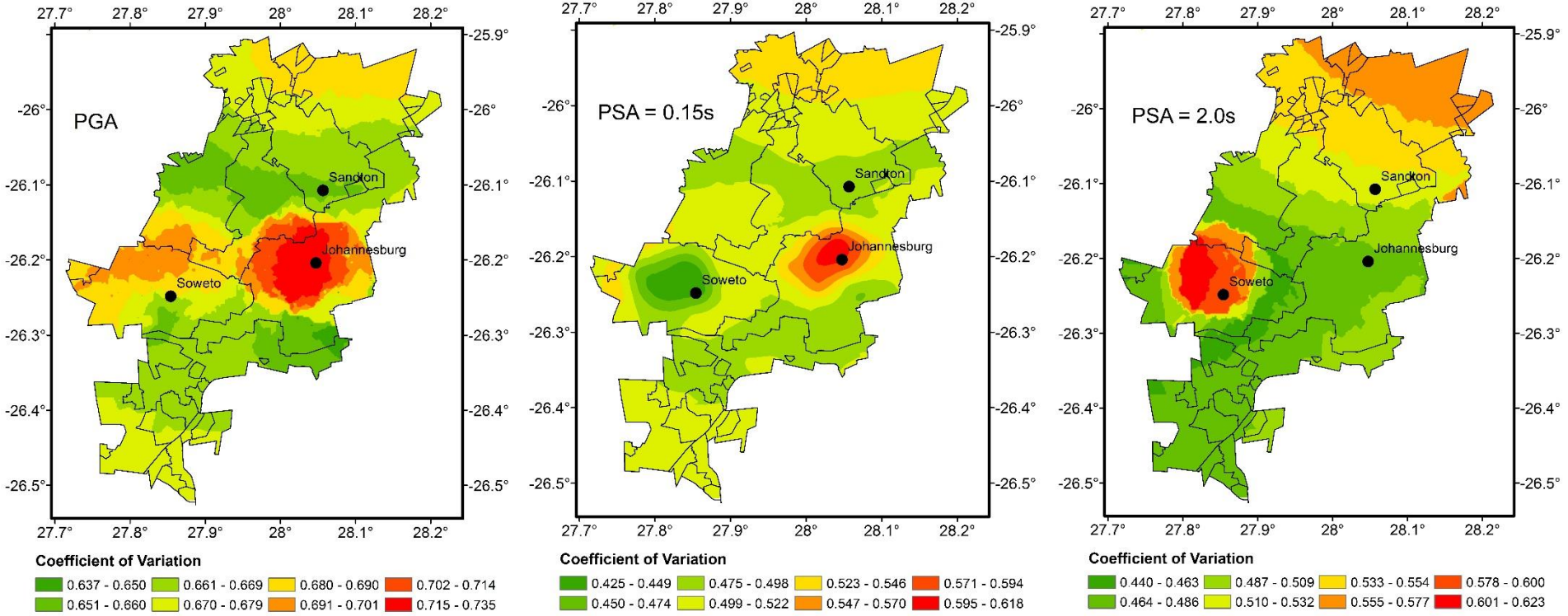


Figure 8-15: COV results for GMPE seismic hazard sensitivity analysis.

8.4. Sensitivity analysis related to local variables

Sensitivity analysis for local variables were performed for individual source zones. The seismic source model developed in this study was used in this assessment. Ideally, all seismic source zones need to be assessed. However, the processing is time consuming and requires large computing power. Therefore, the KOSH seismic source zone was used to illustrate the influence of local variables. This zone was selected since it had moderate impact on the hazard (Figure 8-10; Figure 8-11; Figure 8-12) at all spectral periods.

8.4.1. *b*-value estimation

The estimation of *b*-value is dependent on a number of factors. For a specific source zone, it is possible to have several *b*-values estimated from a single catalogue. Sensitivity results show that *b*-value variations have a slight influence on the hazard results since the COV values are close to 0.1. This parameter needs to be carefully taken into account especially when modelling epistemic uncertainties (i.e. in the logic tree compilation). The values are slightly higher than our threshold of 0.1 with PGA values as high as 0.11 for PGA while PSA 0.15s and 2.0s have values of 0.12 and 0.14 respectively. These values do not indicate strong influence of the variation of *b*-value (Figure 8-16). The variation in the spatial distribution of COV is different for the three spectral periods. For PGA, COV values increases from the southwestern to the northeastern side of the study are while for PSA=0.15s and PSA=2.0s COV values are vice versa.

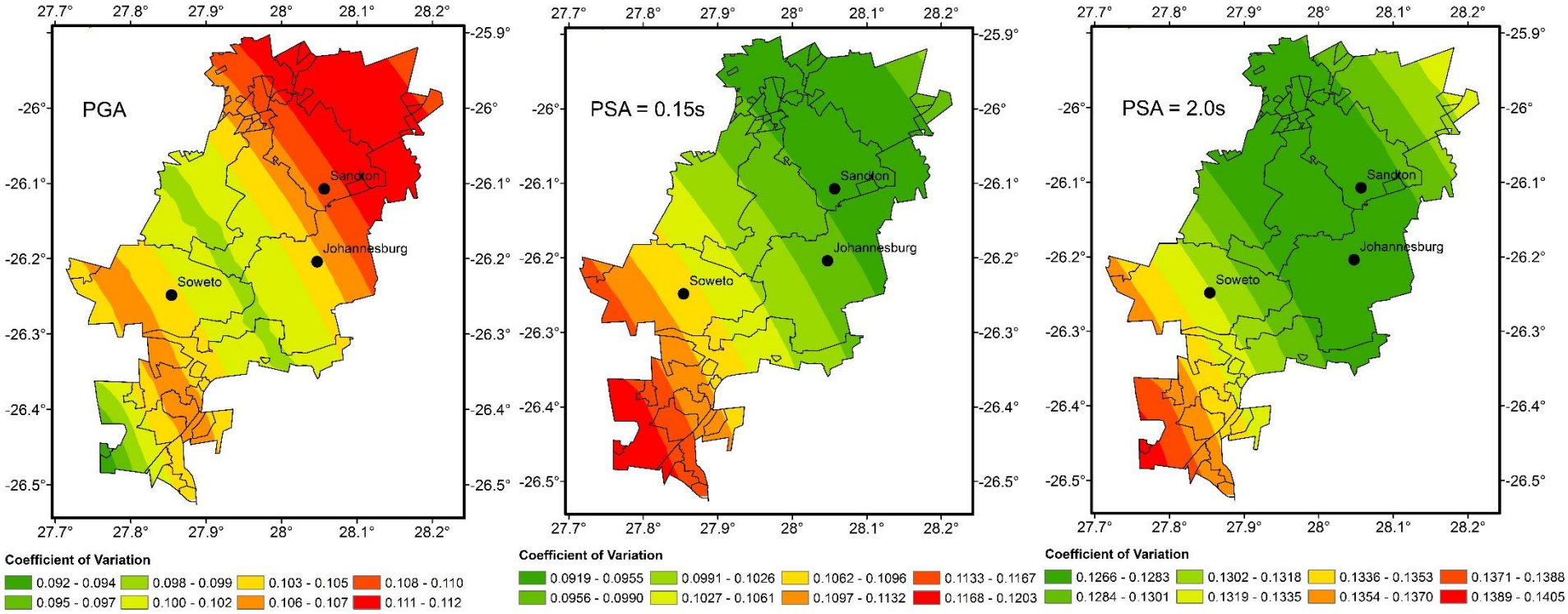


Figure 8-16: COV results for the sensitivity analysis for *b*-value**.**

8.4.2. Activity rate

The activity rate has a critical influence on the final hazard results since it represents the rate of earthquake production. The variation in hazard with activity rates is illustrated strongly by the obtained COV values, where values as high as 0.3 were observed (Figure 8-17). The spatial distribution of COV are similar to that for the *b*-value for all spectral periods.This implies significant influence on the total hazard at all spectral periods. Both activity rate and *b*-value are a product of the catalogue. Therefore, these results show how significant the catalogue compilation process is. Spatial variations not very large within each spectral period.

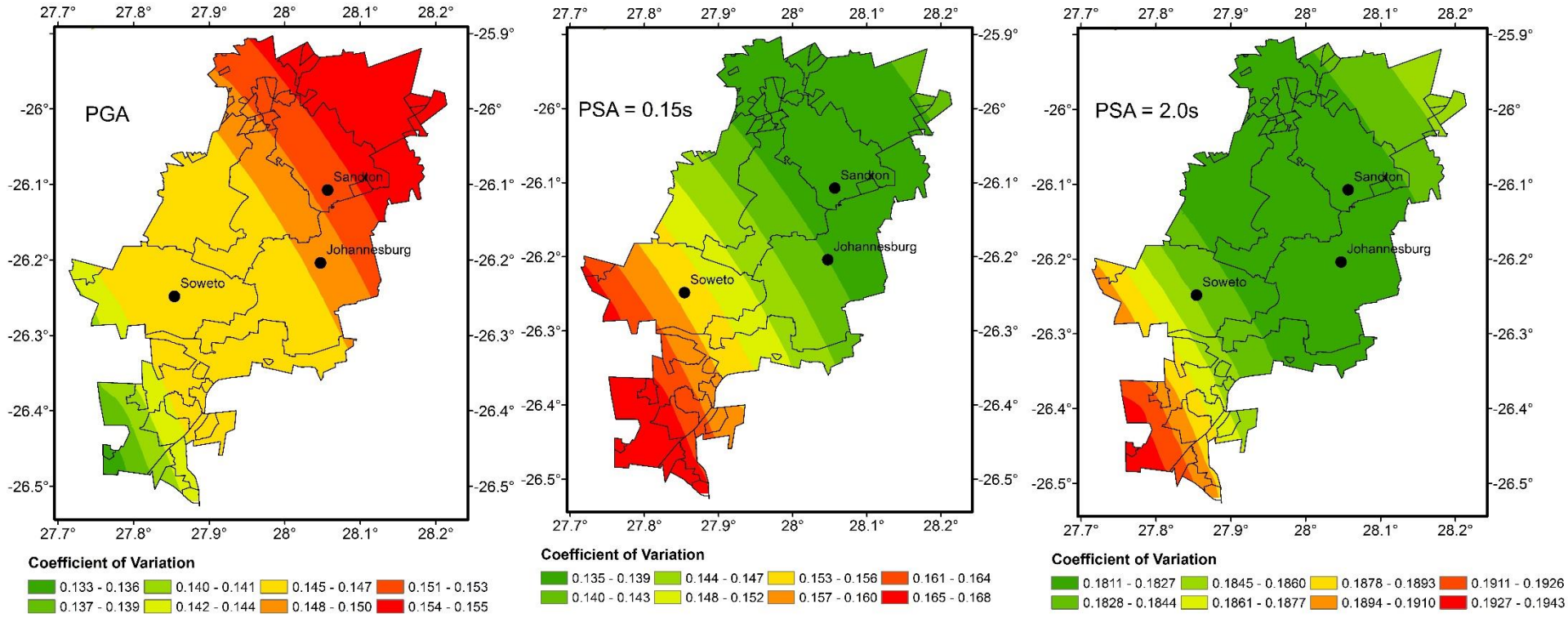


Figure 8-17: COV results for the sensitivity analysis for activity rate.

8.4.3. M_{max} determination

The computed M_{max} values in Table 6-3 were used in computing the hazard. The variation in hazard with M_{max} appears to occur at all spectral period. The strong variation of hazard with M_{max} is reflected in the significant COV values for all spectral periods (Figure 8-18), though stronger variation is observed at the longer period of 2.0s (0.32 – 0.35). The extent of the variation in hazard due to M_{max} variation affects the entire city. COV values increases from the southwestern side towards the northeastern side for all spectral periods. For PGA the central parts of the study area shows the highest COV values. COV values not very different within each spectral period.

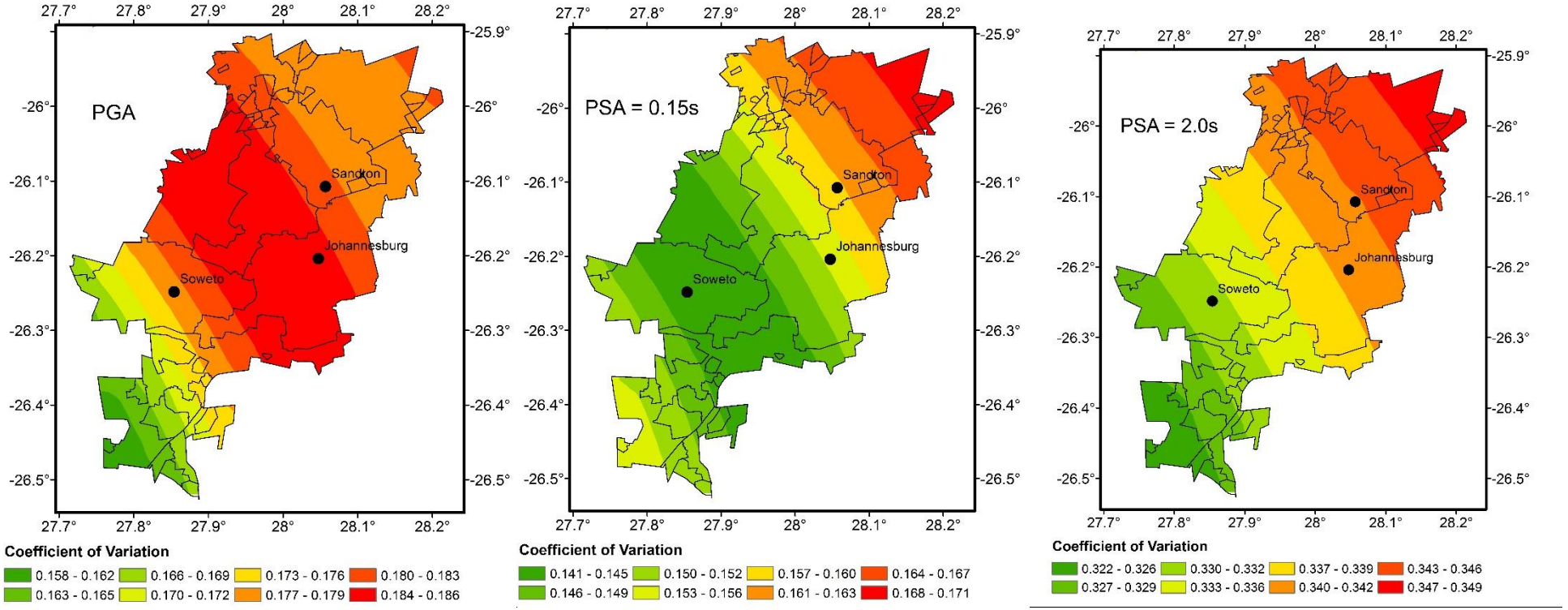


Figure 8-18: COV results for the sensitivity analysis for M_{max}.

8.5. Discussions

The application of sensitivity feedback from the model parameters provided a useful tool to identify those parameters with a major influence on the final hazard. For this purpose, the coefficient of variation was evaluated for the different input parameters to assess their influence on the seismic hazard for the city of Johannesburg. Recurrence parameters were computed from different catalogues developed during the different catalogue processing procedures as well as in the analysis of uncertainties related to some parameters. The *b*-value, the activity rate, the earthquake magnitude limits (M_{min} and M_{max}), and GMPEs were considered as input variables to the PSHA. The influence of uncertainty in model inputs on the variability of PSHA results, as well the influence of the local site effects were investigated.

The hazard was assessed for three spectral periods (PGA, T= 0.15 seconds and T= 2.0 seconds) for 2% probability of exceedance in 50 years. Each hazard computation was performed at 217 sites distributed within the Municipality of Johannesburg. Uncertainty analysis was accomplished by assessing different alternatives for each model and input parameter. For each input parameter, sensitivity analysis was computed through the coefficient of variation (COV) of the final hazard at each site. The output distribution was obtained by evaluating the model at grid points covering the study area for different input values. For peak ground acceleration (PGA) and spectral acceleration at 0.15s and 2.0s, the COV representing the knowledge-based uncertainty in seismic hazard can exceed 0.4 over the Central Johannesburg and diminishes to about 0.1 away from areas of seismic activity. The parameters with high COV values are more influential and need to be fully accounted for in terms of uncertainty.

Sensitivity analysis indicates that the five most important inputs (not in order of impact) that have a profound impact in controlling the final hazard levels are (1) catalogue homogenisation process, (2) method of computing recurrence parameters, (3) temporal variation of the seismic catalogue, (4) seismic source model and (5) GMPEs (Table 8-5). Therefore, to improve understanding and accuracy in the seismic hazard assessment results, it is necessary to focus effort on the analysis and careful study of these parameters and their models. The first four give insight into the limitations of the current earthquake catalogue for Johannesburg. Currently, the earthquake catalogue is limited by a short time period of observation, high location errors leading to poor associations with possible earthquake source structures and heterogeneous magnitude values. All these lead to high uncertainty in the computed parameters. Processes involved in the compilation of the catalogue (e.g. declustering and homogenisation) shows significantly high COV values at all spectral periods.

Delineation of seismic sources is a daunting task for this area, especially due to the unavailability of identified active faults. Areal sources were therefore selected using the available regional geology and seismicity distribution. By using these areal zones, it is possible to represent the conceptual model of the degree of stationarity of seismicity in a reproducible and simple way. However, sensitivity results show that some of the delineated seismic sources actually contributed little to no hazard at all spectral periods. These sources were removed to reduce the computation time as well as the complexity of the source model. It has to be noted that results found in this study might be different for a different study area but it will provide some guidelines for future research.

The fifth input is related to the understanding and prediction of strong earthquake ground motions for South Africa. Knowledge about strong ground motions from South African earthquakes is limited by the lack of large-earthquake ($M \geq 6.0$) recordings in South Africa to develop GMPEs with local data.

Table 8-5: Coefficient of variation ranges for different spectral periods.

Parameter	**Coefficient of variation ranges for different spectral periods**		
	PGA	**T= 0.15s**	**T = 2.0s**
Homogenisation	0.04 – 0.21	0.03 – 0.81	0.10 – 0.32
Declustering	0.06 – 0.19	0.00 – 0.21	0.04 – 0.20
Temporal variation	0.0003 – 0.39	0.004 – 0.53	0.01 - 0.30
Seismic source model	0.00 – 1.00	0.00 – 1.00	0.00 – 1.00
Bedrock shear wave velocity	0.07 – 0.12	0.08 – 0.09	0.19 – 0.21
M_{min}	0.09 – 0.31	0.11 – 0.32	0.00 – 0.09
GMPE	0.64 – 0.74	0.43 – 0.62	0.44 – 0.62
Methods of calculating recurrence parameters	0.024 – 0.33	0.00 – 0.34	0.01 – 0.31
b-value	0.10 – 0.113	0.09 – 0.12	0.13 – 0.14
Activity rate	0.13 – 0.16	0.14 – 0.17	0.18 – 0.19
M_{max}	0.16 – 0.19	0.14 – 0.17	0.32 – 0.35

8.6. Conclusions

Sensitivity analysis was carried out to determine the impact of input parameters and models on the calculation of the seismic hazard for Johannesburg. The key input parameters for PSHA described in the previous chapters are considered as input variables to carry out the sensitivity analysis in this study. Exhaustive analysis to identify and quantify epistemic uncertainties associated with different parameters and methods involved in the computation procedure, have been a key issue of this work.

The hazard was assessed for three spectral periods (PGA, 0.15s, and 2.0s) for bedrock sites for 2% probability of exceedance in 50 years. Sensitivity analysis carried out in this study shows that GMPEs and the catalogue compilation process have the biggest influence on the hazard for Johannesburg and

hence need to be carefully taken into consideration. The Coefficient of Variation (COV) values for most of the parameters analysed were above 0.1 meaning they need to be carefully determined and their uncertainty values need to be incorporated in the hazard computation through a logic tree approach. GMPEs have the highest COV values indicating that the choice of GMPE is the factor that introduces the largest uncertainty in the hazard assessment; followed by the source models, homogenisation, temporal variation of the catalogue, M_{max}, M_{min}, and bedrock velocity. The catalogue processing procedures (homogenisation, declustering and temporal stationarity) also are important factors that must be considered. Since geological and paleo-seismological information provided little to no information to the understanding of seismicity occurrence in the study region so far, the best tool available is the catalogue. Improved analysis of the catalogue will reduce associated uncertainties and hence improve the hazard estimates. All of these results show that a significant effort needs to be put into the determination or selection of these parameters and models.

CHAPTER 9: CONCLUSION

Seismic hazard analysis is a dynamic process, which requires regular updating with emerging new information. In this regard, a quest for new information is always there. However, in order to reduce costs, minimise labour and being redundant, efforts have to be focused on areas that are more influential to the final hazard. This study focused on assessing the uncertainties associated with various models and parameters in the seismic hazard analysis for Johannesburg. Various input parameters influencing the seismic hazard analysis for Johannesburg have been analysed and their influence investigated. The contribution of each parameter was computed through sensitivity analysis. Exhaustive analysis to identify and quantify epistemic uncertainties associated with the different parameters and methods involved in the computation procedure, have been a key issue of this work. The application of sensitivity feedback from the model parameters provided a useful tool to identify those parameters with a major influence on the final hazard, and allowed to reduce the number of possible branches in the logic tree. The epistemic uncertainties associated with studied SHA input parameters and models can therefore be taken into account in seismic hazard using a logic tree formalism. Several conclusions can be drawn from this study, which are very important for other seismic hazard analyses in the region and for decision makers. Sensitivity feedback resulted in a significant reduction in the number of possible branches of the logic tree. COV maps are used to represent both the sensitivity and the relative contribution to the overall uncertainty of each factor. Thus knowledge of the more influential input parameter can serve as a guide for future research to reduce uncertainty for these inputs and hence in the overall uncertainty in these calculations.

Sensitivity analysis results to evaluate the impact of other parameters (e.g. M_{max} and GMPEs) also clearly show that differences in these values results in significant changes to the hazard calculation. All of these results show that substantial effort needs to be put into the determination of these parameters. Most of the global parameters (e.g. GMPEs, seismic source delineation, catalogue compilation processes) affect the hazard because these parameters are not well constrained owing to lack of data.

In this case, the most influential parameter or model in our hazard is the GMPE. Selecting the inappropriate GMPE will certainly result in a wrong hazard assessment. To reduce the uncertainty associated with the selection of suitable GMPEs, ten GMPEs were identified and compared with a local dataset of ground motion to select a suit of GMPEs that could be assumed to fit the local data and thus this region. The comparisons showed that when GMPEs are based on a well assembled database and they are used within their range of validity they can correctly predict the ground motion parameters. The methodology adopted in this study is among the best established methods as of now

for this region. Effort will need to be made to continue assessing or to develop GMPEs for this region as suitable strong motion data from future moderate to large earthquakes are recorded.

Source model delineation is also noted to have a significant impact on the hazard and should be addresses carefully making use of all available information. If alternative reasonable models are available, they could all be implemented in the hazard calculation using a logic tree formalism (e.g. Bommer et al., 2015a; Midzi et al., 2020b). Source delineation may also result in redundant sources being used, which will increase the computation time but without affecting the hazard. Such sources can usually be excluded from the final hazard calculation.

Sensitivity analysis carried out in this study shows that the catalogue compilation processes also influences the hazard (e.g. the homogenisation of the catalogue). The current seismic catalogue for South Africa is characterised by has magnitudes determined using different local magnitude scales (Midzi et al., 2020a). Improved analysis of the catalogue reduces the uncertainty and hence improves the hazard estimates. Therefore, improvements in the current catalogue are essential, as we have highlighted in this study. The several catalogue processing methods done show that the present catalogue is short, not precise and falls short of the requirements needed as an input to SHA. However, most of the shortfalls can be overcome through certain robust assumptions.

The current catalogue is not exhaustive, especially for early instrumental and pre instrumental periods. Although efforts to improve the catalogue through the analysis of macroseismic data is ongoing, more information needs to be searched and incorporated for recurrence parameter calculations. The relocation of pre- and early-instrumental earthquakes was performed using the state of the art software in order to improve the quality and length of the catalogue (Manzunzu *et al. in press*). This was also observed to influence the final hazard calculations from sensitivity results. Therefore, more effort should be devoted in improving locations of the pre- and early-instrumental earthquakes.

Different magnitude scales have been used over the years for magnitude determination at CGS. Therefore careful analysis of the homogenisation process had to be followed. Efforts to try to minimise the uncertainties associated with the homogenisation process was made through the development of new conversion relations (Manzunzu et al., 2020). These relations took into consideration the temporal changes in the magnitude determination in the CGS database. This aspect in the catalogue completely ignored in most previous studies. Sensitivity analysis results show how important it is to correctly homogenise the catalogue, given the observed high COV values of greater than 0.3.

The declustering process was also extensively analysed in order to see if the catalogue resembles the fundamental requirement in seismic hazard analysis for a Poissonian distribution. Eight declustering methods were implemented to cater for the uncertainties associated with the process. Statistical analysis was done to test each declustered catalogue for Poissonian distribution. Of the eight declustering methods used, only the CLUSTER method implemented in SEISAN, Gardner and Knoppoff (1974) and the Grünthal (1985) techniques were statistically significant for Poissonian distribution. The latter two methods produced very similar catalogues, as was expected after reading the literature (e.g. Hainzl et al., 2006). Downstream usage of the compiled catalogue indicated many uncertainties, which resulted in the creation of 36 sets of recurrence parameters from different catalogues created for different uncertainties. These parameters were used in the sensitivity analysis. Results of sensitivity also showed that the recurrence parameters selected for use in seismic hazard analysis have profound influence on the hazard. Different methods for computing recurrence parameters were also observed to result in significantly different values, which influence the hazard. Different methodologies also used to determine M_{max}, produced significantly different values. The sensitivity study showed that varying M_{max} significantly resulted in substantial impact on the hazard.

A major task was to associate the seismicity to some geological phenomena. Though this was possible in general, the scatter in seismicity associated with poor locations especially of small events, makes this a difficult task (Midzi et al., 2020b). The sparsity of the South African National Seismograph Network (SANSN) resulted in large location errors of about 10 km. As a result, it was not possible to conclusively identify active faults that could be used as linear sources in the hazard assessment. Instead, area source zones were created using the seismicity locations and tectonic information. The use of large seismic source zones, made it possible to represent the conceptual model of the degree of stationarity of seismicity in a reproducible and simple way. It is necessary to continue obtaining relevant data and information to identify and characterise seismic sources, especially active faults.

The seismotectonic model also plays an important role in this study. It influenced the source delineation as well as the geometry of the seismic sources. However, reliable information for the characterisation of seismic sources comes mostly from the earthquake catalogue and some regional geology and geophysics that was useful in the delineation of areal sources. It is evident that South Africa behaves like a stable continental region (SCR) with intraplate earthquakes that vary spatially and temporally along complex ancient faults (Hartnady, 2002; Manzunzu et al., 2019). Although new data helped in the development of a new and comprehensive seismotectonic model, it has to be mentioned that the tectonic regimes in South Africa are complex and more information is still needed to delineate and fully characterise the sources.

The importance of collecting new information is emphasized in this study. Diffuse seismicity was used in hypotheses by previous proponent experts (e.g. du Plessis (1996), Hartnady (1996), Partridge, (1995)); however, seismicity is now far better described with new well-located seismic data. Such new information was used in this study to characterise the seismic sources. However, some of the newly available information (e.g. GPS data) does not necessarily improve the models or parameters used in the estimation of the hazard of Johannesburg. Interpretation of GPS data, provides of evidence of deformation in southern Africa; however, the rate of defomatiaon is very small, especially when compared to observations along the East African Rift System or at plate boundaries (Meghraoui et al., 2016; Stamps et al., 2018; Manzunzu et al., 2019).

9.1. Limitations

The present study has some limitations due to scarcity of records for active faults in the study region such as the fault geometry, rupture length, slip rates, etc. this information is helpful in estimating recurrence parameters, especially in regions with short catalogues like South Africa. Another major weakness of all seismic hazard studies in this region is the unavailability of a GMPE designed specifically for South Africa. More work needs to be done in order to understand the attenuation of ground motion in South Africa, which has been indicated as very influential from the sensitivity results. GMPEs need to be developed from local datasets that can be used in SHA. Ideally, it is necessary to have equations for the different sources of earthquakes in South Africa, induced events (mining related) and natural events (tectonic), as well as the different tectonic regimes (cratons and mobile belts). However, this lack of suitable GMPEs was addressed by adopting equations derived for tectonically similar regions especially regions with similar style of faulting.

It was noted that aftershock sequences for earthquakes in slowly deforming stable continents can be significantly longer than those in actively deforming regions (Stein and Liu, 2009; Allen et al., 2018; Lloyd et al., 2019; Shumba et al., 2020; Marimira et al., 2021). In these cases, it is reasonable to expect that aftershocks may continue to represent a non-zero contribution to the short-term hazard forecast. Given that aftershocks are still occurring well after the 2006 Machaze earthquake in Mozambique, should this region be effectively reduced to one earthquake for the purposes of PSHA? This is a question that provokes significant debate among seismologists and one that is difficult to address through standard PSHA processes.

Currently there is no agreed procedure for modelling seismic hazard for induced seismicity areas. This is an important question for South Africa, given that 90% of seismicity recorded in South Africa is from the mining regions. In classical SHA, this poses uncertainties in the assumption of Poissonian

distribution. It may be possible to make further improvements in the seismic hazard estimates by addressing these limitations for the chosen study region.

9.2. Recommendations

The present study concentrates on the sensitivity analysis due to variability in seismicity parameters, seismotectonics and ground motion models. Simplified seismotectonic models developed with the current available data were used to delineate seismic source zones. As future tasks, it is necessary to refine this study by introducing complex fault parameters as well as near-fault effects in the PSHA. Neotectonics within the Kaapvaal Craton needs to be well analysed in order to be understood since it is related to mining-induced activities, especially in the Witwatersrand Basin (Bird et al., 2006; Manzunzu et al., 2017). Analysis of micro-seismicity should be carried out on identified potential active faults to fully understand and delineate them.

In order to reduce the uncertainties due to the earthquake catalogue for Johannesburg, the catalogue may be improved in at least three ways. Firstly, continual and enhanced monitoring of earthquake activity into the future. In this regard, the CGS is making effort by installing cluster seismic networks for monitoring of seismicity in the mining regions; this will help overcome short periods of catalogue incompleteness at small magnitudes and improve our understanding of sources of earthquakes.

Second, some progress can be made by better understanding the sizes and locations of historical seismicity based on intensity reports, (e.g. Flint, 2017; Albini et al., 2014; Manzunzu et al., in press). These earthquakes are important in constraining M_{max} values and also identifying and confirming active faults. The inclusion of pre-historical as well as historical earthquakes is crucial. Instrumental recording of earthquakes in many regions of South Africa began only about 1970; therefore reliable recurrence parameters can be computed for the past 50 years only, which is far too short from typical recurrence rates of SCRs (Calais et al., 2016). A substantial amount of work was conducted as part of this study to evaluate historical seismicity (from 1870 to 1949) from macroseismic information. However, more information is still missing and needs to be determined in order to improve the catalogue.

Third, paleoseismic studies to identify and characterise active faults need to be conducted in order to push back in time our understanding of how often the largest, most damaging earthquakes have occurred during the late Quaternary. In other studies (e.g. Goedhart and Booth, 2016), paleoseismic results show potential magnitude M=8 in South Africa. These historical events are necessary in M_{max} computation as well as increasing the catalogue length. A reliable catalogue of historical earthquakes along with paleoseismological studies is essential to establish the seismic character of the region. The reliable information on the active faults and geodetic measurements of fault movement rates would

improve the present investigation further. Lastly, strong motion database for the region needs to be developed in order to develop GMPEs from local data. The CGS strong motion network needs to be expanded to tectonic regions throughout South Africa to cover the entire distances required in GMPE development.

REFERENCES

Abd el-aal, A.K., El-Eraki, M.A. and Mostafa, S.I., 2015. An extended stochastic method for seismic hazard estimation. *Natural Hazards and Earth System Sciences Discussions*, **3**, pp.7555-7586.

Abd el-aal, A.K., 2010. Modelling of seismic hazard at the northeastern part of greater Cairo metropolitan area, Egypt. *Journal of Geophysics and Engineering*, **7(1)**, pp.75-90.

Abd el-aal, A.K., 2008. Simulating time-histories and pseudo-spectral accelerations from the 1992 Cairo earthquake at the proposed El-Fayoum New City Site, Egypt. *Acta Geophysica*, **56(4)**, pp.1025-1042.

Abrahamson N.A., 2006. Seismic hazard assessment: Problems with current practice and future developments, *First European Conference on Earthquake Engineering and Seismology*, Geneva, Switzerland, 3-8 September 2006

Abrahamson, N.A., 2000. State of the practice of seismic hazard evaluation. In ISRM International Symposium. *International Society for Rock Mechanics*, Melbourne, Australia, 19 – 24 November 2000.

Abrahamson, N.A. and Bommer, J.J., 2005. Probability and uncertainty in seismic hazard analysis. *Earthquake Spectra*, **21(2)**, pp.603-607.

Abrahamson, N. and Silva, W., 2008. Summary of the Abrahamson & Silva NGA ground-motion relations. *Earthquake Spectra*, **24(1)**, pp.67-97.

Abrahamson, N.A. and Youngs, R.R., 1992. A stable algorithm for regression analyses using the random effects model. *Bulletin of the Seismological Society of America*, **82(1)**, pp.505-510.

Adams, A. and Nyblade, A., 2011. Shear wave velocity structure of the southern African upper mantle with implications for the uplift of southern Africa. *Geophysical Journal International*, **186**, 808 – 824.

Akkar, S., Sandıkkaya, M.A. and Bommer, J.J., 2014. Empirical ground-motion models for point-and extended-source crustal earthquake scenarios in Europe and the Middle East. *Bulletin of Earthquake Engineering*, **12(1)**, pp.359-387.

Akkar, S. and Bommer, J.J., 2007. Empirical prediction equations for peak ground velocity derived from strong-motion records from Europe and the Middle East. *Bulletin of the Seismological Society of America*, ***97*(2)**, pp.511-530. doi: 10.1785/0120060141.

Albarello, D., Camassi, R. and Rebez, A., 2001. Detection of space and time heterogeneity in the completeness of a seismic catalog by a statistical approach: an application to the Italian area. *Bulletin of the Seismological Society of America*, ***91*(6)**, pp.1694-1703.

Albini, P., Strasser, F.O. and Flint, N.S., 2014. Earthquakes from 1820 to 1936 in Grahamstown and surroundings (Eastern Cape Province, South Africa). *Bulletin of Earthquake Engineering*, ***12*(1)**, pp.45-78, doi: 10.1007/s10518-013-9562-0

Albini, P., 2012. Investigating the past seismicity of the Eastern Cape Province, South Africa. Report 2012-0099, *Rev.0, Council for Geoscience*, Pretoria, South Africa, pp 453.

Allen, T.I., Griffin, J.D., Leonard, M., Clark, D.J. and Ghasemi, H., 2020. The 2018 national seismic hazard assessment of Australia: Quantifying hazard changes and model uncertainties. *Earthquake Spectra*, ***36*(1_suppl)**, pp.5-43.

Allen, T.I., 2012. *Stochastic ground-motion prediction equations for southeastern Australian earthquakes using updated source and attenuation parameters*. Record 2012/69, Geoscience Australia: Canberra.

Allen, T., Griffin, J. and Clark, D. 2018. *The 2018 National Seismic Hazard Assessment for Australia: model input files*. Record 2018/32. Geoscience Australia, Canberra. http://dx.doi.org/10.11636/Record.2018.032

Algermissen, S.T., Perkins, D.M., Thenhaus, P.C., Hanson, S.L. and Bender, B.L., 1982. *Probabilistic estimates of maximum acceleration and velocity in rock in the contiguous United States* (No. 82-1033). US Geological Survey,.

Amante, C. and Eakins, B.W., 2009. ETOPO1 Global Relief Model converted to PanMap layer format. *NOAA-National Geophysical Data Center, doi*, *10*. doi:10.7289/V5C8276M

Ambraseys, N.N., Douglas, J., Sarma, S.K., and Smit, P.M., 2005. Equations for the estimation of strong ground motions from shallow crustal earthquakes using data from Europe and the Middle East: horizontal peak ground acceleration and spectral acceleration, *Bulletin of the Earthquake Engineering*, **3,** pp.1–53.

Ambraseys, N.N. and Adams, R.D. 1991. Reappraisal of major African earthquakes, south of 20°N, 1900-1930. *Natural Hazards* **4**, pp.389-419.

Ambraseys, N.N. and Adams, R.D., 1992. Reappraisal of major African earthquakes, south of 20°N, 1900-1930. *Tectonophysics* **209**, pp.293-296.

Amorese, D., 2007. Applying a change-point detection method on frequency-magnitude distributions. *Bulletin of the Seismological Society of America*, ***97*(5)**, pp.1742-1749.

Amponsah, P.E., Banoeng-Yakubo, B.K., Panza, G.F. and Vaccari, F., 2009. Deterministic seismic ground motion modelling of the greater Accra metropolitan area, southeastern Ghana. *South African Journal of Geology*, *112***(3-4)**, pp.317-328. doi: 10.2113/gssajg.112.3-4.317.

Anagnos, T. and Kiremidjian, A.S., 1988. A review of earthquake occurrence models for seismic hazard analysis. *Probabilistic Engineering Mechanics*, **3(1).**

Anderson, J.G., 1979. Estimating the seismicity from geological structure for seismic-risk studies. *Bulletin of the Seismological Society of America*, ***69*(1)**, pp.135-158.

Anderson, J.G., Wesnousky, S.G. and Stirling, M.W., 1996. Earthquake size as a function of fault slip rate. *Bulletin of the Seismological Society of America*, ***86*(3)**, pp.683-690.

Andreoli, M.A.G., Doucouré, M., Van Bever Donker, J., Brandt, D. and Andersen, N.J.B., 1996. Neotectonics of southern Africa – a review. *African Geoscience Review,* **3**, pp. 1-16.

Armitage, P., McDonald, I. and Tredoux, M., 2007. A geological investigation of the Waterberg hydrothermal platinum deposit, Mookgophong, Limpopo Province, South Africa. *Applied Earth Science, **116*(3)**, pp.113-129.

Ansal, A., Erdik, M., Studer, J., Springman, S.M., Laue, J., Buchheister, J., Giardini, D., Faeh, D. and Köksal, D., 2004. Seismic microzonation for earthquake risk mitigation in Turkey. In *13th World Conference on Earthquake Engineering, Vancouver, BC,* Canada, August 1-6, 2004.

Ansal, A., Tonuk, G., 2007. Source and site factors in microzonation. *In: Pitilakis, K.D.(Ed.), Earthquake Geotechnical Engineering, 4th International Conference on Earthquake Geotechnical Engineering-Invited Lectures,* pp. 73–92.

Ares, A.F. and Fatehi, A., 2013. Development of probabilistic seismic hazard analysis for international sites, challenges and guidelines. *Nuclear Engineering and Design*, ***259***, pp.222-229.

Assatourians, K. and Atkinson, G.M., 2013. EqHaz: An open-source probabilistic seismic-hazard code based on the Monte Carlo simulation approach. *Seismological Research Letters*, ***84*(3)**, pp.516-524.

Atik, L.A. and Youngs, R.R., 2014. Epistemic uncertainty for NGA-West2 models. *Earthquake Spectra, **30*(3)**, pp.1301-1318.

Atkinson, G.M., 2015. Ground-motion prediction equation for small-to-moderate events at short hypocentral distances, with application to induced-seismicity hazards. *Bulletin of the Seismological Society of America, **105*(2A)**, pp.981-992.

Atkinson, G.M., 2008. Ground-motion prediction equations for eastern North America from a referenced empirical approach: Implications for epistemic uncertainty, *Bulletin of the Seismological Society of America,* **98(3),** pp.1304–1318, doi: 10.1785/0120070199.

Atkinson, G.M., 2004. Empirical attenuation of ground-motion spectral amplitudes in south eastern Canada and the north eastern United States, *Bulletin of the Seismological Society of America,* **94,** pp.1079-1095.

Atkinson, G.M. and Boore, D.M., 2011. Modifications to existing ground-motion prediction equations in light of new data. *Bulletin of the Seismological Society of America*, **101(3)**, pp.1121-1135.

Atkinson, G.M. and Boore, D.M., 2006. Earthquake ground-motion prediction equations for eastern North America. *Bulletin of the Seismological Society of America, **96*(6)**, pp.2181-2205. doi: 10.1785/0120050245.

Atkinson, G.M. and Charlwood, R.G., 1983. Uncertainties in probabilistic seismic hazard assessment as a function of probability level: A case history for Vancouver, British Columbia. *Bulletin of the Seismological Society of America, **73*(4)**, pp.1225-1241.

Baiesi, M. and Paczuski, M., 2004. Scale-free networks of earthquakes and aftershocks. *Physical Review E*, ***69*(6)**, p.066106.

Bakun, W.H. and Wentworth, C.M., 1997. Estimating earthquake location and magnitude from seismic intensity data. *Bulletin of the Seismological Society of America* **87(6)**, 1502-1521.

Baker, J.W., 2008. An introduction to probabilistic seismic hazard analysis (PSHA). *White paper, version*, **1**, p.72.

Balan S.F., Bala A., Ritter J.R.R., Hannich D., Hubber G. and Rohn J., 2007. Geotechnical laboratory tests for microzonation of Bucharest, *International Symposium on Strong Vrancea Earthquakes and Risk Mitigation*, Bucharest, Romania, 4-6 October 2007

Barani, S., Spallarossa, D., Bazzurro, P. and Eva, C., 2007. Sensitivity analysis of seismic hazard for Western Liguria (North Western Italy): a first attempt towards the understanding and quantification of hazard uncertainty. *Tectonophysics*, ***435*(1-4)**, pp.13-35.

Barton E.S., Barton J.M., Callow M.J., Allsopp H.L., Evans I.B. and Welke H.J., 1986. Emplacement ages and implications for the source region of granitoid rocks associated with the Witwatersrand basin, Abstract Geocongress 86, *Geological Society of South Africa*, Johannesburg.

Basson I.J., 2019. Cumulative deformation and original geometry of the Bushveld Complex, *Tectonophysics*, **750**, pp.177–202.

Bayraktarli, Y.Y., Baker, J.W. and Faber, M.H., 2011. Uncertainty treatment in earthquake modelling using Bayesian probabilistic networks. *GeoRisk*, ***5*(1)**, pp.44-58.

Beach, A., Smith, R., 2007. Structural geometry and development of the Witwatersrand Basin, South Africa. In: Ries, A.C., Butler, R.W.H., Graham, R.H. (Eds.), Deformation of the Continental Crust: The Legacy of Mike Coward: *Geological Society, London, Special Publications*, **272**, pp. 533–542

Beauval, C. and Scotti, O., 2004. Quantifying sensitivities of PSHA for France to earthquake catalog uncertainties, truncation of ground-motion variability and magnitude limits. *Bulletin of the Seismological Society of America*, **94(5)**, pp.1579-1594.

Beauval, C., Yepes, H., Palacios, P., Segovia, M., Alvarado, A., Font, Y., Aguilar, J., Troncoso, L. and Vaca, S., 2013. An earthquake catalog for seismic hazard assessment in Ecuador. *Bulletin of the Seismological Society of America*, ***103*(2A)**, pp.773-786.

Bender, B. and Campbell, K.W., 1989. A note on the selection of minimum magnitude for use in seismic hazard analysis. *Bulletin of the Seismological Society of America,* ***79*(1)**, pp.199-204.

Bender, B.K. and Perkins, D.M., 1993. Treatment of parameter uncertainty and variability for a single seismic hazard map. *Earthquake Spectra*, ***9*(2)**, pp.165-195.

Bernreuter, D.L., Savy, J.B., Mensing, R.W., Chen, J.C. and Davis, B.C., 1985. *Seismic hazard characterization of the eastern United States. Volume 1. Methodology and results for ten sites* (No. UCID-20421-Vol. 1). Lawrence Livermore National Lab., CA (USA).

Bird, P., Ben-Avraham, Z., Schubert, G., Andreoli, M. and Viola, G., 2006. Patterns of stress and strain rate in southern Africa, *Journal of Geophysical Research*, **111**, B08402, doi:10.1029/2005JB003882.

Bommer, J.J., 2002. Deterministic vs. probabilistic seismic hazard assessment: an exaggerated and obstructive dichotomy. *Journal of Earthquake Engineering*, **6(spec01)**, pp.43-73.

Bommer, J.J., 2003. Uncertainty about the uncertainty in seismic hazard analysis. *Engineering Geology*, **70(1-2)**, pp.165-168. doi: 10.1016/S0013-7952(02)00278-8.

Bommer, J.J. and Akkar, S., 2012. Consistent source-to-site distance metrics in ground-motion prediction equations and seismic source models for PSHA. *Earthquake Spectra*, ***28*(1)**, pp.1-15.

Bommer, J.J., Akkar, S. and Kale, Ö., 2011. A model for vertical-to-horizontal response spectral ratios for Europe and the Middle East. *Bulletin of the Seismological Society of America* **101**(4), pp.1783-1806.

Bommer, J.J., Coppersmith, K.J., Coppersmith, R.T., Hanson, K.L., Mangongolo, A., Neveling, J., Rathje, E.M., Rodriguez-Marek, A., Scherbaum, F., Shelembe, R., Stafford, P.J. and Strasser, F.O., 2015a. A SSHAC Level 3 Probabilistic Seismic Hazard Analysis for a New-Build Nuclear Site in South Africa, *Earthquake Spectra*, **31(2)**, pp.661–698.

Bommer, J.J., Crowley, H. and Pinho, R., 2015b. A risk-mitigation approach to the management of induced seismicity. *Journal of Seismology*, **19(2),** pp.623-646.

Bommer, J.J. and Crowley, H., 2017. The purpose and definition of the minimum magnitude limit in PSHA calculations. *Seismological Research Letters*, **88(4)**, pp.1097-1106.

Bommer, J.J. and Scherbaum, F., 2008. The use and misuse of logic trees in probabilistic seismic hazard analysis. *Earthquake Spectra*, ***24*(4)**, pp.997-1009.

Bommer, J.J., Douglas, J., Scherbaum, F., Cotton, F., Bungum, H., Fäh, D., 2010. On the selection of ground-motion prediction equations for seismic hazard analysis. *Seismological Research Letters*, **81(5),** pp.783–793.

Bommer, J.J., Douglas, J. and Strasser, F.O., 2003. Style-of-faulting in ground-motion prediction equations. *Bulletin of Earthquake Engineering*, **1(2)**, pp.171-203.

Bommer J.J., Scherbaum F., Bungum H., Cotton F., Sabetta F. and Abrahamson N.A., 2005. On the use of logic trees for ground motion prediction equations. *Bulletin of the Seismological Society of America*, **95(2)**, pp.377-389. doi: 10.1785/0120040073.

Bommer, J.J. and Strasser, F. O., 2011. Seismic Hazard Sensitivity Analyses for the Thyspunt Site, South Africa: Analysis of sensitivity of hazard at longer response periods due to the east African rift and other distant sources. Pretoria.

Bommer, J.J., Strasser, F.O., Pagani, M., and Monelli, D., 2013. Quality assurance for logic-tree implementation in probabilistic seismic hazard analysis for nuclear applications: A practical example, *Seismological Research Letters,* **84**, pp.938–945.

Bonilla, M.G., Mark, R.K. and Lienkaemper, J.J., 1984. Statistical relations among earthquake magnitude, surface rupture length, and surface fault displacement. *Bulletin of the Seismological Society of America, **74*(6)**, pp.2379-2411.

Boore, D.M., Stewart, J.P., Seyhan, E. and Atkinson, G.M., 2014. NGA-West2 equations for predicting PGA, PGV, and 5% damped PSA for shallow crustal earthquakes. *Earthquake Spectra,* **30(3)**, pp.1057-1085.

Boore, D.M., 2003. Simulation of ground motion using the stochastic method. *Pure and applied geophysics*, **160(3-4)**, pp.635-676.

Boore, D.M. and Atkinson, G.M., 2008. Ground-motion prediction equations for the average horizontal component of PGA, PGV, and 5%-damped PSA at spectral periods between 0.01s and 10.0 s. *Earthquake Spectra,* **24(1),** pp.99–138.

Boore, D.M. and Joyner, W.B., 1982. The empirical prediction of ground motion. *Bulletin of the Seismological Society of America, **72*(6B)**, pp.S43-S60.

Booth, P.W.K., Brunsdon G. and Shone, R.W., 2004. A Duplex Model for the Eastern Cape Fold Belt? Evidence from the Palaeozoic Witteberg and Bokkeveld Groups (Cape Supergroup), Near Steytlerville, South Africa, *Gondwana Research*, **7,** pp.211 - 222.

Bormann, P., 2002. IASPEI New Manual of Seismological Observatory Practice (NMSOP). *Geo Forschuags Zentrum Potsdam*, **1(3)**, pp.30-33.

Bowers, D., 1997. The October 30, 1994, seismic disturbance in South Africa: Earthquake or large rock burst? *Journal of Geophysical Research* **102(B5)**, 9843-9857.

Boyd, O.S., 2012. Including foreshocks and aftershocks in time-independent probabilistic seismic-hazard analyses. *Bulletin of the Seismological Society of America,* **102(3)**, pp.909-917.

Brandl G., 1995. Reactivation of certain faults in the Limpopo Belt during Quaternary. Extended Abstract, *Geological Society of South Africa*, Johannesburg, pp.442-444.

Brandt, M.B.C., 2019. Performance of the South African National Seismograph Network from October 2012 to February 2017: spatially varying magnitude completeness. *South African Journal of Geology,* **122(1)**, pp.57-68.

Brandt, M.B.C., 2014. Focal depths of South African earthquakes and mine events. *Journal of the Southern African Institute of Mining and Metallurgy,* **114(10)**, pp.855-862.

Brandt M.B.C. 2008. Review of the seismotectonic provinces and major structures in South Africa with new data, *Council for Geoscience, Report Number 2008-0001*, Pretoria, South Africa.

Brandt, M.B.C., 1997. Implementation of the SEISAN earthquake analysis software for the SUN to analyze the data obtained through the South African National Seismograph Network. *Council for Geoscience, Report CGS 1997-0263*, Pretoria, South Africa.

Brandt, M.B.C., Bejaichund, M., Kgaswane, E.M., Hattingh, E., and Roblin, D.L., 2005. Seismic history of South Africa. *Seismological Series 37, Council for Geoscience*, Pretoria, South Africa.

Brandt, M.B.C. and Saunders, I., 2011a. New regional moment tensors in South Africa. *Seismological Research Letters* **82(1)**, pp.69-80.

Brandt, M.B.C. and Saunders, I., 2011b. Monitoring Seismicity in the Central Rand – Water Ingress related seismicity. *Council for Geoscience, Report CGS 20110-0019*, Pretoria, South Africa.

Brandt, M.B., Grand, S.P., Nyblade, A.A. and Dirks, P.H., 2012. Upper mantle seismic structure beneath Southern Africa: Constraints on the buoyancy supporting the African superswell. *Pure and applied geophysics*, **169(4)**, pp.595-614.

Brandt, M.B., 2012. Middle mantle seismic structure of the African superplume. *Pure and Applied Geophysics*, **170(5)**, pp.845-861. DOI:10.1007/s00024-012-0589-y.

Budnitz, R.J., Apostolakis, G., Boore, D.M., Cluff, L.S., Coppersmith, K.J., Cornell, C.A. and Morris, R.A., 1997a. *Recommendations for probabilistic seismic hazard analysis: guidance on uncertainty and use of experts* (No. NUREG/CR-6372-Vol. 1; UCRL-ID-122160). Nuclear Regulatory Commission, Washington, DC (United States). Div. of Engineering Technology; Lawrence Livermore National Lab., CA (United States); Electric Power Research Inst., Palo Alto, CA (United States); USDOE, Washington, DC (United States).

Budnitz, R.J., Apostolakis, G., Boore, D.M., Cluff, L.S., Coppersmith, K.J., Cornell, C.A. and Morris R.A., 1997b. *Recommendations for probabilistic seismic hazard analysis: Guidance on uncertainty and use of experts* (No. NUREG/CR--6372-VOL. 2). Nuclear Regulatory Commission.

Bulajic, B. and Manic, M., 2006. Selection of the appropriate methodology for the deterministic seismic hazard assessment on the territory of the Republic of Serbia. *Facta universitatis-series: Architecture and Civil Engineering*, ***4*(1)**, pp.41-50.

Burke, K., 1996. The African plate. *South African Journal of Geology*, **99**, pp.341-409.

Burkhard, M. and Grünthal, G., 2009. Seismic source zone characterization for the seismic hazard assessment project PEGASOS by the Expert Group 2 (EG1b). *Swiss Journal of Geosciences*, **102(1)**, pp.149-188.

Calais, E., Camelbeeck, T., Stein, S., Liu, M. and Craig, T.J., 2016. A new paradigm for large earthquakes in stable continental plate interiors. *Geophysical Research Letters*, **43(20)**, pp.10-621.

Calais, E., Freed, A.M., Van Arsdale, R. and Stein, S., 2010. Triggering of New Madrid seismicity by late-Pleistocene erosion. *Nature*, **466(7306)**, pp.608-611.

Calais, E., Ebinger, C., Hartnady, C. and Nocquet, J.M., 2006. Kinematics of the East African Rift from GPS and earthquake slip vector data. *Geological Society, London, Special Publications*, **259(1)**, pp.9-22.

Calais, E., Mattioli, G., DeMets, C., Nocquet, J.M. and Stein, S. 2005. Tectonic strain in plate interiors? *Nature Geoscience*, **438**, E9–E10.

Campbell, K.W., 2014. An evaluation of eastern North American ground-motion models developed using the hybrid empirical method. *Bulletin of the Seismological Society of America*, **104(1)**, pp.347-359.

Campbell, K.W., 2003. Prediction of strong ground motion using the hybrid empirical method and its use in the development of ground-motion (attenuation) relations in eastern North America. *Bulletin of the Seismological Society of America*, **93(3)**, pp.1012-1033.

Campbell, M.J., Machin, D., and Walters, S. J. 2010. *Medical statistics: a textbook for the health sciences.* John Wiley & Sons.

Cao, A. and Gao, S.S., 2002. Temporal variation of seismic b-values beneath north-eastern Japan island arc. *Geophysical research letters*, **29(9)**, pp.48-1.

Castanos, H. and Lomnitz, C., 2002. PSHA: is it science? *Engineering Geology*, **66**, pp.315-317.

Castellaro, S., Mulargia, F. and Kagan, Y.Y., 2006. Regression problems for magnitudes. *Geophysical Journal International*, ***165*(3)**, pp.913-930.

Catuneanu, O. and Eriksson, P.G., 1999. The sequence stratigraphic concept and the Precambrian rock record: an example from the 2.3-2.1 Ga Pretoria Group, Kaapvaal craton. *Precambrian Research*, **97**, pp.215-251.

Charlesworth, E.G. and McCarthy, T.S., 1990. Structural aspects of the eastern part of the Rietfontein fault system, *South African Journal of Geology*, **93,** pp.211–223.

Chiou, B.J. and Youngs, R.R., 2008. An NGA model for the average horizontal component of peak ground motion and response spectra. *Earthquake Spectra*, **24(1)**, pp.173-215.

Chouinard, L. and Rosset, P., 2007. Seismic site effects and seismic risk in Montreal area- the influence of Marine clays, *9th Canadian Conference on Earthquake Engineering*, Ontario, Canada, 26-29 June 2007.

Chow, R. A. C., Fairhead, J. D., Henderson, N.B., and Marshall, P.D., 1980. Magnitude and Q determinations in southern Africa using Lg wave amplitudes. *Geophysical Journal of the Royal Astronomical Society*, **63**, 735-745.

Chunnett, G.K. and Rompel, A.K.K., 2004. Data integration for structural interpretation in the Bushveld Complex. In *International Platinum Conference "Platinum Adding Value,"* Sun City, South Africa, pp. 265-268. October 2004.

Cichowicz, A., Kgaswane, E., van Aswegen, G., Adamos, P., Birch, D., Jele, V., Kometsi, R., Prasad, K., Saunders I., Strasser, F., Tabane, L., and Zulu, B., 2010. Monitoring Seismicity in the Central Rand and East Rand Goldfield – Mine-Flooding Induced Seismicity Part of Strategic Water-Management Project. *Report Number CGS 2010-0056. Council for Geoscience.*

Coppersmith, K. J. and Youngs, R.R., 1986. Capturing uncertainty in probabilistic seismic hazard assessments within interpolate tectonic environments, *Third U.S. National Conference on Earthquake Engineering*, Charleston, South Carolina, USA, August 24-28, 1986

Coppersmith, K.J., Youngs, R.R. and Sprecher, C., 2009. Methodology and main results of seismic source characterization for the PEGASOS Project, Switzerland. *Swiss Journal of Geosciences*, **102(1)**, pp.91-105.

Cornell, D.H., Van Schijndel, V., Ingolfsson, O., Scherstén, A., Karlsson, L., Wojtyla, J. and Karlsson, K., 2011. Evidence from Dwyka tillite cobbles of Archaean basement beneath the Kalahari sands of southern Africa. *Lithosphere*, **125(1-2)**, pp.482-502.

Coward, M.P., 1976. A Discussion on natural strain and geological structure-Archaean deformation patterns in southern Africa. *Philosophical Transactions of the Royal Society of London. Series A, Mathematical and Physical Sciences*, ***283*(1312)**, pp.313-331.

Cornell, D.H., Van Schijndel, V., Ingolfsson, O., Scherstén, A., Karlsson, L., Wojtyla, J. and Karlsson, K., 2011. Evidence from Dwyka tillite cobbles of Archaean basement beneath the Kalahari sands of southern Africa. *Lithosphere*, **125(1-2),** pp.482 - 502.

Cornell, C.A., and Van Marke, E.H., 1969. The major influence on seismic risk. *Proceedings of the Third Conference on Earthquake Engineering*. Santiago, Chile.V: A-1, 69-93.

Cornell, C.A., 1968. Engineering seismic risk analysis. *Bulletin of the Seismological Society of America*, **58(5)**, pp.1583-1606.

Cornell, C.A. and Winterstein, S.R., 1988. Temporal and magnitude dependence in earthquake recurrence models. *Bulletin of the Seismological Society of America*, **78(4),** pp.1522-1537.

Costa, G., Panza, G.F., Suhadolc, P. and Vaccari, F., 1993. Zoning of the Italian territory in terms of expected peak ground acceleration derived from complete synthetic seismograms. *Journal of Applied Geophysics*, **30(1-2)**, pp.149-160.

Cotton, F., Pousse, G., Bonilla, F. and Scherbaum, F., 2008. On the discrepancy of recent European ground-motion observations and predictions from empirical models: Analysis of KiK-net accelerometric data and point-sources stochastic simulations. *Bulletin of the Seismological Society of America*, **98(5)**, pp.2244-2261.

Cotton, F., Scherbaum, F., Bommer, J.J. and Bungum, H., 2006. Criteria for selecting and adjusting ground-motion models for specific target regions: Application to central Europe and rock sites. *Journal of Seismology*, **10(2),** pp.137-156.

Cramer, C.H., 2001a. The New Madrid seismic zone: capturing variability in seismic hazard analyses. *Seismological Research Letters*, **72(6)**, pp.664-672.

Cramer C.H., 2001b. A seismic hazard uncertainty analysis for the New Madrid seismic zone, *Engineering Geology*, **62,** pp. 251 – 266

Cramer C.H., 2002. Uncertainty analysis for seismic hazard in the Southern Illinois Basin, *Seismological Research Letters*, **73(5**), pp.92- 805.

Cramer, C.H., Petersen, M.D. and Reichle, M.S., 1996. A Monte Carlo approach in estimating uncertainty for a seismic hazard assessment of Los Angeles, Ventura, and Orange Counties, California. *Bulletin of the Seismological Society of America*, **86(6)**, pp.1681-1691.

Cramer, C.H., Petersen, M.D., Cao, T., Toppozada, T.R. and Reichle, M., 2000. A time-dependent probabilistic seismic-hazard model for California. *Bulletin of the Seismological Society of America*, **90(1)**, pp.1-21.

Crowley, H., Bommer, J.J., Pinho, R. and Bird, J., 2005. The impact of epistemic uncertainty on an earthquake loss model. *Earthquake Engineering and Structural Dynamics*, **34(14)**, pp.1653-1685.

Crow, C. and Condie, K.C., 1988. Geochemistry and origin of Late Archaean volcanics from the Ventersdorp Supergroup, South Africa. *Precambrian Research*, **42**, pp.19–37.

Dankert, B.T., Hein, K.A.A., 2010. Evaluating the structural character and tectonic history of the Witwatersrand Basin. *Precambrian Research*, **177**, pp.1–22.

Davies, N. and Kijko, A., 2003. Seismic risk assessment: with an application to the South African insurance industry. *South African Actuarial Journal*, **3(1)**, pp.1-28.

De Klerk, W.J. and Reed, J. S., 1988. An account of historical seismic activity in southern Africa with emphasis on the southern and eastern Cape. Report, *Albany Museum*, Grahamstown, South Africa.

Deichmann, N., 2006. Local magnitude, a moment revisited. *Bulletin of the Seismological Society of America*, **96(4A)**, pp.1267-1277.

Delavaud, E., Scherbaum, F., Kuehn, N., and Riggelsen, C., 2009. Information−theoretic selection of ground-motion prediction equations for seismic hazard analysis: An applicability study using Californian data, *Bulletin of the Seismological Society of America*, **99(6)**, pp.3248−3263.

Delvaux D. and Barth, A., 2010. African stress pattern from formal inversion of focal mechanism data, *Tectonophysics*, **482**, pp.105–128.

DeMets, C., Gordon, R.G. and Argus, D.F., 2010. Geologically current plate motions. *Geophysical Journal International,* **181(1)**, pp.1-80.

Dennison, P. I. G. and van Aswegen, G. 1993. Stress modelling and seismicity on the Tanton fault: A case study in a South African gold mine. *In* "Rockbursts and Seismicity in Mines" (R.P. Young, ed.). *Balkema, Rotterdam,* 327 – 335.

Deniz, A., 2006. *Estimation of earthquake insurance premium rates for Turkey*. M.Sc. Thesis, Department of Civil Engineering, METU, Yüksek Lisans Tezi, ODTÜ, Fen Bilimleri Enstitüsü.

Der Kiureghian, A. and Ditlevsen, O., 2009. Aleatory or epistemic? Does it matter? *Structural Safety*, **31(2)**, pp.105-112.

de Wit M.J. and Ransome I.G.D., 1992. Inversion Tectonics of the Cape Fold Belt, Karoo and Cretaceous Basins of Southern Africa, *Balkema, Rotterdam,* Netherlands.

De Wit, M.J., De Ronde, C.E.J., Tredoux, M., Roering, C., Hart, R.J., Armstrong, R.A., Green, R.W.E., Peberdy, E. and Hart, R.A., 1992. Formation of an Archaean continent. *Nature,* **357**, pp.553–562.

Dhansay, T., Musekiwa, C., Ntholi, T., Chevallier, L., Cole, D. and De Wit, M.J., 2017. South Africa's geothermal energy hotspots inferred from subsurface temperature and geology. *South African Journal of Science,* **113(11-12)**, pp.1-7.

Dor, O., Reches, Z. and van Aswegen, G., 2001. Fault Zones Associated with Matjhabeng Earthquake, 1999, South Africa. *Proceedings of the 5th International Symposium on Rockbursts and Seismicity in Mines (RaSiM5).* Johannesburg, South Africa.

Douglas, J., 2018. *Ground motion prediction equations,* 1964-2018, http://www.gmpe.org.uk.

Douglas, J., 2016. *Ground motion prediction equations,* 1964-2014, http://www.gmpe.org.uk.

Douglas, J., 2011. *Ground-motion prediction equations*, 1964–2010, BRGM/RP-59356-FR, 444 pages, 9 illustrations.

Douglas, J., 2010. *Estimation of strong ground motion: Aleatory variability and epistemic uncertainties.* PhD thesis, Université Joseph-Fourier-Grenoble I.

Douglas, J., 2003. Earthquake ground motion estimation using strong-motion records: a review of equations for the estimation of peak ground acceleration and response spectral ordinates. *Earth-Science Reviews,* **61(1-2)**, pp.43-104.

Douglas, J., 2001. *A comprehensive worldwide summary of strong-motion attenuation relationships for peak ground acceleration and spectral ordinates (1969 to 2000).* Imperial College of Science, Technology and Medicine, Civil Engineering Department.

Douglas, J., Bungum, H. and Scherbaum, F., 2006. Ground-motion prediction equations for southern Spain and southern Norway obtained using the composite model perspective. *Journal of Earthquake Engineering*, **10(01),** pp.33-72.

Douglas, J., Cotton, F., Di Alessandro, C., Boore, D.M., Abrahamson, N.A. and Akkar, S., 2012. Compilation and critical review of GMPEs for the GEM-PEER Global GMPEs Project. In *15th World Conference on Earthquake Engineering: 15th WCE.* September 2012.

Douglas, J., Cotton, F., Abrahamson, N.A., Akkar, S., Boore, D.M. and Di Alessandro, C., 2011. Pre-selection of ground motion prediction equations. *Report Produced in Context of GEM GMPE Project, Version: 1.0*.

Douglas, J., Edwards, B., Convertito, V., Sharma, N., Tramelli, A., Kraaijpoel, D., Cabrera, B.M., Maercklin, N. and Troise, C., 2013. Predicting ground motion from induced earthquakes in geothermal areas. *Bulletin of the Seismological Society of America***, 103(3)**, pp.1875-1897.

Douglas, J., Akkar, S., Ameri, G., Bard, P.Y., Bindi, D., Bommer, J.J., Bora, S.S., Cotton, F., Derras, B., Hermkes, M. and Kuehn, N.M., 2014. Comparisons among the five ground-motion models developed using RESORCE for the prediction of response spectral accelerations due to earthquakes in Europe and the Middle East. *Bulletin of Earthquake Engineering*, **12(1)**, pp.341-358.

Douglas, J., Bungum, H. and Scherbaum, F., 2006. Ground-motion prediction equations for southern Spain and southern Norway obtained using the composite model perspective. *Journal of Earthquake Engineering*, **10(01)**, pp.33-72.

du Plessis, A., 1996. Seismicity in South Africa and its Relationship to the Geology of the Region. *CGS Report No. 1996-0019*. (One (1) tube containing the 11 maps associated with this report).

Durrheim, R.J., Anderson, R.L., Cichowicz, A., Ebrahim-Trollope, R., Hubert, G., Kijko, A., McGarr, A., Ortlepp, W.D. and Van der Merwe, N., 2006. *Investigation into the risks to miners, mines, and the public associated with large seismic events in gold mining districts (Vol.1)*. Department of Minerals and Energy, p.50.

Durrheim, R.J. and Mooney, W.D., 1994. Evolution of the Precambrian lithosphere: seismological and geochemical constraints. *Journal of Geophysical Research: Solid Earth*, **99(B8)**, pp.15359-15374.

Durrheim, R.J. and K.L. Riemer, 2016. The history of mining seismology. In De Beer, J.H. ed., 2016. *The History of Geophysics in Southern Africa*. AFRICAN SUN MeDIA.

Dziewonski, A.M., Ekström, G., Woodhouse, J.H. and Zwart, G., 1991. Centroid-moment tensor solutions for July–September 1990. *Physics of the Earth and Planetary Interiors*, **67**, pp.211–220.

Dziewonski, A.M., Ekström, G., Woodhouse, J.H., and Zwart, G., 1987. Centroid-moment tensor solutions for October-December 1986. *Physics of the Earth and Planetary Interiors* **48**, pp.5–17.

Ebel, J.E., 2009. Analysis of aftershock and foreshock activity in stable continental regions: Implications for aftershock forecasting and the hazard of strong earthquakes. *Seismological Research Letters*, **80**(6), pp.1062-1068.

Ebel, J.E. and Kafka, A.L., 1999. A Monte Carlo approach to seismic hazard analysis. *Bulletin of the Seismological Society of America*, **89(4)**, pp.854-866.

Eglington, B.M., 2006. Evolution of the Namaqua-Natal Belt, southern Africa – A geochronological and isotope geochemical review. *Journal of African Earth Sciences*, **46(1-2)**, pp.93-111.

Electric Power Research Institute (EPRI), 2004. *CEUS Ground Motion Project Final Report*, EPRI Report number1009684, Palo Alto, California.

Electric Power Research Institute (EPRI), 1986. *Seismic Hazard Methodology for the Central and Eastern United States*, Vol. 1: Methodology. EPRI Report number NP-4726, Palo Alto, California.

Ellingwood, B.R. and Kinali, K., 2009. Quantifying and communicating uncertainty in seismic risk assessment. *Structural Safety*, ***31*(2)**, pp.179-187.

Enescu, B., Enescu, D. and Ito, K., 2011. Values of b and p: their variations and relation to physical processes for earthquakes in Japan and Romania. *Romanian Journal of Physics*, **56(3-4)**, pp.590-608.

Epstein, B. and Lomnitz, C., 1966. A model for the occurrence of large earthquakes. *Nature*, **211(5052)**, p.954.

Eriksson, P.G., Hattingh, P.J. and Altermann, W., 1995. An overview of the geology of the Transvaal Sequence and Bushveld Complex, South Africa. *Mineralium Deposita*, **30(2)**, pp.98-111.

Eriksson, P.G. and Altermann, W., 1998. An overview of the geology of the Transvaal Supergroup dolomites (South Africa). *Environmental geology*, **36(1-2)**, pp.179-188.

Eriksson, P.G., Bose, P.K., Catuneanu, O., Sarkar, S. and Banerjee, S., 2008. Precambrian clastic epeiric embayments: examples from South Africa and India. In *Dynamics of epeiric seas*, Geological Association of Canada, **48**, pp.119-136.

Eriksson, P. G. and Clendenin, C.W., 1990. A review of the Transvaal Sequence, South Africa. *Journal of African Earth Science* **10(1-2)**, 101-116.

Eriksson, P.G., Mazumder, R., Catuneanu, O., Bumby, A.J., and Ilondo, B.O., 2006. Precambrian continental freeboard and geological evolution: a time perspective. *Earth- Science Reviews*, **79**, pp.165–204.

Esteva L., 1967. Criterios para la construccion de espectros para diseno sısmico. *Proceedings of XII Jornadas Sudamericanas de Ingenierıa Estructural y III Simposio Panamericano de Estructuras*, Caracas, Published later in *Boletın del Instituto de Materiales y Modelos Estructurales*, Universidad Central de Venezuela, No. 19,

Esteva L., 1968. *Bases para la formulacion de decisiones de diseno sismic*, PhD Thesis and Report 182, Universidad Autonoma Nacional de Mexico.

Esteva L., 1969. Seismic Risk and Seismic Design Decisions, in Seismic Design for Nuclear Power Plants, Ed. Hansen, R. J., MIT Press, Cambridge, Mass.

Estrada, G.M., 2012. Analysis of uncertainties associated with different approaches for earthquake risk assessment, *Proceeding of the 15th World Conference on Earthquake Engineering*, Lisbon. Available at http://www.iitk.ac.in/nicee/wcee/article/WCEE2012_5242.pdf

Evernden, J., 1969. Precision of epicenters obtained by small numbers of worldwide stations. *Bulletin of the Seismological Society of America*, **59**, pp.1365–1398.

Faber, M.H., 2005. On the treatment of uncertainties and probabilities in engineering decision analysis. *Journal of Offshore Mechanics and Arctic Engineering*, **127(3)**, pp.243-248.

Fan, G., and Wallace, T., 1995. Focal mechanism of a recent event in South Africa: A study using a sparse very broadband network. *Seismological Research Letters*, **66(5)**, pp.13-18.

FEMA, 2003. Recommended Provisions for Seismic Regulations for New Buildings and Other Structures (FEMA 450).

Fenton, C.H. and Bommer, J.J., 2006. The Mw7 Machaze, Mozambique, earthquake of 23 February 2006. *Seismological Research Letters*, **77(4)**, pp.426-439.

Fernández, L., 1980. Adaptation of the Richter seismic local magnitude scale to South Africa. *Geological Survey of South Africa*. Report number 1980-0175. Pretoria.

Fernandez, L.M. and Guzman, J.A., 1979. Seismic history of Southern Africa, *Seismological Series Geological Survey of South Africa* **9**, p.38.

Finsen, W.S., 1950. The geographical distribution of some South African earthquakes. *Circular No. 110*, Union Observatory, Johannesburg.

Fishwick, S. and Bastow, I.D., 2011. Towards a better understanding of African topography: a review of passive-source seismic studies of the African crust and upper mantle. *Geological Society, London, Special Publications*, **357(1)**, pp.343-371.

Fitzenz, D.D. and Nyst, M., 2015. Building time-dependent earthquake recurrence models for probabilistic risk computations. *Bulletin of the Seismological Society of America*, **105(1)**, pp.120-133.

Foster, A.N. and Jackson, J.A., 1998. Source parameters of Large African earthquake: implications for crustal rheology and regional kinematics, *Geophysical Journal International* **134**, pp.422-448.

Fourie, C.J.S., Henry, G. and Maré, L.P., 2014. The structure of the Karoo-age Ellisras Basin in Limpopo Province, South Africa, in the light of new airborne geophysical data. *South African Journal of Geology*, **117(2)**, pp.193-210.

Flinn, E.A., 1965. Confidence regions and error determinations for seismic event location. *Reviews of Geophysics*, **3(1)**, pp.157-185.

Flint N.S. 2017. The Microzonation of Johannesburg: A seismic history of the Johannesburg area, *CGS report number 2017-0040 (Rev. 0)*. Council for Geoscience, Pretoria.

Frankel, A., 1994. Implications of felt area-magnitude relations for earthquake scaling and the average frequency of perceptible ground motion. *Bulletin of the Seismological Society of America*, **84(2),** 462-465.

Frankel, A., 1995. Mapping seismic hazard in the central and eastern United States. *Seismological Research Letters*, **66(4)**, pp.8-21.

Frankel, A.D., Mueller, C., Barnhard, T., Perkins, D., Leyendecker, E., Dickman, N., Hanson, S. and Hopper, M., 1996. *National seismic-hazard maps: documentation June 1996*, *Open-File Report 96-532*, U.S. Department of the Interior, U.S. Geological Survey.

Frisenda, M., Massa, M., Spallarossa, D., Ferretti, G. and Eva, C., 2005. Attenuation relationship for low magnitude earthquakes using standard seismometric records, *Journal of Earthquake Engineering*, **9**, pp.23–40

Fukushima, Y., 1996. Scaling relations for strong ground motion prediction models with M^2 terms, *Bulletin of the Seismological Society of America*, **86**, pp.329–336.

Gane, P.G., 1939 A Statistical Study of the Witwatersrand Earth Tremors, *The Journal of the Chemical, Metallurgical and Mining Society of South Africa*, **40**, pp.155 - 172.

Gane, P.G. and Oliver, H. O., 1953. South African earthquakes - 1949 to December 1952, *Transactions of the Geological Society of South Africa*, **56**, pp.21 - 33.

Gardner, J.K. and Knopoff, L. 1974. Is the sequence of earthquakes in Southern California, with aftershocks removed, Poissonian? *Bulletin of the Seismological Society of the America*, **64(9)**, pp.1363-1367.

Gardonio, B., Jolivet, R., Calais, E. and Leclère, H., 2018. The April 2017 Mw6. 5 Botswana earthquake: an intraplate event triggered by deep fluids. *Geophysical Research Letters*, ***45*(17)**, pp.8886-8896.

Gasperini, P, Bernardini, F, Valensise, G, and Boschi, E., 1999. Defining seismogenic sources from historical earthquakes felt reports. *Bulletin of the Seismological Society of America*, **89**, pp.94-110.

Gasperini, P., Vannucci, G., Tripone, D. and Boschi, E., 2010. The location and sizing of historical earthquakes using the attenuation of macroseismic intensity with distance. *Bulletin of the Seismological Society of America*, **100(5A)**, pp.2035-2066.

Gephart, J.W. and Forsyth, D.W., 1984. An improved method for determining the regional stress tensor using earthquake focal mechanism data: application to the San Fernando earthquake sequence. *Journal of Geophysical Research: Solid Earth*, **89(B11)**, pp.9305-9320.

Gibowicz, S.J. and Kijko, A., 1994. *An Introduction to Mining Seismology*, San Diego: Academic Press.

Giner, J.J., Molina, S. and Jauregui, P., 2002. Advantages of using sensitivity analysis in seismic hazard assessment: a case study of sites in southern and eastern Spain. *Bulletin of the Seismological Society of America*, **92,** pp.543–554.

Goedhart, M.L., Booth, P.W.K., 2016. A palaeoseismic trench investigation of early Holocene neotectonic faulting along the Kango Fault, southern Cape Fold Belt, South Africa – Part I: stratigraphic and structural features. *South African Journal of Geology*, **119(3)**, pp.545-568.

Goes, S.D., 1996. Irregular recurrence of large earthquakes: an analysis of historic and paleoseismic catalogs. *Journal of Geophysical Research: Solid Earth*, **101(B3)**, pp.5739-5749.

Gomberg, J., 1991. Seismicity and detection/location threshold in the southern Great Basin seismic network. *Journal of Geophysical Research: Solid Earth*, **96(B10**), pp.16401-16414.

Gomez, K.A. and Gomez, A.A., 1984. *Statistical procedures for agricultural research*. John Wiley and Sons.

Good, N. and De Wit, M.J., 1997. The Thabazimbi-Murchison lineament of the Kaapvaal craton, South Africa: 2700 Ma of episodic deformation. *Journal of the Geological Society*, **154(1)**, pp.93-97.

Gore, J., James, D.E., Zengeni, T.G., Gwavava, O., 2009. Crustal structure of the Zimbabwe craton and the Limpopo Belt of southern Africa: new constraints from seismic data and implications for its evolution. *South African Journal of Geology*, **112**, pp.213–228.

Gordon, R.G. and Stein, S., 1992. Global tectonics and space geodesy. *Science*, **256(5055),** pp.333-342.

Graves, R.W., Aagaard, B.T., Hudnut, K.W., Star, L.M., Stewart, J.P. and Jordan, T.H., 2008. Broadband simulations for Mw 7.8 southern San Andreas earthquakes: Ground motion sensitivity to rupture speed. *Geophysical Research Letters*, **35**, L22302.

Green, R.W.E. and Bloch, S., 1971. The Ceres, South Africa, earthquake of September 29, 1969: I. Report on some aftershocks. *Bulletin of the Seismological Society of America*, **61(4),** pp.851-859.

Grobbelaar, M.R.G., Birch, D. and Cichowicz, A., 2017, March. Comparison of data from complementary seismograph networks in a mining district. In *Proceedings of the Eighth International Conference on Deep and High Stress Mining* (pp. 117-124). Australian Centre for Geomechanics.

Grünthal, G., Wahlström, R., 2001. Sensitivity of parameters for probabilistic seismic hazard analysis using a logic tree approach. *Journal of Earthquake Engineering*, **5,** pp309–328.

Grünthal, G., 1985. The up-dated earthquake catalogue for the German Democratic Republic and adjacent areas—Statistical data characteristics and conclusions for hazard assessment.

Proceedings 3rd International Symposium on the Analysis of Seismicity and Seismic Risk, Czechoslovak Academy of Science, Prague, 19-25.

Gutenberg, B., and Richter, C.F. 1956. *Seismicity of the Earth and associated phenomena*. Princeton University Press.

Gutenberg, B. and Richter, C.F., 1944. Frequency of earthquakes in California. *Bulletin of the Seismological Society of America*, **34(4)**, pp.185-188.

Gupta, I.D., 2002. The state of the art in seismic hazard analysis. *ISET Journal of Earthquake Technology*, **39(4)**, pp.311-346.

Gupta, I.D., 2006, December. Defining source-to-site distances for evaluation of design earthquake ground motion. In *Proceedings of the 13th Symposium on Earthquake Engineering, Roorkee*, **1**, pp.295-306.

Hainzl, S., Scherbaum, F., and Beauval, C., 2006. Estimating background activity based on interevent-time distribution. *Bulletin of the Seismological Society of the America*, **96(1)**, pp.313-320.

Hälbich, I.W., 1983. A geodynamic model for the Cape Fold Belt (CFB). In: *Geodynamics of the Cape Fold Belt: A Contribution to the National Geodynamics Programme*, A.P.G. Sönghe and I.W. Hälbich (*eds*.), *Special Publication 12, chapter 15, 177-184, Geological Society of South Africa*, Johannesburg.

Hanks, T., and Kanamori, H., 1979. A moment magnitude scale. *Journal of Geophysical Research*, **84**, pp.2348–2350.

Hanks, T.C. and Bakun, W.H., 2008. M-log A observations for recent large earthquakes. *Bulletin of the Seismological Society of America*, **98(1)**, pp.490-494.

Hartnady, C.J.H., 2002. Earthquake hazard in Africa: perspectives on the Nubia-Somalia boundary. *South African Journal of Science*, **98**, pp.425-427.

Hartnady, C.J.H., 1990. Seismicity and plate boundary evolution in south eastern Africa. *South African Journal of Geology*, **93**, pp.473-484.

Hartnady, C.J.H., 1996. Seismotectonic Provinces of South Africa: Critical Review and New Proposals. *CGS Report number 1996-029*.

Hartnady, C.J.H., 1985. Uplift, faulting, seismicity, thermal spring and possible incipient volcanic activity in the Lesotho-Natal Region, SE Africa: The Quathlamba Hotspot Hypothesis. *Tectonics*, ***4*(4)**, pp.371-377.

Hartnady, C.J.H. and Partridge, T.C. 1995. Neotectonic uplift in southern Africa: A brief review and geodynamic conjecture. Extended Abstracts Centennial *Geocongress, Geological Society of South Africa*, **I**, pp.456-459.

Hartzell, S., Meremonte, M., Ramírez-Guzmán, L. and McNamara, D., 2013. Ground motion in the presence of complex topography: Earthquake and ambient noise sources. *Bulletin of the Seismological Society of America*, **104(1)**, pp.451-466. Doi: 10.1785/0120130088

Hassaballa, A., Mohamed, A.R.E. and Sobaih, M., 2011. Sensitivity analysis of parameters for probabilistic seismic hazard for Sudan. *Journal of Science and Technology*, **12(02)**, pp.105-116.

Heidbach, O., Rajabi, M., Cui, X., Fuchs, K., Müller, B., Reinecker, J., Reiter, K., Tingay, M., Wenzel, F., Xie, F. and Ziegler, M.O., 2018. The World Stress Map database release 2016: Crustal stress pattern across scales. *Tectonophysics*, **744,** pp.484-498.

Henderson, N.B., 1974. Earthquake magnitude determination based on short period crustal waves. *Rhodesian Meteorological Service, Meteorological Notes*, Series A, No. 42.

Holland, M., 2011. *Hydrogeological Characterisation of Crystalline Basement Aquifers within the Limpopo Province, South Africa*. PhD Thesis. University of Pretoria, South Africa.

Hong, H. P., and Goda, K. 2006. A comparison of seismic-hazard and risk deaggregation, *Bulletin of the Seismological Society of America,* **96**, 2021-2039.

Horner-Johnson, B.C., Gordon, R.G. and Argus, D.F., 2007. Plate kinematic evidence for the existence of a distinct plate between the Nubian and Somalian plates along the Southwest Indian Ridge. *Journal of Geophysical Research: Solid Earth*, **112(B05418)**.

Huang, D., Wang, J.P., Brant, L. and Chang, S.C., 2012, September. Deterministic seismic hazard analysis considering non-controlling seismic sources and time factors. In *International Conference on Scalable Uncertainty Management* (p. 550-557). Springer, Berlin, Heidelberg.

Hutton, K., Woessner, J. and Hauksson, E., 2010. Earthquake monitoring in southern California for seventy-seven years (1932–2008). *Bulletin of the Seismological Society of America*, **100(2),** pp.423-446.

Hutton, L.K., and Boore, D.M., 1987. The ML scale in Southern California. *Bulletin of the Seismological Society of America,* **77(6),** pp.2074-2094.

Iervolino, I., Giorgio, M. and Polidoro, B., 2014. Sequence-based probabilistic seismic hazard analysis. *Bulletin of the Seismological Society of America*, **104(2)**, pp.1006-1012.

Ishimoto, M., and Iida K., 1939. Observations of earthquakes registered with the microseismograph constructed recently. *Bulletin of the Earthquake Research Institute, Tokyo University*, **17, 644,** pp.443–478.

Jelsma, H., Barnett, W., Richards, S., Lister, G., 2009. Tectonic setting of kimberlites. *Lithosphere*, **112S**, 155–165.

Jensen B.L., 1991. *Source parameters and seismotectonics of three earthquakes in the stable continental interior of Africa*. MSc Thesis, Memphis State University.

Jestin F., Huchon P., and Gaulier J.M., 1994. The Somalia plate and the East African rift system: present-day kinematics, *Geophysical Journal International*, **116**, pp.637-654.

Johnson, M.R., Anhaeusser, C.R. and Thomas, R.J., 2006. The Geology of South Africa. *Geological Society of South Africa and Council for Geoscience*, pp.461-499

Johnston, A.C., 1994. The stable continental region earthquake database. *The Earthquakes of Stable Continental Regions: Assessment of Large Earthquake Potential. EPRI Report. TR, 102261*, pp.3-1.

Johnston, A.C., 1996. Seismic moment assessment of earthquakes in stable continental regions – I. Instrumental seismicity. *Geophysical Journal International*, **124**, pp.381-414.

Johnston, A.C., Coppersmith, K.J., Kanter, L.R., and C.A. Cornell 1994. The Earthquakes of Stable Continental Regions. *Final Report submitted to Electric Power Research Institute (EPRI)*.

Jordan, T.H. and Sverdrup, K.A., 1981. Teleseismic location techniques and their application to earthquake clusters in the South-central Pacific. *Bulletin of the Seismological Society of America*, **71**, pp.1105–1130.

Joyner, W.B. and Boore, D.M., 1981. Peak horizontal acceleration and velocity from strong-motion records including records from the 1979 Imperial Valley, California, earthquake. *Bulletin of the Seismological Society of America*, **71(6)**, pp.2011-2038.

Julià, J., Nyblade, A.A., Durrheim, R., Linzer, L., Gök, R., Dirks, P. and Walter, W., 2009. Source mechanisms of mine-related seismicity, Savuka mine, South Africa. *Bulletin of the Seismological Society of America*, **99(5)**, pp.2801-2814, doi: 10.1785/0120080334.

Kafka, A.L., 2007. Does seismicity delineate zones where future large earthquakes are likely to occur in intraplate environments? In: *Continental Intraplate Earthquakes: Science, Hazard, and Policy Issues*, S. Stein & S. Mazzotti (*eds.*), Geological Society of America Special Paper **425**, pp. 35-48.

Kanamori, H. and Anderson, D.L., 1975. Theoretical basis of some empirical relations in seismology. *Bulletin of the Seismological Society of America*, **65(5)**, pp.1073-1095.

Kgaswane, E.M., Nyblade, A.A., Durrheim, R.J., Julià, J., Dirks, P.H. and Webb, S.J., 2012. Shear wave velocity structure of the Bushveld Complex, South Africa. *Tectonophysics*, **554,** pp.83-104.

Kijko 2014. Program manual: HA3- Seismic hazard assessment for selected area.

Kijko, A., 2012. On Bayesian procedure for maximum earthquake magnitude estimation. *Research in Geophysics*, **2(1)**, p.7.

Kijko, A., 2011. Introduction to Probabilistic Seismic Hazard Analysis. In *Encyclopedia of Solid Earth Geophysics* (pp. 1107-1121). Springer, Dordrecht.

Kijko, A., 2004. Estimation of the maximum earthquake magnitude m_{max}. *Pure Applied Geophysics*, **161(8)**, pp.1655–1681.

Kijko, A., 1994. Seismological outliers: L1 or adaptive Lp norm application. *Bulletin of the Seismological Society of America*, **84(2)**, pp.473-477.

Kijko, A., Graham, G., Bejaichund, M., Roblin, D.L. and Brandt, M.B.C., 2003. Probabilistic peak ground acceleration and spectral seismic hazard maps for South Africa, *Council for Geoscience*, report number 2003-0053.

Kijko, A. and Graham, G., 1999. "Parametric-historic" Procedure for probabilistic seismic hazard analysis Part II: Assessment of Seismic Hazard at Specified Site. P*ure and Applied Geophysics*, **154(1)**, pp.1-22.

Kijko, A. and Graham, G., 1998. Parametric-historic procedure for probabilistic seismic hazard analysis Part I: estimation of maximum regional magnitude Mmax. *Pure and Applied Geophysics*, **152(3)**, pp.413-442, doi: 10.1007/s000240050161.

Kijko, A., Lasocki, S. and Graham, G., 2001. Non-parametric seismic hazard in mines. P*ure and Applied Geophysics*, **158(9-10)**, pp.1655-1675.

Kijko, A. and Sellevoll, M.A., 1989. Estimation of earthquake hazard parameters for incomplete and uncertain data files: Part I Utilization of extreme and complete catalogs with different threshold magnituse. *Bulletin of the Seismological Society of America*, **79(3)**, pp.645-654.

Kijko, A., Smit, A. and Sellevoll, M.A., 2016. Estimation of earthquake hazard parameters from incomplete data files. Part III. Incorporation of uncertainty of earthquake-occurrence model. *Bulletin of the Seismological Society of America*, **106(3)**, pp.1210-1222.

Kijko, A. and Singh, M. 2011. Statistical tools for maximum possible earthquake estimation. *Acta Geophysica*, **59(4)**, pp.674–700.

Kinabo, B.D., Atekwana, E.A., Hogan, J.P., Modisi, M.P., Wheaton, D.D. and Kampunzu, A.B., 2007. Early structural development of the Okavango rift zone, NW Botswana. *Journal of African Earth Sciences*, **48(2-3)**, pp.125-136.

King, L.C. and Maud, R. M., 1964. *The geology of Durban and environs*, Geological survey, Government printer, Pretoria, 49 pp.

Kinnaird, J.A., McDonald, I., 2005. An introduction to mineralisation in the Northern Limb of the Bushveld Complex. Applied Earth Science: *Transactions of the Institutions of Mining and Metallurgy: Section B*, **114 (4)**, pp.194–198.

Klügel J.U., 2005. Problems in the application of the SSHAC probability method for assessing earthquake hazards at Swiss nuclear power plants, *Engineering Geology*, **78**, pp. 285-307.

Klügel, J.U., 2008. Seismic hazard analysis—Quo vadis? *Earth-Science Reviews*, **88(1-2)**, pp.1-32.

Knopoff, L., and Gardner, J.K., 1972. Higher seismic activity during local night on the raw worldwide earthquake catalog. *Geophysical Journal*, **28**, 311-313.

Knopoff, L. and Kagan, Y., 1977. Analysis of the theory of extremes as applied to earthquake problems. *Journal of Geophysical Research*, ***82*(36)**, pp.5647-5657.

Konstantinou, K.I., 2014. Moment magnitude–rupture area scaling and stress-drop variations for earthquakes in the Mediterranean region. *Bulletin of the Seismological Society of America*, **104(5)**, pp.2378-2386.

Kositcin, N., Krapež, B., 2004. Relationship between detrital zircon age-spectra and the tectonic evolution of the Late Archaean Witwatersrand Basin, South Africa. *Precambrian Research*, **129**, pp.141–168.

Kövesligethy, R.D., 1906. A makroszeizmikus rengések feldolgozása. *Mathematikai és Természettudományi Értesítõ*, **24**, pp.349-368.

Kowsari, M., Halldórsson, B., Eftekhari, N., Snæbjörnsson, J.Þ. and Jónsson, S., 2019. Sensitivity Analysis of Seismicity Parameters and Ground Motion Models Used in PSHA to Its Input Assumptions: A Case Study of Husavik, North Iceland. *Conference: In Proceedings of the Northquake 2019 workshop (Ed. S. Jónsson et al.)*, Húsavík Academic Centre, pp.64-65, 21-24 May 2019.

Kowsari, M., Halldorsson, B. and Snæbjörnsson, J.Þ., 2017. On the probabilistic seismic hazard estimate for Husavik, north Iceland, on the basis of Monte Carlo methods. In *16th World Conference on Earthquake Engineering (16WCEE)*, Santiago, Chile.

Kramer, S.L., 1996. *Geotechnical earthquake engineering*. In Prentice–Hall International series in Civil Engineering and Engineering Mechanics. *Prentice-Hall, New Jersey*.

Krige, L.J., 1936. The Swaziland and Fauresmith Earthquakes of January 1936. *Transactions of the Geological Society of South Africa*, **39**, pp.429-40.

Krige, L.J, and Maree, B.D., 1948. Earthquakes in South Africa. Bulletin No. 20, *Geological Survey of South Africa*, 14pp [in Afrikaans; English translation, 1951].

Krige, L.J., and Maree, B.D., 1951. Earthquakes in South Africa. *Bulletin of the Geological Survey of South Africa*, **20**, pp.1-14.

Krige, L.J., and Venter, F.A.. 1933. The Zululand Earthquake of the 31st December 1932. *Transactions of the Geological Society of South Africa*, **36**, 101-112.

Krige, L.J. and Venter, F.A., 1936. The Swaziland and Fauresmith earthquakes of January 1936 *Transactions of the Geological Society of South Africa*, **39**, pp. 429-440.

Krinitzsky, E.L., 1993. Earthquake probability in engineering—Part 2: Earthquake recurrence and limitations of Gutenberg-Richter b-values for the engineering of critical structures: The third Richard H. Jahns distinguished lecture in engineering geology. *Engineering geology*, ***36*(1-2)**, pp.1-52. doi: 10.1016/0013-7952(93)90017-7.

Krinitzsky, E.L., 1995a. Deterministic versus probabilistic seismic hazard analysis for critical structures. *Engineering Geology*, **40**, 1–7.

Krinitzsky, E.L., 1995b. Problems with logic trees in earthquake hazard evaluation. *Engineering Geology*, **39**, 1–3.

Krinitzsky, E.L., 2002. Epistematic and aleatory uncertainty: a new shtick for probabilistic seismic hazard analysis. *Engineering Geology*, **66(1-2)**, pp.157-159.

Krinitzsky, E.L., 2003. How to combine deterministic and probabilistic methods for assessing earthquake hazards. *Engineering Geology*, **70(1-2)**, pp.157-163.

Krüger F., Reichman, S. and Scherbaum, F., 2011. Moment tensor solution for the 29 September 1969 Ceres earthquake. *SSHAC Level 3 Workshop 1*, Cape Town.

Kulkarni, R. B., Youngs R. R. and Coppersmith K. J., 1984. Assessment of Confidence Intervals for Results of Seismic Hazard Analysis, *Eighth World Conference on Earthquake Engineering*, San Francisco, USA.

Kværna, T., Ringdal, F., Schweitzer, J. and Taylor, L., 2002. Optimized seismic threshold monitoring–part 1: regional processing. P*ure and Applied Geophysics*, **159(5)**, pp.969-987.

Lasocki, S. and Orlecka-Sikora, B., 2008. Seismic hazard assessment under complex source size distribution of mining-induced seismicity. *Tectonophysics*, **456(1-2)**, pp.28-37.

Le Goff, B., Fitzenz, D. and Beauval, C. 2010. Towards a bayesian seismotectonic zoning for use in Probabilistic Seismic Hazard Assessment (PSHA), *In AIP Conference Proceedings*, pp. 242–249. doi: 10.1063/1.3573623.

Le Goff, B. and Fitzenz, D. D. 2012. Combining seismic and geologic data for reproducible seismic source models, *In 15th World Conference on Earthquake Engineering.* Lisbon, December 2011. Available at: http://www.iitk.ac.in/nicee/wcee/article/WCEE2012_4914.pdf

Leonard, M., 2010. Earthquake fault scaling: Self-consistent relating of rupture length, width, average displacement, and moment release. *Bulletin of the Seismological Society of America*, ***100*(5A)**, pp.1971-1988.

Letlatsa, G.M., 2004. *Geological conditions and enviromental impact of the Mohale dam, Lesotho highlands water project.* PhD Thesis, Faculty of Science, University of Free State, Bloemfontein, South Africa.

Lienert, B.R.E. and Havskov, J., 1995. A computer program for locating earthquakes both locally and globally, *Seismological Research Letters*, **66,** 26–36.

Lithgow-Bertelloni, C. and Silver, P.G., 1998. Dynamic topography, plate driving forces and the African superswell. *Nature*, **395(6699)**, pp.269– 272.

Liu, L., Zoback, M.D. and Segall, P., 1992. Rapid intraplate strain accumulation in the New Madrid seismic zone. *Science*, ***257*****(5077)**, pp.1666-1669.

Liu, M., Stein, S. and Wang, H., 2011. 2000 years of migrating earthquakes in North China: How earthquakes in midcontinents differ from those at plate boundaries. *Lithosphere*, ***3*****(2)**, pp.128-132.

Liu, M., Luo, G., Wang, H. and Stein, S., 2014. Long aftershock sequences in North China and Central US: implications for hazard assessment in mid-continents. *Earthquake Science*, ***27*****(1)**, pp.27-35.

Lloyd, R., Biggs, J. and Copley A., 2019. The decade-long Machaze–Zinave aftershock sequence in the slowly straining Mozambique Rift. *Geophysical Journal International*, **217,** pp.504–531.

Lombardi, A.M., Akinci, A., Malagnini, L. and Mueller, C.S., 2005. Uncertainty analysis for seismic hazard in Northern and Central Italy. *Annals of Geophysics*, **48(6)**, pp 853-865.

Lomnitz-Adler, J. and Lomnitz, C., 1979. A modified form of the Gutenberg-Richter magnitude-frequency relation. *Bulletin of the Seismological Society of America*, **69(4)**, pp.1209-1214.

Luen, B., and Stark, P.B. 2012. Poisson tests of declustered catalogues. *Geophysical Journal International*, **189**, pp.691-700.

Lund, B. and Slunga, R., 1999. Stress tensor inversion using detailed microearthquake information and stability constraints: Application to Ölfus in southwest Iceland. *Journal of Geophysical Research: Solid Earth*, **104(B7)**, pp.14947-14964.

Magrin, A., Parvez, I.A., Vaccari, F., Peresan, A., Rastogi, B.K., Cozzini, S., Bisignano, D., Romanelli, F., Choudhury, P., Roy, K.S. and Mir, R.R., 2016. Neo-deterministic definition of seismic and tsunami hazard scenarios for the territory of Gujarat (India). In *Earthquakes and their impact on society*, (eds. D'Amico S.), pp. 193-212, Springer, Cham.

Magrin, A., Peresan, A., Kronrod, T., Vaccari, F. and Panza, G.F., 2017. Neo-deterministic seismic hazard assessment and earthquake occurrence rate. *Engineering Geology*, **229**, pp.95-109. doi: 10.1016/j.enggeo.2017.09.004.

Main, I., 2000. Apparent breaks in scaling in the earthquake cumulative frequency-magnitude distribution: fact or artifact? *Bulletin of the Seismological Society of America*, **90(1)**, pp.86-97.

Main, I., Naylor, M., Greenhough, J., Touati, S., Bell, A.F. and McCloskey, J., 2011. Model selection and uncertainty in earthquake hazard analysis. *Applications of Statistics and Probability in Civil Engineering*, (eds. Faber, Köhler and Nishijima), pp.735-743.

Malservisi, R., Hugentobler, U., Wonnacott, R. and Hackl, M., 2003. How rigid is a rigid plate? Geodetic constraint from the TrigNet CGPS network, South Africa. *Geophysical Journal International*. **192**(3), 918–28.

Mangongolo, A., Strasser, F.O., Saunders, I. and Rathod, G.W., 2017. Depths of earthquakes in South Africa. *Seismological Research Letters*, **88(4)**, pp.1078-1088.

Manzi, M.S., Gibson, M.A., Hein, K.A., King, N. and Durrheim, R.J., 2012. Application of 3D seismic techniques to evaluate ore resources in the West Wits Line goldfield and portions of the West Rand goldfield, South Africa. *Geophysics*, **77(5)**, pp.WC163-WC171.

Manzi, M.S.D., Hein, K.A.A., Durrheim, R. and King, N., 2013. Seismic attribute analysis to enhance detection of thin gold-bearing reefs: South Deep gold mine, Witwatersrand basin, South Africa. *Journal of Applied Geophysics*, **98**, pp.212-228.

Manzi, M., Cooper, G., Malehmir, A., Durrheim, R. and Nkosi, Z., 2015. Integrated interpretation of 3D seismic data to enhance the detection of the gold-bearing reef: Mponeng Gold mine, Witwatersrand Basin (South Africa). *Geophysical Prospecting*, **63(4)**, pp.881-902.

Manzunzu, B., Midzi, V., Durrheim, R.J., Pule, T.G.and Flint, N. (*In press)*. Quantitative evaluation of source parameters of historical earthquakes in southern Africa. *Journal of Seismology.*

Manzunzu, B., Brandt, M.B.C., Midzi, V., Durrheim, R.J., Saunders, I. and Mulabisana, T.F., 2020. Towards a homogeneous moment magnitude determination for earthquakes in South Africa: Reduction of associated uncertainties. *Journal of African Earth Sciences*, **173,** p.104051.

Manzunzu, B. and Midzi, V., 2019. Uncertainties associated with the Seismic Hazard Analysis for Johannesburg (ST-0040-1331), *Council for Geoscience,* report number 2019-0072.

Manzunzu B., Midzi, V., Mulabisana, T. F., Zulu, B., Pule, T.G., Myendeki, S. and Rathod G.W. 2019. Seismotectonics of South Africa, *Journal of African Earth Sciences,* **149**, pp.271-279.

Manzunzu, B., Midzi, V., Mangongolo, A. and Essrich, F., 2017. The aftershock sequence of the 5 August 2014 Orkney earthquake (M L 5.5), South Africa. *Journal of Seismology*, ***21*(6)**, pp.1323-1334.

Manzunzu, B. and Midzi, V., 2015. The Curious Case of the 1919 Swaziland Earthquake. *Seismological Research Letters*, **86(3)**, pp.803-809.

Marimira, K., Manzunzu, B., Shumba, B.T., Midzi, V. and Saunders, I., 2021. Aftershock sequence of 22 September 2016, Manica-Zinave earthquake (Mw5. 6), Mozambique. *Journal of African Earth Sciences*, **177**, p.104146.

Mark, R.K., 1977. Application of linear statistical models of earthquake magnitude versus fault length in estimating maximum expectable earthquakes. *Geology*, **5(8)**, pp.464-466.

Marsan, D., 2003. Triggering of seismicity at short timescales following Californian earthquakes. *Journal of Geophysical Research: Solid Earth*, **108(B5)**, pp.1-14.

Marshall, T.R., 1987. Morphotectonic analysis of the Wesselsbron panveld. *South African Journal Geology*, **90**, pp.209–218.

Massa, M., P. Morasca, L. Moratto, S. Marzorati, G. Costa and Spallarossa, D., 2008. Empirical ground motion prediction equations for northern Italy using weak and strong motion amplitudes, frequency content and duration parameters, *Bulletin of the Seismological Society of America*, **98,** pp.1319-1342

Matthews, M. V., Ellsworth, W. L. and Reasenberg, P. A. 2002. A Brownian model for recurrent earthquakes, *Bulletin of the Seismological Society of America*, **92(6),** pp. 2233-2250.

Maury, J., Cornet, F.H. and Dorbath, L., 2013. A review of methods for determining stress fields from earthquakes focal mechanisms; Application to the Sierentz 1980 seismic crisis (Upper Rhine graben). *Bulletin de la Societe Geologique de France*, **184(4-5)**, pp.319-334.

Mavonga, T., 2010. Seismic hazard assessment and volcanogenic seismicity for the Democratic Republic of Congo and surrounding areas, western rift valley of Africa. PhD thesis, *University of the Witwatersrand, Johannesburg, South Africa*.

McCalpin, J.P., 2009. Application of paleoseismic data to seismic hazard assessment and neotectonic research. *International Geophysics*, **95**, pp.1-106.

McCarthy, T.S., 2006. The Witwatersrand Supergroup. In: Johnson, M.R., Anhaeusser, C.R., Thomas, R.J. (Eds.), The Geology of South Africa. *Geological Society of South Africa, Johannesburg/Council for Geosciences*, Pretoria, pp. 155–186.

McCarthy T. S. and Rubidge B. S., 2005. Journey into the Past. Struik, Cape Town.

McCarthy, T. S., Stanistreet, I. G., Cadle, A. B., and Durrheim, R. J., 1990. The geology of the Ventersdorp Supergroup (Bezuidenhout Valley) outlier to the east of Johannesburg and its relevance to the tectonics of a Witwatersrand Basin margin. *South African Journal of Geology* **93**, 289–309.

McGarr, A. and Fletcher, J. B., 2005. Development of ground–motion prediction equations relevant to shallow mining–induced seismicity in the Trail Mountain area, Emery County, Utah, *Bulletin of the Seismological Society of America*, **95**, 31-47.

McGuire, R. K., 1976. *FORTRAN computer program for seismic risk analysis* (No. 76-67). US Geological Survey, Denver, Colorado.

McGuire, R. K., 1978. *FRISK: Computer program for seismic risk analysis using faults as earthquake sources* (No. 78-1007). US Geological Survey.

McGuire, R. K., 1993. Computations of seismic hazard. *Annali di Geofisica*, **36(3–4)**, pp.181–200.

McGuire, R. K., 2001. Deterministic vs. probabilistic earthquake hazards and risks. *Soil Dynamics and Earthquake Engineering*, ***21*(5)**, pp.377-384. doi: 10.1016/S0267-7261(01)00019-7

McGuire, R. K., 2004. *Seismic hazard and risk analysis*. Earthquake Engineering Research Institute.

McGuire, R. K., 2008. Probabilistic seismic hazard analysis: Early history. *Earthquake Engineering & Structural Dynamics*, ***37*(3)**, pp.329-338.

McGuire, R. K. and Shedlock, K. M., 1981. Statistical uncertainties in seismic hazard evaluations in the United States. *Bulletin of the Seismological Society of America*, **71(4)**, pp.1287-1308.

Meghraoui, M., Amponsah, P., Ayadi, A., Ayele, A., Ateba, B., Bensuleman, A., Delvaux, D., El Gabry, M., Fernandes, R., Midzi, V., Roos, M. and Timoulali, Y. 2016. The Seismotectonic Map of Africa, *Episodes*, **39**(1), doi:10.18814/epiiugs/2016/v39i1/8923.

Mello J.T., 2017. *Neotectonics: A study of the recent seismic activities of the Pliocene Epoch in Thabazimbi and Warmbaths, Limpopo Province, South Africa*. BSc thesis, University of Pretoria.

Merz, H.A. and Cornell, C.A., 1973. Seismic risk analysis based on a quadratic magnitude-frequency law. *Bulletin of the Seismological Society of America*, **63(6-1)**, pp.1999-2006.

Michael, A.J., 1987. Use of focal mechanisms to determine stress: a control study. *Journal of Geophysical Research*, **92**, pp.357–368

Midzi, V., Pule, T., Mulabisana, T., Zulu B. and Manzunzu, B. 2020a. Reassessment of source parameters of 'major' southern African earthquakes, *South African Journal of Geology*, **123(1),** 59-74, doi:10.25131/sajg.123.0002.

Midzi, V., Manzunzu, B., Mulabisana, T., Zulu, B.S., Pule, T. and Myendeki, S., 2020b. Probabilistic seismic hazard maps for South Africa. *Journal of African Earth Sciences*, **162**, p.103689. https://doi.org/10.1016/j.jafrearsci.2019.103689

Midzi, V. and Manzunzu, B., 2014. Large recorded earthquakes in sub-Saharan Africa. *Extreme Natural Hazards, Disaster Risks and Societal Implications*, ***1*,** p.214. DOI: 10.1017/CBO9781139523905.020

Midzi, V., Saunders, I., Manzunzu, B., Kwadiba, M.T., Jele, V., Mantsha, R., Marimira, K.T., Mulabisana, T.F., Ntibinyane, O., Pule, T. and Rathod, G.W., 2018. The 03 April 2017 Botswana M6.5 earthquake: Preliminary results. *Journal of African Earth Sciences*, **143**, pp.187-194.

Midzi, V., Zulu, B., Manzunzu, B., Mulabisana, T., Pule, T., Myendeki, S. and Gubela, W., 2015a. Macroseismic survey of the ML5. 5, 2014 Orkney earthquake. *Journal of Seismology*, **19(3)**, pp.741-751.

Midzi, V., Manzunzu, B., Zulu, B.S., Mulabisana, T., Myendeki, S. and Mangongolo, A., 2015b. Impact of Recent Moderately Sized Earthquakes in South Africa: Macroseismic Investigations of the 18 November and 2 December 2013 Earthquakes. *South African Journal of Geology*, **118(4),** pp.373-388.

Midzi, V., Hlatywayo, D.J., Chapola, L.S., Kebede, F., Atakan, K., Lombe, D.K., Turyomurugyendo, G. and Tugume, F.A., 1999. Seismic hazard assessment in Eastern and Southern Africa. *Annals of Geophysics*, **42(6),** pp.1067-1083.

Mignan, A., Werner, M.J., Wiemer, S., Chen, C.C. and Wu, Y.M., 2011. Bayesian estimation of the spatially varying completeness magnitude of earthquake catalogs. *Bulletin of the Seismological Society of America*, **101(3),** pp.1371-1385. doi: 10.1785/0120100223.

Mignan, A. and Woessner, J., 2012. *Theme IV–Understanding Seismicity Catalogs and their Problems*: Estimating the magnitude of completeness for earthquake catalogs, Technical Report doi: https://doi. org/10.5078/corssa-00180805, Community Online Resource for Statistical Seismicity Analysis.

Milesi J.P., Frizon de Lamotte, D., de Kock, G., and Toteu, F. 2010. Tectonic map of Africa, *Commision for Geological Map of the World (CCGM)*

Miller, R.D., Xia, J., Park, C.B., Ivanov, J.M., 1999. Multichannel Analysis of Surface Waves to Map Bedrock. Kansas Geological Survey, *The Leading Edge*, pp. 1392–1396.

Milne, W.G. and Davenport, A.G., 1969. Distribution of earthquake risk in Canada. *Bulletin of the Seismological Society of America*, **59(2)**, pp.729-754.

Modie, B.N., 2007. *The palaeozoic palynostratigraphy of the Karoo supergroup and palynofacies insight into palaeoenvironmental interpretations, Kalahari Karoo basin, Botswana*. PhD Thesis, Universite De Bretagne Occidentale

Mogren, S., 2020. Engineering bedrock depth estimation and ground response analysis of the northern Jeddah urban area, western Saudi Arabia. *Journal of King Saud University-Science*, **32(4)**, pp.2445-2453.

Molchan, G.M., Keilis-Borok, V.I. and Vilkovich, G.V., 1970. Seismicity and principal seismic effects. *Geophysical Journal International*, **21(3)**, pp.323-335.

Molina, S., Lindholm, C.D. and Bungum, H., 2001. Probabilistic seismic hazard analysis: zoning free versus zoning methodology. *Bollettino di Geofisica (selected papers from the 27th ESC, Lisbon, 2000)*, **42**, pp.19-39.

Molina, S. and Lindholm, C.D., 2007. Estimating the confidence of earthquake damage scenarios: examples from a logic tree approach. *Journal of Seismology*, **11(3)**, pp.299-310.

Molnar, P., 1979. Earthquake recurrence intervals and plate tectonics. *Bulletin of the Seismological Society of America*, **69(1)**, pp.115-133.

Montessus de Ballore, M. F., 1896. Seismic phenomena in the British Empire. *Quarterly Journal of the Geological Society*, **52(1-4)**, pp.651-668.

Moore, J.M., Tsikos, H. and Polteau, S., 2001. Deconstructing the Transvaal Supergroup, South Africa: implications for Palaeoproterozoic palaeoclimate models. *Journal of African Earth Sciences*, **33(3-4)**, pp.437-444.

Morgan, W.J., 1983. Hotspot tracks and the early rifting of the Atlantic. In *Developments in Geotectonics*, **19,** pp. 123-139. Elsevier.

Mulabisana, T.F., 2016. *Compiling a homogeneous earthquake catalogue for Southern Africa*. MSc Thesis, University of Witwatersrand.

Mulabisana, T., Meghraoui, M., Midzi, V., Saleh, M., Ntibinyane, O., Kwadiba, T., Manzunzu, B., Seiphemo, O., Pule, T. and Saunders, I., 2021. Seismotectonic Analysis of the 2017 Moiyabana Earthquake (MW6. 5; Botswana), Insights from field investigations, aftershock and InSAR studies. *Journal of African Earth Sciences*, p.104297.

Mulargia, F., Stark, P.B. and Geller, R.J., 2017. Why is probabilistic seismic hazard analysis (PSHA) still used? *Physics of the Earth and Planetary Interiors*, **264**, pp.63-75.

Musmeci, F. and Vere-Jones, D., 1992. A space-time clustering model for historical earthquakes. *Annals of the Institute of Statistical Mathematics*, **44(1)**, pp.1-11.

Musson, R. M. W., 2008. The case for large (M>7) earthquakes felt in the UK in historical times. In The Historical Seismology: Interdisciplinary Studies of Past and Recent Earthquakes, edited by J. Fréchet, M. Meghraoui, M. Stucchi, *Springer Netherlands*, ISBN: 978-1-4020-8221-4 (Print) 978-1-4020-8222-1, DOI 10.1007/978-1-4020-8222-1_9

Musson, R.M.W., 2009. MEEP 2.0 User Guide. Earth Hazards and Systems Programme Open Report OR/09/045, *British Geological Survey*, 16pp.

Musson, R.M.W., 2000. The use of Monte Carlo simulations for seismic hazard assessment in the United Kingdom, *Annals of Geophysics*, **43(1)**, pp. 1–9. doi: 10.4401/ag-3617.

Musson, R.M.W., 1996. Determination of parameters of historical British earthquakes. *Annali di Geofisica* **29(5),** 1041-1047.

Musson, R.M.W., Jiménez, M.J., 2008. Macroseismic estimation of earthquake parameters. NERIES Technical Report NA4-D3, 41pp

Musson, R.M.W. and Sargeant, S.L., 2007. Eurocode 8 seismic hazard zoning maps for the UK. *British Geological Survey Technical Report*, CR/07/125. 70 pp.

Myers, R.E., McCarthy, T.S. and Stanistreet, I.G., 1990. A tectono-sedimentary reconstruction of the development and evolution of the Witwatersrand Basin, with particular emphasis on the Central Rand Group. *South African Journal of Geology*, **93(1)**, pp.180-201.

Nath, S.K., 2007. Seismic microzonation framework-principles and applications, *Proceedings of the Workshop on Microzonation, Indian Institute of Science, Bangalore,* 26 –27 June 2007, India, pp. 9–35.

NEHRP, 2009. *NEHRP recommended seismic provisions for new buildings and other structures* (FEMA-P750). FEMA, Washington DC.

Nekrasova, A., Kossobokov, V., Peresan, A., Aoudia, A. and Panza, G.F., 2011. A multiscale application of the Unified Scaling Law for Earthquakes in the Central Mediterranean area and Alpine region. *Pure and Applied Geophysics*, **168(1-2)**, pp.297-327. doi: 10.1007/s00024-010-0163-4.

Newman A., Schneider, J., Stein, S. and Mendez, A. 2001. Uncertainties in seismic hazard maps for the New Madrid seismic zone and implications for seismic hazard communications, *Seismological Research Letters*, **72**, pp.647 – 663

Nguuri, T.K., Gore, J., James, D.E., Webb, S.J., Wright, C., Zengeni, T.G., Gwavava, O., Snoke, J.A. and Kaapvaal Seismic Group, 2001. Crustal structure beneath southern Africa and its implications for the formation and evolution of the Kaapvaal and Zimbabwe cratons. *Geophysical Research Letters*, **28**(13).

Nilsen, T. and Aven, T., 2003. Models and model uncertainty in the context of risk analysis. *Reliability Engineering and System Safety*, **79(3)**, pp.309-317.

Nishenko, S.P. and Buland, R., 1987. A generic recurrence interval distribution for earthquake forecasting. *Bulletin of the Seismological Society of America*, **77(4**), pp.1382-1399.

Nocquet, J.M. and Calais, E., 2003. Crustal velocity field of Western Europe from permanent GPS array solutions, 1996–2001. *Geophysical Journal International*, **154(1)**, pp.72-88.

Nuttli, O.W., 1973. Seismic wave attenuation and magnitude relations for eastern North America. *Journal of Geophysical Research*, **78**(5), pp.876-885.

Nuttli, O.W., 1983. Empirical magnitude and spectral scaling relations for mid-plate and plate-margin earthquakes. *Tectonophysics*, **93(3-4)**, pp.207-223.

Nyblade, A.A., and Robinson, S.W., 1994. The African superswell. *Geophysical Research Letters*, **21**, 765–768.

Ordaz M., 2004. Some Integrals Useful in Probabilistic Seismic Hazard Analysis, *Bulletin of the Seismological Society of America*, **94(4)**, pp. 1510–1516.

Oliver, H.O. 1956. South African earthquakes – January 1953 to December 1955. *Transactions of the Geological Society of South Africa*, **59**, 123-129.

Ottemöller, L., Voss, P. and Havskov, J., 2018. SEISAN: earthquake analysis software for windows, solaris, linux and macosx, University of Bergen.

Pagani, M., Monelli, D., Crowley, H., Danciu, L., Field, E.H., Wiemer, S. and Giardini, D., 2010. *GEM1 hazard: description of input models, calculation engine and main results*. GEM Technical Report 2010-3. GEM Foundation, Pavia, Italy.

Panza, G.F., 2017. NDSHA: Robust and reliable seismic hazard assessment. *Proceedings, International Conference on Disaster Risk Mitigation*, Dhaka, Bangladesh, September 23 - 24, 2017.

Panza, G.F., Kossobokov, V.G., Peresan, A. and Nekrasova, A., 2014. Why are the standard probabilistic methods of estimating seismic hazard and risks too often wrong? In *Earthquake Hazard, Risk and Disasters*, pp. 309-357. doi: 10.1016/B978-0-12-394848-9.00012-2.

Panza G.F., Romanelli F., Vaccari F., Decanini L. and Mollaioli F., 2003. Perspectives of innovative approaches in seismic hazard evaluation. *Proceedings, Fourth International Conference of Earthquake Engineering and Seismology*, Tehran, Islamic Republic of Iran, 12-14 May 2003

Partridge, T.C., 1995. A review of existing data on neotectonics and palaeoseismicity to assist in the assessment of seismic hazard at possible nuclear power station sites in South Africa, *Council for Geoscience* Report no 34.

Parvez, I.A. and Ram, A., 1997. Probabilistic assessment of earthquake hazards in the north-east Indian peninsula and Hindukush regions. P*ure and Applied Geophysics*, **149(4)**, pp.731-746.

Pasyanos, M.E. and Nyblade, A.A., 2007. A top to bottom lithospheric study of Africa and Arabia. *Tectonophysics*, **444(1-4)**, pp.27-44.

Paté-Cornell, M.E., 1996. Uncertainties in risk analysis: Six levels of treatment. *Reliability Engineering & System Safety*, **54(2-3),** pp.95-111.

Patwardhan, A.S., Kulkarni, R.B. and Tocher, D., 1980. A semi-Markov model for characterizing recurrence of great earthquakes. *Bulletin of the seismological society of America*, **70(1)**, pp.323-347.

Peruzza, L. and Pace, B., 2002. Sensitivity analysis for seismic source characteristics to probabilistic seismic hazard assessment in central Apennines (Abruzzo area). *Bollettino di Geofisica Teorica ed Applicata*, **43(1-2)**, pp.79-100.

Petersen, M.D., Frankel, A.D., Harmsen, S.C., Mueller, C.S., Haller, K.M., Wheeler, R.L., Wesson, R.L., Zeng, Y., Boyd, O.S., Perkins, D.M. and Luco, N., 2008. *Documentation for the 2008 update of the United States national seismic hazard maps* (No. 2008-1128). Geological Survey (US).

Petersen, M.D., Moschetti, M.P., Powers, P.M., Mueller, C.S., Haller, K.M., Frankel, A.D., Zeng, Y., Rezaeian, S., Harmsen, S.C., Boyd, O.S. and Field, N., 2015a. The 2014 United States national seismic hazard model. *Earthquake Spectra*, **31(S1)**, pp.S1-S30, doi: https://doi.org/10.1193/120814EQS210M.

Petersen, M.D., Mueller, C.S., Moschetti, M.P., Hoover, S.M., Rubinstein, J.L., Llenos, A.L., Michael, A.J., Ellsworth, W.L., McGarr, A.F., Holland, A.A. and Anderson, J.G., 2015b. Incorporating induced seismicity in the 2014 United States National Seismic Hazard Model: Results of 2014 workshop and sensitivity studies, Report no: Open-File Report 2015–1070. Available at: http://dx.doi.org/10.3133/ofr20151070.

Petersen, M.D., Mueller, C.S., Moschetti, M.P., Hoover, S.M., Rukstales, K.S., McNamara, D.E., Williams, R.A., Shumway, A.M., Powers, P.M., Earle, P.S. and Llenos, A.L., 2018. One-Year Seismic Hazard forecast for the central and eastern United States from Induced and Natural Earthquakes. *Seismological Research Letters*, **89(3)**, pp.1049-1061.

Pezeshk, S., Zandieh, A. and Tavakoli, B., 2011. Hybrid Empirical Ground-Motion Prediction Equations for Eastern North America Using NGA Models and Updated Seismological Parameters, *Bulletin of the Seismological Society of America*, **101**(4), 1859-1870.

Pule, T., Midzi, V., Manzunzu, B., Zulu, B., Mulabisana, T., Rathod, G. and Mphahlele, K., 2018. The macroseismic survey of the M4.6, 2017 Stilfontein earthquake. In *Proceedings of 16th European Conference on Earthquake Engineering* (pp. 18-21).

Rabinowitz, N. and Steinberg, D.M., 1991. Seismic hazard sensitivity analysis: a multi-parameter approach. *Bulletin of the Seismological Society of America*, ***81*(3)**, pp.796-817.

Rabinowitz, N., Steinberg, D.M., and Leonard, G., 1993. Technical note: When does seismic hazard jump? *Earthquake Spectra*, **9**, pp. 877 – 883

Rabinowitz, N., Steinberg, D. M., and Leonard, G., 1998. Logic trees, sensitivity analysis, and data reduction in probabilistic seismic hazard assessment, *Earthquake Spectra*, **14**, pp.189 – 201

Reasenberg, P., 1985. Second-order moment of central Californian seismicity, 1969-1982. *Journal of Geophysical Research*, **90**, 5479-5495.

Rebez, A. and Slejko, D., 2000. Sensitivity analysis on the input parameters in probabilistic seismic hazard assessment, *Soil Dynamics of Earthquake Engineering*, **20**, pp. 341 –351

Reiter L., 1990. *Earthquake hazard analysis: Issues and insights*, Columbia University Press, New York.

Richter, C.F., 1935. An instrumental earthquake scale. *Bulletin of the Seismological Society of America*, **25**, 1-32.

Richter, C.F., 1958. *Elementary Seismology.* W.H. Freeman, San Francisco, 768 pp.

Rietbrock, A., Strasser, F. and Edwards, B., 2013. A stochastic earthquake ground-motion prediction model for the United Kingdom, *Bulletin of the Seismological Society of America*, **103**, 57-77.

Ringdal, F., 1975. On the estimation of seismic detection thresholds. *Bulletin of the Seismological Society of America*, **65(6)**, pp.1631-1642.

Rohmer, J., Douglas, J., Bertil, D., Monfort, D. and Sedan, O., 2014. Weighing the importance of model uncertainty against parameter uncertainty in earthquake loss assessments. *Soil Dynamics and Earthquake Engineering*, **58**, pp.1-9.

Rydelek, P.A. and Sacks, I.S., 1989. Testing the completeness of earthquake catalogues and the hypothesis of self-similarity. *Nature*, **337(6204)**, pp.251-253.

Rydelek, P.A. and Sacks, I.S., 2003. Comment on "Minimum magnitude of completeness in earthquake catalogs: Examples from Alaska, the Western United States, and Japan," by Stefan Wiemer and Max Wyss. *Bulletin of the Seismological Society of America*, **93(4)**, pp.1862-1867.

Ryden, N., 2004. *Surface Wave Testing of Pavements.* Doctoral Thesis, Department of Engineering Geology. Lund Institute of Technology, Lund University.

Ryder, J. A., and Jager, J. A. 2002. *A textbook on rock mechanics for tabular hard rock mines.* Johannesburg : Safety in Mines Research Advisory Committee (SIMRAC).

Sabetta, F., Lucantoni, A., Bungum, H., Bommer, J.J., 2005. Sensitivity of PSHA results to ground motion prediction relations and logic-tree weights. *Soil Dynamics and Earthquake Engineering*, **25**, 317–329.

Sabetta, F. and Pugliese A., 1987. Attenuation of peak horizontal acceleration and velocity from Italian strong-motion records. *Bulletin of the Seismological Society of America*, **77(5)**, pp. 1491– 1513

Sagar, S. and Leonard, M., 2007. Mapping the Magnitude of completeness of the Australian earthquake catalogue. *In Proceedings of the Australian Earthquake Engineering Society Conference, Wallongong.* http://aees.org.au/wp-content/uploads/2013/11/46-Sagar-Stephen.pdf.

Salazar, W., 2018. Principles of Probabilistic Seismic Hazard Assessment (PSHA) and Site Effect Evaluation and Its Application for the Volcanic Environment in El Salvador. *Earthquakes: Forecast, Prognosis and Earthquake Resistant Construction*, p.119.

Saltelli, A. and Annoni, P., 2010. How to avoid a perfunctory sensitivity analysis. *Environmental Modelling and Software*, ***25*(12)**, pp.1508-1517.

Saltelli, A., Chan, K., and Scott, E.M., 2000. *Sensitivity analysis*. Wiley New York.

Santamarina, J.C., Klein, K.A., Fam, M.A., 2001. *Soil and Waves.* John Wiley and Sons Incoporation, New York.

Santulin, M., Tamaro, A., Rebez, A., Slejko, D., Sani, F., Martelli, L., Bonini, M., Corti, G., Poli, M.E., Zanferrari, A., Marchesini, A., Busetti, M., Dal Cin. M., Spallarossa, D., Barani, S., Scafidi, D., Barreca, G., and Monaco, C., 2017. Seismogenic zonation as a branch of the logic tree for the new Italian seismic hazard map – MPS16: preliminary outline, *Bulletino di Geofisica Teorica ed Applicata,* **48(4)**, pp.313-342.

Saria, E., Calais, E., Stamps, D.S., Delvaux, D. and Hartnady, C.J.H., 2014. Present-day kinematics of the East African Rift. *Journal of Geophysical Research: Solid Earth*, ***119*(4)**, pp.3584-3600.

Saunders I, Brandt, M., Molea, T., Akromah, L. and Sutherland, B. 2010. Seismicity of southern Africa during 2006 with special reference to the MW 7 Machaze earthquake. *South African Journal of Geology*. **113,** pp.369-380.

Saunders I., Brandt, M., Steyn, J., Roblin, D. and Kijko, A. 2008. The South African Seismograph Network. *Seismological Research Letters*, **79,** pp. 203-210.

Saunders, I., Ottemöller, L., Brandt, M.B. and Fourie, C.J., 2013. Calibration of an M L scale for South Africa using tectonic earthquake data recorded by the South African National Seismograph Network: 2006 to 2009. *Journal of Seismology*, **17(2)**, pp.437-451.

Saunders, I., Kijko, A. and Fourie, C.J.S., 2016. Statistical evaluation of seismic event location accuracy by the South African National Seismograph Network over four decades. *South African Journal of Geology*, **119(1)**, pp.291-304.

Scherbaum, F., Delavaud E., and Riggelsen C., 2009. Model selection in seismic hazard analysis: An information-theoretic perspective, *Bulletin of the Seismological Society of America*, **99(6)**, pp. 3234–3247

Scherbaum, F., Bommer, J.J., Bungum, H., Cotton, F. and Abrahamson, N.A., 2005. Composite ground-motion models and logic trees: methodology, sensitivities, and uncertainties. *Bulletin of the Seismological Society of America*, **95(5)**, pp.1575-1593.

Scherbaum, F. and Kuehn, N.M., 2011. Logic tree branch weights and probabilities: summing up to one is not enough. *Earthquake Spectra*, **27(4)**, pp.1237-1251.

Scherbaum, F., Schmedes, J. and Cotton, F., 2004. On the conversion of source-to-site distance measures for extended earthquake source models. *Bulletin of the Seismological Society of America*, **94(3)**, pp.1053-1069.

Scherbaum, F., Seif, S. and Kuehn, N.M., 2011, December. On the relationship between Fourier and response spectra: Consequences for the adjustment of empirical ground-motion prediction equations for regional differences. In *American Geophysical Union Fall Meeting Abstracts*, December 2011, S53B-2298.

Scherbaum, F., Delavaud, E. and Riggelsen, C., 2009. Model selection in seismic hazard analysis: an information-theory perspective, *Bulletin of the Seismological Society of America*, **99**, pp.3234-3247.

Schlittenhardt, J., Spies, T., Kopera, J. and Morales, W., 2014. A simple model for probabilistic seismic hazard analysis of induced seismicity associated with deep geothermal systems. *Energy Procedia*, **59**, pp.105-112.

Schorlemmer, D. and Woessner, J., 2008. Probability of detecting an earthquake. *Bulletin of the Seismological Society of America*, **98(5)**, pp.2103-2117.

Scholz, C.H., 1968. The frequency-magnitude relation of micro-fracturing in rock and its relation to earthquakes. *Bulletin of the Seismological Society of America*, **58(1)**, pp.399-415.

Schulte, S., and Mooney, W.D., 2005. An updated global earthquake catalogue for stable continental regions: reassessing the correlation with ancient rifts. *Geophysical Journal International*, **161,** pp. 707–721.

Schwartz, D. P. and Coppersmith, K. J., 1984. Fault behavior and characteristic earthquakes: Examples from the Wasatch and San Andreas Fault Zones, *Journal of Geophysical Research*, **89(B7)**, pp. 5681-5698.

Segwabe, T., 2008. *The geological framework and depositional environments of the coal-bearing Karoo Strata in the Central Kalahari Karoo Basin, Botswana.* PhD thesis, Rhodes University.

Sen, T.K., 2012. Magnitude-Recurrence Relationship and its Effect on Uniform Hazard Spectra: A Current Assessment, *Proceeding to 15th World Conference on Earthquake Engineering, Lisbon*. Available at http://www.iitk.ac.in/nicee/wcee/article/WCEE2012_0143.pdf

Shearer, P.M., and Stark, P.B., 2012. Global risk of big earthquakes has not recently increased. *Proceedings of US National Academy of Sciences*, **109**, pp. 717–721.

Shi, Y., and Bolt, B. A., 1982. The standard error of the magnitude frequency b-value, *Bulletin of the Seismological Society of America*, **72(5), pp.**1677–1687.

Shimazaki, K. and Nakata, T., 1980. Time-predictable recurrence model for large earthquakes. *Geophysical Research Letters*, **7(4)**, pp.279-282.

Shoja–Taheri, J., Naserieh, S. and Hadi, G., 2010. A test of the applicability of NGA models to the strong ground-motion data in the Iranian plateau. *Journal of Earthquake Engineering*, **14**, pp.278 – 292.

Shudofsky, G.N., 1985. Source mechanism and focal depths of East African earthquakes using Rayleigh-wave inversion and body-wave modelling, *Geophysical Journal of the Royal Astronomical Society* **83**(3), pp.563-614.

Shumba, B.T., Midzi, V., Manzunzu, B., Ottemöller, L. and Marimira, K.T., 2020. Source parameters of the moderate Mozambique–Zimbabwe border earthquake on 22 December 2018. *Journal of African Earth Sciences*, **166,** p.103829.

Shumilina, L.S., Gusev, A.A. and Pavlov, V.M., 2000. An improved technique for determination of seismic hazard. *Journal of Earthquake Prediction Research*, **8(1)**, pp.104-110.

Sieberg, A., 1932. Erdbebengeographie. In: Gutenberg, B. (ed.), Handbuch der Geophysik, **4,** Bornträger, Berlin, Germany.

Silva, W., Gregor, N. and Darragh, R., 2002. Development of regional hard rock attenuation relations for central and eastern North America. *Pacific Engineering and Analysis, El Cerrito, CA*.

Simon, R.E., Wright, C., Kgaswane, E.M., and Kwadiba, M.T.O., 2002. The P wave speed structure below and around Kaapvaal craton to depths of 800 km, from travel-times and waveforms of local and regional earthquakes and mining-induced tremors. Geophysical Journal International, **151**, pp.132–145.

Simon, R.E., Wright, C., Kwadiba, M.T.O., and Kgaswane, E.M., 2003. Mantle structure and composition to 800-km depth beneath southern Africa and surrounding oceans from broadband body waves. Lithosphere, **71**, pp.353–367. doi:10.1016/S0024-4937(03)00121-X

Simmons, N.A., Forte, A.M. and Grand, S.P., 2006. Constraining mantle flow with seismic and geodynamic data: a joint approach. *Earth and Planetary Science Letters*, **246(1-2)**, pp.109-124.

Singh M., 2016. *Seismic sources, seismotectonics and earthquake recurrence for the KZN coastal regions.* PhD thesis, University of KwaZulu-Natal, South Africa.

Singh, M., Akombelwa, M. and Maud, R. 2013. Geo-database compilation for seismo-tectonic investigations for the KZN coastal regions, *SASGI Proceedings – Stream 2*.

Singh, M., Kijko, A. and Durrheim, R., 2011. First-order regional seismotectonic model for South Africa. *Natural Hazards*, **59(1)**, pp.383-400.

Singh, M., Kijko, A. and Durrheim, R., 2009. Seismotectonic models for South Africa: Synthesis of geoscientific information, problems, and the way forward. *Seismological research letters*, **80(1)**, pp.71-80.

Singh, M., and Hattingh, E., 2009. Short communication: Collection of isoseismal maps for South Africa. *Natural Hazards*, **50**(2), pp.403-408.

Smit, A., 2019. *A generic probabilistic model for natural hazard assessment.* PhD thesis, University of Pretoria.

Smit, L., Fagereng, Å., Braeuer, B. and Stankiewicz, J., 2015. Microseismic activity and basement controls on an active intraplate strike-slip fault, Ceres–Tulbagh, South Africa. *Bulletin of the Seismological Society of America*, **105(3)**, pp.1540-1547.

Smith, A.J., Beukes, N.J. and Gutzmer, J., 2013. The composition and depositional environments of Mesoarchean iron formations of the West Rand Group of the Witwatersrand Supergroup, South Africa. *Economic Geology*, **108(1)**, pp.111-134.

Smith, R. A., 1984. The lithostratigraphy of the Karoo Supergroup in Botswana. *Bulletin Geological Survey Botswana* **26**, 239pp.

Snoke, J.A., 2003. FOCMEC: Focal mechanism determinations. *International Handbook of Earthquake and Engineering Seismology*, **85**, pp.1629-1630.

Sobol, I.M., 1993. Sensitivity estimates for nonlinear mathematical models. *Mathematical Modelling and Computational Experiments*, **1(4)**, pp.407-414.

Sobol, I.M. and Kucherenko, S.S., 2005. Global sensitivity indices for nonlinear mathematical models, Review. *Wilmott Magazine*, **1**, pp.56-61.

Sokolov, V. and Ismail-Zadeh, A., 2015. Seismic hazard from instrumentally recorded, historical and simulated earthquakes: application to the Tibet–Himalayan region. *Tectonophysics*, ***657***, pp.187-204.

Somerville, P., Graves, R., Collins, N., Song, S.G., Ni, S. and Cummins, P., 2009. Source and ground motion models of Australian earthquakes, *Proceedings of the 2009 Annual Conference of the Australian Earthquake Engineering Society*.

Spada, M., Wiemer, S. and Kissling, E., 2011. Quantifying a potential bias in probabilistic seismic hazard assessment: seismotectonic zonation with fractal properties. *Bulletin of the Seismological Society of America*, **101(6)**, pp.2694-2711.

Stacey, T.R. and Wesseloo, J., 1998. Evaluation and upgrading of records of stress measurement data in the mining industry, Report number: GAP155b, *SIMRAC.*

Stamps, D. S., E. Calais, E. Saria, C. Hartnady, J. M. Nocquet, C. J. Ebinger, and R. M. Fernandes, 2008. A kinematic model for the East African Rift, Geophysical Research Letters, **35**, L05304, doi:10.1029/2007GL03278.

Stamps, D.S., Saria, E. and Kreemer, C., 2018. A geodetic strain rate model for the East African Rift system. *Scientific reports*, **8(1)**, pp.1-8.

Stamps, D. S., Flesch, L. M., Calais, E. and Ghosh, A. 2014. Current kinematics and dynamics of Africa and the East African Rift System. *Journal of Geophysical Research: Solid Earth.* **119(6),** pp.5161–86.

Stanistreet., 1.O., McCarthy, T.S., Charlesworth, E.G., Meyers, R.E. and Armstrong. R.A., 1986. Pre-Transvaal tectonics aLcrig the northel'n margin of the Witwatersrand Basin. *Tectonophysics*, **131**, pp. 53 - 74.

Stein, S. and Liu, M., 2009, Long aftershock sequences within continents and implications for earthquake hazard assessment, *Nature*, **462(7269),** pp.87–89.

Stepp J.C., 1972. Analysis of completeness of the earthquake sample in the Puget Sound area and its effect on statistical estimates of earthquake hazard, *Proceedings of the 1st International Conference on Microzonation*, **2**, pp.897–910.

Stewart, R.A., Reimold, W.U. and Charlesworth, E.G., 2004. Tectonosedimentary model for the Central Rand goldfield, Witwatersrand basin, South Africa. *South African Journal of Geology*, **107(4)**, pp.603-618.

Stewart, J.P., Douglas, J., Javanbarg, M., Bozorgnia, Y., Abrahamson, N.A., Boore, D.M., Campbell, K.W., Delavaud, E., Erdik, M. and Stafford, P.J., 2015. Selection of ground motion prediction equations for the Global Earthquake Model. *Earthquake Spectra*, **31(1)**, pp.19-45.

Stevenson, F., Higgs, R.M. and Durrheim, R.J., 2003. Seismic imaging of precious and base-metal deposits in Southern Africa. *Hardrock Seismic Exploration. Edited by DW Eaton, B. Milkereit, and MH Salisbury. Society of Exploration Geophysicists, Tulsa, Okla*, pp.141-156.

Strasser, F.O., Albini, P., Flint, N.S. and Beauval, C., 2015. Twentieth century seismicity of the Koffiefontein region (Free State, South Africa): Consistent determination of earthquake catalogue parameters from mixed data types. *Journal of Seismology*, **19(4)**, pp.915-934.

Stucchi, M., Albini, P., Mirto, M. and Rebez, A., 2004. Assessing the completeness of Italian historical earthquake data. *Annals of Geophysics*, **47(2-3),** pp.659-673.

Taborda, R. and Roten, D., 2014. Physics-based ground-motion simulation. *Encyclopedia of Earthquake Engineering*, Springer-Verlag Berlin Heidelberg pp.1-33.

Tankard, A. J., Jackson, M.P.A., Eriksson, K.A., Hobday, D.K., Hunter, D.R. and Minter, W.E.L. 1982. *Crustal Evolution of Southern Africa, 3.8 Billion Years of Earth History*, **523** pp., Springer-Verlag, New York.

Tavakoli, B., 2002. Sensitivity of seismic hazard evaluations to uncertainties determined from seismic source characterization. *Journal of Seismology*, **6(4)**, pp.525-545.

Terrier, M., Bles, J.L., Godefroy, P., Dominique, P., Bour, M. and Martin, C., 2000. Zonation of Metropolitan France for the application of earthquake-resistant building regulations to critical facilities Part 1: Seismotectonic zonation. *Journal of Seismology*, **4(3)**, pp.215-230.

Thenhaus, P. C. and Campbell, K. W. 2003. Seismic Hazard Analysis. In Chen, W.F. and Scawthorn, C., editors, *Earthquake Engineering Handbook*., pp 1-50. CRC Press.

Theron, J.N., 1974. The seismic history of the south-western Cape province. In: Van Wyk, W.L. and L.E. Kent (Eds.). The earthquake of 29 September 1969 in the south-western Cape Province, South Africa. *Seismological Series 4*, Geological Survey of South Africa.

Tinti, S. and Mulargia, F., 1985. Effects of magnitude uncertainties on estimating the parameters in the Gutenberg-Richter frequency-magnitude law. *Bulletin of the Seismological Society of America*, **75(6)**, pp.1681-1697.

Tocher, D., 1958. Earthquake energy and ground breakage. *Bulletin of the Seismological Society of America*, **48(2)**, pp.147-153.

Toro, G.R., Abrahamson, N.A. and Schneider, J.F., 1997. Model of strong ground motions from earthquakes in central and eastern North America: best estimates and uncertainties. *Seismological Research Letters*, **68(1)**, pp.41-57.

Toro, G.R. 2002. Modification of the Toro et al. (1997) attenuation equations for large magnitudes and short distances, Technical Report, Risk Engineering.

Tucholke, B.E., Houtz, R.E. and Barrett, D.M., 1981. Continental crust beneath the Agulhas plateau, southwest Indian Ocean. *Journal of Geophysical Research: Solid Earth*, **86(B5)**, pp.3791-3806.

Turyomurugyendo, G. (1996), *Some aspects of seismic hazard in the east and south African region*, MSc Thesis, Institute of Solid Earth Physics, University of Bergen, Bergen, Norway.

Udias, A. and Rice, J., 1975. Statistical analysis of microearthquake activity near San Andreas geophysical observatory, Hollister, California. *Bulletin of the Seismological Society of America*, **65(4),** pp.809-827.

Uhrhammer, R.A., 1986. Characteristics of northern and central California seismicity (abs.). *Earthquake Notes* **57**, p.21.

USNRC, 2012. *Central and Eastern United States Seismic Source Characterization for Nuclear Facilities*. NUREG-2115, US Nuclear Regulatory Commission, Washington D.C.

Van der Westhuizen, W.A., De Bruiyn, H. and Meintjes, P.G., 1991. The Ventersdorp Supergroup: An overview. *Journal of African Earth Sciences*, **13**, pp.83–105.

van Elk, J., Doornhof, D., Bommer, J.J., Bourne, S.J., Oates, S.J., Pinho, R. and Crowley, H., 2017. Hazard and risk assessments for induced seismicity in Groningen. *Netherlands Journal of Geosciences*, **96(5)**, pp.s259-s269.

Vanmarcke, E. H. and Cornell, C. A., 1969. *Analysis of Uncertainty in Ground Motion and Structural Response Due to Earthquakes*, School of Engineering, Massachusetts Institute of Technology, Department of Civil Engineering, Research Report, R 69-24.

Van Stiphout, T., Zhuang, J., and Marsan, D., 2012. Seismicity declustering. Community Online Ressource for Statistical Seismicity Analysis, doi:10:5078/corssa-52382934. Available at http://www.corssa.org.

Vavryčuk, V., 2014. Iterative joint inversion for stress and fault orientations from focal mechanisms. *Geophysical Journal International*, **199(1)**, pp.69-77.

Vermeulen, P.J., 2014. *Extension of the parametric-Historic procedure for probabilistic seismic hazard analysis*, MSc thesis, University of Pretoria.

Vermeulen, P.J., 2020. *Problems in parameter estimation in probabilistic seismic hazard analysis and some solutions*, PhD thesis, University of Pretoria.

Veneziano, D., Cornell, C.A. and O'hara, T., 1984. Historic method for seismic hazard analysis. *Electric Power Research Institute, Report NP-3438, Palo Alto*.

Vinnik, L., Oreshin, S., Kosarev, G., Kiselev, S. and Makeyeva, L., 2009. Mantle anomalies beneath southern Africa: evidence from seismic S and P receiver functions. *Geophysical Journal International*, **179(1)**, pp.279-298.

Viola, G., Andreoli, M., Ben-Avraham, Z., Stengel, I. and Reshef, M., 2005. Offshore mud volcanoes and onland faulting in southwestern Africa: neotectonic implications and constraints on the regional stress field. *Earth and Planetary Science Letters*, **231(1-2)**, pp.147-160.

von Seggern, D.H., 2004. Seismic background noise and detection threshold in the Southern Great Basin Digital Seismic Network. *Bulletin of the Seismological Society of America*, **94(6)**, pp.2280-2298.

Voster C. J., 2003. Simplified Geology of South Africa, Lesotho and Swaziland, *Council for Geoscience*

Vorobieva, I., Narteau, C., Shebalin, P., Beauducel, F., Nercessian, A., Clouard, V., and Bouin M.P., 2013. Multiscale Mapping of Completeness Magnitude of Earthquake Catalogs. *Bulletin of the Seismological Society of America*, **103(4)**, pp.2188-2202.

Vrouwenvelder, A.C.W.M., 2003. Uncertainty analysis for flood defence systems in The Netherlands. In *Bedford, T. Gelder, PHAJM van, Safety and Reliability. Proceedings of ESREL, European Safety and Reliability Conference 2003, Maastricht*, the Netherlands, 15-18 June 2003, 11-18. AA Balkema Publishers; Swets & Zeitlinger.

Wagner, G.S. and Langston, C.A., 1988. East African earthquake body wave inversion with implications for continental structure and deformation. *Geophysical Journal International*, **94(3)**, pp.503-518.

Wang, J.P. and Huang, D., 2014. Deterministic seismic hazard assessments for Taiwan considering non-controlling seismic sources. *Bulletin of Engineering Geology and the Environment*, ***73*(2)**, pp.635-641.

Wells, D. L. and Coppersmith, K. J., 1994. New empirical relationships among magnitude, rupture length, rupture width, rupture area and surface displacement, *Bulletin of the Seismological Society of America*, **84(4)**, pp.974-1002.

Wesnousky, S.G., 1994. The Gutenberg-Richter or characteristic earthquake distribution, which is it? *Bulletin of the Seismological Society of America*, **84(6)**, pp.1940-1959.

Wesnousky, S.G., 2008. Displacement and geometrical characteristics of earthquake surface ruptures: Issues and implications for seismic-hazard analysis and the process of earthquake rupture. *Bulletin of the Seismological Society of America*, **98(4)**, pp.1609-1632.

Wheeler, R.L., 2009. *Methods of Mmax estimation east of the Rocky Mountains* (No. 2009-1018). US Geological Survey.

White, S., Stollhofen, H., Stanistreet, I.G. and Lorenz, V., 2009. Pleistocene to recent rejuvenation of the Hebron Fault, SW Namibia. *Geological Society, London, Special Publications*, **316(1)**, pp.293-317.

Wiemer, S., Garcia-Fernandez, M. and Burg, J.P., 2009. Development of a seismic source model for probabilistic seismic hazard assessment of nuclear power plant sites in Switzerland: the view from PEGASOS Expert Group 4 (EG1d). *Swiss Journal of Geosciences*, **102(1)**, pp.189-209.

Wiemer, S., 2001. A software package to analyze seismicity: ZMAP. *Seismological Research Letters*, **72(3)**, pp.373-382 https://doi.org/10.1785/gssrl.72.3.373

Wiemer, S., and Wyss, M., 2000. Minimum magnitude of complete reporting in earthquake catalogs: examples from Alaska, the Western United States, and Japan. *Bulletin of the Seismological Society of America*, **90(3),** pp.859-869.

Wiemer, S. and Katsumata, K., 1999. Spatial variability of seismicity parameters in aftershock zones, *Journal of Geophysical Research*, **104(13**), pp.13135-13151.

Wiemer, S., McNutt, S.R. and Wyss, M., 1998. Temporal and three-dimensional spatial analyses of the frequency–magnitude distribution near Long Valley Caldera, California. *Geophysical Journal International*, **134(2)**, pp.409-421.

Wiemer, S. and Wyss, M. 1997. Mapping the frequency-magnitude distribution in asperities: An improved technique to calculate recurrence times? *Journal of Geophysical Research*, **102**, pp.15115-15128.

Winter, T., Trinh, P.T., Lacassin, R., Yem, N.T. and Costaz, J., 1994. Advantage of a deterministic approach of seismic risk for dam design: the Hoa Binh dam case (Vietnam). In *P. Taponnier and Nguyen Dinh Xuyen (réd.) Proceedings of the International Workshop on Seismic Hazards in South East Asia. Hanoi, 1er-4 février,* pp. 249-254.

Woessner, J. and Wiemer, S., 2005. Assessing the quality of earthquake catalogues: Estimating the magnitude of completeness and its uncertainty. *Bulletin of the Seismological Society of America,* **95(2)**, pp.684-698.

Woessner, J. and Giardini, D., 2012. Seismic hazard estimates for the Euro-Mediterranean region: A community-based probabilistic seismic hazard assessment. In *Proceedings of 15th World Conference on Earthquake Engineering (15WCEE)* (p. 4337). 15th World Conference on Earthquake Engineering (15WCEE).

Woo, G., 1996. Kernel estimation methods for seismic hazard area source modelling. *Bulletin of the Seismological Society of America,* **86(2)**, pp.353-362.

Wood, H.E., 1913. On the occurrence of earthquakes in South Africa. *Bulletin of the Seismological Society of America*, **3(3)**, pp.113-120.

Wood HE. 1914. Witwatersrand earth tremors. *Journal of the Chemical, Metallurgical and Mining Society of South Africa,* **14,** 423-426.

Wong I. G., 1993. Tectonic stresses in mine seismicity: Are they significant? *In* "Rockbursts and Seismicity in Mines" (R.P. Young, ed.). *Balkema, Rotterdam*, 273 – 278.

Wright, C. and Fernández, L.M., 2003. Chapter 79.48: South Africa. *In: Lee, W.H.K., H. Kanamori and P.C. Jennings (Eds), International Handbook of Earthquake and Engineering Seismology. International Geophysics* **81**(B), 1433-1434.

Wright, C., Walls, E.J. and Carneiro, D.D.J., 2000. The seismic velocity distribution in the vicinity of a mine tunnel at Thabazimbi, South Africa. *Journal of Applied Geophysics*, **44(4)**, pp.369-382.

Wright, C., Kwadiba, M.T.O., Kgaswane, E.M. and Simon, R.E., 2002. The structure of the crust and upper mantle to depths of 320 km beneath the Kaapvaal craton, from P wave arrivals generated by regional earthquakes and mining-induced tremors. *Journal of African Earth Sciences,* **35(4),** pp.477-488.

Wu, S.C., Cornell, C.A. and Winterstein, S.R., 1995. A Hybrid Recurrence Model and Its Implication on Seismic Hazard Results, *Bulletin of the Seismological Society of America,* **85(1)**, pp.1-16.

Wyss, M., Hasegawa, A., Wiemer, S. and Umino, N., 1999. Quantitative mapping of precursory seismic quiescence before the 1989, M 7.1 off-Sanriku earthquake, Japan, *Annali di Geofisica,* **42(5)**, pp.851-869.

Yakovlev, G., Turcotte, D.L., Rundle, J.B. and Rundle, P.B., 2006. Simulation-based distributions of earthquake recurrence times on the San Andreas fault system. *Bulletin of the Seismological Society of America*, **96(6)**, pp.1995-2007.

Yen, Y.T. and Ma, K.F., 2011. Source-scaling relationship for M 4.6–8.9 earthquakes, specifically for earthquakes in the collision zone of Taiwan. *Bulletin of the Seismological Society of America*, **101(2)**, pp.464-481.

Youngs, R.R. and Coppersmith, K.J., 1985. Implications of fault slip rates and earthquake recurrence models to probabilistic seismic hazard estimates. *Bulletin of the Seismological society of America*, **75(4)**, pp.939-964.

Zaliapin, I., Gabrielov, A., Keilis-Borok, V. and Wong, H., 2008. Clustering analysis of seismicity and aftershock identification. *Physical Review Letters*, **101(1)**, p.018501.

Zoller, G. and Hainzl, S., 2007. Recurrence time distributions of large earthquakes in a stochastic model for coupled fault systems: the role of fault interaction. *Bulletin of the Seismological Society of America*, **97(5)**, pp.1679-1687.

Zöller, G. and Holschneider, M., 2016. The maximum and the maximum expected earthquake magnitude for production-induced earthquakes at the gas field in Groningen, The Netherlands. *Bulletin of the Seismological Society of America*, **106(6)**, pp.2917–2921.

Zuccolo, E., Vaccari, F., Peresan, A. and Panza, G.F., 2011. Neo-deterministic and probabilistic seismic hazard assessments: a comparison over the Italian territory. *Pure and Applied Geophysics*, **168(1-2)**, pp.69-83.

Zulu, B.S., 2018. *Time-dependent seismic hazard assessment in the mining regions of the Gauteng province, South Africa*, MSc thesis. University of Witwatersrand.

Zuniga, R., and Wyss, M., 1995. Inadvertent changes in magnitude reported in earthquake catalogs: Influence on b-value estimates, *Bulletin of the Seismological Society of America*, **85,** 1858–1866.

APPENDIX:

Appendix A.

A.1. List of macroseismic event analysed in this study.

Table A1: List of earthquakes analysed in this study with the newly determined source parameters.

ID	Time of the event					Previously published locations by CGS			Solutions obtained in this study				Province
	Year	Mon	Day	Hr	Min	Lat	Long	Mag	Long	Lat	Mag	Rank	
1	1870	8	3	13	20	-28.3	29.1	5.0	29.42	28.25	5.5	2	KZN
2	1903	7	31	20	43				24.88	-28.84	4.8	2	NC
3	1906	12	10	8	12	-26.9	31.3	4.3	31.13	-26.67	5.3	2	ESWAT
4	1908	2	2	22	25				28.07	-26.19	3.0	3	GP
5	1908	2	7	18	20				28.05	-26.25	3.4	3	GP
6	1908	9	10	17	53				28.04	-26.18	2.8	2	GP
7	1908	9	24	18	50	-24	30.5	4.0	30.13	-23.81	3.4	2	LIM
8	1908	9	26	21	7	-29	26	5.0	26.00	-29.07	5.8	1	FS
9	1908	12	25	14	8	-26.0	28.0	3.7	27.95	-26.00	4.1	2	GP
10	1909	6	23	22	25				28.02	-26.21	3.1	2	GP
11	1909	8	5	8	37	-22.2	29	5.0	29.09	-22.62	5.1	2	BOTS
12	1910	3	9	1	29				28.03	-26.21	3.1	3	GP
13	1910	8	16	11	15				28.05	-26.21	3.2	3	GP
14	1910	9	9	13	30				27.99	-26.26	3.0	2	GP
15	1910	10	21	18	40	-30.5	24.7	5.0	25.00	-29.50	6.2	1	NC
16	1912	2	20	13	0	-29.5	25	6.2	25.00	-29.50	6.2	1	FS
17	1912	5	25	18	34				28.05	-26.21	3.1	2	GP
18	1912	5	27	18	43				28.06	-26.20	3.3	3	GP
19	1912	11	16	23	43	-29.7	25.1	4.0	25.09	-29.21	5.7	2	FS
20	1913	3	15	18	28				28.06	-26.18	3.1	2	GP
21	1913	4	5	23	11				28.04	-26.20	2.8	2	GP
22	1913	9	5	14	37				28.05	-26.20	3.1	3	GP
23	1913	12	21	0	28				28.06	-26.22	3.3	3	GP
24	1914	11	11	2	14				28.05	-26.21	3.3	2	GP
25	1914	12	2	21	40				28.05	-26.19	3.0	2	GP
26	1915	1	19	18	32				28.07	-26.21	3.5	2	GP
27	1915	4	19	20	44				28.04	-26.21	3.8	2	GP
28	1915	6	19	21	53				28.05	-26.18	3.7	2	GP
29	1915	6	24	7	49				28.06	-26.18	3.3	2	GP
30	1915	6	28	4	15				28.04	-26.20	3.6	3	GP
31	1916	7	27	17	45	-25.7	31.3	4.0	30.93	-25.27	4.4	2	MP

ID	Time of the event					Previously published locations by CGS			Solutions obtained in this study				Province
	Year	Mon	Day	Hr	Min	Lat	Long	Mag	Long	Lat	Mag	Rank	
32	1916	8	27						28.07	-26.22	3.3	2	GP
33	1918	7	17	20	10				28.07	-26.21	3.3	2	GP
35	1924	10	16	1	10				28.02	-26.23	3.6	2	GP
36	1924	11	25	2	31	-24.9	28.2	3.7	28.30	-24.91	3.9	3	LIM
37	1927	5	2	6	52				27.99	-26.20	3.3	2	GP
38	1928	11	19	18	34				28.03	-26.21	3.6	2	GP
39	1932	8	9			-33.3	26.5	5.0	26.50	-33.40	5.7	1	EC
40	1932	12	31	6	30	-28.3	32.5	6.3	32.22	-28.43	6.1	1	KZN
41	1936	1	12	5	17	-27.00	31.00	5.0	31.61	-27.34	5.1	1	SWAZ
42	1936	1	16	9	32	-29.8	25.3	5.0	25.42	-29.40	5.4	1	FS
43	1938	2	10	20	4	-27.8	31.3	4.3	31.75	-28.14	4.3	2	KZN
44	1940	2	29	23	40	-28.6	28.2	4.3	28.85	-28.10	4.4	2	KZN
45	1940	5	19	18	16	-22.5	33.5	6.2	30.78	-22.55	6.5	2	LIM
46	1940	11	10	21	0	-24	30.2	5.0	30.15	-24.12	5.2	2	LIM
47	1944	11	12	10	55	-29	27.7	4.3	27.62	-29.09	4.5	3	SA-LES